TÉCNICO LISBOA

UNIVERSIDADE DE LISBOA

INSTITUTO SUPERIOR TÉCNICO

Hairy black holes and bosonic stars:

linear and non-linear solutions and their properties

Nuno André Moreira Santos

Supervisor:	Doctor Carlos Alberto Ruivo Herdeiro
Co-supervisors:	Doctor Nicolás Sanchis-Gual
	Doctor David Matthew Hilditch

Thesis approved in public session to obtain the PhD Degree in

Physics

Jury final classification: **Pass with Distinction**

2025

UNIVERSIDADE DE LISBOA
INSTITUTO SUPERIOR TÉCNICO

Hairy black holes and bosonic stars:

linear and non-linear solutions and their properties

Nuno André Moreira Santos

Supervisor:	Doctor Carlos Alberto Ruivo Herdeiro
Co-supervisors:	Doctor Nicolás Sanchis-Gual
	Doctor David Matthew Hilditch

Thesis approved in public session to obtain the PhD Degree in

Physics

Jury final classification: **Pass with Distinction**

Jury

Chairperson: Doctor Ilídio Pereira Lopes, Instituto Superior Técnico, Universidade de Lisboa

Members of the Committee:
Doctor Sam Richard Dolan, School of Mathematical and Physical Sciences, The University of Sheffield, Reino Unido
Doctor David Matthew Hilditch, Instituto Superior Técnico, Universidade de Lisboa
Doctor Eugen Radu, Departamento de Matemática - Centro de Investigação e Desenvolvimento em Matemática e Aplicações (CIDMA), Universidade de Aveiro
Doctor Richard Pires Brito, Instituto Superior Técnico, Universidade de Lisboa

Funding Institution

FCT: Fundação para a Ciência e a Tecnologia

2025

A Natureza é partes sem um todo.
Alberto Caeiro

Resumo

O paradigma do buraco negro de Kerr é, à data, o mais bem sucedido na explicação da natureza dos objetos astrofísicos mais compactos do Universo. No entanto, certos problemas teóricos em aberto, bem como as limitações das observações atuais, motivam a procura de alternativas, cujas propriedades desafiam o paradigma vigente. Entre as muitas possibilidades, apenas algumas parecem ser sólidas e de potencial relevância astrofísica. É esse o caso dos buracos negros com cabelo sincronizado e das estrelas bosónicas, duas famílias de objetos compactos exóticos cuja existência depende de campos bosónicos hipotéticos.

Esta tese de doutoramento é uma compilação de trabalhos de investigação sobre a física desses objetos compactos. Os capítulos são, na sua maioria, reimpressões de trabalhos de investigação publicados em revistas científicas com revisão por pares. O Capítulo 2 estuda em detalhe o estado fundamental dos buracos negros com cabelo de Proca, nomeadamente as suas versões lineares, conhecidas como nuvens estacionárias. O Capítulo 3 discute a lógica subjacente à existência de nuvens estacionárias, que requer um mecanismo de retroalimentação. O Capítulo 4 apresenta um limite superior para a "pilosidade" de buracos negros com cabelo sincronizado formados através do crescimento e saturação do modo superradiante dominante de buracos negros de Kerr. O Capítulo 5 considera esses buracos negros cabeludos de um ponto de vista termodinâmico. Apesar de serem entropicamente favorecidos, estes objetos compactos são localmente instáveis no conjunto canónico, mesmo quando bifurcam de buracos negros de Kerr localmente estáveis, correspondendo, por isso, a uma nova fase. Por fim, o Capítulo 6 analisa perturbações radiais lineares de estrelas bosónicas esfericamente simétricas no domínio da frequência, confirmando e estendendo resultados existentes na literatura. Inclui o cálculo dos modos normais fundamentais destas estrelas, bem como uma discussão sobre critérios de estabilidade linear.

Palavras-chaves: relatividade geral, buracos negros com cabelo, estrelas bosónicas, campos bosónicos fundamentais, teoria de perturbações

Abstract

The Kerr black hole paradigm reigns supreme in explaining the nature of the most compact astrophysical objects in the Universe. However, lingering theoretical questions and the limitations of current observations motivate the search for alternatives, whose properties defy the current paradigm. Among the many possibilities, only a few appear to be sound and of potential astrophysical relevance. This is the case of black holes with synchronized hair and bosonic stars, two families of exotic compact objects that spring from the existence of as yet hypothetical bosonic fields.

This doctoral thesis is a compilation of research papers on the physics of these compact objects. The chapters are, for the most part, reprints of research papers published in peer-reviewed journals. Chapter 2 studies in detail the ground state of the Proca hairy black holes, namely their linear strand, known as stationary clouds Chapter 3 discusses the rationale behind the existence of stationary clouds, which requires a feedback mechanism. Chapter 4 presents an upper limit on the "hairiness" of black holes with synchronized hair formed through the growth and saturation of the dominant superradiant mode of Kerr black holes. Chapter 5 considers these hairy black holes from a thermodynamic point of view. Despite being entropically favored, they are found to be locally unstable in the canonical ensemble even when branched off from locally stable Kerr black holes and thus correspond to a new phase. Finally, Chapter 6 delves into linear radial perturbations of spherically symmetric bosonic stars in the frequency domain, confirming and extending previous results in the literature. It includes the computation of their fundamental normal modes as well as a discussion about criteria for linear stability.

Keywords: general relativity, hairy black holes, bosonic stars, fundamental bosonic fields, perturbation theory

Acknowledgements

First and foremost, I would like to express my sincere gratitude to my supervisor, Carlos Herdeiro, for his guidance, patience, and encouragement throughout my doctoral journey. His expertise in gravitation was instrumental in shaping this research and keeping me focused. I am particularly grateful for the insightful discussions as well as the opportunities to attend national and international conferences, and visit Brazil and Mexico on an exchange. I would also like to acknowledge my co-supervisors, David Hilditch and Nicolás Sanchis-Gual and, for their support and encouragement.

I am indebted to the Center for Astrophysics and Gravitation (CENTRA) at Instituto Superior Técnico, and to the Gravitational Geometry and Dynamics Group (Gr@v), from the Center for Research & Development in Mathematics and Applications (CIDMA), at the University of Aveiro, for providing stimulating academic environments and the resources necessary to complete this research. I would like to particularly thank Cristina Grosso, Marta Santos and Rita Sousa for being of great assistance to me in dealing with bureaucracy and making my secondments possible.

I would like to thank Prof. Luís Crispino and Prof. Juan Carlos Degollado for their kindness and generosity during my research visits to Universidade Federal do Pará (Pará, Brazil) and Universidad Nacional Autónoma de México (Morelos, Mexico), respectively. Their warm hospitality helped to make my visits smoother.

I am grateful to my collaborators—Alexandre Pombo, Carolina Benone, Ernesto Contreras, Eugen Radu, Etevaldo Costa, João Oliveira, Luís Crispino, Miguel Zilhão, Mikaela Carrasco and Pedro Ildefonso—for their invaluable work and dedication.

I would like to acknowledge to Fundação para a Ciência e Tecnologia for the financial support through grant number SFRH/BD/143407/2019, which made this research possible.

On a personal note, I am thankful to my office and lunch mates over the past four years—Alexandre, Giorgio, João, José, Ivo, Manuel— and to all my colleagues at Gr@v for the brainstormings, coffee breaks, and words of encouragement that kept me going.

A special thanks to Mariana Alves and Rafael Galupa from Cartas com Ciência and Maria Coelho Rosa from Between – Partnerships 4 Development for the opportunity to attend the School of Humanness, promoted by the Erasmus+ project "HUMANNESS: EU Social Challenges and Civic Engagement for Solidarity", in Eastern Uganda, where some of the last pages of this thesis were written. Paradoxically (or not), the change of scenery in the very last moment has made everything easier.

Finally, my deepest gratitude goes to my family—my parents, my grandmother and my aunt—and friends—, my friends, especially Alexandre, Beatriz, Lídia and Samuel, for their unwavering support, and, last but not least, Rafael for his patience, kindness and love.

Publications

This doctoral thesis is a compilation of the following peer-reviewed research papers:

- N. M. Santos, C. L. Benone, L. C. B. Crispino, C. A. R. Herdeiro and E. Radu, *Black holes with synchronised Proca hair: linear clouds and fundamental non-linear solutions*, *JHEP* **07** (2020) 010 [2004.09536]
- N. M. Santos and C. A. R. Herdeiro, *Stationary scalar and vector clouds around Kerr–Newman black holes*, *Int. J. Mod. Phys. D* **29** (2020) 2041013 [2005.07201]
- N. M. Santos and C. A. R. Herdeiro, *Black holes, stationary clouds and magnetic fields*, *Phys. Lett. B* **815** (2021) 136142 [2102.04989]
- C. A. R. Herdeiro, E. Radu and N. M. Santos, *A bound on energy extraction (and hairiness) from superradiance*, *Phys. Lett. B* **824** (2022) 136835 [2111.03667]
- N. M. Santos, C. A. R. Herdeiro and E. Radu, *Thermodynamic stability of quasi-bald asymptotically flat black holes*, *Phys. Rev. D* **106** (2022) 124005 [2207.10089]
- N. M. Santos, C. L. Benone and C. A. R. Herdeiro, *Radial stability of spherical bosonic stars and critical points*, *JCAP* **06** (2024) 068 [2404.07257]

During the years of my doctoral program, I also coauthored the following the following peer-reviewed research papers (not included herein):

- A. M. Pombo, J. M. S. Oliveira and N. M. Santos, *Coupled scalar-Proca soliton stars*, *Phys. Rev. D* **108** (2023) 044044 [2304.13749]
- P. Ildefonso, M. Zilhão, C. Herdeiro, E. Radu and N. M. Santos, *Self-interacting dipolar boson stars and their dynamics*, *Phys. Rev. D* **108** (2023) 064011 [2307.00044]
- C. A. R. Herdeiro, E. Radu, N. Sanchis-Gual, N. M. Santos and E. dos Santos Costa Filho, *The non-spherical ground state of Proca stars*, *Phys. Lett. B* **852** (2024) 138595 [2311.14800]

- M. Carrasco-H., N. M. Santos and E. Contreras, *Spontaneous scalarization in Einstein-power-Maxwell-scalar models*, *Phys. Dark Univ.* **45** (2024) 101529 [2405.20442]

Contents

Chapter 1

Introduction

What is the nature of compact astrophysical objects? This has been one of the most pressing questions in astronomy and astrophysics over the past century. The current paradigm conceives of stellar-mass compact objects as compact stellar remnants, the leftover cores of massive stars after their nuclear fuel runs out. The term encompasses the three main traits of compact objects: white dwarfs, neutron stars and black holes. They all have much higher mass-to-radius ratios than ordinary stars, and hence higher densities and stronger surface gravitational fields. White dwarfs are the remnants of the lightest stars, have masses comparable to that of the Sun, but are of the size of the Earth. They are supported by electron degeneracy pressure. Neutron stars are the remnants of some massive stars, also have masses comparable to that of the Sun, but are of the size of a city, resulting in supranuclear densities. They are supported by neutron degeneracy pressure. When a massive star cannot counterbalance the pull of gravity by any means, it leaves behind a *black hole* [11], a region of spacetime where gravity is so strong that nothing can escape from it—not even electromagnetic radiation. The boundary of this region is called the *event horizon*. A stellar-mass black hole is thus a completely collapsed star.

1.1 A brief history of black hole physics

1.1.1 Theoretical achievements

John Michell [12] and Pierre-Simon Laplace [13], both born in 18th century, are credited as the first to propose that sufficiently massive stars could have a surface escape velocity exceeding the speed of light. Although their understading of gravity was based on Newton's law of universal gravitation, their ideas remarkably foreshadowed

the concept of black hole, which was not fully realized until Eintein's theory of general relativity in 1915 [14]. Found by Schwarzschild that same year [15], the first exact solution of Einstein's equations in vacuum, which is the metric of a spherically symmetric spacetime of mass M, already revealed the existence of a particular hypersurface, the event horizon, characterized by the Schwarzschild radius $R_S = 2GM/c^2$, within which communication with external observers is not possible. Behind this "one-way membrane" is a singularity, where the strength of gravity becomes infinite and general relativity is expected to break down. The significance of the Schwarzschild radius was first realized by Oppenheimer and Snyder in 1939, who studied the continued gravitational contraction of a pressureless star in spherical symmetry [16]. They found that the radius of the star approaches asymptotically its Schwarzschild radius, with the star closing itself off from any communication with a distant observer. The Oppenheimer-Snyder collapse turned black holes into more than theoretical speculation. Despite providing a more concrete understanding of their hypothetical formation and properties, it remained unclear whether or not perturbations—in particular, those caused by rotation—could prevent the formation of black holes through gravitational collapse.

It was not until nearly half a century later, in 1963, that Kerr found a new exact vacuum solution of Einstein's equations that describes a rotating object of mass M and angular momentum J [17]. Since astrophysical objects typically rotate, Kerr's solution was a breakthrough in bridging general relativity and astrophysics, and marked the beginning of the *golden age of black hole physics* (1963-1973). If until then many physicists viewed black holes as a speculative hypothesis, Kerr's achievement was a game changer—it was quickly pointed out that quasars, discovered shortly before [18], could be powered by supermassive Kerr black holes. This cemented the *black hole paradigm*, i.e. the idea that astrophysical black holes do exist.

In the decade following Kerr's seminal work, a number of uniqueness and "no-hair" theorems came to light. The former [19–21] state that the only possible stationary and axisymmetric black hole solutions of the Einstein equations are the Kerr solutions, completely characterized by two parameters only—the total mass M and the total angular momentum J, subject to the constraint $M^2 - (J/M)^2 > 0$. Together with "no-hair" theorems (see [22, 23] for reviews), these results contributed to the *Kerr hypothesis* (or "*no-hair*" *conjecture*), stating that the gravitational collapse in the presence of any type of matter-energy yields a Kerr black hole. Quoting Chandrasekhar's personal reflection in a lecture on Shakespeare, Newton and Beethoven [24], the Kerr hypothesis asserts that *an exact solution of Einstein's equations of general relativity [...] provides the absolute exact representation of untold numbers of massive black holes that populate*

the universe." If true, this expectation means that, unlike planets, stars or other astrophysical objects, black holes do not have structural freedom, with only two degrees of freedom, and are very similar to one another. In other words, two black holes with the same mass and angular momentum are indistinguishable.

Also during the golden era, Penrose reconsidered the physics of gravitational collapse without the assumption of spherical symmetry, and analyzed the problem from a topological viewpoint. For that purpose, he introduced the key concept of *trapped surface*, a closed two-dimensional surface that only allows light rays to converge to the singularity, and showed that "deviations from spherical symmetry cannot prevent space-time singularities from arising" [25] (see [26] for a review).[1]

The golden age of black hole physics culminated in the formulation of *black hole thermodynamics*. In 1972, Hawking realized that the area of a black hole's event horizon can never decrease with time [28]. The presence of a naked singularity (i.e. a singularity not hidden behind an event horizon) would be the only possibility to evade Hawking's area theorem. However, naked singularities are excluded by the (weak) cosmic censorship conjecture [29], which states that such singularities cannot form from gravitational collapse. One year later, Bekenstein noticed that Hawking's area theorem bore a very close resemblance to the second law of thermodynamics and identified the area of a black hole as playing the role of entropy [30]. This observation led him to realize that a black hole should indeed be assigned an entropy proportional to its area.[2]

In the meantime, Bardeen, Carter and Hawking formulated the laws of black hole mechanics [31]. A side-by-side comparison of the first law of black-hole mechanics with the first law of thermodynamics indicates that the surface gravity plays a role mathematically equivalent to temperature. Although this equivalence was not noted then, it was not until 1975 that Hawking made the remarkable discovery that black holes emit particles at a steady rate as if they were black bodies with a temperature proportional to the surface gravity [32, 33]. The physical temperature of a black hole is thus proportional to the surface gravity. According to Hawking, the generalized second law of thermodynamics will only hold if one accepts spontaneous particle creation by black hole. Although Hawking radiation from astrophysical black holes is dull and therefore unlikely to be detected any time soon, it surely poses serious challenges to theoretical physics, most notably the information loss paradox, i.e. the breakdown of quantum unitary evolution [34]. The quest to solve this paradox together with

[1] This result owes Roger Penrose half of the 2020 Nobel Prize in Physics "for the discovery that black hole formation is a robust prediction of the general theory of relativity" [27].

[2] Bekenstein mentions in [30] that it was Greif who first considered the possibility of defining the entropy of a black hole but failed to put forward a concrete proposal.

the search for a rationale behind the microscopic nature of the Bekenstein-Hawking entropy have proven to be a convoluted but still fruitful and enlightening path towards a quantum theory of gravity.

1.1.2 Astronomical evidence

Once viewed as exotic, black holes gradually became a cornerstone in physics. Observational astronomy has strengthened both the black hole paradigm and the Kerr hypothesis over the past 60 years (see [35] for a recent review). The body of evidence includes observations of:

- *X-ray binaries and quasars.* The first evidence for the existence of black holes emerged in the 1960s with the discovery of both X-ray binaries in the Milky Way [36] as well as quasi-stellar radio sources (or quasars) in massive galactic nuclei [18]. While the former are candidates for stellar-mass black holes (8–20 $M_\odot$), the latter are plausibly supermassive black holes (10^6–10^{10} $M_\odot$).

- *Stellar orbits in the Galactic Center.* Over the past half century, cumulative evidence for non-stellar mass concentrations at the center of most galaxies has strengthned the black hole paradigm. The evidence comes from observations of stellar orbits in both the optical and infrared bands, e.g. from the Hubble Space Telescope, and, more recently, the James Webb Telescope, as well as in the radio band, from very-long-baseline interferometry of first and second generations, e.g. from the Event Horizon Telescope Collaboration and the GRAVITY Collaboration, respectively. The Milky Way in particular harbours a compact, non-thermal radio source at its center (Saggitarius A*), compatible with a supermassive black hole with 4.3×10^6 $M_\odot$ [37, 38].[3]

- *Shadows.* If there is a black hole between a point light source and a distant observer, only photons with a sufficiently large impact parameter can reach the latter. Those not reaching the distant observer form a depression of light known as "shadow". In an astrophysical setting, this is essentially the silhouette or dark region observed against the bright background of the surrounding hot gas and matter being accreted by the black hole. During a 2017 campaign, the Event Horizon Telescope Collaboration has directly observed the immediate environment of both M87* [39] and Saggitarius A* [38], with the "shadows" being consistent with those predicted by general relativity.

[3]This finding owes Reinhard Genzel and Andrea Ghez half of the 2020 Nobel Prize in Physics "for the discovery of a supermassive compact object at the center of our galaxy" [27].

- *Gravitational waves.* Compact binary mergers lose energy through the emission of gravitational waves. Their dynamics can be divided into three phases: the inspiral, the merger and the ringdown. In the inspiral phase, the two compact objects are initially at large orbital radii. As they lose energy, the inspiral rate increases, and so do the orbital speed, the gravitational-wave strain and the gravitational-wave amplitude, leading to the characteristic "chirp" waveform. Initially in a wide orbit around each other, they gradually spiral inward, Eventually, the compact objects reach the innermost stable orbit, where relativistic effects become important. The binary then transitions to the merger phase, during which the compact objects plunge, i.e. rapidly spiral toward each other and coalesce to form a new compact object. Following the merger, the remnant undergoes the ringdown: it settles into its final, quiescent state, radiating away the excess energy through quasi-normal modes. The quest for the direct detection of gravitational waves started in the 1960s.

  The first direct detection of gravitational waves, labeled as GW150914 [40], is compatible with the coalescence of two black holes.[4] Since the first detection and up to the end of the third observing run, aLIGO and aLIGO together with Virgo and KAGRA have detected ~ 100 candidates for compact binary mergers, including black hole–black hole merger, black hole–neutron star mergers, and neutron star–neutron star mergers [41]. The current catalogue provides the strongest evidence ever for the existence of (stellar-mass) black holes.

Collectively, these astronomical observations contribute to a robust body of evidence supporting the existence of both stellar-mass and supermassive Kerr black holes. Yet, due to limitations in instrumental capabilities and/or incomplete information, such evidence is not conclusive, and the classification of the most compact astrophysical objects in the Universe as actual black holes is still uncertain. In light of this, it is worth considering if all or any part of them are something else rather than Kerr black holes. Raising this possibility fits into testing both the black hole paradigm and the Kerr hypothesis. While this holds value *per se*, the quest for *exotic compact objects* has also been fueled by some open problems in cosmology and general relativity, such as the information loss paradox and the quantum description of the event horizon, or the nature of dark matter.

[4] This achievement owe Reiner Weiss, Barry Barish and Kip Thorne the 2017 Nobel Prize in Physics "for decisive contributions to the LIGO detector and the observation of gravitational waves" [27].

1.2 Exotic compact objects

Exotic compact objects are here loosely defined as hypothetical objects that can challenge the black hole paradigm and/or the Kerr hypothesis. As plausible candidates for astrophysical objects, they must be sufficiently dim not to have been detected by state-of-the-art observations across the electromagnetic spectrum. Some can be as compact as Kerr black holes, and mimic their phenomenology, even when lacking an event horizon. Such definition encompasses:

- *Horizonless exotic compact objects*—exotic compact objects without an event horizon. They appear within modified theories of gravity and/or in the presence of (self-gravitating) exotic matter or exotic states of matter. A number of proposals has been put forward over the past decades (see [42] for a review). Examples include boson stars [43, 44], anisotropic stars [45], wormholes [46], gravastars [47], or fuzzballs [48].

- *Hairy black holes*—exotic compact objects with an event horizon or, equivalently, black holes endowed with hair. The very first example challenging the "no-hair" conjecture was found whithin Einstein–Yang-Mills theory in 1989 [49]. This finding put hairy black holes on the agenda since then, but with a shift from non-Abelian fields to scalar fields over the past years (see [23] for a historical perspective). The possibilities are numerous, even when restricted to four-dimensional, asymptotically-flat solutions with regular geometry on and outside the event horizon (see [22] for a review on black holes with scalar hair). Of particular interest are families of solutions bifurcating from Kerr-Newman black holes, namely black holes with synchronized hair [50] and scalarized black holes [51–53].

This thesis is mainly focused on boson stars and black holes with synchronized hair, which appear in Einstein's gravity minimally coupled to a complex bosonic field. In the case of a scalar field, the action reads

$$\mathcal{S} = \int \mathrm{d}^4x \sqrt{-g} \left[\frac{R}{2\kappa} - \hbar \left(g^{ab} \nabla_a \Phi \nabla_b \bar{\Phi} + \mu^2 \Phi \bar{\Phi} \right) \right] , \tag{1.1}$$

where $\kappa = 8\pi G/c^3$, Φ is a complex scalar field, and the overbar $\bar{\cdot}$ denotes complex conjugation. Both families of compact objects rely on the existence of a putative bosonic field of mass $m = \hbar\mu/c$, where μ is the inverse Compton wavelength, relatable to wave dark matter. The latter is nothing but dark matter that exhibits wave-like

behavior, i.e. whose de Broglie wavelength exceeds the average interparticle separation. From measurements of the dark matter density in the neighborhood of the Sun [54–56], it can be shown that the latter holds if $m \lesssim 30\ \mathrm{eV}/c^2$. The term encompasses fuzzy dark matter [57], the QCD axion [58] and axion-like particles (ALPs), whose possible mass spans a wide range. Fuzzy dark matter in particular refers to ultralight bosonic fields ($m \sim 10^{-22}$–$10^{-20}\ \mathrm{eV}/c^2$) weakly coupled to ordinary matter. Such fields are ubiquitous in string theory [59] and physics beyond the Standard Model [60], and can have a relic abundance that matches today's observed dark matter density [61].

The basic features and phenomenological aspects of bosonic stars and black holes with synchronized hair will be outlined in the following.

1.2.1 Bosonic stars

One of the earliest mentions of boson stars can be traced back to a paper published by Kaup in 1968 [43], followed by a paper by Ruffini and Bonazzola in 1969 [44]. As first conceived by Kaup, boson stars are nothing but the descendents of Wheeler's «gravitational electromagnetic entity» (or simply *geon*), a localized non-singular solution of the Einstein–Maxwell equations [62]. They are solitonic (i.e. particle-like) solutions of Einstein's gravity minimally coupled to a massive, complex scalar field with harmonic time dependence (see [63–65] for reviews). Their evolution is described by the Einstein–Klein–Gordon equations. Boson stars are held together not by the electromagnetic or strong nuclear forces as in ordinary matter, but rather by the dispersive nature of the scalar field, akin to that underlying the Heisenberg uncertainty principle. The dispersiveness counterbalances its self-gravity, preventing the scalar field from collapsing into a black hole. From a condensed matter physics perspective, these stars can be regarded as Bose–Einstein condensates at vanishing temperature.

Boson stars come in different flavours in the literature. They can have charge [66] or rotation [67, 68], and exist in modified theories of gravity, in Newtonian gravity [44] or even in the absence of gravity (Q–balls [69]). Their features are mainly shaped by the scalar field's self-interactions, expressed in different classes of potentials. Three particularly relevant classes of boson stars are:

- *mini-boson stars*, composed of a non-interacting scalar field, whose maximum mass, $\sim 0.633\, m_{\mathrm{P}}^2/m$ [43] (with $m \lesssim 30\ \mathrm{eV}/c^2$), is much smaller than the corresponding Chandrasekhar limit for a fermion star, $\sim m_{\mathrm{P}}^3/m^2$ [70].

- *massive boson stars*, composed of a scalar field with a quartic self-interaction potential of the form $\lambda|\Phi|^4/4$ [71], whose maximum mass depends on the coupling

constant λ, and can be comparable to or even larger than the corresponding Chandrasekhar limit.

- *solitonic boson stars*, composed of a scalar field with a solitonic potential of the form $m^2|\Phi|^2(1-2|\Phi|^2/v_0^2)$, whose maximum mass depends on v_0, $\sim 0.0198 m_{\rm P}^4/(m v_0^2)$.

Additionally, although boson stars are often thought of as condensates of spin–0 fields, they can likewise be composed of spin–1 (or Proca) fields [72], in which case they are called Proca stars. Collectively, they are commonly referred to as *bosonic stars*.

Just like their scalar relatives, Proca stars exhibit a rich landscape of variety. Despite their similitude, boson stars and Proca stars are significantly different from each other. The ground state of static boson stars is characterized by a spherically symmetric energy distribution, whereas that of static Proca stars in the ground state turns out to be axially symmetric [9] (see also [73]). As for stationary configurations, boson stars are prone to non-axisymmetric instabilities that ultimately lead to black hole formation, while Proca stars are dynamically stable [74].

From an astrophysical standpoint, bosonic stars stand out from other exotic compact objects because, unlike most of them, they have a formation mechanism. They can be formed by gravitational cooling, i.e. the (relativistic) virialization through the ejection of bosonic radiation [75–77] (see also [78]). Rotating bosonic stars in particular share several features with black holes, being often regarded as black hole mimickers. As a matter of fact, the putative fundamental field they are composed of is assumed to not interact with baryonic matter, making them as elusive as black holes. The addition of (either attractive or repulsive) self-interactions can make these compact objects as heavy and compact as black holes. Furthermore, bosonic stars can also have ergoregions (and be prone to ergoregion instabilities [79]) and light rings (and be prone to light-ring instabilities [80, 81]).

If bosonic stars are to be an alternative to black holes or coexist with them, they should explain all or at least part of the (radio, X-ray, and gravitational-wave) observations given as evidence of their existence, respectively.

As for radio observations, if Sgr A* is modelled as a very compact rotating boson star with a *stationary* accretion torus around it, the latter produces images which bear close resemblance with those of a rapidly-rotating Kerr black hole, showing in particular an effective shadow and light-ring-like structures [82]. On the other hand, general relativistic magnetohydrodynamic simulations of accreting black holes and static mini-boson stars reveal that the differences in the synthetic reconstructed

images (under realistic astronomical observing conditions) can be detected by the Event Horizon Telescope Collaboration [83]. It has been suggested in particular that a (static) mini-boson star is an unlikely candidate to describe Sgr A* [84], but this hypothesis deserves further investigation. There are some indications that such dissimilarities may soften or even vanish when replacing a boson star by a Proca star [85–87]. Nonetheless, an in-depth study of this scenario (and its variants) should be considered to make a conclusive argument.

As regards X-rays observations, synthetic X-ray reflection spectra of accretion disks around bosonic stars suggest that current missions only rule out the most dilute as well as the most compact configurations [88, 89]. Future X-ray missions, such as eXTP [90], are expected to put stringent constraints on exotic compact objects, namely through precision quasi-periodic-oscillation spectroscopy [91].

Like neutron stars and black holes, bosonic stars can be sources of gravitational waves whose characteristic strain and frequency lie in the detection sensitivity range of current and future detectors. Binary bosonic stars in particular are an ideal target of gravitational-wave astronomy. Although the early inspiral phase is blind to the structure and composition of the compact objects [92], they become important in the late inspiral and merger phases [93, 94, 42]. In principle, gravitational-wave observations can help constrain the "equation of state" of bosonic stars, placing bounds in their potential. Nevertheless, equal-mass, head-on collisions of two boson stars suggest their gravitational-wave signals might be indistinguishable from those of two black holes [95]. In fact, exotic binaries can mimic the ringdown phase of binary black holes, even when their quasi-normal mode spectra are unalike [96]. An illustration of this degeneracy is the event GW190521 [97], interpreted as a merger of two black holes, which is also consistent with the merger of two rotating Proca stars [98] (see also [99]).

1.2.2 Black holes with synchronized hair

Black holes with synchronized hair are (four-dimensional) asymptotically-flat, stationary solutions of Einstein's gravity minimally coupled to a complex bosonic field which are regular on and outside an event horizon (see [22] for a review). Unlike most hairy black holes, these solutions are sourced by matter with canonical kinetic energy, a minimal coupling to gravity. As originally conceived [50], these compact objects are characterized by three global charges: the mass M, the angular momentum J, and the Noether charge Q. The latter is a consequence of the $U(1)$ global symmetry of the complex field. In other words, the Noether charge is a primary hair. Since the field is not gauged, the Noether charge is not associated with a Gauss law and cannot

be measured at spatial infinity. Both the mass and the angular momentum can be expressed as $M = M_H + M_\psi$ and $J = J_H + J_\psi$, where M_H and J_H (M_ψ and J_ψ) are the mass and angular momentum inside (outside) the event horizon, respectively. The proportions of mass and angular momentum outside the horizon, $p = M_\psi/M$ and $q = J_\psi/J$, both ranging from 0 to 1, measure the amount of hair (or *hairiness*).

The parameter space of black holes with synchronized hair continuously connects Kerr black holes with rotating bosonic stars. They reduce to the former in the limit of vanishing field (*Kerr limit*, $p = q = 0$) and to the latter in the limit of vanishing event horizon size (*solitonic limit*, $p = q = 1$). Their properties can vary significantly across the parameter space. For instance, they (*i*) always feature an ergo-region that is limited by either an ergo-sphere or an ergo-Saturn [100]; (*ii*) can violate the Kerr bound in terms of asymptotic and/or horizon quantities, i.e. J/M^2 and/or J_H/M_H^2 can be greater than unity [101]; (*iii*) can have quadrupole moments and orbital angular velocities at the innermost stable circular orbit considerably larger than those of comparable Kerr black holes.

The existence of these solutions was first established for a complex scalar field [50] (see also [102] for details on the numerical strategy for their construction). The physical rationale behind it can be understood from a linear analysis, i.e. disregarding the matter's backreaction on the spacetime and considering the latter to be that of a Kerr black hole. In the case of a scalar field, this amounts to solving the Klein-Gordon equation in Kerr spacetime. The non-trivial separability of this problem was first unveiled via separation of variables by Carter [103], shortly after noting the complete integrability of the Hamilton-Jacobi equation for Kerr geodesics [104]. In Boyer-Lindquist coordinates (t, r, θ, φ), this can be achieved by taking an ansatz for the scalar field of the form [105]

$$\Phi(t, r, \theta, \varphi) = e^{-i\omega t} f(r, \theta) e^{+im\varphi} \ , \tag{1.2}$$

where ω is the (angular) frequency and m is the azimuthal harmonic index. The scalar function f can be further separated as $f(r, \theta) = S_{\ell m}(\theta) R_{\ell m}(r)$, where $S_{\ell m}$ are the spheroidal harmonics of degree ℓ and order m (see [106] for a review), and $R_{\ell m}$ satisfies the radial Teukolsky equation [105, 107], which can be cast in a Schrödinger-like form. Despite that, as opposed to the hydrogen atom problem in quantum mechanics, in general, the Klein-Gordon equation does allow for bound states, i.e. solutions with real frequency, $\Im(\omega) = 0$. The event horizon requires only purely ingoing waves should be present therein, precluding the existence of bound states. Mathematically speaking, the (non-linear) boundary value problem is not Hermitian and therefore the

frequencies are complex, the imaginary part being associated with either the decay, if $\Im(\omega) < 0$, or the growth, if $\Im(\omega) > 0$, rate of the corresponding *quasi-bound state*. If $\Re(\omega)/m > \Omega_H$, then $\Im(\omega) < 0$, and the quasi-bound state decays exponentially in time, with e-folding $1/|\Im(\omega)|$. This is the decaying regime. On the other hand, if $\Re(\omega)/m < \Omega_H$, then $\Im(\omega) > 0$, and the quasi-bound state grow exponentially in time, with e-folding $1/\Im(\omega)$. This is the superradiant regime, in which energy and angular momentum can be extracted from the Kerr black hole. Something special happens at the onset of superradiance,

$$\frac{\Re(\omega)}{m} = \Omega_H \ , \tag{1.3}$$

i.e. when the (real part of the) frequency synchronizes with the angular velocity of the event horizon: bound states, $\Im(\omega) = 0$, in the sense of quantum mechanics, do exist. These are commonly referred to as *stationary clouds*. They were first found for extremal Kerr black holes [108], in which case the radial equation becomes a confluent hypergeometric equation, similarly to that arising in the hydrogen atom problem in quantum mechanics, and can be solved analitically. The analysis was then extended (for the most part, numerically) to sub-extremal Kerr black holes [109–114], and generalized to ungauged and/or gauged scalar fields around Kerr-Newman holes [115–117], Reissner-Nordström-Melvin black holes [3], black holes in string theory [118, 119], BTZ black holes [120], regular black holes [121], and to Proca fields around Kerr(-Newman) black holes [1, 2].

Stationary clouds are marginal and lead to new families of stationary solutions: black holes with synchronized hair. They can be thought of as the non-linear continuations of stationary clouds, the latter being a natural seed in a root-finding algorithm [122].

While the foregoing discussion was restricted to the original family of such hairy black holes [50], generalizations are possible. Examples include families with electric charge [123], radial and polar nodes [124], higher azimuthal winding number [125], self-interacting hair [126, 127], higher-dimensional Myers-Perry black holes [128, 129], asymptotically anti-de Sitter [130].

Kerr black holes can grow hair through superradiance and become black holes with synchronized hair. A bosonic field with $\Re(\omega) < m\Omega_H$ and mass in an appropriate range triggers a superradiant instability that efficiently extracts energy and angular momentum from a Kerr black hole, spinning it down. Superradiance feeds the bosonic field on energy and angular momentum. At the linear level, this fuels an exponential growth in time known as "black-hole bomb" [131] (see also [132–134]). When the black hole spins down enough to meet the synchronization condition in Eq. (1.3), the process stalls. The non-linear evolution of the "black-hole bomb" remained an open question for

decades and was only achieved very recently. The detailed phenomenology depends on whether the field is real or complex. As for self-interacting real fields, the superradiant instability can drive the system to a "bosenova" [135], a phenomenon analogous to the supernova-like explosions observed in Bose-Einstein condensates. "Bosenovas" may give rise to observable gravitational-wave signals [136]. In the case of free complex fields, on the other hand, non-linearities saturate the growth by superradiance, leading the system to new (quasi-)stationary equilibrium configurations without any explosive phenomena [137]. The latter are precisely black holes with synchronized hair [138].

Black holes with synchronized hair grown by superradiance are themselves prone to superradiant instabilities [139]. For sufficiently Kerr-like configurations with scalar hair, their growth rate is comparable to those of a massive scalar field in Kerr spacetime. Thus, such compact objects should not be the endpoint of the evolution of superradiant instabilities, but rather transient configurations. Their lifetime, though, can be very large. For supermassive black holes, it can actually exceed the Hubble time [140]. The (effective) stability against superradiance does not preclude the possibility of these hairy black holes being plagued by other (as yet unknown) instabilities that may threaten their astrophysical viability.

Since black holes with synchronized hair are non-linear combinations of Kerr black holes and bosonic stars, their phenomenology should be Kerr-like in the Kerr limit and non-Kerr-like in the solitonic limit. This expectation is confirmed, for instance, by studies of their lensing and shadows using backward ray-tracing [141–144] (see [145] for a review). The lensing and shadows of Kerr-like configurations might be indistinguishable from those of comparable Kerr black holes. The state of affairs significantly changes when considering non-Kerr-like configurations. The size, shape and topology of their shadow can be utterly different, and their lensing exhibits chaotic patterns, induced by the emergence of stable light rings [143]. On the observational side, current constraints from the Event Horizon Telescope are compatible with superradiantly-grown black holes with synchronized hair [146]. The light source considered in the aforementioned studies is a celestial sphere sufficiently far away from the compact object. More realistic astrophysical scenarios should include accretion disks, though. In general, the differences in imaging between hairy and Kerr black holes remain, although an emitting torus of matter can partly mask them [147] (see also [148, 149]). The effects of the hair have also been examined in the context of Bondi-Hoyle-Lyttleton accretion [150], with the morphology of the flow past a black hole with syncronized hair being fairly similar to that past a Kerr black hole. As the black holes becomes hairier and hairier, the angle of the bow shock becomes wider and wider and the stagnation point moves

further and further away from the compact object. Bondi-Hoyle-Lyttleton accretion naturally produces quasi-periodic oscillations in the shock cone [151], whose spectrum is richer in the presence of hair and might be a fingerprint for an ultralight bosonic field (see also [91] for an account of quasi-periodic oscillations in the X-ray flux from an accreting hairy black hole).

As for X-ray spectroscopy, a proof of concept study of the iron Kα line expected in the reflection spectrum of black holes with synchronized hair showed some regions of their parameter space could be ruled out by current observations [152], which is nevertheless consistent with Kerr-like configurations.

Lastly, as far as gravitational-wave signatures are concerned, there is a distinctive lack of dynamical evolutions of black holes with synchronized hair in the literature, from which template waveforms could be extracted to build new libraries that can be compared with real data. A first step in that direction considered extreme-mass-ratio inspirals in such spacetimes, by using a formalism that combines exact orbital dynamics of geodesic motion with the quadrupole formula [153, 154]. On the observational side, the LIGO-Virgo-KAGRA Collaboration Collaborations have recently searched for gravitational-wave signals resulting from the depletion of a scalar cloud around a rotating black hole using data from the third observing run of Advanced LIGO, and did not find evidence for such signals [155].

In summary, current observations can only rule out regions in the parameter space wherein these hairy black holes deviate significantly from their hairless counterparts, but not those wherein deviations are negligible, i.e. sufficiently close to the Kerr limit, in which superradiance may be able to create such compact objects.

1.3 Outline of the thesis

This thesis is a compilation of research works on bosonic stars and black holes with synchronized hair. The following chapters are reprints from peer-reviewed journal publications co-authored by me.

Part I – Black holes with synchronzied hair

- Chapter 2, reprinted from [1, 2], deals with black holes with synchronized Proca hair, both at the linear and non-linear levels. Firstly, the linear solutions are studied in detail for the first time using the Lunin–Frolov–Krtouš–Kubizňák (LFKK) ansatz for the separability of the Proca equation in the Kerr–NUT–(A)dS family of spacetimes [156], which relies on the existence of a principal tensor, i.e.

a non-degenerate closed conformal Killing–Yano 2-form [157]. The ansatz eases the problem of solving the Proca equation, breaking it down into two second-order ordinary differential equations, which in turn facilitates the study of stationary clouds' dependence on the different "quantum" numbers. Since the Proca field is a spin-1 field, they are labelled by four, and not three, such numbers: $\{n, \ell, j, m\}$, where the orbital angular momentum ℓ and the total angular momentum j may not coincide. Secondly, the parameter space of non-linear solutions in the ground state is constructed and compared with that of solutions in the first-excited state as well as that of their scalar counterparts. Illustrative examples of Kerr-like and non-Kerr-like black holes are provided, with an emphasis on the morphology of surfaces of constant energy density, as it might offer hints to their dynamical stability.

- Chapter 3, reprinted from [3], discusses the conditions for the existence of stationary clouds. As suggested by several examples, they only exist if (i) the spacetime allows for the possibility of superradiance, and (ii) a trapping mechanism is present. The former, which can be traced back to the existence of an ergoregion, is needed for the matter to be in equilibrium with respect to the event horizon. The latter is necessary for matter to accumulate in its vicinity. There is a variety of trapping mechanisms. For example, the (bare or effective) mass of a bosonic field creates a potential barrier that prevents it from dispersing and escaping to infinity. The two conditions are often considered independent from each other. In the case of stationary clouds around Kerr black holes (say), superradiance is not related with the trapping mechanism whatsoever, the latter being assured by the bare mass of the field. However, this is not necessarily the case: a single ingredient might satisfy both conditions simultaneously. To illustrate this, the work studies stationary clouds of massless, neutral scalar fields around Reissner-Nordström black holes immersed in a uniform magnetic field, i.e. Reissner-Nordström-Melvin black holes. These are electrovacuum solutions whose asymptotics resemble those of the magnetic Melvin universe [158]. Their magnetic field induces rotation (and thereby superradiance), and, at the same time, traps the field in the neighborhood of the black hole. Stationary clouds are here obtained both semi-analytically (using the method of matched asymptotic expansion) and numerically (using a shooting method).

- Chapter 4, reprinted from [4], is about the dynamical formation of black holes with synchronized hair. More precisely, it explores how hairy such black holes

can be when formed by the growth and saturation of superradiant instabilities. Hawking's area theorem sets an upper limit of 29% for the efficiency of energy extraction from Kerr black holes [159]. This upper limit corresponds to the case of an extremal Kerr black hole. In light of this maximal efficiency, the proportion of energy stored in superradiance-induced hair is expected not to exceed 29%. Recent evolutions of the dominant superradiant mode of a complex Proca field could only reach 9%, though, despite considering a near-extremal Kerr black hole [137]. Similar evolutions for the scalar case are as yet to be performed. The work queries whether the "hairiness" of such black holes can be much closer to the thermodynamic bound. For that purpose, the evolution of superradiant instabilities is assumed to be nearly conservative. Accordingly, the Kerr bound should be satisfied throughout the growth and saturation of the dominant superradiant mode. This allows one to scan the parameter space and estimate a bound on the "hairiness".

- Chapter 5, reprinted from [5], addresses a poorly explored aspect of asymptotically-flat hairy black holes: their thermodynamic stability. The four laws of black-hole mechanics describe black holes as thermal systems [31]. Because of this, basic concepts in classical thermodynamics do have a meaning in this context. An example is the notion of thermodynamic equilibrium, which can be local or global. The former (the latter) occurs when the equilibrium configuration of a thermal system corresponds to a local (global) maximum of the entropy. Following previous results on the thermodynamic stability of the canonical black holes in general relativity [160], the work investigates for the first time the local thermodynamic stability of black holes with synchronized hair in the canonical ensemble, also considering scalarized black holes in Einstein-Maxwell-scalar theories for comparison. The study is based on the admissable specific heats and evinces the contrast between thermodynamic and dynamic stabilities.

Part II – Bosonic stars

- Chapter 6, reprinted from [6], considers the mode stability of different families of spherically symmetric bosonic stars, namely boson stars with different potentials and Proca stars. More concretely, the parameter space of equilibrium solutions is obtained and reviewed, and their radial normal modes are computed. The latter amounts to solving a boundary value problem for the perturbation mode frequency squared, whose sign is connected with the stability of the corresponding

mode. This has been done in detail for mini-boson stars [161], but results for other families were sparse or even lacking in the literature. The work aims at (partially) filling that gap as well as dispeling some misconceptions about the stability of boson stars.

The thesis closes with an outlook and perspectives in Chapter 7.

Part I

Black holes with synchronized hair

Chapter 2

Reprint of *JHEP* 07 (2020) 010 and *Int. J. Mod. Phys. D* 29 (2020)

Published for SISSA by Springer
Received: April 24, 2020
Revised: May 25, 2020
Accepted: June 5, 2020
Published: July 1, 2020

Black holes with synchronised Proca hair: linear clouds and fundamental non-linear solutions

Nuno M. Santos,[a] **Carolina L. Benone,**[b] **Luís C.B. Crispino,**[c] **Carlos A.R. Herdeiro**[d] **and Eugen Radu**[d]

[a] *Centro de Astrofísica e Gravitação — CENTRA and Departamento de Física, Instituto Superior Técnico — IST, Universidade de Lisboa — UL, Avenida Rovisco Pais 1, 1049, Lisboa, Portugal*
[b] *Campus de Salinópolis, Universidade Federal do Pará, 68721-000, Salinópolis, Pará, Brazil*
[c] *Faculdade de Física, Universidade Federal do Pará, 66075-110, Belém, Pará, Brazil*
[d] *Centre for Research and Development in Mathematics and Applications (CIDMA) and Departamento de Matemática da Universidade de Aveiro, Campus de Santiago, 3810-183 Aveiro, Portugal*

E-mail: nunomoreirasantos@tecnico.ulisboa.pt, benone@ufpa.br, crispino@ufpa.br, herdeiro@ua.pt, eugen.radu@ua.pt

Abstract: Recent studies have made key progress on the black hole/solitonic solutions of the Einstein-Proca system. Firstly, fully non-linear dynamical evolutions of the Kerr black hole superradiant instability, triggered by a Proca field, have shown the formation of a new equilibrium state, a spinning black hole with synchronised Proca hair. Secondly, non-linear evolutions of spinning Proca stars have established that they are dynamically stable, unlike their scalar cousins. Thirdly, separability of the Proca equation on the Kerr background has been achieved. Motivated by these results, in this paper we reconsider Kerr black holes with synchronised Proca hair. The separability of the Proca equation on the Kerr background allows us to examine the stationary Proca clouds in greater detail, in particular their dependence on the different quantum numbers. These stationary clouds occur at a set of existence lines in the Kerr parameter space, from which the black holes with synchronised Proca hair bifurcate. We construct the domain of existence of these black holes, comparing the fundamental states missed in the original study with the first excited states and with the cousin scalar model, giving illustrative examples of Kerr-like and non-Kerr-like BHs. In the vanishing event horizon limit, these hairy black holes connect to the fundamental states of spinning Proca stars, which include the dynamically stable solutions.

Keywords: Black Holes, Classical Theories of Gravity

ArXiv ePrint: 2004.09536

https://doi.org/10.1007/JHEP07(2020)010

JHEP07(2020)010

Contents

JHEP07(2020)010

1 Introduction

Successfully tested up to the TeV scale, the Standard Model of particle physics turns out to describe but a tiny fraction of the matter-energy density of the Universe. It does not explain the phenomenological evidence for the existence of dark matter and dark energy, which are believed to make up about 95% of the Cosmos [1]. Many models have been put forward to explain the dark side of the Universe. Some, in particular, relate dark matter to hypothetical new, ultralight bosonic particles which are sufficiently weakly coupled to ordinary matter to have remained elusive to past and present experimental searches [2, 3].

Bosonic particles have an interesting interaction with Kerr black holes (BHs). They can extract the BH's rotational energy through a radiation enhancement mechanism known as superradiance [4]. For Kerr BHs, superradiance occurs when the phase angular velocity of the boson, ω, fulfills the condition

$$\frac{\omega}{m_j} < \Omega_{\rm H} \equiv \frac{a}{2Mr_{\rm H}}\,, \tag{1.1}$$

where m_j is the boson's azimuthal total angular momentum and $\Omega_{\rm H}$, $r_{\rm H} = M + \sqrt{M^2 - a^2}$ are, respectively, the BH's horizon angular velocity and event horizon (Boyer-Lindquist) radial coordinate, in terms of the BHs's ADM mass M and total angular momentum

$J = Ma$. The enhancement is most efficient when the reduced Compton wavelength of the boson, $\lambda_{\rm C} = \hbar/(\mu c)$, is comparable to the BH's gravitational radius, $R_{\rm G} = GM/c^2$, i.e.

$$\alpha \equiv \frac{R_{\rm G}}{\lambda_{\rm C}} = \frac{GM\mu}{\hbar c} \approx 0.15 \left(\frac{M}{106 M_\odot}\right) \left(\frac{\mu c^2}{10^{-17}\ eV}\right) \sim 1\,, \tag{1.2}$$

where μ is the boson's mass; α is the so-called gravitational fine-structure constant. For the known astrophysical BH masses, ranging between $1 - 10^{10}\ M_\odot$, this implies that the bosonic particles are ultralight, with a mass range of roughly $10^{-10} - 10^{-20}\ eV$.

The non-vanishing bosonic field mass plays the role of a mirror, trapping the bosons in the vicinity of the BH and creating a recurrent energy/angular momentum enhancement of the bosonic state. At the linear level, i.e. disregarding the bosons' backreaction on the background spacetime, the energy feeding of the particles fuels an exponential growth known as superradiant instability, or 'BH bomb' [5]. At the non-linear level, the exponential superradiant growth stalls when the inequality (1.1) saturates, i.e.

$$\frac{\omega}{m_j} = \Omega_{\rm H}\,. \tag{1.3}$$

One may say the (phase angular velocity of the) cloud and the (horizon angular velocity of the) BH synchronise. A simple entropic estimate shows that up to about 29% of the BH's energy could be mined, in an astrophysical timescale, by this process. The result is a classical condensate (often dubbed as *cloud* but also as BH '*hair*') which is stationary with respect to the slowed-down BH [6–8]: a Kerr BH with synchronised bosonic hair. These are stationary BH solutions of Einstein's gravity minimally coupled to complex bosons, first discussed in [9] for scalar and in [10] for vector bosons. They challenge the *no-hair* hypothesis [11] (see also [12, 13]) *even* in General Relativity. According to this hypothesis, BHs that could form dynamically in the presence of astrophysically (potentially) relevant generic matter-energy are fully characterised by global charges associated with Gauss laws, such as M and J, and have no other degrees of freedom, broadly referred to as 'hair'.

The domain of existence of BHs with synchronised bosonic hair has two important boundaries. Firstly, for vanishing horizon size it yields the set of spinning bosonic stars, which have long been known in the scalar case [14, 15], but only recently constructed in the vector case, *a.k.a.* Proca stars [16]. Very recently, it has been shown that the spinning scalar stars suffer from a non-axisymmetric instability, whereas the spinning Proca stars are dynamically robust [17]. This suggests that the Proca case may be dynamically more interesting. Secondly, for vanishing bosonic field, the hairy BHs bifurcate from the Kerr family at the Kerr solutions that admit linear bound states of the corresponding massive bosonic field. These states exist at the threshold of superradience, i.e. when eq. (1.3) holds, and are commonly known as *stationary clouds*.

Stationary clouds around Kerr BHs were first found in the scalar case and around an extremal ($a = M$) BH [18]. Remarkably, in this particular case the radial function can be solved analytically in terms of confluent hypergeometric functions. This analysis has then be extended, typically using numerical methods, to other regimes and other BHs — see e.g. [19–36]. Stationary clouds in the Kerr case are analogous to the atomic orbitals in the

JHEP07(2020)010

hydrogen atom [37] — see also [38]. They are finite on and outside the BH's event horizon, decay exponentially at spatial infinity and can be labeled by four quantum numbers: n, the number of nodes of the radial function; ℓ, the orbital angular momentum; j, the total angular momentum; and m_j, the projection of the total angular momentum along the BH's axis of rotation. Similar configurations have also been obtained in analogue models of gravity such as the draining bathtub vortex [39, 40].

Most studies of stationary clouds around rotating BHs have focused on the scalar case, whose equations of motion are separable on the Kerr spacetime. As for the massive vector bosons, it remained unclear for decades whether the Proca equation was separable or not on Kerr and the only study of clouds tackled the problem by solving the corresponding partial differential equations [10] — see also [41]. Recently, however, the separability of the Proca equation for a large family of spacetimes that includes the Kerr BH was established using a proper ansatz [hereafter the Lunin-Frolov-Krtouš-Kubizňák (LFKK) ansatz] [42]. This development has allowed more detailed studies of the Proca superradiant instability — see e.g. [43, 44]. The first goal of this paper is to make use of this development to determine and characterize the stationary vector clouds around Kerr BHs in terms of $\{n, \ell, j, m_j\}$.

The stationary (scalar or vector) clouds define an existence line on the Kerr parameter space from which the BHs with synchronised hair bifurcate [9, 10]. There is a discrete set of families of BHs with synchronised hair, labelled by the parameters (n, m_j); the parameters (ℓ, j) do not have significance when going from the linear to the non-linear theory. In the scalar case, the fundamental family of hairy BHs has *nodeless* scalar field profiles, corresponding to $n = 0$ and $m_j = 1$ [45]; nodeful solutions, i.e. with $n \neq 0$, are excited states with higher energy [46]. The same holds for the solitonic limit. In the particular case of spherical, static scalar boson stars ($m_j = 0$), it has been shown dynamically that the $n > 0$ excited states decay into the fundamental $n = 0$ ground state [47].

In the original study of Proca stars [16] it was proved that, for static spherical Proca stars, one of the profile functions of the Proca potential must have at least one node; there are no nodeless solutions. In consistency with this observation, the spinning Proca stars reported in the same paper had one node for the corresponding function. Subsequently, the original study of BHs with synchronised Proca hair constructed BH solutions that also have one node of the same function [10]. It was observed in [8] when interpreting the results in [7], however, that in the spinning case (but not in the static case) there are nodeless Proca stars, and also hairy BHs with Proca hair, and these are the true fundamental states. Nonetheless, the latter have not been studied in detail in the literature. The second goal of this paper is, therefore, to report a detailed study of the fundamental solutions of these hairy BHs. In particular, their solitonic limit corresponds precisely to the solutions that have been recently shown to be dynamically robust [17] — see also [48].

This paper is organised as follows. In section 2 we consider the linear analysis of the stationary clouds on a fixed Kerr geometry. In section 2.1 the relativistic quantum-mechanical description of vector bosons is briefly addressed. The notation introduced therein will be useful to label the stationary clouds. Section 2.2 reviews the Proca equation on a curved spacetime, introduces the LFKK ansatz for the Proca field and presents the radial and angular equations it yields for the Kerr case, in Boyer-Lindquist coordinates.

JHEP07(2020)010

Section 2.3 then sets the stage for the numerical integration of those equations and covers the results. Section 3 deals with the non-linear analysis. After briefly describing the setup in section 3.1, the domain of existence of the fundamental BHs with Proca hair is discussed in section 3.2 and compared with that of the first excited states of hairy BHs and the cousin scalar model. In section 3.3 we analyse illustrative solutions of both hairy BHs and spinning Proca stars. Finally, a concise overview of the work is sketched in section 4, together with some closing remarks on future prospects. Appendix A provides some illustrations of the vector spherical harmonics.

Natural units ($G = c = 1$) are consistently used throughout the text. Additionally, the metric signature $(-,+,+,+)$ is adopted.

2 Linear analysis: stationary clouds on a fixed Kerr geometry

2.1 Vector bosons

In relativistic quantum mechanics, particles are described by the orbital angular momentum $\hat{\boldsymbol{L}}$ and the intrinsic angular momentum $\hat{\boldsymbol{S}}$. The components of the individual operators satisfy the angular momentum commutation relations, i.e.

$$[\hat{L}_a, \hat{L}_b] = i\hbar\epsilon_{abc}\hat{L}_c\,, \qquad [\hat{S}_a, \hat{S}_b] = i\hbar\epsilon_{abc}\hat{S}_c\,, \qquad [\hat{\boldsymbol{L}}, \hat{\boldsymbol{S}}] = 0\,,$$

where $a, b, c = 1, 2, 3$. The eigenstates of the operators $\hat{\boldsymbol{L}}^2$ (and $\hat{L}_z$) and $\hat{\boldsymbol{S}}^2$ (and $\hat{S}_z$), respectively denoted as $|\ell, m_\ell\rangle$ and $|s, m_s\rangle$, where $|m_\ell| \leqslant \ell$ and $|m_s| \leqslant s$, satisfy

$$\begin{aligned} \hat{\boldsymbol{L}}^2\,|\ell, m_\ell\rangle &= \hbar^2\ell(\ell+1)\,|\ell, m_\ell\rangle\ , & \hat{L}_z\,|\ell, m_\ell\rangle &= \hbar m_\ell\,|\ell, m_\ell\rangle\ , \\ \hat{\boldsymbol{S}}^2\,|s, m_s\rangle &= \hbar^2 s(s+1)\,|s, m_s\rangle\ , & \hat{S}_z\,|s, m_s\rangle &= \hbar m_s\,|s, m_s\rangle\ . \end{aligned}$$

The total angular momentum $\hat{\boldsymbol{J}}$ is the sum of the orbital and intrinsic angular momenta, i.e. $\hat{\boldsymbol{J}} = \hat{\boldsymbol{L}} + \hat{\boldsymbol{S}}$. Thus, according to the angular momentum addition theorem, the eigenstates of the operator $\hat{\boldsymbol{J}}^2$, here denoted by $|\ell, s, j, m_j\rangle$, can be expressed in terms of the eigenstates $|\ell, m_\ell\rangle$ and $|s, m_s\rangle$ as [49]

$$|\ell, s, j, m_j\rangle = \sum_{m_\ell + m_s = m_j} C^{\ell s j}_{m_\ell m_s m_j}\,|\ell, m_\ell\rangle \otimes |s, m_s\rangle\ ,$$

where the coefficients $C^{\ell s j}_{m_\ell m_s m_j}$, with $j = |\ell - s|, \ldots, \ell + s - 1, \ell + s$ and $|m_j| \leqslant j$, are the Clebsch-Gordan coefficients. These eigenstates satisfy

$$\begin{aligned} \hat{\boldsymbol{L}}^2\,|\ell, s, j, m_j\rangle &= \hbar^2\ell(\ell+1)\,|\ell, s, j, m_j\rangle\ , & \hat{\boldsymbol{S}}^2\,|\ell, s, j, m_j\rangle &= \hbar^2 s(s+1)\,|\ell, s, j, m_j\rangle\ , \\ \hat{\boldsymbol{J}}^2\,|\ell, s, j, m_j\rangle &= \hbar^2 j(j+1)\,|\ell, s, j, m_j\rangle\ , & \hat{J}_z\,|\ell, s, j, m_j\rangle &= \hbar m_j\,|\ell, s, j, m_j\rangle\ , \end{aligned}$$

and therefore $\{\ell, s, j, m_j\}$ are legitimate quantum numbers.

Vector bosons are characterized by $s = 1$, which means that the quantum number j can take a single value when $\ell = 0$ ($j = 1$) and three different values when $\ell > 0$ ($j = \ell - 1, \ell, \ell + 1$). In this case, the eigenstates of the operator $\hat{\boldsymbol{J}}^2$ in the spherical

JHEP07(2020)010

coordinate representation are the ('pure-orbital') vector spherical harmonics $\boldsymbol{Y}^{\ell}_{j,m_j}$, which can be expressed in terms of the scalar spherical harmonics Y_{j,m_j} as

$$\boldsymbol{Y}^{j-1}_{j,m_j} = \frac{1}{\sqrt{j(2j+1)}}\left[r\boldsymbol{\nabla} + j\hat{\boldsymbol{e}}_{(r)}\right] Y_{j,m_j}\,, \tag{2.1}$$

$$\boldsymbol{Y}^{j}_{j,m_j} = -\frac{i}{\sqrt{j(j+1)}}[\boldsymbol{r}\times\boldsymbol{\nabla}]Y_{j,m_j}\,, \tag{2.2}$$

$$\boldsymbol{Y}^{j+1}_{j,m_j} = \frac{1}{\sqrt{(j+1)(2j+1)}}\left[r\boldsymbol{\nabla} - (j+1)\hat{\boldsymbol{e}}_{(r)}\right] Y_{j,m_j}\,, \tag{2.3}$$

where

$$\hat{\boldsymbol{e}}_{(r)} = \boldsymbol{\partial}_r\,, \qquad \hat{\boldsymbol{e}}_{(\theta)} = \frac{1}{r}\boldsymbol{\partial}_\theta\,, \qquad \hat{\boldsymbol{e}}_{(\varphi)} = \frac{1}{r\sin\theta}\boldsymbol{\partial}_\varphi\,,$$
$$\boldsymbol{\nabla} = \hat{\boldsymbol{e}}_{(r)}\partial_r + \hat{\boldsymbol{e}}_{(\theta)}\frac{1}{r}\partial_\theta + \hat{\boldsymbol{e}}_{(\varphi)}\frac{1}{r\sin\theta}\partial_\varphi\,.$$

The vector spherical harmonics have parity $\hat{\boldsymbol{\Pi}} = (-1)^{\ell+1}$. Thus, upon a parity transformation, $\boldsymbol{Y}^{\ell}_{j,m_j}$ acquires a factor of $(-1)^j$, when $j = \ell \pm 1$, and of $(-1)^{j+1}$, when $j = \ell$. $\boldsymbol{Y}^{j\pm1}_{j,m_j}$ ($\boldsymbol{Y}^{j}_{j,m_j}$) are said to have electric-type (magnetic-type) parity: they correspond to the magnetic (electric) field of electric multipole radiation and the electric (magnetic) field of magnetic multipole radiation [50, 51]. The explicit form and a graphic representation of the first few 'pure-orbital' vector harmonics are provided in appendix A.

In curved spacetimes, $\{\ell, j, m_j\}$ are not in general legitimate quantum numbers, since curvature can break the conservation of angular momentum.[1] However, in Schwarzschild spacetime, the total angular momentum $\hat{\boldsymbol{J}}$ is still conserved. This means that vector bosons only have definite total angular momentum. Such definiteness is broken in Kerr spacetime, in which the total angular momentum is no longer conserved. Nevertheless, choosing $\hat{J}_z$ to be aligned with the symmetry axis of Kerr spacetime at spatial infinity, m_j remains a conserved quantity.

It is convenient to use the quantum numbers $\{\ell, j, m_j\}$ to identify vector bosons, always bearing in mind that they are only physically meaningful in Minkowski spacetime. In particular, in the following, vector states will be labelled with $|\ell, j, m_j\rangle \equiv |\ell, s=1, j, m_j\rangle$.

2.2 Proca equation

The Lagrangian density of a massive complex vector boson A^α reads

$$\mathcal{L}_{\rm M} = -\frac{1}{4}F_{\alpha\beta}\bar{F}^{\alpha\beta} - \frac{1}{2}\mu^2 A_\alpha \bar{A}^\alpha\,, \tag{2.4}$$

where $F_{\alpha\beta} = 2A_{[\beta;\alpha]}$. $F_{\alpha\beta}$ is the electromagnetic-field tensor, which is antisymmetric and gauge invariant, $\alpha, \beta = 0, 1, 2, 3$ and μ is the boson's mass. The variation of the action integral $\mathcal{S} = \int_V \mathrm{d}^4x\sqrt{-g}\ \mathcal{L}_{\rm M}$ with respect to the field $\bar{A}^\alpha$ leads to the Proca field equation [52]:

$$\nabla_\beta F^{\alpha\beta} + \mu^2 A^\alpha = 0\,. \tag{2.5}$$

[1] Intrinsic angular momentum is expected to be conserved in curved spacetimes, though, otherwise curvature could induce transitions between particles or fields with different spins.

JHEP07(2020)010

Writing the equation in terms of the electromagnetic four-potential A^α,

$$\nabla_\beta \nabla^\alpha A^\beta - \Box A^\alpha + \mu^2 A^\alpha = 0\,, \tag{2.6}$$

its four-divergence reads

$$\nabla_\alpha \nabla_\beta \nabla^\alpha A^\beta - \nabla_\alpha (\Box A^\alpha) + \mu^2 \nabla_\alpha A^\alpha = 0\,. \tag{2.7}$$

Using the identities

$$\nabla_{[\alpha} \nabla_{\beta]} A^\beta = \frac{1}{2} R^\beta{}_{\gamma\alpha\beta} A^\gamma = -\frac{1}{2} R_{\alpha\beta} A^\beta\,, \tag{2.8}$$

$$\nabla_{[\alpha} \nabla_{\beta]} (\nabla^\alpha A^\beta) = R_{\alpha\beta} \nabla^{[\alpha} A^{\beta]}\,, \tag{2.9}$$

it follows that, for Ricci-flat spacetimes ($R_{\alpha\beta} = 0$), such as the Kerr spacetime, eq. (2.7) reduces to

$$\nabla_\alpha A^\alpha = 0\,. \tag{2.10}$$

This means that any massive complex vector boson minimally coupled to Einstein's gravity in a Ricci-flat spacetime satisfies the Lorenz condition. Moreover, under these conditions, the Proca equation (2.6) simplifies to

$$(\Box - \mu^2) A^\alpha = 0\,. \tag{2.11}$$

The dynamics of the divergenceless electromagnetic four-potential A^α is thus encoded in a set of four Klein-Gordon equations, one per component. The non-trivial separability of the Klein-Gordon equation in Kerr spacetime was first unveiled via variable separation by Carter [53], shortly after noting the complete integrability of the Hamilton-Jacobi equation for Kerr geodesics [54]. Carter's seminal work broke down the original second-order partial differential equation (PDE) into two coupled second-order ordinary differential equations (ODEs), and paved the way for a thorough study of Kerr linear perturbations.

Although the four equations of motion (2.11) are individually separable for a specific ansatz, the separability does not extend to the Lorenz condition (2.10). In fact, the separability of these five second-order PDEs is not trivial and was only achieved recently via the LFKK ansatz [42] (see also ref. [55]), following [56]. This separability has been established for the Kerr-NUT-(A)dS family of spacetimes. The LFKK ansatz, which embodies the explicit and hidden symmetries of the metric, is

$$A^\alpha = B^{\alpha\beta} \nabla_\beta Z\,, \tag{2.12}$$

where $B^{\alpha\beta}$ is the polarisation tensor[2] and Z is an auxiliary complex scalar function for which a multiplicative separation of variables will hold — cf. eq. (2.17) below. The polarisation tensor $B^{\alpha\beta}$ is defined in terms of the principal tensor[3] $h_{\alpha\beta}$ as

$$B^{\alpha\gamma} \left(g_{\gamma\beta} + i \frac{h_{\gamma\beta}}{\lambda} \right) = \delta^\alpha_\beta\,, \tag{2.13}$$

where λ plays the role of a separation constant.

[2] In [55], the authors named $B^{\alpha\beta}$ *polarisation tensor* without clarifying how the tensor encodes the different polarisations of massive vector bosons. It is worth pointing out that, as opposed to the polarisation tensors usually found in the literature, $B^{\alpha\beta}$ is not totally symmetric.

[3] The separability of the Hamilton-Jacobi, Klein-Gordon, and Dirac equations in Kerr-NUT-(A)dS spacetimes can be traced back to the existence of the principal tensor. For a review, see [57].

JHEP07(2020)010

To solve the Proca equation in the Kerr background with the ansatz (2.12) one proceeds as follows. In Boyer-Lindquist coordinates (t, r, θ, φ), the Kerr metric reads

$$\boldsymbol{g} = -\frac{\Delta}{\Sigma}\left[\mathbf{d}t - a\sin^2\theta\,\mathbf{d}\varphi\right]^2 + \frac{\Sigma}{\Delta}\mathbf{d}r^2 + \Sigma\,\mathbf{d}\theta^2 + \frac{\sin^2\theta}{\Sigma}\left[a\,\mathbf{d}t - (r^2+a^2)\,\mathbf{d}\varphi\right]^2 , \tag{2.14}$$

where $\Sigma \equiv r^2 + a^2\cos^2\theta$ and $\Delta \equiv r^2 - 2Mr + a^2$. The Kerr spacetime is stationary and axisymmetric; it has an event horizon at $r = r_{\rm H}$, the largest root of Δ. In Boyer-Lindquist coordinates, the Killing vectors associated with these continuous symmetries are $\boldsymbol{\xi}_t = \boldsymbol{\partial}_t$ and $\boldsymbol{\xi}_\varphi = \boldsymbol{\partial}_\varphi$, respectively. Its principal tensor reads

$$\begin{aligned}\boldsymbol{h} = &-(r\mathbf{d}r + a^2\sin\theta\cos\theta\mathbf{d}\theta)\wedge\mathbf{d}t \\ &+ a\sin\theta[r\sin\theta\mathbf{d}r + (r^2+a^2)\cos\theta\mathbf{d}\theta]\wedge\mathbf{d}\varphi\,.\end{aligned} \tag{2.15}$$

Using the metric and principal tensor, one constructs the polarization tensor. Its symmetric and antisymmetric parts are

$$B^{(\alpha\beta)} = \frac{\lambda^2}{\Sigma}\left[\frac{1}{q_r}\begin{pmatrix} -\frac{(r^2+a^2)^2}{\Delta} & 0 & 0 & -\frac{a(r^2+a^2)}{\Delta} \\ 0 & \Delta & 0 & 0 \\ 0 & 0 & 0 & 0 \\ -\frac{a(r^2+a^2)}{\Delta} & 0 & 0 & -\frac{a^2}{\Delta}\end{pmatrix} + \frac{1}{q_\theta}\begin{pmatrix} a^2\sin^2\theta & 0 & 0 & a \\ 0 & 0 & 0 & 0 \\ 0 & 0 & 1 & 0 \\ a & 0 & 0 & \csc^2\theta\end{pmatrix}\right],$$

$$B^{[\alpha\beta]} = -\frac{i\lambda}{\Sigma}\left[\frac{r}{q_r}\begin{pmatrix} 0 & -(r^2+a^2) & 0 & 0 \\ (r^2+a^2) & 0 & 0 & a \\ 0 & 0 & 0 & 0 \\ 0 & -a & 0 & 0\end{pmatrix} + \frac{a\cos\theta}{q_\theta}\begin{pmatrix} 0 & 0 & -a\sin\theta & 0 \\ 0 & 0 & 0 & 0 \\ a\sin\theta & 0 & 0 & \csc\theta \\ 0 & 0 & -\csc\theta & 0\end{pmatrix}\right],$$

respectively, where

$$q_r = r^2 + \lambda^2\,, \qquad q_\theta = \lambda^2 - a^2\cos^2\theta\,. \tag{2.16}$$

Note that the r-dependent terms are decoupled from the θ-dependent terms, apart from the common factor $1/\Sigma$.

Additionally, we take the complex scalar function in eq. (2.12) with the form

$$Z(t, r, \theta, \varphi) = e^{-i\omega t}R(r)Q(\theta, \varphi)\,, \qquad Q(\theta, \varphi) = S(\theta)e^{+im_j\varphi}\,, \tag{2.17}$$

where R and S are dubbed radial and angular functions, respectively, and ω and m_j are the eigenvalues related to the aforementioned isometries.

With this construction, the ansatz (2.12) reduces the Proca equation to the two separated equations

$$q_r\frac{\mathrm{d}}{\mathrm{d}r}\left[\frac{\Delta}{q_r}\frac{\mathrm{d}R}{\mathrm{d}r}\right] + \left[\frac{K_r^2}{\Delta} + \frac{2\lambda^2 - q_r}{q_r}\sigma\lambda - q_r\mu^2\right]R = 0\,, \tag{2.18}$$

$$\frac{q_\theta}{\sin\theta}\frac{\mathrm{d}}{\mathrm{d}\theta}\left[\frac{\sin\theta}{q_\theta}\frac{\mathrm{d}S}{\mathrm{d}\theta}\right] - \left[\frac{K_\theta^2}{\sin^2\theta} + \frac{2\lambda^2 - q_\theta}{q_\theta}\sigma\lambda - q_\theta\mu^2\right]S = 0\,, \tag{2.19}$$

where

$$K_r = (r^2+a^2)\omega - am_j\,, \qquad K_\theta = m_j - a\omega\sin^2\theta\,, \qquad \sigma = \frac{a(m_j - a\omega)}{\lambda^2} + \omega\,. \tag{2.20}$$

JHEP07(2020)010

As mentioned in section 2.1, vector states can have electric-type or magnetic-type parity. The ansatz (2.12) encodes all the electric-type states and the magnetic-type states with $j = |m_j|$ [37, 43]. It remains unclear, however, whether all the magnetic-type states are captured by the LFKK ansatz or not. If so, further study of the Proca equation in Kerr spacetime may shed some light on how to recover all of them. If not, a new question arises: whether it is possible to find a new ansatz which contains all the states.

In the following, all physical quantities will be expressed in terms of the boson's reduced Compton wavelength. It is therefore convenient to set $\lambda_{\rm C} = \mu^{-1} = 1$.

2.3 Stationary vector clouds around Kerr black holes

In general, eqs. (2.18) and (2.19) form a non-standard coupled eigenvalue problem with an eigenvalue pair $\{\omega, \lambda\}$. To construct the stationary vector clouds around Kerr BHs, we need to find the bound states whose phase angular velocity fulfills the synchronization condition (1.3). Since ω is fixed *a priori*, the eigenvalue pair can be chosen to be either $\{M, \lambda\}$ or $\{a, \lambda\}$. The existence of stationary clouds is only allowed for specific values of the background parameters M and a. Such quantization follows from the regularity of the bound states and results in an *existence line* in the two-dimensional Kerr parameter space defined by (M, a) or, alternatively, $(M, \Omega_{\rm H})$.

The next subsections summarise the algorithm to solve the radial equation (2.18) together with the synchronization condition and therefore determine the existence lines of stationary vector clouds around Kerr BHs. For convenience, eqs. (2.18) and (2.19) will be considered as written in terms of $r_{\rm H}$ and a instead of M and a. For this purpose, using the identity

$$M = \frac{r_{\rm H}^2 + a^2}{2r_{\rm H}}\,, \tag{2.21}$$

the function Δ may be written as

$$\Delta = r^2 - (r_{\rm H}^2 + a^2)\frac{r}{r_{\rm H}} + a^2\,. \tag{2.22}$$

2.3.1 Angular equation

In the Minkowski limit, the phase angular velocity equals the inverse of the reduced Compton wavelength: $\omega = \mu = 1$. Hence, eq. (2.19) can be written in the form[4]

$$\hat{\boldsymbol{J}}^2 Q_0 = \lambda_0^{\rm E}(\lambda_0^{\rm E} - 1)Q_0\,, \tag{2.23}$$

where Q_0 denotes the leading-order form of the function Q at spatial infinity and the superscript 'E' will become clear in the remainder of the present section. $\hat{\boldsymbol{J}}^2$ coincides with the square of the orbital angular momentum operator,

$$\hat{\boldsymbol{J}}^2 = -\frac{1}{\sin\theta}\frac{\partial}{\partial\theta}\left(\sin\theta\frac{\partial}{\partial\theta}\right) - \frac{1}{\sin^2\theta}\frac{\partial^2}{\partial\varphi^2}\,, \tag{2.24}$$

[4]As opposed to the angular equation governing the dynamics of massless scalar bosons in the Kerr geometry, eq. (2.19) does not reduce to the spherical harmonic differential equation when $a\omega = 0$ (i.e. when $a = 0$ or $\omega = 0$), but only when $a = 0$, i.e. in the Schwarzschild limit. Note, however, that eq. (2.23) corresponds to the Minkowski limit ($M = 0$, $a = 0$) of eq. (2.19), for which the condition $\omega = \mu$ holds.

JHEP07(2020)010

whose eigenfunctions are the well-known scalar spherical harmonics of degree j and order m_j, Y_{j,m_j}. In particular, $\hat{\boldsymbol{J}}^2 Y_{j,m_j}(\theta,\varphi) = j(j+1)Y_{j,m_j}(\theta,\varphi)$. Since the Kerr spacetime is asymptotically flat, j may be defined as the total angular momentum at spatial infinity.

The quadratic equation $\lambda_0^{\rm E}(\lambda_0^{\rm E}-1) = j(j+1)$ has two different solutions:

$$\lambda^{\rm E}_{0,-} = -j\,, \quad \lambda^{\rm E}_{0,+} = j+1\,. \tag{2.25}$$

This means that, at leading order, the electromagnetic four-potential $A^\alpha = (A^t, \boldsymbol{A})$ takes the form

$$\begin{aligned}
A^t_0 &= \frac{\lambda^{\rm E}_0}{r^2+(\lambda^{\rm E}_0)^2}\left(-\lambda^{\rm E}_0\partial_t Z_0 + ir\partial_r Z_0\right) = \frac{i\lambda^{\rm E}_0}{r}\partial_r Z_0 + \ldots = i\lambda^{\rm E}_0\frac{e^{-i\omega t}}{r}\partial_r R^{[\infty]}_0 Y_{j,m_j} + \ldots\,,\\
A^r_0 &= \frac{\lambda^{\rm E}_0}{r^2+(\lambda^{\rm E}_0)^2}\left(-ir\partial_t Z_0 + \lambda^{\rm E}_0\partial_r Z_0\right) = -\frac{i\lambda^{\rm E}_0}{r}\partial_t Z_0 + \ldots = -\lambda^{\rm E}_0\frac{e^{-i\omega t}}{r}R^{[\infty]}_0 Y_{j,m_j} + \ldots\,,\\
A^\theta_0 &= \frac{1}{r^2}\partial_\theta Z_0 = \frac{e^{-i\omega t}}{r^2}R^{[\infty]}_0\partial_\theta Y_{j,m_j}\,,\\
A^\varphi_0 &= \frac{1}{r^2\sin^2\theta}\partial_\varphi Z_0 = \frac{e^{-i\omega t}}{r^2\sin^2\theta}R^{[\infty]}_0\partial_\varphi Y_{j,m_j}\,,
\end{aligned}$$

where $R^{[\infty]}_0$ is the leading-order form of the function R at spatial infinity. The spatial part of A^α can be written as

$$\begin{aligned}
\boldsymbol{A}_0 &= \frac{e^{-i\omega t}}{r}R^{[\infty]}_0\left[-\lambda^{\rm E}_0 Y_{j,m_j}\boldsymbol{\partial}_r + \frac{1}{r}(\partial_\theta Y_{j,m_j})\boldsymbol{\partial}_\theta + \frac{1}{r\sin^2\theta}(\partial_\varphi Y_{j,m_j})\boldsymbol{\partial}_\varphi\right]\\
&= \frac{e^{-i\omega t}}{r}R^{[\infty]}_0\left[-\lambda^{\rm E}_0 Y_{j,m_j}\hat{\boldsymbol{e}}_{(r)} + (\partial_\theta Y_{j,m_j})\hat{\boldsymbol{e}}_{(\theta)} + \frac{1}{\sin\theta}(\partial_\varphi Y_{j,m_j})\hat{\boldsymbol{e}}_{(\varphi)}\right]\\
&= \frac{e^{-i\omega t}}{r}R^{[\infty]}_0\left[r\boldsymbol{\nabla} - \lambda^{\rm E}_0\hat{\boldsymbol{e}}_{(r)}\right]Y_{j,m_j}\\
&= \sqrt{2j+1}\frac{e^{-i\omega t}}{r}R^{[\infty]}_0 \times \begin{cases} \sqrt{j}\;\boldsymbol{Y}^{j-1}_{j,m_j}, & \text{for } \lambda^{\rm E}_0 = \lambda^{\rm E}_{0,-}\\ \sqrt{j+1}\;\boldsymbol{Y}^{j+1}_{j,m_j}, & \text{for } \lambda^{\rm E}_0 = \lambda^{\rm E}_{0,+}\end{cases}\,.
\end{aligned} \tag{2.26}$$

The angular dependence of $\boldsymbol{A}_0$ is described by the 'pure-orbital' vector spherical harmonics in flat space. Equation (2.26) with eigenvalues $\lambda^{\rm E}_{0,\mp}$, corresponds to the $j = \ell \pm 1$ electric-type states of the vector field (cf. section 2.1). This explains the superscript 'E'.

In the ZAMO frame, characterized by the tetrad

$$\begin{aligned}
\hat{\boldsymbol{e}}^\bullet_{(t)} &= \frac{1}{\sqrt{\Xi\Sigma\Delta}}\left[\Xi\boldsymbol{\partial}_t + 2Mar\boldsymbol{\partial}_\varphi\right]\,, & \hat{\boldsymbol{e}}^\bullet_{(r)} &= \sqrt{\frac{\Delta}{\Sigma}}\boldsymbol{\partial}_r\,,\\
\hat{\boldsymbol{e}}^\bullet_{(\theta)} &= \frac{1}{\sqrt{\Sigma}}\boldsymbol{\partial}_\theta\,, & \hat{\boldsymbol{e}}^\bullet_{(\varphi)} &= \frac{\sqrt{\Sigma}}{\sqrt{\Xi}\sin\theta}\boldsymbol{\partial}_\varphi\,,
\end{aligned}$$

where $\Xi \equiv (r^2+a^2)^2 - a^2\Delta\sin^2\theta$, the electric field $\boldsymbol{E}$ and the magnetic field $\boldsymbol{B}$ have the following components:

$$E_{(a)} = F_{\alpha\beta}\hat{e}^{\bullet\alpha}_{(a)}\hat{e}^{\bullet\beta}_{(t)}\,, \qquad B_{(a)} = -\frac{1}{2}\epsilon_{\alpha\beta\gamma\delta}F^{\gamma\delta}\;\hat{e}^{\bullet\alpha}_{(a)}\hat{e}^{\bullet\beta}_{(t)}\,,$$

JHEP07(2020)010

with $\epsilon_{\alpha\beta\gamma\delta} \equiv \sqrt{-g}\ [\alpha\beta\gamma\delta]$, where $[\alpha\beta\gamma\delta]$ is the four-dimensional Kronecker delta. The leading-order terms of $E_{(a)}$ and $B_{(a)}$ are then given by

$$
\begin{aligned}
E_{0(r)} &= -i\lambda_0^{\mathrm{E}} \frac{e^{-i\omega t}}{r} R_0^{[\infty]} Y_{j,m_j}\,, & B_{0(r)} &= 0\,,\\
E_{0(\theta)} &= i\frac{e^{-i\omega t}}{r} R_0^{[\infty]} \partial_\theta Y_{j,m_j}\,, & B_{0(\theta)} &= -\frac{e^{-i\omega t}}{r\sin\theta}\frac{\mathrm{d}R_0^{[\infty]}}{\mathrm{d}r}\partial_\varphi Y_{j,m_j}\,,\\
E_{0(\varphi)} &= i\frac{e^{-i\omega t}}{r\sin\theta} R_0^{[\infty]} \partial_\varphi Y_{j,m_j}\,, & B_{0(\varphi)} &= \frac{e^{-i\omega t}}{r}\frac{\mathrm{d}R_0^{[\infty]}}{\mathrm{d}r}\partial_\theta Y_{j,m_j}\,,
\end{aligned}
$$

or

$$
\begin{aligned}
\boldsymbol{E}_0 &= i\frac{e^{-i\omega t}}{r} R_0^{[\infty]} \left[r\boldsymbol{\nabla} - \lambda_0^{\mathrm{E}}\hat{\boldsymbol{e}}_{(r)}\right] Y_{j,m_j}\\
&= i\sqrt{2j+1}\frac{e^{-i\omega t}}{r} R_0^{[\infty]} \times \begin{cases} \sqrt{j}\ \boldsymbol{Y}^{j-1}_{j,m_j}, & \text{for } j-\ell = +1\\ \sqrt{j+1}\ \boldsymbol{Y}^{j+1}_{j,m_j}, & \text{for } j-\ell = -1 \end{cases},\\
\boldsymbol{B}_0 &= \frac{e^{-i\omega t}}{r}\frac{\mathrm{d}R_0^{[\infty]}}{\mathrm{d}r}[\boldsymbol{r}\times\boldsymbol{\nabla}]Y_{j,m_j} = i\sqrt{j(j+1)}\frac{e^{-i\omega t}}{r}\frac{\mathrm{d}R_0^{[\infty]}}{\mathrm{d}r}\boldsymbol{Y}^{j}_{j,m_j}\,,
\end{aligned}
$$

where we used the fact that $\hat{\boldsymbol{e}}^{\bullet}_{(a)} \to \hat{\boldsymbol{e}}_{(a)}$ as $r \to +\infty$. The electric field $\boldsymbol{E}_0$ depends on the difference $j-\ell$, whereas the magnetic field $\boldsymbol{B}_0$ does not.

When $\alpha \ll 1$, the angular eigenstates and eigenvalues for the electric-type states may be written as an expansion in α. The next-to-leading order corrections to the angular eigenfunctions induce couplings to vector spherical harmonics of the same parity and thus the angular functions Q have definite parity. For future reference, we present the expansion for the angular eigenvalues below [37]:

$$
\lambda^{\mathrm{E}}_{\pm} = \sum_{n=0}^{\infty} \lambda^{\mathrm{E}}_{n,\pm}\alpha^n\,, \tag{2.27}
$$

where the first terms of the series are given by

$$
\lambda^{\mathrm{E}}_{1,\pm} = -\frac{m_j a}{M\lambda^{\mathrm{E}}_{0,\pm}}\,, \tag{2.28}
$$

$$
\lambda^{\mathrm{E}}_{2,\pm} = -\frac{\lambda^{\mathrm{E}}_{0,\pm}}{2\hat{n}^2(2\lambda^{\mathrm{E}}_{0,\pm}-1)} + \frac{a^2(\lambda^{\mathrm{E}}_{0,\pm}+1)[(\lambda^{\mathrm{E}}_{0,\pm})^2 - m_j^2]}{M^2(\lambda^{\mathrm{E}}_{0,\pm})^3[2(\lambda^{\mathrm{E}}_{0,\pm})^2+1]}\,, \tag{2.29}
$$

$$
\lambda^{\mathrm{E}}_{3,\pm} = \frac{m_j a}{M}\left[\frac{1}{\hat{n}^2(2\lambda^{\mathrm{E}}_{0,\pm}-1)} + \frac{a^2(\lambda^{\mathrm{E}}_{0,\pm}+2)[(\lambda^{\mathrm{E}}_{0,\pm})^2 - m_j^2]}{M^2(\lambda^{\mathrm{E}}_{0,\pm})^5(2\lambda^{\mathrm{E}}_{0,\pm}+1)}\right]\,, \tag{2.30}
$$

with $\hat{n} \equiv n+\ell+1$. $\hat{n} \in \mathbb{N}$ is the principal quantum number and $n \in \mathbb{N}_0$ is the node number — see subsubsection 2.3.3.

Equation (2.23) allows us to recover the electric-type states of A^a solely. The magnetic-type states with $j = \ell = |m_j|$, the only ones which are known to be captured by the LFKK ansatz, can be recovered considering the limits

$$
\lambda^{\mathrm{M}}_0 \equiv \lim_{\alpha\to 0}\lambda^{\mathrm{M}} = 0\,, \qquad \chi \equiv \lim_{\alpha\to 0}\frac{a}{M}\frac{\alpha}{\lambda^{\mathrm{M}}} = m_j \pm 1\,, \tag{2.31}
$$

JHEP07(2020)010

where the superscript 'M' labels all quantities related to magnetic-type states with $j = |m_j|$. As first shown in [37], the leading-order form of $\boldsymbol{A}$ is proportional to the vector spherical harmonic $\boldsymbol{Y}^{j}_{j,j}$. Unluckily, no expansion of $\lambda^{\rm M}$ in powers of α is known. However, when considering marginally-bound states ($\omega^2 = \mu^2 = 1$), the angular eigenvalue yields

$$\lim_{\omega^2\to\mu^2} \lambda^{\rm M} = \frac{2a}{m_j + 1 - a\omega + \sqrt{(m_j + 1 - a\omega)^2 + 4a\omega}}\,, \tag{2.32}$$

which vanishes in the Schwarzschild limit ($a \to 0$).

Both the third-order expansion in α for $\lambda^{\rm E}$ in eq. (2.27) and the limiting value of $\lambda^{\rm M}$ (with $j = |m_j|$) in eq. (2.32) suffice to perform the numerical integration of the radial equation with great accuracy when $\alpha \ll 1$ — see subsubsection 2.3.3.

2.3.2 Radial equation

The integration of the radial equation is performed via the expansion

$$\mathbb{R}(r) = \sum_{n=0}^{N} c_n (r - r_{\rm H})^n\,,$$

for the radial function R in eq. (2.18). N is the number of terms of the partial sum and the coefficients $\{c_n\}_{n=0,\ldots,N}$ are functions of[5] $r_{\rm H}$, a, μ, m_j and λ, which, in turn, depends on ℓ and j. Plugging the expansion into eq. (2.18) and equating coefficients order by order, it is possible to write $\{c_n\}_{n=1,\ldots,N}$ in terms of c_0. The latter is usually set to 1. The choice of N should be a trade-off between computational time and accuracy. Once the coefficients $\{c_n\}_{n=0,\ldots,N}$ are defined, one fixes the numerical values of $r_{\rm H}$, μ, ℓ, j and m_j, assigns a guess value to a and computes the corresponding guess value for λ.

The radial equation is then integrated from $r = r_{\rm H}(1 + \delta)$, with $\delta \ll 1$, to $r = r_\infty$, where r_∞ stands for the numerical value of infinity. The solution must satisfy the boundary conditions

$$R(r = r_{\rm H}) = \mathbb{R}(r = r_{\rm H})\,, \qquad R'(r = r_{\rm H}) = \mathbb{R}'(r = r_{\rm H})\,, \tag{2.33}$$

where the prime denotes differentiation with respect to r.

The previous step is repeated for different guess values of a, until the solution satisfies the boundary conditions

$$R(r = r_\infty) \to 0\,, \qquad R'(r = r_\infty) \to 0\,. \tag{2.34}$$

2.3.3 Results

When scanning the parameter space in search of stationary vector clouds with fixed quantum numbers (ℓ, j, m_j), solutions with different numbers of nodes n ($n \in \mathbb{N}_0$) are found. Thus, each vector state may be labelled using the notation $|n, \ell, j, m_j\rangle$. Configurations with $n = 0$ ($n \in \mathbb{N}$) are dubbed fundamental (excited) states. The greater the node number n, the more energetic the state. It is worth stressing out that, although the notation is

[5] In general, the coefficients $\{c_n\}_{n=0,\ldots,N}$ also depend on ω. However, here ω is fully defined via eq. (1.3).

JHEP07(2020)010

similar to the one introduced in ref. [37], these synchronised states were not explored there. The notation $|n,\ell,j,m_j\rangle$ refers here to bound states whose frequencies are real and defined by eq. (1.3), and not to quasi-bound states, whose spectra was derived in ref. [37] and is given by

$$\omega^{(\mathrm{V})}_{|n,\ell,j,m_j\rangle} = 1 - \frac{\alpha^2}{2\hat{n}^2} - \frac{\alpha^4}{8\hat{n}^4} + \frac{f_{\mathrm{V}}(n,\ell,j)}{\hat{n}^3}\alpha^4 + \frac{h_{\mathrm{V}}(\ell,j)}{\hat{n}^3}\frac{m_j a}{M}\alpha^5 + \dots\,, \tag{2.35}$$

with $j = \ell \pm 1, \ell$ and where[6]

$$f_{\mathrm{V}}(n,\ell,j) = -\frac{4(6\ell j + 3\ell + 3j + 2)}{(\ell+j)(\ell+j+1)(\ell+j+2)} + \frac{2}{\hat{n}}\,,$$
$$h_{\mathrm{V}}(\ell,j) = \frac{16}{(\ell+j)(\ell+j+1)(\ell+j+2)}\,.$$

The frequencies and corresponding instability rates were computed analytically in [37] via matched asymptotic expansions, except for the magnetic-type ($j = \ell$) vector states. The expression in eq. (2.35) for $j = \ell$ is a conjecture. Nonetheless, the authors of [37] confirmed that the conjectured frequencies do agree with those found numerically without relying on separability of the Proca equation. In fact, the analytic approximation is accurate when $\alpha \lesssim 0.2$, even for near-extremal Kerr BHs.

Vector instability rates are proportional to the factor $(\omega - m_j\Omega_{\mathrm{H}})$ and thus vanish whenever the synchronization condition holds. In that case, the contour lines for which

$$\omega^{(\mathrm{V})}_{|n,\ell,j,m_j\rangle} = m_j\Omega_{\mathrm{H}} \tag{2.36}$$

constitute an analytical approximation to the *existence lines* of stationary vector clouds in the parameter space of Kerr BHs. For future reference, theses curves will be referred to as *analytical existence lines* (AEL), whereas those obtained via the numerical algorithm laid out in subsubsection 2.3.2 will be named *numerical existence lines* (NEL). Additionally, all existence lines will be presented in a (M,Ω_{H})-plane normalized to the boson's mass μ, in which the domain of existence of Kerr BHs is shaded light green.

The mass spectrum of Kerr BHs which support stationary vector clouds may be derived by solving eq. (2.36) for α. This yields

$$\alpha = \hat{n}(2\varpi)^{1/2}\left[1 - \frac{1}{4}g_{\mathrm{V}}\varpi + \frac{7}{32}g_{\mathrm{V}}^2\varpi^2 - \frac{33}{128}g_{\mathrm{V}}^3\varpi^3 + \dots\right]\,, \tag{2.37}$$

where

$$\varpi = 1 - m_j\Omega_{\mathrm{H}}\,, \qquad g_{\mathrm{V}} = 1 - 8\hat{n}f_{\mathrm{V}}\,. \tag{2.38}$$

[6]Note that [37] $\omega^{(\mathrm{V})}_{|n,j,j,m_j\rangle} = \omega^{(\mathrm{S})}_{|n,j,m_j\rangle}$, where $\omega^{(\mathrm{S})}_{|n,j,m_j\rangle}$ denotes the frequency of a massive scalar quasi-bound state with quantum numbers $\{n,j,m_j\}$. This suggests that the magnetic-type vector states are equivalent to the scalar states with the same total angular momentum. If so, it should be possible to show that eq. (2.18) for magnetic-type states and its scalar counterpart are equivalent, at least in some limiting case.

JHEP07(2020)010

The first two terms in eq. (2.37) depend on n, ℓ and m_j, but not on j. The next-to-leading-order term, which depends on j through $g_{\rm V}$, must be taken into account to capture the leading-order behavior of stationary vector clouds.

The existence lines for the vector states $|0,\ell,1,1\rangle$ with[7] $\ell \in \{0,1,2\}$ are shown in figure 1 (top panel). When $m_j = 1$, the line corresponding to the lowest values of $\Omega_{\rm H}$ belongs to the electric-type state $|0,0,1,1\rangle$, which is therefore the fundamental mode with $m_j = 1$. The analytical existence line for the electric-type state $|0,0,1,1\rangle$ is in agreement with its numerical counterpart when $\alpha \ll 1$. As α increases to values near the extremal case $a = M$ (black solid line), the two lines diverge from each other. This behavior appears to be a generic feature of existence lines corresponding to states for which $j = m_j$ and $\ell < j$ (see figure 1 — bottom panel). The discrepancy, whose source remains unclear, suggests that higher-order corrections to the α-expansion in eq. (2.35) are needed when describing clouds around rapidly-rotating Kerr BHs. On the other hand, the analytical and numerical existence lines for the electric-type state $|0,2,1,1\rangle$, for which $j = m_j$ but $\ell > j$, appear to overlap over the full range of α.

When $\{n, j, m_j\}$ are fixed, the existence lines move towards greater values of $\Omega_{\rm H}$ as the orbital angular momentum ℓ increases. In fact, the larger the value of ℓ, i.e. the greater the energy of the state, the greater must the angular velocity $\Omega_{\rm H}$ be for stationary equilibrium. Moreover, the existence lines converge in the limit of vanishing mass, i.e. $M \to 0$, which reflects the fact that the spacetime becomes insensible to the cloud's features. These trends were also found for stationary scalar clouds around Kerr BHs [21].

The variation of the node number n when $\{\ell, j, m_j\}$ are fixed yields identical behavior. The existence lines for the vector states $|n,0,1,1\rangle$ with $n \in \{0,1,2\}$ are plotted in figure 1 (bottom panel). The node number plays a similar role to that of the principal quantum number in the description of hydrogen's energy levels: the larger the node number n, the more energetic the state. Given two existence lines with the same $\{\ell, j, m_j\}$, the one with the largest node number n lies to the right with respect to other in the $(M, \Omega_{\rm H})$-plane. Additionally, they converge in the limit of vanishing M.

The radial profile of the clouds **I**, **II** and **III** in figure 1 (bottom panel) are displayed in figure 2 (top panel). The function R is finite over the whole r domain outside the event horizon and vanishes (exponentially) as $r \to +\infty$, as required by asymptotic flatness. Besides, the local maximum closest to the event horizon decreases with increasing n.

Finally, figure 2 (bottom panel) shows the dependence of the *radius* of the cloud, hereafter denoted by $r_{\rm C}$, on the rotation parameter a for different vector stationary clouds with $n = 0$. $r_{\rm C}$ is defined as the value of r closest to $r_{\rm H}$ that locally maximizes the function $4\pi|R|^2$. Its value diverges in the Schwarzschild limit ($a \to 0$), in accordance with the fact that Schwarzschild BHs cannot carry stationary vector clouds. Moreover, the minimum of $r_{\rm C}$, which occurs at $a = M$, is finite, which means that Kerr BHs do not support sufficiently tight clouds. Similar observations were already reported for stationary scalar clouds in [21].

[7] The existence of clouds with vanishing orbital angular momentum ($\ell = 0$) is a distinctive feature of stationary vector clouds. This is intimately linked to a non-vanishing intrinsic angular momentum, as stationary scalar clouds with $\ell = 0$ do not exist.

JHEP07(2020)010

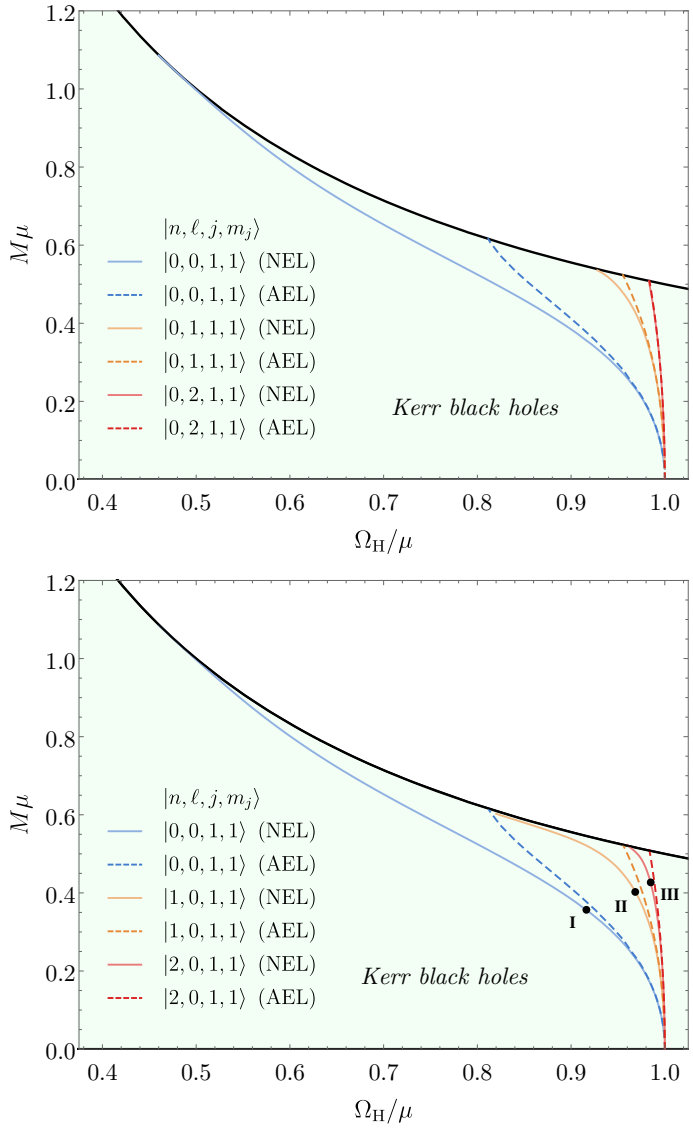

Figure 1. Existence lines for the vector stationary clouds in the $(M, \Omega_{\rm H})$-plane. The black solid line refers to extremal ($a = M$) Kerr BHs. (Top panel) $|0, \ell, 1, 1\rangle$ with $\ell \in \{0, 1, 2\}$. The $\ell = 0$ vector states are the least energetic, as they correspond to lower values of $\Omega_{\rm H}$. The energy increases with ℓ. (Bottom panel) $|n, 0, 1, 1\rangle$ with $n \in \{0, 1, 2\}$. The $n = 0$ vector states are the least energetic, as they correspond to lower values of $\Omega_{\rm H}$. The energy increases with n.

It is worth clarifying the limitations of the linear analysis presented herein: eq. (2.18) was integrated using expansions for λ around $\alpha = 0$. These are good approximations as long as $\alpha \lesssim 0.2$ [37]. The existence lines shown in figure 1 comprises values of $\alpha = M\mu$ ranging between 0 and 1. Although the quantitative results for $\alpha \gtrsim 0.2$ may be less accurate, their qualitative features are rather robust and not compromised by the approximations. Indeed, the numerical existence line for the fundamental $m_j = 1$ state, which spans greater values of α, is consistent with the "bald" boundary of the domain of existence of Kerr BHs with Proca hair to be presented in the following section.

JHEP07(2020)010

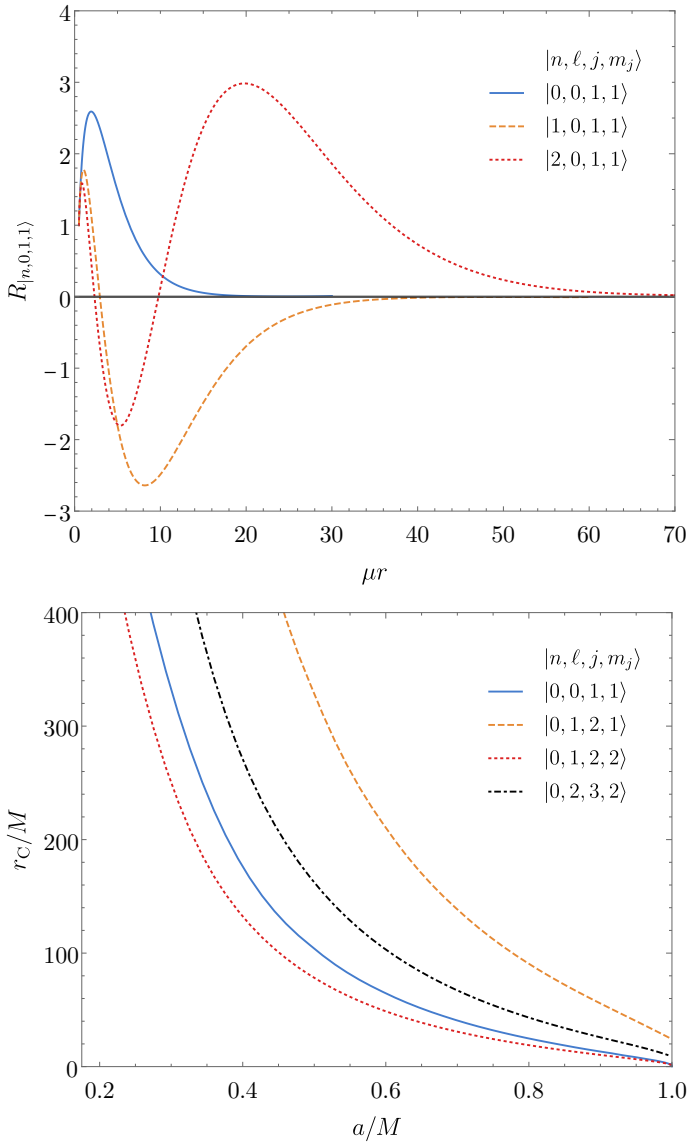

Figure 2. (Top panel) Radial profiles of the bound states **I**, **II** and **III** in figure 1 (bottom panel), characterized by $\mu r_{\rm H} = 0.5$. The radial functions are normalized so that $R(r_{\rm H}) = 1$. The cloud is especially close to the event horizon when $n = 0$. (Bottom panel) *Radius* of different stationary vector clouds with $n = 0$, as a function of a/M.

3 Non-linear analysis: hairy black holes and Proca stars

We now address the fully non-linear solutions of the Einstein-complex-Proca model, described by the action

$$\mathcal{S} = \int \mathrm{d}^4x\sqrt{-g}\left(\frac{R}{16\pi} + \mathcal{L}_{\rm M}\right) , \tag{3.1}$$

where $\mathcal{L}_{\rm M}$ is the Proca Lagrangian density (2.4). Varying this action one obtains the Proca equations (2.5) and the Einstein equations

$$R_{\alpha\beta} - \frac{1}{2}Rg_{\alpha\beta} = 8\pi T_{\alpha\beta} , \tag{3.2}$$

JHEP07(2020)010

where the Proca energy-momentum tensor is:

$$T_{\alpha\beta} = \frac{1}{2}(F_{\alpha\sigma}\bar{F}_{\beta\gamma} + \bar{F}_{\alpha\sigma}F_{\beta\gamma})g^{\sigma\gamma} - \frac{1}{4}g_{\alpha\beta}F_{\sigma\tau}\bar{F}^{\sigma\tau} + \frac{1}{2}\mu^2\left[A_\alpha\bar{A}_\beta + \bar{A}_\alpha A_\beta - g_{\alpha\beta}A_\sigma\bar{A}^\sigma\right] . \tag{3.3}$$

We follow the conventions of [10]. More details on the formalism can be found therein. If one linearises the model (3.1) in the Proca field, one ends up with the vacuum Einstein equations and a test Proca field on a fixed curved background (that solves the vacuum Einstein equations). This corresponds precisely to the analysis of section 2.

3.1 The ansatz

To find the hairy BHs that bifurcate from the linear clouds that were studied in section 2 we use the metric ansatz[8]

$$\boldsymbol{g} = -e^{2F_0}N\mathbf{d}t^2 + e^{2F_1}\left(\frac{\mathbf{d}r^2}{N} + r^2\mathbf{d}\theta^2\right) + e^{2F_2}r^2\sin^2\theta\,(\mathbf{d}\varphi - W\mathbf{d}t)^2 , \tag{3.4}$$

where

$$N \equiv 1 - \frac{r_{\rm H}}{r} , \tag{3.5}$$

and F_i, W are functions of the spheroidal coordinates (r,θ). The parameter $r_{\rm H}$ is the radial coordinate of the event horizon, which is θ-independent.

For the Proca potential, we use an ansatz that depends on four functions (V, H_a). All these functions depend on (r,θ). The ansatz has a harmonic time and azimuthal dependence, which introduces a (positive) frequency, $\omega > 0$, and the azimuthal harmonic index, $m \in \mathbb{Z}$:

$$\boldsymbol{A} = e^{i(m\varphi-\omega t)}\left(iV\mathbf{d}t + H_1\mathbf{d}r + H_2\mathbf{d}\theta + iH_3\sin\theta\mathbf{d}\varphi\right) . \tag{3.6}$$

Here, m should be identified with m_j of section 2 and we shall focus on $m = 1$. We follow closely [10], wherein all details can be found, namely: the explicit equations of motion for this ansatz (in appendix B therein) and the boundary conditions at the horizon, spatial infinity and on the axis (in section 4 therein). Details on the numerical method can be found in section 3.3 of [45]. The key feature for the existence of these BHs is the synchronisation condition (1.3), where $\Omega_{\rm H} = W(r_{\rm H})$, the non-diagonal metric function in eq. (3.4), which on the horizon is independent of θ, and m, ω are the parameters in the Proca ansatz (3.6).

3.2 Domain of existence

When finding solutions via a relaxation method, such as the Newton-Raphson method used for this work, the initial guess plays a key role to guarantee convergence to the desired solutions. In [45], the construction of hairy BHs started from the spinning Proca stars in [16], which have one node for the temporal component of the Proca potential, V. Consequently, the hairy BHs reported in [45] also have one node in V. At that point, it was found no evidence for nodeless solutions of either spinning Proca stars or BHs with

[8]The Kerr metric in this coordinate system, together with the relation between r in eq. (3.4), used in this section, and the radial Boyer-Lindquist coordinate used in section 2, can be found in appendix A of [45].

JHEP07(2020)010

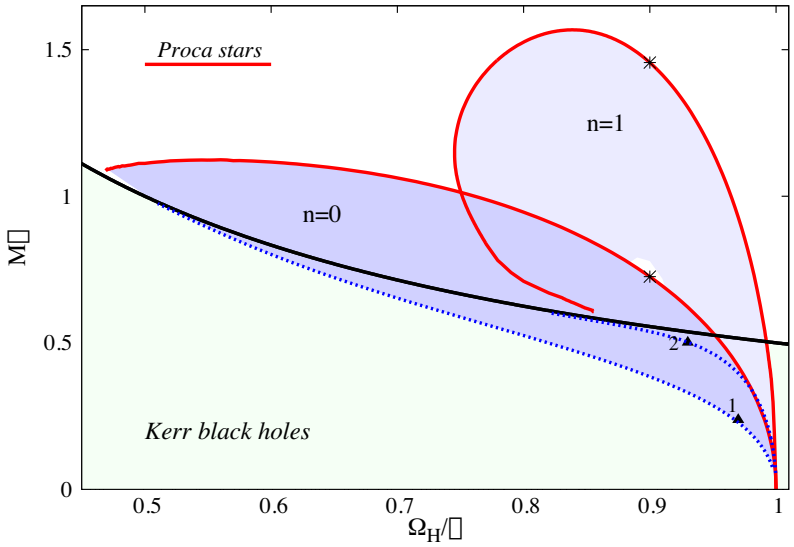

Figure 3. Domain of existence of the $n = 0$ (fundamental state) and $n = 1$ (excited state) BHs with synchronised Proca hair with $m = 1$ in an ADM mass vs. angular velocity diagram, in units of μ. The black solid line corresponds to extremal Kerr BHs; non-extremal Kerr BHs exist below that line, in the light green shaded region. Two Proca star solutions and two hairy BH solutions were highlighted (as stars and triangles), to be analysed in section 3.3.

Proca hair, even though it was stated in [45] that no proof for the inexistence of nodeless solutions could be established (except for spherical Proca stars).

These results were reconsidered after the numerical evolutions of the Kerr superradiant instability have been reported [7]. The data describing the equilibrium points attained in these evolutions matched spinning BHs with Proca hair and a nodeless Proca potential temporal component V, first constructed in [8], wherein their domain of existence was exhibited. This domain of existence is shown in figure 3, together with the domain of existence of the nodeful ($n = 1$) solutions reported in [45]. The hairy BHs exist in the blue shaded regions. In each case ($n = 0$ or $n = 1$) the domain of existence is bounded by the solitonic limit (red solid lines) wherein the hairy BHs become spinning Proca stars with the same n, and by the bald limit (blue dotted lines), wherein they meet the Kerr parameter space at the corresponding existence line, with $m_j = m$, the same n and $(\ell, j) = (0, m_j)$. Thus, the two blue dotted lines plotted in figure 3 correspond to the blue ($n = 0$) and yellow ($n = 1$) numerical existence lines plotted in figure 1 (bottom panel).

The existence line from which the *fundamental* non-linear solutions bifurcate follows a similar rationale to that observed for the scalar case [9]. For a given $m = m_j$, the existence line with $\ell = 0$ and $j = m_j$ is the leftmost one in the Kerr parameter space plotted in figure 1. Thus it represents the threshold between the Kerr BHs that are stable against all modes with that m_j and the ones that are unstable against at least one such mode. Since m_j is the only of the three quantum numbers (ℓ, j, m_j) that remains significant in the non-linear theory — it is associated to an isometry –, for each m_j the existence line whence the hairy BHs bifurcate is the one with $(\ell, j) = (0, m_j)$. BHs emerging from the

JHEP07(2020)010

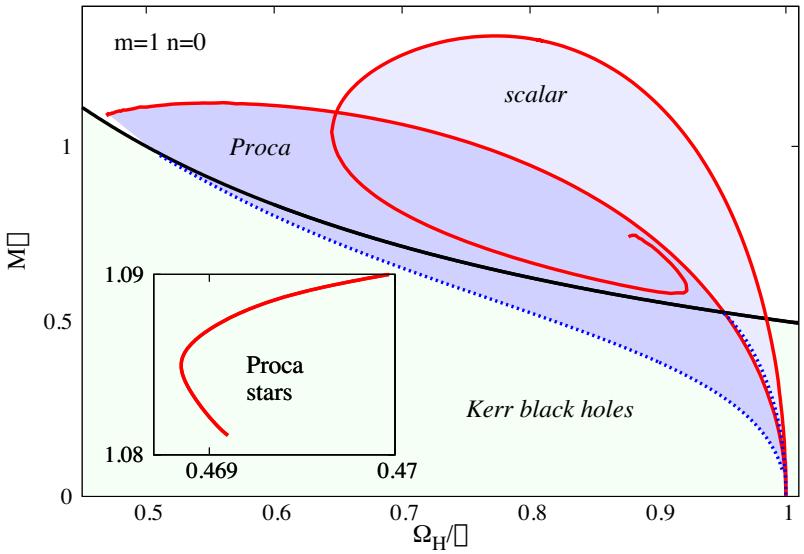

Figure 4. Similar representation of the domain of existence as in figure 3, but now comparing the $(n, m) = (0, 1)$ (fundamental states) Kerr BHs with synchronised scalar and Proca hair. The inset shows a detail of the backbending of the fundamental Proca stars line, as it attains the minimal frequency.

other existence lines with $m = 1$ are likely to exist but are excited states, with either more radial or angular nodes.

Inspection of figure 3 reveals two main features. Firstly, as expected, the excited states ($n = 1$) can attain a larger ADM mass; secondly, the fundamental states of the BHs with Proca hair exist for a larger ω-range; this also seems intuitive: excited states require a larger minimum angular velocity.[9] The same trends are observed when comparing the fundamental states $(n, m) = (0, 1)$ of the scalar and the Proca hairy BHs — figure 4, with the scalar case playing the role of the excited Proca family, in this comparison. This had already been observed for the solitonic limit in [48]. In the bald limit, this means that the fundamental Proca existence line spans lower $\Omega_{\rm H}$ BHs. This is a manifestation of the well-known fact that the superradiant instability is stronger for the vector case [5].

Unlike the scalar or the excited Proca case, in the case of $n = 0$ spinning Proca stars, that compose the (red solid line) boundary of the domain of existence, it was not possible to explore the domain of solutions after the backbending, i.e. when the minimum frequency is attained — see inset in figure 4. The reason is that these solutions become rather compact and hence strong gravity configurations, making their computation numerically challenging. To assess this, we have used the same measure of compactness as, e.g. in [45, 58], namely:

$$\text{Compactness}^{-1} \equiv \frac{R_{99}}{2M_{99}}\,, \tag{3.7}$$

where R_{99} is the perimetral radius that contains 99% of the star's mass, M_{99}. We recall that bosonic stars do not have a surface where a discontinuity of the energy density occurs;

[9] A similar trend can be observed in the scalar case, comparing $n = 0$ with $n = 1$ solutions [46].

JHEP07(2020)010

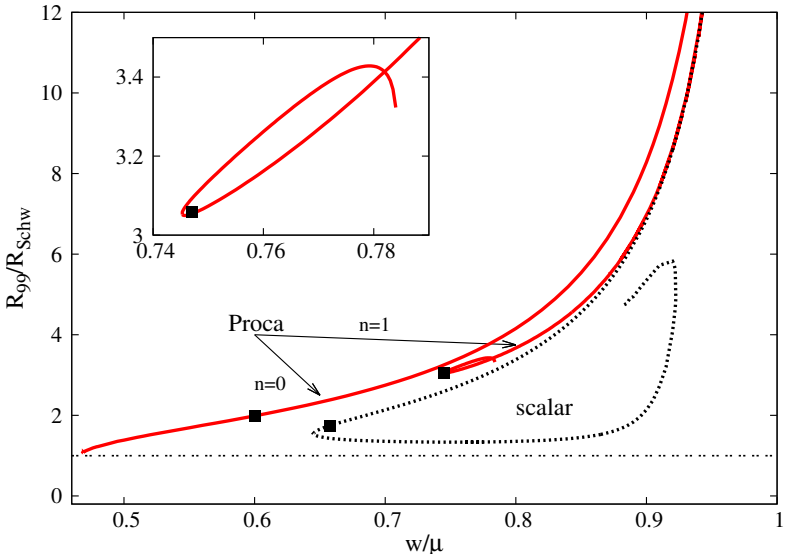

Figure 5. Inverse compactness of the three families of solutions: $n = 0$ and $n = 1$ Proca stars (red solid lines) and $n = 0$ scalar boson stars (black dotted line), all with $m = 1$. The inset exhibits a detail of the $n = 1$ Proca stars line. The squares mark the first occurrence of an ergo-region along the family of bosonic stars.

rather, they decay exponentially, vanishing only at infinity. The perimetral radius is a geometrically meaningful radial coordinate R: a circumference along the equatorial plane has perimeter $2\pi R$. The inverse compactness of the $n = 0, 1$ Proca stars and $n = 0$ scalar boson stars, all with $m = 1$, is shown in figure 5. One observes that the inverse compactness is always greater than unity, meaning that all these stars are less compact than a BH. Moreover, the fundamental Proca stars become the most compact ones, precisely at the backbending, where they attain an inverse compactness $\lesssim 1.1$.

Another token of strong field gravity is the formation of ergo-regions in spinning spacetimes. In the solitonic limit, both the scalar and vector spinning stars do not have ergo-regions when $\omega \to \mu$ (see figures 3 and 4), corresponding to the dilute regime where the stars are not compact and not strongly relativistic. Moving along the spiral and away from this dilute regime, in all cases the ergo-region appears in the first branch, i.e., before the first backbending and for quite compact stars. The first occurrence of an ergo-region along the sequence of bosonic stars is marked with a square in figure 5. The comparison between the three different cases shows that compactness is not the only factor determining the existence of an ergo-region. For all three cases (Proca with $n = 0, 1$ and scalar with $n = 0$) the ergo-region of these stars is toroidal. In the family of the hairy BHs, this toroidal region adds up to the ergo-sphere around the spinning horizon. We have not scanned in detail the parameter space but one will get a rich ergo-region structure, including ergo-Saturns, analogous to those found for BHs with synchronised scalar hair ($n = 0$) [59], Proca hair ($n = 1$) [10] and other cousin models, e.g. [34, 35, 60, 61].

JHEP07(2020)010

3.3 Analysis of specific solutions

In order to get a better intuition on the impact of the node number on the solutions let us consider a comparative study between the profile functions of two spinning Proca stars, one with $n = 0$ and another with $n = 1$, and both with the same frequency $\omega/\mu = 0.9$. These two configurations are highlighted as two stars in figure 3.

In figure 6 we compare the metric functions of the two illustrative Proca stars in terms of a compactified radial coordinate, to have an overview of the whole radial domain, and for three different θ-values. Whereas in the fundamental state all metric functions are rather smooth and monotonic, in the first excited state there is some extra structure, mostly noticeable along the equatorial plane ($\theta = \pi/2$). The metric function W, in particular, is no longer monotonic. The nodeless vs. nodeful structure of the $n = 0$ vs. $n = 1$ spinning Proca stars becomes evident in figure 7. One observes, in particular, that all four Proca potential functions have the same number of nodes, $n = 0$ or $n = 1$, for each star. Moreover, the temporal and radial component of the potential have a trivial structure along the $\theta = 0$ symmetry axis. Finally, the extra structure of the excited states becomes clear when analysing more invariant quantities, such as the Noether charge density, the Ricci curvature scalar and the Komar energy density, that are exhibited in figure 8.

The Noether charge results from the global U(1) symmetry of eq. (3.1), which is invariant under the global transformation $A_\beta \to e^{i\chi}A_\beta$, where χ is a constant. Thus, a conserved 4-current exists

$$J^\alpha = \frac{i}{2}\left[\bar{F}^{\alpha\beta}A_\beta - F^{\alpha\beta}\bar{A}_\beta\right], \qquad \nabla_\alpha J^\alpha = 0\,. \tag{3.8}$$

The Noether charge, Q, which is interpreted as the particle number (indeed becomes the particle number upon quantisation), is obtained integrating the time component of this current on a spacelike hypersurface Σ:

$$Q = \int_\Sigma \mathrm{d}^3x\ J^t\,. \tag{3.9}$$

The Noether charge density is thus J^t, which is plotted in the top panel of figure 8.

The Komar energy density results from the Komar mass computed at infinity. Using Gauss's law, one relates the latter with the horizon Komar mass $M_{\rm H}$ (in the cases which have a horizon) and a volume integral on a spacelike hypersurface between the horizon and infinity. One obtains [45] (where k^α is the asymptotic timelike Killing vector field):

$$M = M_{\rm H} - 2\int_\Sigma \mathrm{d}S_\alpha\left(T^\alpha_\beta k^\beta - \frac{1}{2}Tk^\alpha\right) \equiv M_{\rm H} + M^{(\mathcal{P})}\,, \tag{3.10}$$

where $M^{(\mathcal{P})}$ is the energy contained in the Proca field (outside a horizon, in case there is one):

$$M^{(\mathcal{P})} \equiv -\int_\Sigma \mathrm{d}r\mathrm{d}\theta\mathrm{d}\varphi\sqrt{-g}(2T^t_t - T^\alpha_\alpha)\,. \tag{3.11}$$

The integrand is the Proca energy density, which is plotted in the second from bottom panels of figure 8. A similar analysis can be done for the Komar angular momentum

JHEP07(2020)010

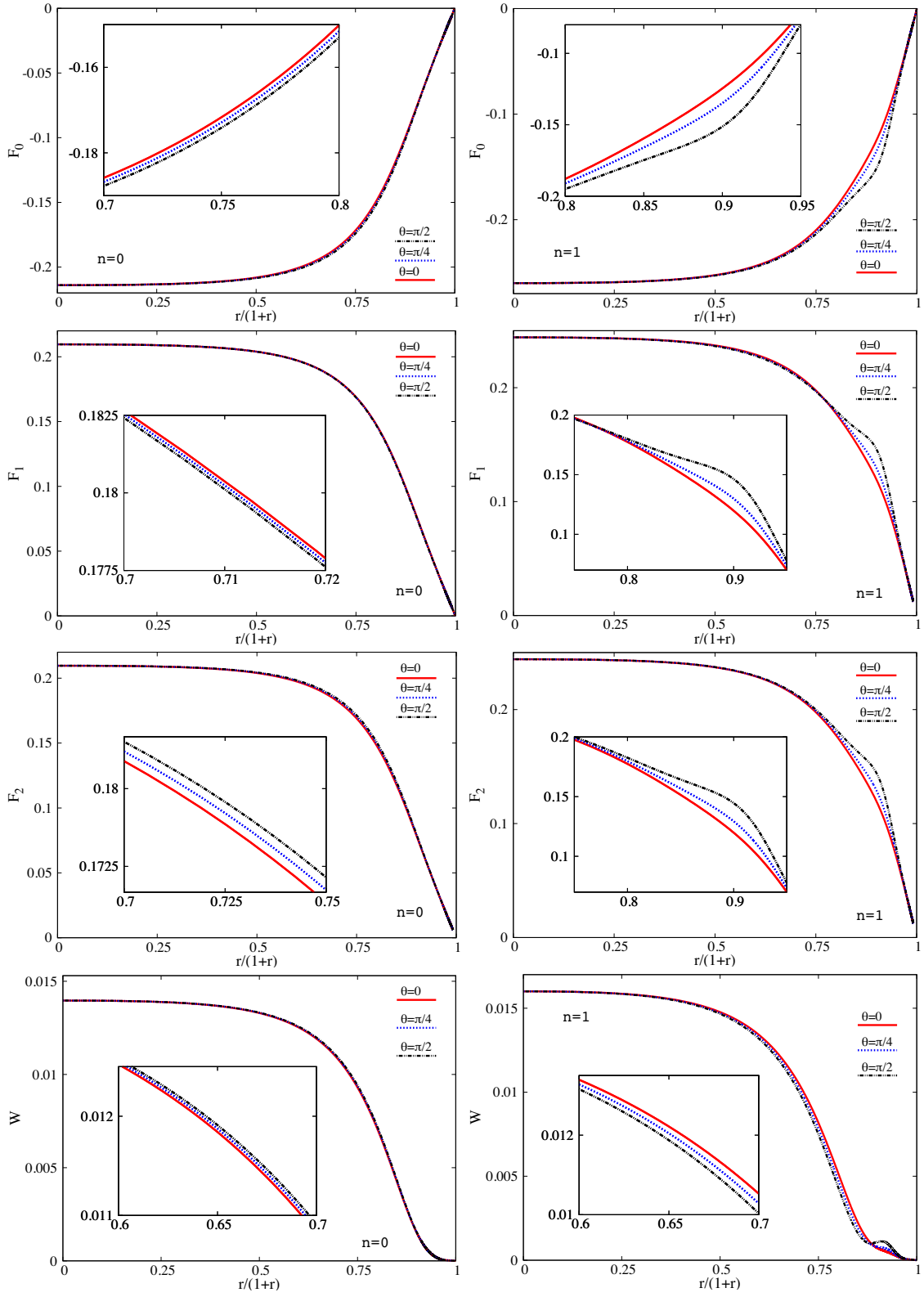

Figure 6. Metric functions of two Proca stars: $n = 0$ (left panels) and $n = 1$ (right panels).

JHEP07(2020)010

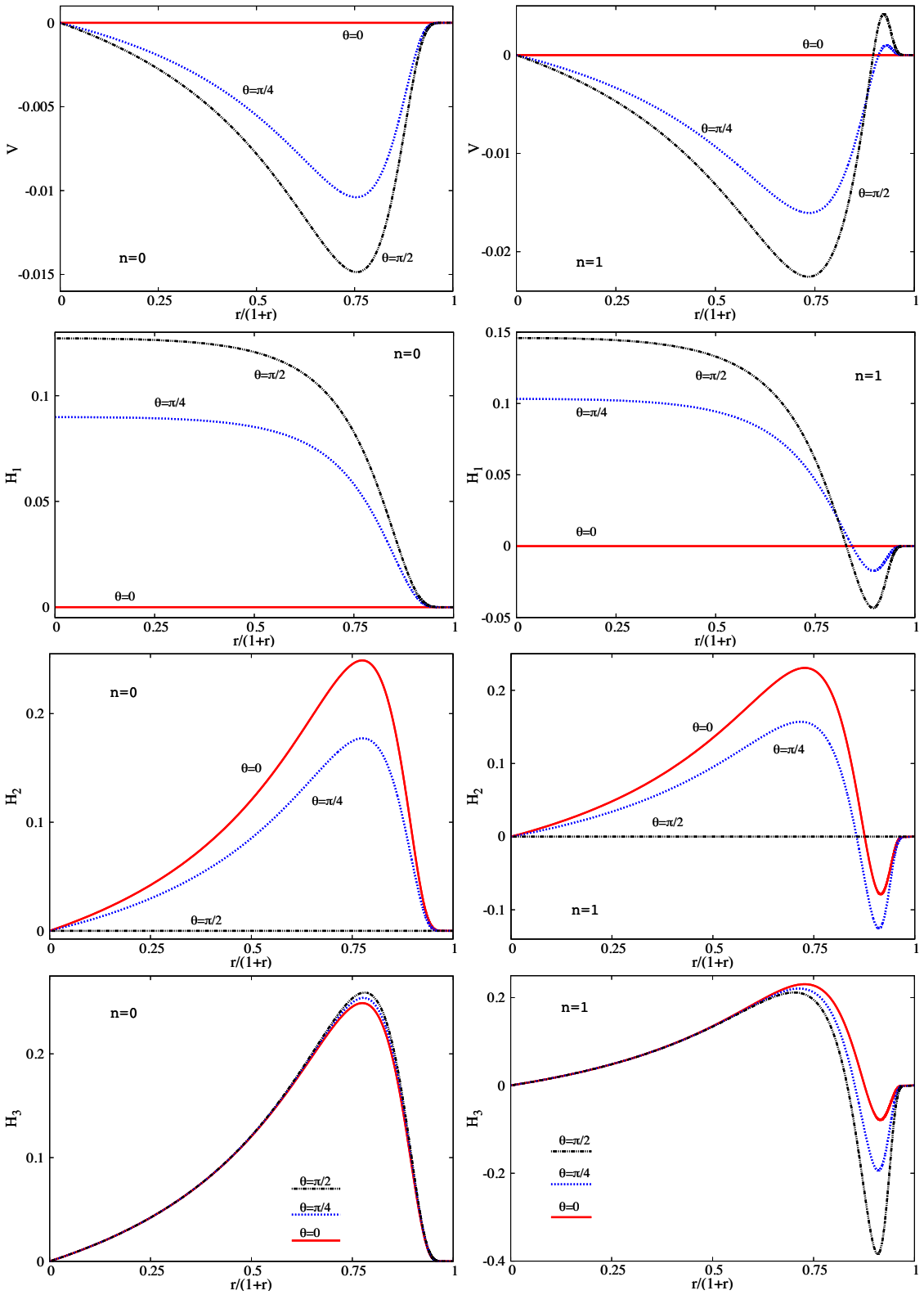

Figure 7. Same as in figure 6, but for the Proca potential functions.

JHEP07(2020)010

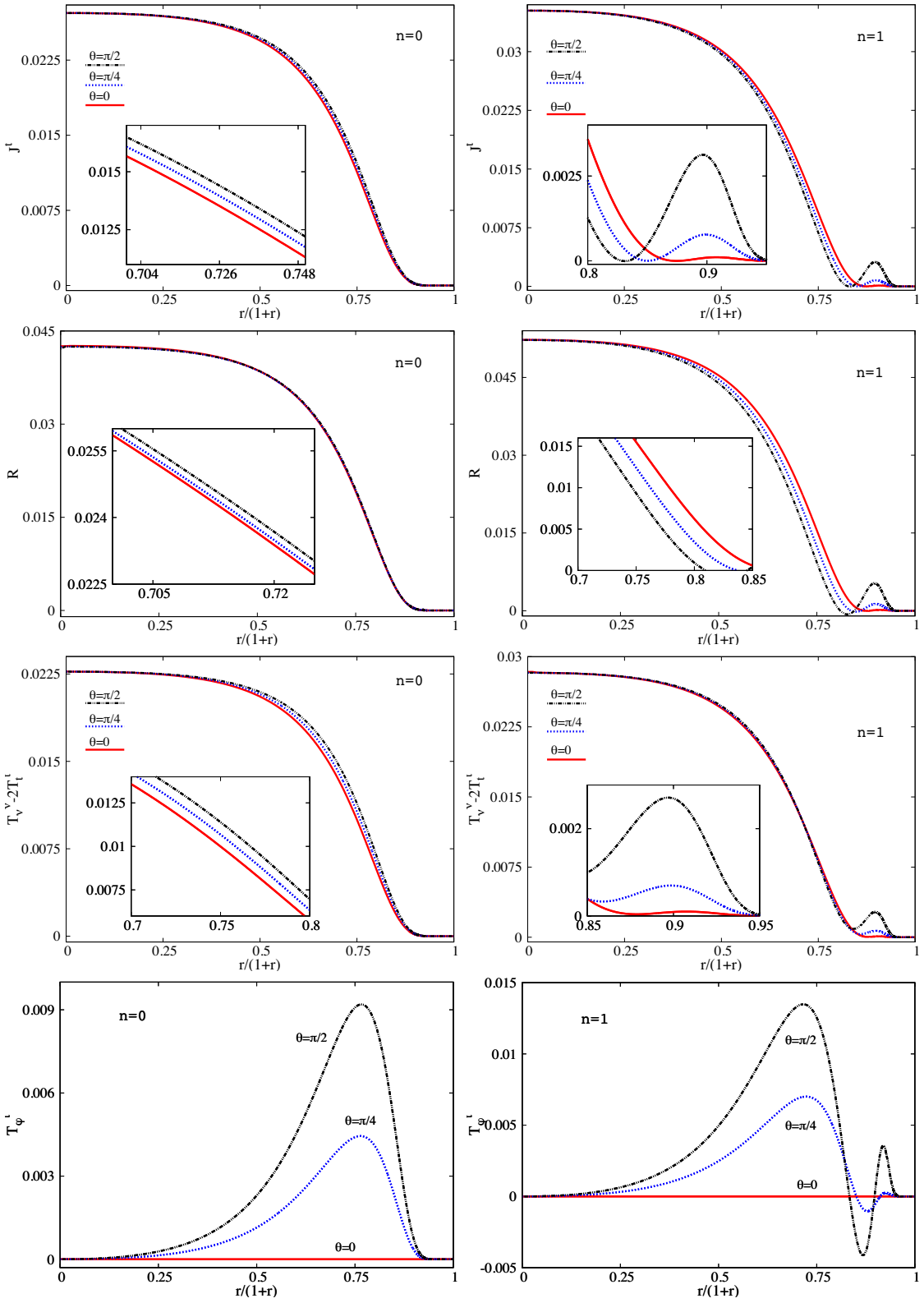

Figure 8. Same as in figures 6 and 7, but for some physical quantities.

JHEP07(2020)010

density, showing that the Komar angular momentum density is T^t_φ [45], plotted in the bottom panels of figure 8.

All invariant quantities in figure 8 demonstrate that whereas the $n = 1$ stars have a Saturn-like morphology — which was observed in [45] –, with the energy density or the particle number having a global maximum at the centre and a local maximum at some radial distance, the fundamental states are spheroidal. This contrasts with the toroidal shape of the fundamental spinning scalar boson stars [14]. This morphological difference was argued to be related to the different dynamical stability of the fundamental states of scalar/vector spinning bosonic stars [17].

We now turn to hairy BHs. The single most important observation concerning hairy BHs in this model is that they can be quite Kerr-like or strongly non-Kerr-like. This follows from the fact that the hairy BHs interpolate between the Kerr family and a solitonic limit (Proca stars) whose properties and phenomenology can be quite different from Kerr. So, here we shall focus on two illustrative solutions that exemplify this range of possibilities.

First, we consider an example of a fairly Kerr-like BH with Proca hair, with $n = 0$. It is chosen in the region where these BHs matched the endpoint of the dynamical evolutions reported in [7] — see [8]. Moreover, within this region, it is chosen to be as hairy as those evolutions suggest a hairy BH can be, when forming dynamically from the superradiant instability of Kerr BHs. This hairy BH, labelled $\mathrm{HBH}_\mathbf{1}$, has[10] [all quantities in eqs. (3.12) and (3.13) are given in units of μ, which was omitted]

$$\left[M, \frac{M_\mathrm{H}}{M};\ J, \frac{J_\mathrm{H}}{J};\ j, j_\mathrm{H};\ \Omega_\mathrm{H}, r_\mathrm{H}\right]_\mathbf{1} = (0.239, 0.905;\ 0.055, 0.607;\ 0.98, 0.726;\ 0.97, 0.3)\,, \tag{3.12}$$

where $j \equiv J/M^2$ and $j_\mathrm{H} \equiv J_\mathrm{H}/M_\mathrm{H}^2$ are the dimensionless spin in terms of global and horizon quantities, respectively. Thus, $\mathrm{HBH}_\mathbf{1}$ has 9.5% of its energy and 39.3% of its spin outside the horizon. These were roughly the maximal values of extraction via superradiance observed in [7]. Also note that both j and j_H are smaller than unity; thus the hairy BH obeys the Kerr bound, both in terms of horizon and asymptotic quantities. It is known that spinning BHs with synchronised hair can violate the Kerr bound — see e.g. [9, 62].

Second, we consider an example of a fairly non-Kerr-like BH with Proca hair, with $n = 0$. This hairy BH, labelled $\mathrm{HBH}_\mathbf{2}$, has

$$\left[M, \frac{M_\mathrm{H}}{M};\ J, \frac{J_\mathrm{H}}{J};\ j, j_\mathrm{H};\ \Omega_\mathrm{H}, r_\mathrm{H}\right]_\mathbf{2} = (0.501, 0.231;\ 0.392, 0.022;\ 1.56, 0.642;\ 0.93, 0.2). \tag{3.13}$$

Thus, $\mathrm{HBH}_\mathbf{2}$ has 76.9% of its energy and 97.8% of its spin outside the horizon. Moreover, this BH violates the Kerr bound in terms of asymptotic quantities, since $j = 1.56 > 1$, but not in terms of horizon quantities. In this sense it behaves more like a star. Both these solutions are marked with triangles, and labelled with the corresponding numbers, in figure 3.

In figure 9 we exhibit the metric functions outside the horizon for the two hairy BHs. In the case of $\mathrm{HBH}_\mathbf{1}$, the insets show a *comparable Kerr BH*, that is with the same total mass

[10] Do not confuse the dimensionless spin j in this section with the total angular momentum j of section 2.

JHEP07(2020)010

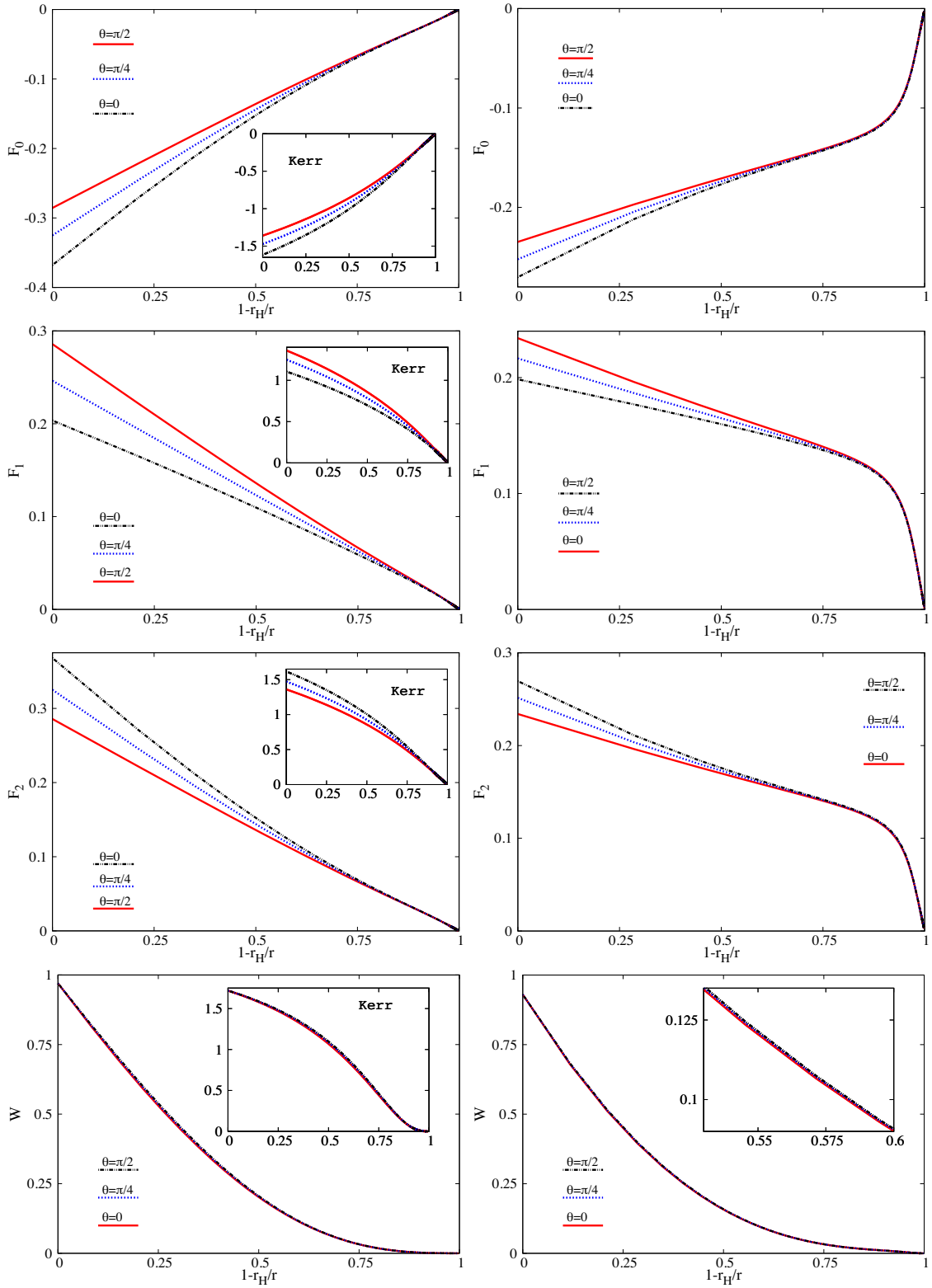

Figure 9. Metric functions of $\mathrm{HBH_1}$ (left panel) and $\mathrm{HBH_2}$ (right panel).

JHEP07(2020)010

M and angular momentum J. In order to make the latter comparison, the Kerr metric is expressed in the gauge (3.4) — see appendix A in [45]. No comparable Kerr BH exists for $\mathrm{HBH}_{\mathbf{2}}$, as the latter violates the Kerr bound. Again we use a compactified radial coordinate. The metric functions of $\mathrm{HBH}_{\mathbf{1}}$ already show some qualitative differences relatively to those of the comparable Kerr BH. The latter has a considerably higher $\Omega_{\mathrm{H}}/\mu \simeq 1.72$; indeed $\mathrm{HBH}_{\mathbf{1}}$ and the comparable Kerr roughly correspond to the two points in figure 5 of [8], representing the longest migration. On the other hand, the metric functions of $\mathrm{HBH}_{\mathbf{2}}$ are a hybrid between the Kerr metric functions and those of a Proca star — see figure 6 (left panels). Indeed, as can be seen from the physical parameters in eq. (3.13), $\mathrm{HBH}_{\mathbf{2}}$ has over three quarters of the total mass and almost the totality of the angular momentum stored in the Proca field outside the horizon. Thus, it is more accurately described as a spinning Proca star with a BH horizon at its centre, than as a BH horizon surrounded by a Proca cloud. The latter is an appropriate description for $\mathrm{HBH}_{\mathbf{1}}$.

In figure 10 the Proca potentials are shown for the two hairy BHs. One can appreciate the difference in boundary conditions as compared to the Proca stars in figure 7. V, H_2, H_3 are non-zero on the BH horizon and zero at the origin, for stars; H_1 is the opposite. On the other hand, the most apparent differences between $\mathrm{HBH}_{\mathbf{1}}$ and $\mathrm{HBH}_{\mathbf{2}}$ are the larger magnitude of the Proca potential functions for the latter, together with a steeper behaviour. This is intuitive from the fact the second BH has a much larger fraction of its energy in the Proca field.

Finally, in figure 11 we represent some physical quantities of the two hairy BH solutions. The Noether charge density is one order of magnitude larger for $\mathrm{HBH}_{\mathbf{2}}$ and with a steeper profile. This impacts on the Ricci scalar curvature, known to manifest the spacetime deformation due to matter, which has a clear lump outside the horizon for the hairiest solution. The Komar energy and angular momentum densities are also larger in magnitude and with sharper profiles, becoming asymptotically more similar to those of the Proca star exhibited in figure 8 (left panels).

4 Conclusion

In this paper we have analysed linear vector clouds of a massive Proca field around a Kerr BH and the BHs with synchronised Proca hair that can be considered as the non-linear realisations of these clouds. Our analysis has been inspired by a series of fairly recent developments that motivates revisiting the Einstein-(complex)-Proca model and its BH and solitonic solutions. Notice, however, that the linear analysis in section 2 does not depend on the fact that the Proca field is complex, unlike the analysis in section 3, where the existence of the stationary solutions describing hairy BHs and Proca stars relies on the field being complex.

Concerning the linear analysis of section 2, the key physical property of these bound-state configurations is the synchronization of their phase angular velocity with the event horizon angular velocity. Furthermore, they resemble the hydrogen's atomic orbitals and can be described in terms of $\{n, \ell, j, m_j\}$. The quantum numbers label the existence lines of stationary vector clouds in the two-dimensional parameter space of Kerr BHs. These

JHEP07(2020)010

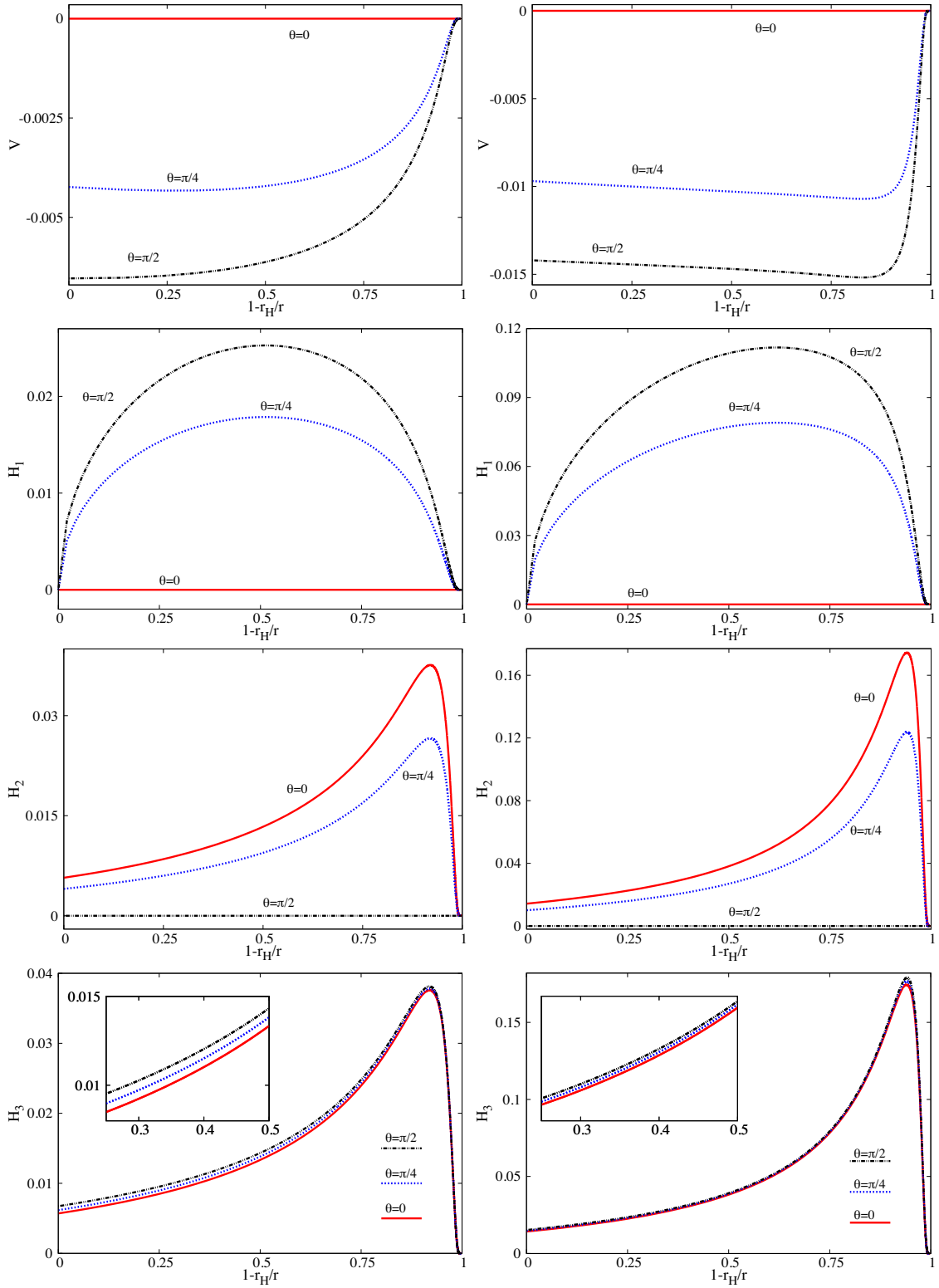

Figure 10. Proca potential functions of $\mathrm{HBH_1}$ (left panel) and $\mathrm{HBH_2}$ (right panel).

JHEP07(2020)010

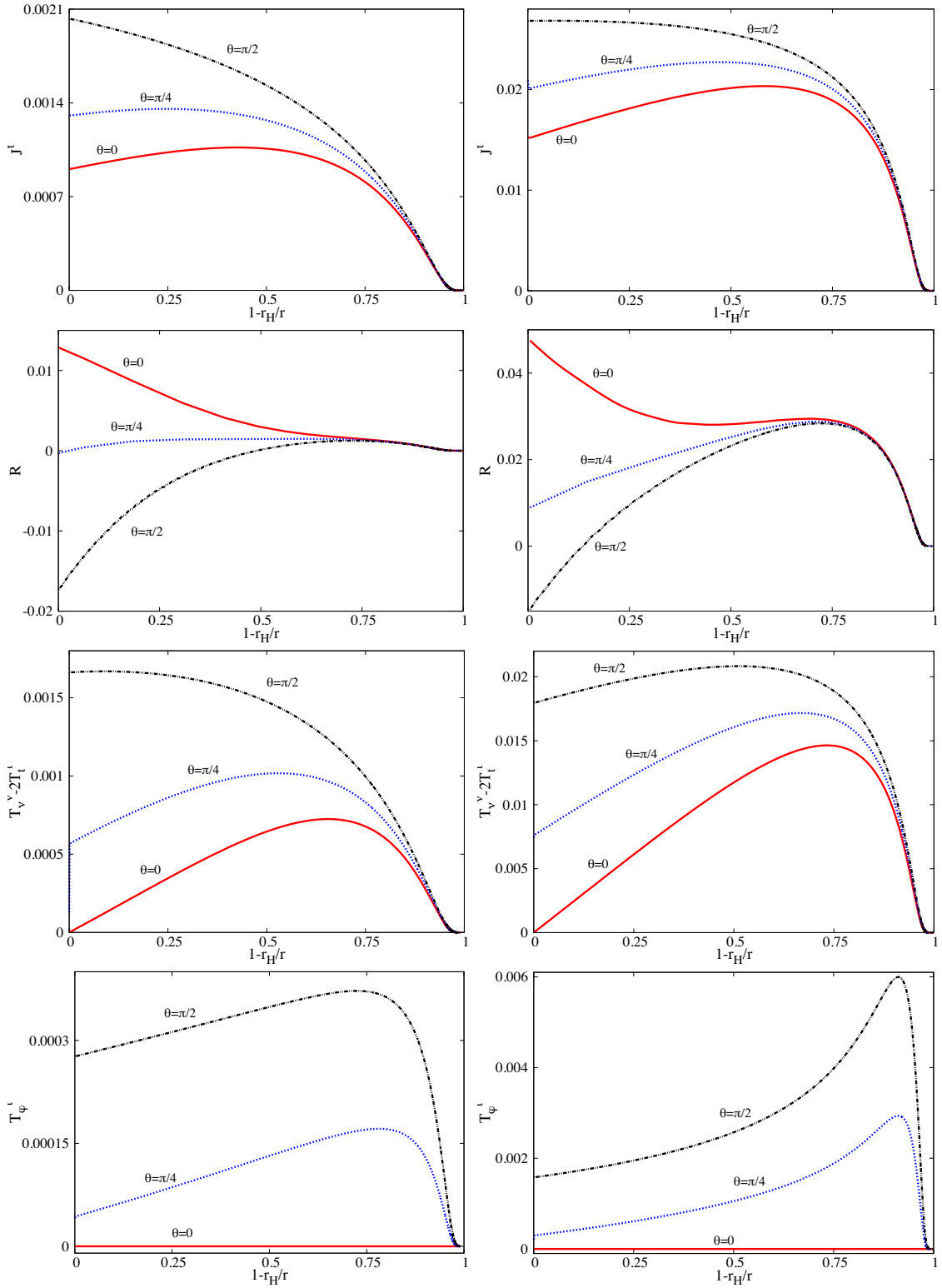

Figure 11. Some physical quantities for $\mathrm{HBH_1}$ (left panel) and $\mathrm{HBH_2}$ (right panel).

JHEP07(2020)010

curves mark the bifurcation of the Kerr family towards the new family of BHs with Proca hair and constitute one of the boundaries of the domain of existence of the latter [10].

As for massive scalar bosons [21], the analysis of the vector clouds shows that, for a fixed value of the azimuthal total angular momentum m_j, the cloud's energy, which is proportional to its phase angular velocity, is mainly determined by the node number n, and the orbital angular momentum ℓ. The bound-state $|0,0,1,1\rangle$ has the lowest possible energy and higher values of n and/or ℓ correspond to higher-energy states. Thus, the existence line of this bound state is wherein the fundamental states of the hairy BHs bifurcate from. Moreover, despite not having a relevant impact on the cloud energy, the total angular momentum j allows for the existence of $\ell = 0$ bound states, which is rooted in the non-vanishing intrinsic angular momentum of the bosons.

The existence lines obtained numerically were compared with analytical approximations recently reported in the literature [37]. In general, the agreement is excellent for all values of the Kerr BH's rotation parameter, except when $j = m_j$ and $\ell < j$. In this case, a discrepancy arises for near-extremal Kerr BHs; the reason behind this observation remains to be clarified.

The analysis' starting point was the LFKK ansatz [42] for the separation of the Proca equation. This ansatz prevents the need for approximations or time-consuming numerical algorithms when studying massive vector bosons in Kerr-NUT-(A)dS spacetimes and has already been used to address quasi-bound states in the Kerr and Kerr-Newman backgrounds [37, 42–44, 63]. This ansatz, however, does decouple and separate the torsion-modified Proca equation (known as Troca equation) in the Chong-Cvetič-Lü-Pope spacetime of $D = 5$ minimal gauged supergravity [44] and in the Kerr-Sen spacetime of low-energy heterotic string theory [44]. Note that all these works focused on the dynamics of massive vector bosons in the frequency domain, in which the particles are described as monochromatic waves. Future research should then dive into a yet-to-be-explored time-domain analysis of these simplified equations of motion. Of particular interest would be to perform long-time evolutions of massive vector Gaussian wave packets in superradiance-prone spacetimes.

Concerning the non-linear analysis in section 3, here we have exhibited the domain of existence of the fundamental states of BHs with synchronised Proca hair and compared some of their properties with the first excited states, discussed in [10], and the cousin hairy BHs obtained in the scalar case [9, 45]. Then, we have analysed some illustrative solutions of both the solitonic limit (Proca stars) and hairy BHs. We emphasise that all the solutions considered here have azimuthal harmonic index m ($\equiv m_j$) $= 1$. Higher m solutions also exist, corresponding to another sort of excitation.[11] There are two main ideas to retain from our results.

Firstly, there are morphological differences between the cases compared herein, which may have various implications. This is summarised in figure 12, where surfaces of constant

[11] Higher m increases the number of nodes in the azimuthal direction. An in-depth study of the higher m solutions in the scalar case is found in [34]. Some particular higher m solutions in the Proca case can be found in [17]. We remark that $n = 0$ spinning Proca stars with $m > 1$ possess surfaces of constant energy density with a toroidal morphology.

JHEP07(2020)010

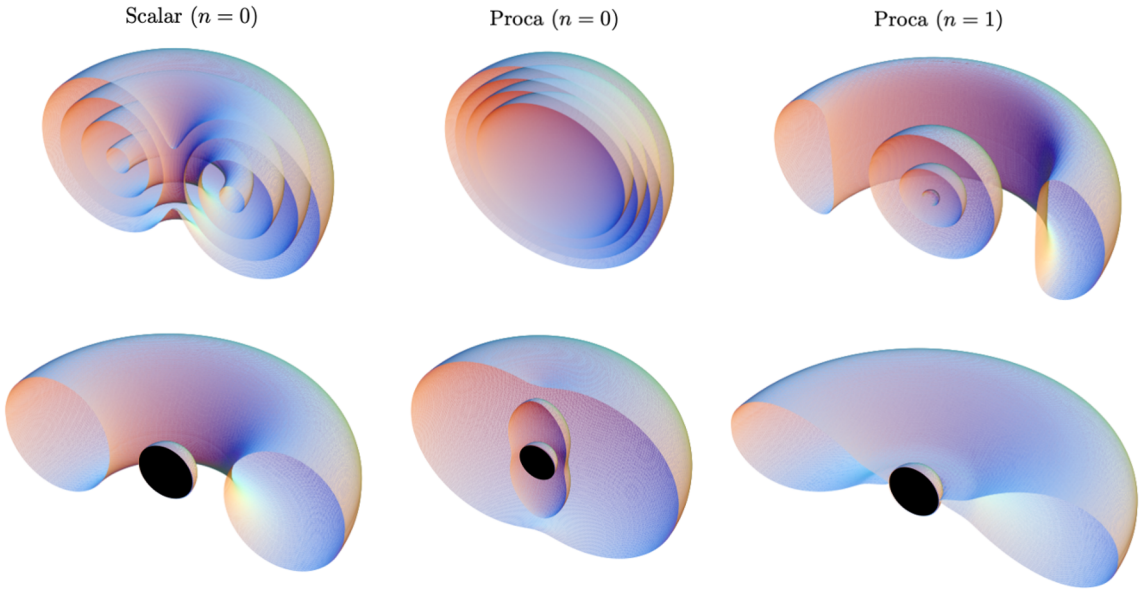

Figure 12. Morphology of the surfaces of constant energy density of scalar ($n = 0$) and vector/Proca ($n = 0$ and $n = 1$) spinning bosonic stars (top panels) and BHs with synchronised hair of the corresponding type (bottom panels). For the BHs, the black disk represents the horizon. All these solutions have $m = 1$. The hairy BHs bifurcate from clouds with $\ell = 0$. Besides further radial excitations (with higher n), these families of solutions possess azimuthal excitations (with higher m) and also further polar-angular excitations (corresponding, in the linear limit, to higher ℓ).

scalar or Proca density for stars and hairy BHs are exhibited for the three families of solutions we have compared. Spinning scalar bosonic stars ($n = 0$) are toroidal; spinning vector stars with $n = 0$ are spheroidal and with $n = 1$ have a Saturn-like morphology. The corresponding hairy BHs are a non-linear bound state of such a star with a horizon, deforming the star's morphology.

Secondly, in all these families of hairy BHs, in particular in the $n = 0$ BHs with Proca hair, there are Kerr-like solutions, but also rather non-Kerr-like examples. At the moment, at least one formation channel for the hairy Kerr-like solutions is known — superradiance; $\mathrm{HBH}_\mathbf{1}$ discussed in section 3.3 belongs to this set. The solution shows already some interesting deviations from Kerr and it will be very interesting to analyse how these deviations impact on astrophysical observables. In this respect, one could reconsider some of the analysis done for the scalar case or for the excited BHs with Proca hair, namely of shadows [64, 65], X-ray spectroscopy [66, 67] or quasi-periodic oscillations [68]. Of course, one of the most interesting open questions concerns the dynamical properties of these BHs, including quasi-normal modes. The recently established dynamical robustness of spinning Proca stars [17] has paved the way to perform dynamical evolutions of these BHs, from which one could, in particular, extract waveforms for binary evolutions. Work in this direction is underway.

JHEP07(2020)010

Acknowledgments

We would like to thank N. Sanchis-Gual for reading a draft of this paper. The authors thank Conselho Nacional de Desenvolvimento Científico e Tecnológico (CNPq) and Coordenação de Aperfeiçoamento de Pessoal de Nível Superior (Capes) — Finance Code 001, in Brazil, for partial financial support. This work is supported by the Center for Astrophysics and Gravitation (CENTRA) and by the Center for Research and Development in Mathematics and Applications (CIDMA) through the Portuguese Foundation for Science and Technology (FCT — Fundação para a Ciência e a Tecnologia), references UIDB/04106/2020, UIDB/00099/2020 and UIDP/04106/2020. We acknowledge support from the projects PTDC/FIS-OUT/28407/2017 and CERN/FIS-PAR/0027/2019 and from national funds (OE), through FCT, I.P., in the scope of the framework contract foreseen in the numbers 4, 5 and 6 of the article 23, of the Decree-Law 57/2016, of August 29, changed by Law 57/2017, of July 19. This work has further been supported by the European Union's Horizon 2020 research and innovation (RISE) programme H2020-MSCA-RISE-2017 Grant No. FunFiCO-777740. The authors would like to acknowledge networking support by the COST Action CA16104.

A Vector spherical harmonics

The components of the first few ('pure-orbital') vector spherical harmonics $\boldsymbol{Y}^{\ell}_{j,m_j}$ in terms of the spherical unit vectors $\{\hat{\boldsymbol{e}}_{(r)}, \hat{\boldsymbol{e}}_{(\theta)}, \hat{\boldsymbol{e}}_{(\varphi)}\}$ are

$$\boldsymbol{Y}^{0}_{1,1} = -\frac{1}{2\sqrt{2\pi}}\begin{pmatrix}1\\ i\\ 0\end{pmatrix}, \qquad \boldsymbol{Y}^{1}_{1,1} = -\frac{1}{4}\sqrt{\frac{\pi}{3}}\begin{pmatrix}\cos\theta\\ i\cos\theta\\ -e^{i\varphi}\sin\theta\end{pmatrix},$$

$$\boldsymbol{Y}^{1}_{2,1} = -\frac{1}{4}\sqrt{\frac{3}{\pi}}\begin{pmatrix}\cos\theta\\ i\cos\theta\\ e^{i\varphi}\sin\theta\end{pmatrix}, \qquad \boldsymbol{Y}^{1}_{2,2} = \frac{1}{4}\sqrt{\frac{3}{\pi}}e^{i\varphi}\sin\theta\begin{pmatrix}1\\ i\\ 0\end{pmatrix},$$

$$\boldsymbol{Y}^{2}_{1,1} = \frac{1}{8\sqrt{\pi}}\begin{pmatrix}3e^{2i\varphi}\sin^2\theta - 3\cos^2\theta + 1\\ i(-3e^{2i\varphi}\sin^2\theta - 3\cos^2\theta + 1)\\ 6e^{i\varphi}\sin\theta\cos\theta\end{pmatrix}, \quad \boldsymbol{Y}^{2}_{2,1} = -\frac{1}{8}\sqrt{\frac{5}{\pi}}\begin{pmatrix}e^{2i\varphi}\sin^2\theta + 3\cos^2\theta - 1\\ i(-e^{2i\varphi}\sin^2\theta + 3\cos^2\theta - 1)\\ -2e^{i\varphi}\sin\theta\cos\theta\end{pmatrix},$$

$$\boldsymbol{Y}^{2}_{2,2} = \frac{1}{4}\sqrt{\frac{5}{\pi}}e^{i\varphi}\sin\theta\begin{pmatrix}\cos\theta\\ i\cos\theta\\ -e^{i\varphi}\sin\theta\end{pmatrix}, \qquad \boldsymbol{Y}^{2}_{3,1} = \frac{1}{8\sqrt{\pi}}\begin{pmatrix}e^{2i\varphi}\sin^2\theta - 6\cos^2\theta + 2\\ i(-e^{2i\varphi}\sin^2\theta - 6\cos^2\theta + 2)\\ -8e^{i\varphi}\sin\theta\cos\theta\end{pmatrix},$$

$$\boldsymbol{Y}^{2}_{3,2} = -\frac{1}{2}\sqrt{\frac{5}{2\pi}}e^{i\varphi}\sin\theta\begin{pmatrix}\cos\theta\\ i\cos\theta\\ e^{i\varphi}\sin\theta\end{pmatrix}, \qquad \boldsymbol{Y}^{2}_{3,3} = -\frac{1}{8}\sqrt{\frac{15}{\pi}}e^{2i\varphi}\sin^2\theta\begin{pmatrix}1\\ i\\ 0\end{pmatrix}.$$

Their real part are displayed in figure 13.

JHEP07(2020)010

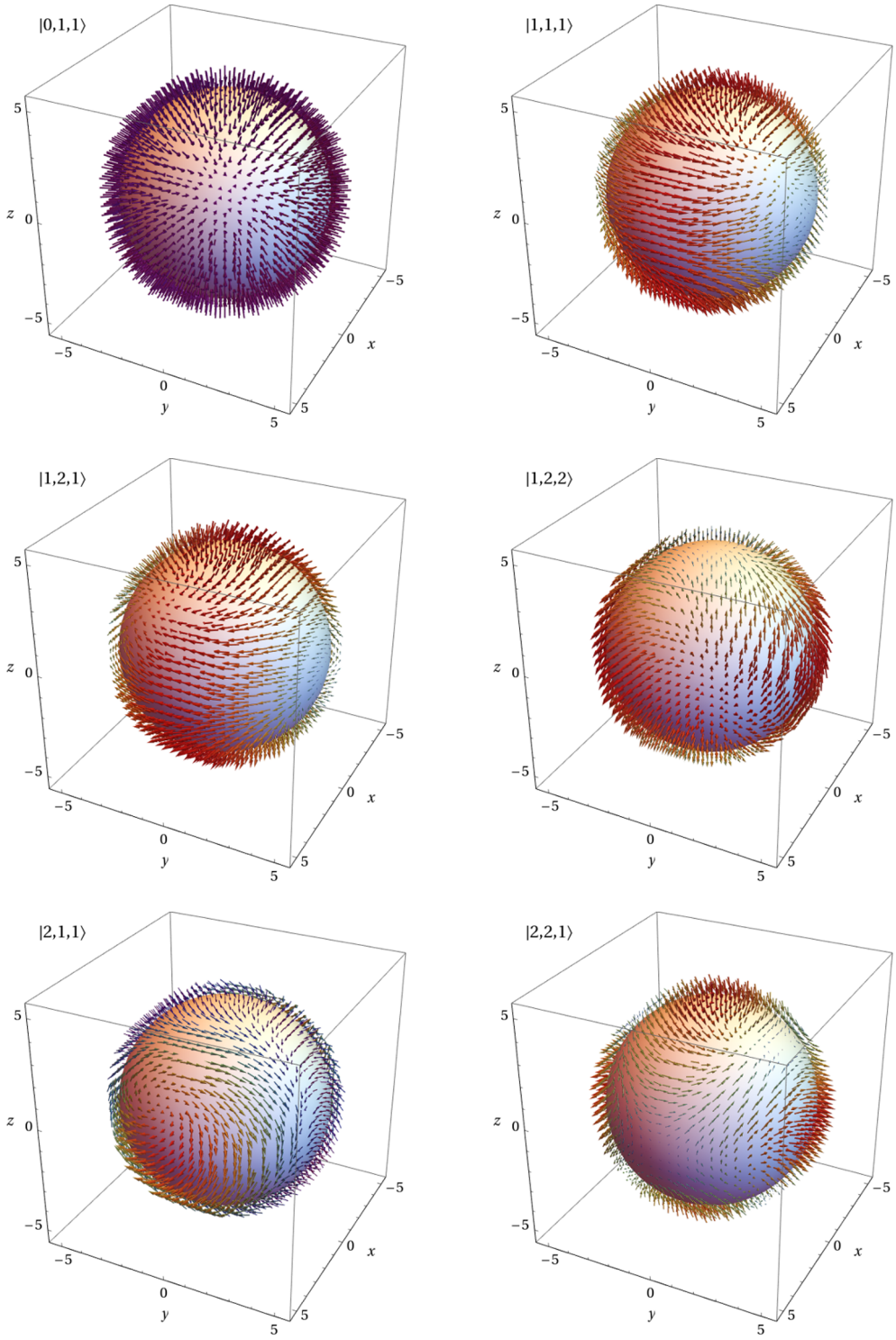

Figure 13. Real part of the first few ('pure-orbital') vector spherical harmonics $\boldsymbol{Y}^{\ell}_{j,m_j}$ in the three-dimensional real coordinate space ($x = r\sin\theta\cos\varphi$, $y = r\sin\theta\sin\varphi$, $z = r\cos\theta$).

JHEP07(2020)010

References

[1] Planck collaboration, *Planck 2018 results. VI. Cosmological parameters*, arXiv:1807.06209 [INSPIRE].

[2] A. Suárez, V.H. Robles and T. Matos, *A Review on the Scalar Field/Bose-Einstein Condensate Dark Matter Model*, *Astrophys. Space Sci. Proc.* **38** (2014) 107 [arXiv:1302.0903] [INSPIRE].

[3] L. Hui, J.P. Ostriker, S. Tremaine and E. Witten, *Ultralight scalars as cosmological dark matter*, *Phys. Rev. D* **95** (2017) 043541 [arXiv:1610.08297] [INSPIRE].

[4] R. Brito, V. Cardoso and P. Pani, *Superradiance*: Energy Extraction, Black-Hole Bombs and Implications for Astrophysics and Particle Physics, vol. 906, Springer (2015), [https://doi.org/10.1007/978-3-319-19000-6] [arXiv:1501.06570] [INSPIRE].

[5] W.H. Press and S.A. Teukolsky, *Floating Orbits, Superradiant Scattering and the Black-hole Bomb*, *Nature* **238** (1972) 211 [INSPIRE].

[6] N. Sanchis-Gual, J.C. Degollado, P.J. Montero, J.A. Font and C. Herdeiro, *Explosion and Final State of an Unstable Reissner-Nordström Black Hole*, *Phys. Rev. Lett.* **116** (2016) 141101 [arXiv:1512.05358] [INSPIRE].

[7] W.E. East and F. Pretorius, *Superradiant Instability and Backreaction of Massive Vector Fields around Kerr Black Holes*, *Phys. Rev. Lett.* **119** (2017) 041101 [arXiv:1704.04791] [INSPIRE].

[8] C.A.R. Herdeiro and E. Radu, *Dynamical Formation of Kerr Black Holes with Synchronized Hair: An Analytic Model*, *Phys. Rev. Lett.* **119** (2017) 261101 [arXiv:1706.06597] [INSPIRE].

[9] C.A.R. Herdeiro and E. Radu, *Kerr black holes with scalar hair*, *Phys. Rev. Lett.* **112** (2014) 221101 [arXiv:1403.2757] [INSPIRE].

[10] C. Herdeiro, E. Radu and H. Rúnarsson, *Kerr black holes with Proca hair*, *Class. Quant. Grav.* **33** (2016) 154001 [arXiv:1603.02687] [INSPIRE].

[11] R. Ruffini and J.A. Wheeler, *Introducing the black hole*, *Phys. Today* **24** (1971) 30 [INSPIRE].

[12] C.A.R. Herdeiro and E. Radu, *Asymptotically flat black holes with scalar hair: a review*, *Int. J. Mod. Phys. D* **24** (2015) 1542014 [arXiv:1504.08209] [INSPIRE].

[13] V. Cardoso and L. Gualtieri, *Testing the black hole 'no-hair' hypothesis*, *Class. Quant. Grav.* **33** (2016) 174001 [arXiv:1607.03133] [INSPIRE].

[14] F.E. Schunck and E.W. Mielke, *Rotating boson star as an effective mass torus in general relativity*, *Phys. Lett. A* **249** (1998) 389 [INSPIRE].

[15] S. Yoshida and Y. Eriguchi, *Rotating boson stars in general relativity*, *Phys. Rev. D* **56** (1997) 762 [INSPIRE].

[16] R. Brito, V. Cardoso, C.A.R. Herdeiro and E. Radu, *Proca stars: Gravitating Bose-Einstein condensates of massive spin 1 particles*, *Phys. Lett. B* **752** (2016) 291 [arXiv:1508.05395] [INSPIRE].

[17] N. Sanchis-Gual et al., *Nonlinear Dynamics of Spinning Bosonic Stars: Formation and Stability*, *Phys. Rev. Lett.* **123** (2019) 221101 [arXiv:1907.12565] [INSPIRE].

[18] S. Hod, *Stationary Scalar Clouds Around Rotating Black Holes*, *Phys. Rev. D* **86** (2012) 104026 [*Erratum ibid.* **86** (2012) 129902] [arXiv:1211.3202] [INSPIRE].

JHEP07(2020)010

[19] S. Hod, *Stationary resonances of rapidly-rotating Kerr black holes*, *Eur. Phys. J. C* **73** (2013) 2378 [arXiv:1311.5298] [INSPIRE].

[20] S. Hod, *Kerr-Newman black holes with stationary charged scalar clouds*, *Phys. Rev. D* **90** (2014) 024051 [arXiv:1406.1179] [INSPIRE].

[21] C.L. Benone, L.C.B. Crispino, C. Herdeiro and E. Radu, *Kerr-Newman scalar clouds*, *Phys. Rev. D* **90** (2014) 104024 [arXiv:1409.1593] [INSPIRE].

[22] S. Hod, *Quasi-Bound States of Massive Scalar Fields in the Kerr Black-Hole Spacetime: Beyond the Hydrogenic Approximation*, *Phys. Lett. B* **749** (2015) 167 [arXiv:1510.05649] [INSPIRE].

[23] H.M. Siahaan, *Instability of charged massive scalar fields in bound states around Kerr-Sen black holes*, *Int. J. Mod. Phys. D* **24** (2015) 1550102 [arXiv:1506.03957] [INSPIRE].

[24] S. Hod, *Spinning Kerr black holes with stationary massive scalar clouds: The large-coupling regime*, *JHEP* **01** (2017) 030 [arXiv:1612.00014] [INSPIRE].

[25] S. Hod, *The large-mass limit of cloudy black holes*, *Class. Quant. Grav.* **32** (2015) 134002 [arXiv:1607.00003] [INSPIRE].

[26] Y. Huang and D.-J. Liu, *Scalar clouds and the superradiant instability regime of Kerr-Newman black hole*, *Phys. Rev. D* **94** (2016) 064030 [arXiv:1606.08913] [INSPIRE].

[27] C. Bernard, *Stationary charged scalar clouds around black holes in string theory*, *Phys. Rev. D* **94** (2016) 085007 [arXiv:1608.05974] [INSPIRE].

[28] I. Sakalli and G. Tokgoz, *Stationary Scalar Clouds Around Maximally Rotating Linear Dilaton Black Holes*, *Class. Quant. Grav.* **34** (2017) 125007 [arXiv:1610.09329] [INSPIRE].

[29] H.R.C. Ferreira and C.A.R. Herdeiro, *Stationary scalar clouds around a BTZ black hole*, *Phys. Lett. B* **773** (2017) 129 [arXiv:1707.08133] [INSPIRE].

[30] M. Richartz, C.A.R. Herdeiro and E. Berti, *Synchronous frequencies of extremal Kerr black holes: resonances, scattering and stability*, *Phys. Rev. D* **96** (2017) 044034 [arXiv:1706.01112] [INSPIRE].

[31] Y. Huang, D.-J. Liu, X.-H. Zhai and X.-Z. Li, *Scalar clouds around Kerr-Sen black holes*, *Class. Quant. Grav.* **34** (2017) 155002 [arXiv:1706.04441] [INSPIRE].

[32] Y. Huang, D.-J. Liu, X.-h. Zhai and X.-z. Li, *Instability for massive scalar fields in Kerr-Newman spacetime*, *Phys. Rev. D* **98** (2018) 025021 [arXiv:1807.06263] [INSPIRE].

[33] G. García and M. Salgado, *Obstructions towards a generalization of no-hair theorems: Scalar clouds around Kerr black holes*, *Phys. Rev. D* **99** (2019) 044036 [arXiv:1812.05809] [INSPIRE].

[34] J.F.M. Delgado, C.A.R. Herdeiro and E. Radu, *Kerr black holes with synchronised scalar hair and higher azimuthal harmonic index*, *Phys. Lett. B* **792** (2019) 436 [arXiv:1903.01488] [INSPIRE].

[35] J. Kunz, I. Perapechka and Y. Shnir, *Kerr black holes with parity-odd scalar hair*, *Phys. Rev. D* **100** (2019) 064032 [arXiv:1904.07630] [INSPIRE].

[36] G. García and M. Salgado, *Existence or absence of superregular boson clouds around extremal Kerr black holes and its connection with number theory*, *Phys. Rev. D* **101** (2020) 044040 [arXiv:1909.12987] [INSPIRE].

JHEP07(2020)010

[37] D. Baumann, H.S. Chia, J. Stout and L. ter Haar, *The Spectra of Gravitational Atoms*, *JCAP* **12** (2019) 006 [arXiv:1908.10370] [INSPIRE].

[38] A. Arvanitaki and S. Dubovsky, *Exploring the String Axiverse with Precision Black Hole Physics*, *Phys. Rev. D* **83** (2011) 044026 [arXiv:1004.3558] [INSPIRE].

[39] C.L. Benone, L.C.B. Crispino, C. Herdeiro and E. Radu, *Acoustic clouds: standing sound waves around a black hole analogue*, *Phys. Rev. D* **91** (2015) 104038 [arXiv:1412.7278] [INSPIRE].

[40] C.L. Benone, C.B. Crispino, Luís, C.A.R. Herdeiro and M. Richartz, *Synchronized stationary clouds in a static fluid*, *Phys. Lett. B* **786** (2018) 442 [arXiv:1809.03952] [INSPIRE].

[41] W.E. East, *Superradiant instability of massive vector fields around spinning black holes in the relativistic regime*, *Phys. Rev. D* **96** (2017) 024004 [arXiv:1705.01544] [INSPIRE].

[42] V.P. Frolov, P. Krtouš, D. Kubizňák and J.E. Santos, *Massive Vector Fields in Rotating Black-Hole Spacetimes: Separability and Quasinormal Modes*, *Phys. Rev. Lett.* **120** (2018) 231103 [arXiv:1804.00030] [INSPIRE].

[43] S.R. Dolan, *Instability of the Proca field on Kerr spacetime*, *Phys. Rev. D* **98** (2018) 104006 [arXiv:1806.01604] [INSPIRE].

[44] R. Cayuso et al., *Massive vector fields in Kerr-Newman and Kerr-Sen black hole spacetimes*, *JHEP* **04** (2020) 159 [arXiv:1912.08224] [INSPIRE].

[45] C. Herdeiro and E. Radu, *Construction and physical properties of Kerr black holes with scalar hair*, *Class. Quant. Grav.* **32** (2015) 144001 [arXiv:1501.04319] [INSPIRE].

[46] Y.-Q. Wang, Y.-X. Liu and S.-W. Wei, *Excited Kerr black holes with scalar hair*, *Phys. Rev. D* **99** (2019) 064036 [arXiv:1811.08795] [INSPIRE].

[47] J. Balakrishna, E. Seidel and W.-M. Suen, *Dynamical evolution of boson stars. 2. Excited states and selfinteracting fields*, *Phys. Rev. D* **58** (1998) 104004 [gr-qc/9712064] [INSPIRE].

[48] C. Herdeiro, I. Perapechka, E. Radu and Y. Shnir, *Asymptotically flat spinning scalar, Dirac and Proca stars*, *Phys. Lett. B* **797** (2019) 134845 [arXiv:1906.05386] [INSPIRE].

[49] D. Griffiths, *Introduction of Quantum Mechanics*, Prentice Hall, Inc., (1995).

[50] K.S. Thorne, *Multipole Expansions of Gravitational Radiation*, *Rev. Mod. Phys.* **52** (1980) 299 [INSPIRE].

[51] M. Maggiore, *Gravitational Waves. Volume 1: Theory and Experiments*, Oxford University Press, Oxford, U.K. (2007).

[52] A. Proca, *Théorie non relativiste des particules à spin entier*, *J. Phys. Radium* **9** (1938) 61.

[53] B. Carter, *Hamilton-Jacobi and Schrödinger separable solutions of Einstein's equations*, *Commun. Math. Phys.* **10** (1968) 280 [INSPIRE].

[54] B. Carter, *Global structure of the Kerr family of gravitational fields*, *Phys. Rev.* **174** (1968) 1559 [INSPIRE].

[55] P. Krtouš, V.P. Frolov and D. Kubizňák, *Separation of Maxwell equations in Kerr-NUT–(A)dS spacetimes*, *Nucl. Phys. B* **934** (2018) 7 [arXiv:1803.02485] [INSPIRE].

[56] O. Lunin, *Maxwell's equations in the Myers-Perry geometry*, *JHEP* **12** (2017) 138 [arXiv:1708.06766] [INSPIRE].

JHEP07(2020)010

[57] V. Frolov, P. Krtouš and D. Kubizňák, *Black holes, hidden symmetries and complete integrability*, *Living Rev. Rel.* **20** (2017) 6 [arXiv:1705.05482] [INSPIRE].

[58] P. Amaro-Seoane, J. Barranco, A. Bernal and L. Rezzolla, *Constraining scalar fields with stellar kinematics and collisional dark matter*, *JCAP* **11** (2010) 002 [arXiv:1009.0019] [INSPIRE].

[59] C. Herdeiro and E. Radu, *Ergosurfaces for Kerr black holes with scalar hair*, *Phys. Rev. D* **89** (2014) 124018 [arXiv:1406.1225] [INSPIRE].

[60] C. Herdeiro, I. Perapechka, E. Radu and Y. Shnir, *Gravitating solitons and black holes with synchronised hair in the four dimensional $O(3)$ σ-model*, *JHEP* **02** (2019) 111 [arXiv:1811.11799] [INSPIRE].

[61] J. Kunz, I. Perapechka and Y. Shnir, *Kerr black holes with synchronised scalar hair and boson stars in the Einstein-Friedberg-Lee-Sirlin model*, *JHEP* **07** (2019) 109 [arXiv:1904.13379] [INSPIRE].

[62] C.A.R. Herdeiro and E. Radu, *How fast can a black hole rotate?*, *Int. J. Mod. Phys. D* **24** (2015) 1544022 [arXiv:1505.04189] [INSPIRE].

[63] N. Siemonsen and W.E. East, *Gravitational wave signatures of ultralight vector bosons from black hole superradiance*, *Phys. Rev. D* **101** (2020) 024019 [arXiv:1910.09476] [INSPIRE].

[64] P.V.P. Cunha, C.A.R. Herdeiro, E. Radu and H.F. Rúnarsson, *Shadows of Kerr black holes with scalar hair*, *Phys. Rev. Lett.* **115** (2015) 211102 [arXiv:1509.00021] [INSPIRE].

[65] P.V.P. Cunha, C.A.R. Herdeiro and E. Radu, *EHT constraint on the ultralight scalar hair of the M87 supermassive black hole*, *Universe* **5** (2019) 220 [arXiv:1909.08039] [INSPIRE].

[66] Y. Ni, M. Zhou, A. Cardenas-Avendano, C. Bambi, C.A.R. Herdeiro and E. Radu, *Iron Kα line of Kerr black holes with scalar hair*, *JCAP* **07** (2016) 049 [arXiv:1606.04654] [INSPIRE].

[67] M. Zhou, C. Bambi, C.A.R. Herdeiro and E. Radu, *Iron Kα line of Kerr black holes with Proca hair*, *Phys. Rev. D* **95** (2017) 104035 [arXiv:1703.06836] [INSPIRE].

[68] N. Franchini et al., *Constraining black holes with light boson hair and boson stars using epicyclic frequencies and quasiperiodic oscillations*, *Phys. Rev. D* **95** (2017) 124025 [arXiv:1612.00038] [INSPIRE].

JHEP07(2020)010

International Journal of Modern Physics D
(2020) 2041013 (17 pages)

DOI: 10.1142/S0218271820410138

Stationary scalar and vector clouds around Kerr–Newman black holes

Nuno M. Santos*,‡ and Carlos A. R. Herdeiro†

*Centro de Astrofísica e Gravitação – CENTRA
Departamento de Física, Instituto Superior Técnico – IST
Universidade de Lisboa – UL, Avenida Rovisco Pais 1, 1049, Lisboa, Portugal
†Centre for Research and Development in Mathematics and Applications (CIDMA)
Departamento de Matemática da Universidade de Aveiro
Campus de Santiago, 3810-183 Aveiro, Portugal
‡nunomoreirasantos@tecnico.ulisboa.pt

Received 27 February 2020
Revised 7 May 2020
Accepted 14 May 2020
Published 13 July 2020

Massive bosons in the vicinity of Kerr–Newman black holes can form pure bound states when their phase angular velocity fulfills the synchronization condition, i.e. at the threshold of superradiance. The presence of these stationary clouds at the linear level is intimately linked to the existence of Kerr black holes with synchronized hair at the nonlinear level. These configurations are very similar to the atomic orbitals of the electron in a hydrogen atom. They can be labeled by four quantum numbers: n, the number of nodes in the radial direction; ℓ, the orbital angular momentum; j, the total angular momentum; and m_j, the azimuthal total angular momentum. These synchronized configurations are solely allowed for particular values of the black hole's mass, angular momentum and electric charge. Such quantization results in an existence surface in the three-dimensional parameter space of Kerr–Newman black holes. The phenomenology of stationary scalar clouds has been widely addressed over the last years. However, there is a gap in the literature concerning their vector cousins. Following the separability of the Proca equation in Kerr(–Newman) spacetime, this paper explores and compares scalar and vector stationary clouds around Kerr and Kerr–Newman black holes, extending previous research.

Keywords: Black holes; massive bosons; superradiance.

1. Introduction

Energy extraction from Kerr black holes was first devised in 1969 by Penrose,[1] who conceived a *gedankenexperiment* whereby a particle disintegrates within the ergoregion of a Kerr black hole into two other particles in such a way that the black hole loses energy. In general, the efficiency of the Penrose process is low: the extracted

energy is at most about a fifth of the infalling energy for particles decaying close to the event horizon of extremal Kerr black holes.[2,3] More importantly, the minimum relative velocity between the two end-products of the decay must be greater than half the speed of light for energy to be extracted. The Penrose process is thus unlikely to occur and be relevant in conceivable astrophysical scenarios.

In 1971, Zel'Dovich showed that low-frequency electromagnetic waves scattered off a rotating conducting cylinder are amplified, later suggesting that, under particular circumstances, this enhancement occurs for any wave impinging on a rotating object.[4,5] Misner conjectured that Kerr black holes would not be an exception.[6] This rather odd proposal opened the door to black hole superradiance,[7] which may be thought as the wave analogue of the Penrose process.

For Kerr black holes, superradiance is triggered when the phase angular velocity ω of a boson state satisfies

$$\frac{\omega}{m_j} < \Omega_{\rm H} \equiv \frac{a}{r_+^2 + a^2}, \tag{1}$$

where m_j is the boson's azimuthal total angular momentum and $\Omega_{\rm H}$ and $r_+ = M + \sqrt{M^2 - a^2}$ are, respectively, the black hole's horizon angular velocity and event horizon (Boyer–Lindquist) radial coordinate, written in terms of the black hole's ADM mass M and total angular momentum $J = Ma$. When the bosons are massive, they remain trapped in the vicinity of the black hole — as if they were enclosed by a reflective cavity. When Eq. (1) is fulfilled, bosons extract energy from the black hole and, as a result, the trapped boson states grow exponentially with time, creating superradiant instabilities.[8] These arise even when the bosons' backreaction on the geometry is negligible — a fairly good approximation for a plethora of astrophysical systems —, which means that superradiance is a linear phenomenon, although it persists at fully nonlinear level.[9]

From a dynamical viewpoint, energy extraction from the black hole stalls as soon as Eq. (1) saturates, i.e.

$$\frac{\omega}{m_j} = \Omega_{\rm H} \ . \tag{2}$$

The endpoint is a classical boson condensate — colloquially referred to as *cloud* or *hair* — which is stationary with respect to the slowed-down black hole.[10–12] These equilibrium configurations are solutions of Einstein's gravity minimally coupled to complex massive bosons, first unveiled for scalar bosons[13] and then extended to vector bosons.[14] Kerr black holes with synchronized hair evade well-known uniqueness theorems[15] — which state that asymptotically-flat stationary black holes in scalar– or vector–(electro–)vacuum general relativity are necessarily Kerr(–Newman) black holes[16–18] — and defy the *no-hair* conjecture — according to which the gravitational collapse in the presence of any type of matter-energy must give birth to a Kerr(–Newman) black hole.[19,20]

These hairy black holes reduce to synchronized bound states between Kerr black holes and (scalar or vector) bosons at the linear level. These states exist at the

threshold of superradiance and are commonly known as stationary clouds. They are very similar to the atomic orbitals of the electron in a hydrogen atom in the sense that they are regular on and outside the event horizon, decay exponentially at spatial infinity and can be labeled by four quantum numbers: n, the number of nodes in the radial direction; ℓ, the orbital angular momentum; j, the total angular momentum; and m_j, the projection of the total angular momentum along the black hole's axis of symmetry.

These synchronized bound states were first found for massive scalar bosons around extremal ($a = M$) Kerr black holes[21] and later around rapidly-rotating black holes.[22] While the phenomenology of stationary scalar clouds has been widely addressed in the literature over the last years,[23–40] little is known about the physical properties of their vector cousins.[25] This discrepancy makes sense under the view that, as opposed to the Klein–Gordon equation,[41,42] the decoupling and separation of the Proca equation in Kerr spacetime was solely achieved very recently via the Lunin–Frolov–Krtouš–Kubizňák (LFKK) ansatz.[43] Following this breakthrough, which extends to the Kerr–NUT–(A)dS family of spacetimes, the properties of massive vector bosons started to be further explored in a number of spacetimes,[44–49] most notably the Kerr spacetime.

The main goal of this paper is to apply the LFKK ansatz to characterize and compare stationary scalar and vector clouds around Kerr(–Newman) black holes, complementing some results presented in Refs. 24 and 49.

The paper is organized as follows. Section 2 reviews some key features of Kerr–Newman spacetime. Section 3 introduces the Klein–Gordon and Proca equations and the corresponding ansätze for their separability and presents the separated equations. Section 4 covers a comparative analysis of stationary scalar and vector clouds around Kerr and Kerr–Newman black holes. An overview of this paper is sketched in Sec. 5, together with some closing remarks.

2. Kerr–Newman geometry

The Kerr–Newman solution is the most general black hole solution to the Einstein–Maxwell equations for an asymptotically flat, stationary and axisymmetric spacetime with a connected event horizon. It describes a black hole with mass M, angular momentum J and electric charge Q (as measured from spatial infinity). A Kerr–Newman black hole is said to be sub-extremal if $a^2 + Q^2 < M^2$ and extremal if $a^2 + Q^2 = M^2$, where $a = J/M$ is the specific angular momentum. In Boyer–Lindquist coordinates (t, r, θ, φ), the solution reads

$$\begin{aligned} \boldsymbol{g} &= \Sigma\left(-\frac{\Delta}{\Xi}\mathbf{d}t^2 + \frac{\mathbf{d}r^2}{\Delta} + \mathbf{d}\theta^2\right) + \frac{\Xi}{\Sigma}\sin^2\theta(\mathbf{d}\varphi - \Omega\mathbf{d}t)^2, \\ \boldsymbol{A} &- \frac{Qr}{\Sigma}(\mathbf{d}t - a\sin^2\theta\mathbf{d}\varphi), \end{aligned} \tag{3}$$

where

$$\begin{aligned} \Sigma &= r^2 + a^2\cos^2\theta, & \Delta &= r^2 - 2Mr + a^2 + Q^2, \\ \Xi &= (r^2+a^2)^2 - \Delta a^2 \sin^2\theta, & \Omega &= \frac{(2Mr - Q^2)a}{\Xi} \ . \end{aligned} \tag{4}$$

The line element has a curvature singularity at $\Sigma = 0$ and coordinate singularities at $\Delta = 0$ when $a^2 + Q^2 \leq M^2$, which solves for $r = r_\pm \equiv M \pm \sqrt{M^2 - a^2 - Q^2}$. The hypersurface $r = r_+$ ($r = r_-$) is the outer (inner) horizon.

Being stationary and axisymmetric, the Kerr–Newman spacetime does not depend explicitly on t nor on φ. The two linearly independent Killing vectors associated with these two isometries are $\boldsymbol{\xi} = \boldsymbol{\partial}_t$ and $\boldsymbol{\eta} = \boldsymbol{\partial}_\varphi$, respectively. The Killing vector $\boldsymbol{\xi}$ is null on the hypersurface $r = r_{\rm E} \equiv M + \sqrt{M^2 - Q^2 - a^2\cos^2\theta}$, known as stationary limit surface or ergosphere. This hypersurface is timelike except in the points in which $\boldsymbol{\eta} = 0$, where it coincides with the outer horizon and becomes null. $\boldsymbol{\xi}$ is timelike outside the ergosphere and spacelike in the spacetime region between the outer horizon and the ergosphere ($r_+ < r < r_{\rm E}$). The points where $\boldsymbol{\eta} = 0$ define the axis of symmetry.

The dragging potential Ω is constant on $r = r_+$, where it has the value

$$\Omega_{\rm H} \equiv \frac{a}{r_+^2 + a^2} \ . \tag{5}$$

$\Omega_{\rm H}$ is thus the angular velocity of the outer horizon. The Killing vector $\boldsymbol{\chi} = \boldsymbol{\xi} + \Omega_{\rm H}\boldsymbol{\eta}$ is null on the hypersurface $r = r_+$ and is timelike outside it. Observers moving along curves of constant r and θ with angular velocity $\Omega_{\rm H}$ follow the integral curves of $\boldsymbol{\chi}$ and thus rotate rigidly with the black hole.

The Kerr–Newman solution admits a principal tensor, i.e. a nondegenerate closed conformal Killing–Yano 2–form $\boldsymbol{h}$ which obeys the equations[a]

$$\boldsymbol{\nabla h} = \boldsymbol{g} \wedge \boldsymbol{\xi}, \qquad \boldsymbol{\xi} = \frac{1}{3}\boldsymbol{\nabla} \cdot \boldsymbol{h} \ . \tag{6}$$

This reads

$$\boldsymbol{h} = r(\mathbf{d}t - a\sin^2\theta \mathbf{d}\varphi) \wedge \mathbf{d}r - a\cos\theta \left[a\mathbf{d}r - (r^2+a^2)\mathbf{d}\varphi\right] \wedge \mathbf{d}\cos\theta \ . \tag{7}$$

The Hodge dual of $\boldsymbol{h}$ is a Killing–Yano tensor $\boldsymbol{f} = \star\boldsymbol{h}$, whose square is the Killing tensor

$$\boldsymbol{K} = -\boldsymbol{f}\cdot\boldsymbol{f} = \boldsymbol{h}\cdot\boldsymbol{h} - \frac{1}{2}\boldsymbol{g}h^2, \tag{8}$$

which relates to the Killing vectors by $\boldsymbol{\eta} = \boldsymbol{K}\cdot\boldsymbol{\xi}$.

[a]The dot ($\cdot$) denotes contraction of two subsequent tensors with respect to their two neighbor indices.

3. Equations of motion

The dynamics of massive scalar (Φ) and vector ($\boldsymbol{A}$) bosons in curved spacetimes is ruled by similar equations:

$$(\Box - \mu_{\rm s}^2)\Phi = 0, \tag{9}$$

$$(\Box - \mu_{\rm v}^2)\boldsymbol{A} = 0, \tag{10}$$

where $\Box \equiv \nabla_a \nabla^a$ is the D'Alembert operator and $\mu_s/\mu_{\rm v}$ stands for the mass of the scalar/vector boson. Equation (9) is the Klein–Gordon equation, whereas Eq. (10) is the Proca equation. The Proca equation is nothing but a set of four Klein–Gordon equations, supplemented by the Lorenz condition

$$\boldsymbol{\nabla} \cdot \boldsymbol{A} = 0, \tag{11}$$

which is automatically satisfied, thanks to the nonvanishing mass $\mu_{\rm v}$.

It has long been known that the Klein–Gordon equation in Kerr–Newman spacetime allows a multiplicative separation of variables of the form[50,51]

$$\Phi(t, r, \theta, \phi) = e^{-i\omega t} R_{\rm s}(r) Q_{\rm s}(\theta, \phi), \quad Q_{\rm s}(\theta, \phi) = S_{\rm s}(\theta) e^{+i m_j \phi}, \tag{12}$$

where ω and m_j are the eigenvalues of $i\boldsymbol{\xi}$ and $-i\boldsymbol{\eta}$, respectively. This ansatz reduces Eq. (9) to two linear differential equations in the coordinates r and θ. These equations take the form

$$\frac{\mathrm{d}}{\mathrm{d}r}\left[\Delta \frac{\mathrm{d}R_{\rm s}}{\mathrm{d}r}\right] + \left[\frac{K_r^2}{\Delta} - (\mu_{\rm s}^2 r^2 + a^2\omega^2 - 2m_j a\omega + \lambda_{\rm s})\right] R_{\rm s} = 0, \tag{13}$$

$$\frac{1}{\sin\theta}\frac{\mathrm{d}}{\mathrm{d}\theta}\left[\sin\theta \frac{\mathrm{d}S_{\rm s}}{\mathrm{d}\theta}\right] - \left[\frac{m_j^2}{\sin^2\theta} - \nu^2\cos^2\theta - \lambda_{\rm s}\right] S_{\rm s} = 0, \tag{14}$$

where $K_r = (r^2 + a^2)\omega - a m_j$ and $\nu^2 \equiv a^2(\omega^2 - \mu_{\rm s}^2)$ is the degree of spheroidicity. Equations (13)–(14) are only coupled via the boson mass μ_s, the Killing eigenvalues $\{\omega, m_j\}$, the black hole parameters $\{M, a, Q\}$ and the separation constant $\lambda_{\rm s}$. When $\nu = 0$ (i.e. when the degree of spheroidicity vanishes), Eq. (14) reduces to the associated Legendre equation and the separation constant becomes $\lambda_s = j(j+1)$, $j \in \mathbb{N}_0$. The canonical solutions are the associated Legendre polynomials of degree j and order m_j. The angular dependence of Φ is thus described by the scalar spherical harmonics of degree j and order m_j when either $a = 0$ or $\omega^2 = \mu_{\rm s}^2$. In general, however, it is given by scalar spheroidal harmonics. When $\nu \ll 1$, the separation constant can be written as a series expansion around $\nu = 0$,

$$\lambda_{\rm s} = \sum_{k=0}^{+\infty} f_{\rm s}^{(k)} \nu^{2k}, \text{ with } f_{\rm s}^{(0)} = \ell(\ell+1), \ f_{\rm s}^{(1)} = h(\ell+1) - h(\ell) - 1, \ldots,$$

where $h(\ell) \equiv 2\ell(\ell^2 - m^2)/(4\ell^2 - 1)$. Series expansions for large and real ν and for large and pure imaginary ν are also known.[52] For generic degree of spheroidicity, MATHEMATICA built-in function SPHEROIDALEIGENVALUE, for instance, retrieves high-precision results.

The Proca equation, on the other hand, was believed not to separate in the Kerr–Newman spacetime. Until recently, the Hartle–Thorne formalism for slowly rotating spacetimes[53] was the only available (semi-)analytical technique to study massive vector bosons in Kerr spacetime.[54,55] However, a new ansatz by Lunin for the separability of Maxwell's equations in the Myers–Perry-(A)dS family of spacetimes[56] was further developed by Frolov–Krtouš–Kubizňák,[57,58] who realized that the separability does extend to the Proca equation (and the Lorenz condition) in the Kerr–NUT–(A)dS family.[43] The LFKK ansatz relies on the existence of hidden symmetries and allows Eq. (9) to be separated into ordinary differential equations. This novel approach has already been applied to separate the torsion-modified Proca equation (known as Troca equation) in the Chong–Cvetič–Lü–Pope spacetime of $D = 5$ minimal gauged supergravity[45] and to study the superradiant instability of massive vector bosons in the Kerr–Newman and Kerr–Sen spacetimes.[48]

The LFKK ansatz for $\boldsymbol{A}$ takes the strikingly simple form

$$\boldsymbol{A} = \boldsymbol{P} \cdot \boldsymbol{\nabla} Z, \tag{15}$$

where $\boldsymbol{P}$ is the *polarization tensor* and Z is a complex scalar function. $\boldsymbol{P}$ is covariantly defined in terms of the metric $\boldsymbol{g}$ and the principal tensor $\boldsymbol{h}$ as

$$\boldsymbol{P} \cdot \left(\boldsymbol{g} + \frac{i}{\lambda_{\rm v}} \boldsymbol{h} \right) = \mathbf{1}, \tag{16}$$

where $\lambda_{\rm v}$ is a complex constant and $\mathbf{1}$ is the four-dimensional identity matrix. Given the ansatz in Eq. (15), the Proca equation *and* the Lorenz condition allows a multiplicative separation of variables for Z,

$$Z(t, r, \theta, \phi) = e^{-i\omega t} R_{\rm v}(r) Q_{\rm v}(\theta, \phi), \quad Q_{\rm v}(\theta, \phi) = S_{\rm v}(\theta) e^{+i m_j \phi}, \tag{17}$$

where, as before, ω and m_j are the eigenvalues of $i\boldsymbol{\xi}$ and $-i\boldsymbol{\eta}$, respectively. The separated equations in Kerr–Newman spacetime are[b]

$$q_r \frac{\mathrm{d}}{\mathrm{d}r} \left[\frac{\Delta}{q_r} \frac{\mathrm{d}R_{\rm v}}{\mathrm{d}r} \right] + \left[\frac{K_r^2}{\Delta} + \frac{2\lambda_{\rm v}^2 - q_r}{q_r} \sigma \lambda_{\rm v} - q_r \mu_{\rm v}^2 \right] R_{\rm v} = 0, \tag{18}$$

$$\frac{q_\theta}{\sin\theta} \frac{\mathrm{d}}{\mathrm{d}\theta} \left[\frac{\sin\theta}{q_\theta} \frac{\mathrm{d}S_{\rm v}}{\mathrm{d}\theta} \right] - \left[\frac{K_\theta^2}{\sin^2\theta} + \frac{2\lambda_{\rm v}^2 - q_\theta}{q_\theta} \sigma \lambda_{\rm v} - q_\theta \mu_{\rm v}^2 \right] S_{\rm v} = 0, \tag{19}$$

where

$$\begin{aligned} q_r &= r^2 + \lambda_{\rm v}^2, & q_\theta &= \lambda_{\rm v}^2 - a^2 \cos^2\theta, \\ \sigma &= a(m_j - a\omega)/\lambda_{\rm v}^2 + \omega, & K_\theta &= m_j - a\omega \sin^2\theta \ . \end{aligned} \tag{20}$$

Just like Eqs. (13)–(14), Eqs. (18)–(19) are only coupled via the boson mass $\mu_{\rm v}$, the Killing eigenvalues $\{\omega, m_j\}$, the black hole parameters $\{M, a, Q\}$ and the complex

[b]The explicit form of the polarization tensor $\boldsymbol{P}$ in the Kerr(–Newman) spacetime can be found written in Boyer–Lindquist coordinates in Ref. 49.

constant $\lambda_{\rm v}$. The latter may be loosely interpreted as a separation constant[c]. Equation (18) shares two singular points with Eq. (13), $r = r_{\pm}$, and features additional poles at $r = \pm i\lambda_{\rm v}$. When $a = 0$, Eq. (18) reduces to the associated Legendre equation provided that $\lambda_{\rm v}^{\rm E}(\lambda_{\rm v}^{\rm E}-1) = j(j+1)$, which solves for $\lambda_{{\rm v},-}^{\rm E} = -j$ and $\lambda_{{\rm v},+}^{\rm E} = j+1$, where the superscript "E" refers to the electric-type states. Indeed, an asymptotic analysis of Eq. (18) reveals that the angular dependence of the leading-order form of the spatial part of $\boldsymbol{A}$ is described by the electric-type "pure-orbital" vector spherical harmonics in flat space.[59,60] More concretely, $\lambda_{{\rm v},\mp}^{\rm E}$ correspond to the $j = \ell \pm 1$ electric–type states and can be written as a series expansion around $M\mu_{\rm v} = 0$,[46]

$$\lambda_{{\rm v},\pm}^{\rm E} = \sum_{k=0}^{+\infty} f_{{\rm v},\pm}^{(k)} (M\mu_{\rm v})^k, \tag{21}$$

where

$$f_{{\rm v},+}^{(0)} = j+1,\ f_{{\rm v},-}^{(0)} = -j$$
$$f_{{\rm v},+}^{(1)} = -\frac{m_j a}{j(j+1)M},\ f_{{\rm v},-}^{(1)} = \frac{m_j a}{jM}, \ldots$$

The magnetic-type states with $j = \ell = |m_j|$ can be recovered by taking the limits[44]

$$\lim_{M\mu_{\rm v}\to 0} \lambda_{\rm v}^{\rm M} = 0, \quad \lim_{M\mu_{\rm v}\to 0} \frac{\mu_{\rm v} a}{\lambda_{\rm v}^{\rm M}} = m_j \pm 1, \tag{22}$$

where the superscript "M" refers to states with $j = |m_j|$. Unluckily, no series expansion of $\lambda_{\rm v}^{\rm M}$ around $M\mu_{\rm v} = 0$ is known. In the marginally-bound limit ($\omega^2 = \mu_{\rm v}^2$), however, the separation constant takes the value

$$\lim_{\omega^2\to\mu_{\rm v}^2} \lambda_{\rm v}^{\rm M} = \frac{2a}{m_j + 1 - a\omega + \sqrt{(m_j+1-a\omega)^2 + 4a\omega}}, \tag{23}$$

which vanishes in the Schwarzschild limit.

A potential caveat concerning the use of the LFKK ansatz is the fact that it might not capture all magnetic-type states. To the best of the authors' knowledge, only electric-type states and magnetic-type states with $j = |m_j|$ have so far been reported.[43,44,46]

4. Stationary scalar and vector clouds

Quasi-bound states have frequencies whose real part is smaller than the boson mass μ, $\mathrm{Re}(\omega) < \mu$. Also, they behave as purely ingoing waves in the outer horizon's vicinity and decay exponentially at spatial infinity (as measured by a comoving observer), i.e.

$$R|_{y\to-\infty} \sim e^{-i(\omega - m_j\Omega_{\rm H})y}, \quad R|_{y\to+\infty} \sim y^{-1} e^{-\sqrt{\mu^2-\omega^2}\,y}, \tag{24}$$

[c]In Ref. 43, the authors first perform the separation of the Lorenz condition. This yields the separated equations, but with an additional constant, which is the actual separation constant. When separating the Proca equation, however, the new constant is fixed in terms of the boson mass $\mu_{\rm v}$ and the complex constant $\lambda_{\rm v}$. That is why $\lambda_{\rm v}$ can be referred to as a separation constant.

where the subscripts "s" and "v" were (and will hereafter be) omitted to avoid clutter and y is the tortoise coordinate, defined by

$$y(r) = r + \frac{r_+^2}{r_+ - r_-}\log(r - r_+) - \frac{r_-^2}{r_+ - r_-}\log(r - r_-)\ . \tag{25}$$

These states can be labeled by four "quantum" numbers: $n \in \mathbb{N}_0$, the number of nodes in the radial direction; ℓ, the orbital angular momentum; j, the total angular momentum; and m_j, the projection of the total angular momentum along the black hole's axis of symmetry, which defines the number of nodes in the azimuthal direction. In general, only n and m_j are legitimate "quantum" numbers in the sense that they describe values of conserved quantities. Both orbital and total angular momenta are not conserved in rotating spacetimes. However, it is still convenient to use ℓ and j to label scalar ($j = \ell$) and vector ($j = \ell - 1, \ell, \ell + 1$) states, always bearing in mind that they are only physically meaningful in Minkowski spacetime.

When the (phase angular velocity of the) boson and the (horizon angular velocity of the) black hole synchronize, the oscillatory behavior close to the outer horizon vanishes and the resulting radial profiles become similar to those of the atomic orbitals of the electron in a hydrogen atom. In the following, synchronized scalar and vector states will be labeled with $|n, j, m_j\rangle$ and $|n, \ell, j, m_j\rangle$, respectively.

These synchronized states are only supported by Kerr–Newman black holes in a particular domain of the 3-parameter space described by the dimensionless quantities $\{M\mu, a\mu, Q\mu\}$ or, equivalently,[d] $\{r_+\mu, a\mu, Q\mu\}$ — the latter is the gauge used in this paper. A simple direct-integration shooting method[61] suffices to scan the parameter space in search of synchronized (scalar and vector) states. To impose the desired behavior close to the outer horizon, R is written as a series expansion around $r = r_+$,

$$R|_{r\to r_+} \sim \sum_{k=0}^{+\infty} c_{(k)}(r - r_+)^k, \tag{26}$$

where $c_{(0)} = 1$ and the coefficients $\{c_{(k)}\}_{k>0}$ are obtained by solving either Eq. (13) or (18) order by order. The coefficients depend on the boson mass μ, the Killing eigenvalues $\{\omega, m_j\}$, the black hole parameters $\{r_+, a, Q\}$ and the corresponding separation constant. Fixing $\{\ell, j, m_j\}$ and the black hole parameters $\{r_+\mu, Q\mu\}$, for instance, Eq. (13) or (18) is then integrated from $r = r_+(1 + \delta_+)$, with $\delta_+ \ll 1$, to $r = r_\infty$, where r_∞ stands for the numerical value of the radial coordinate at spatial infinity.

Numerical solutions with the appropriate boundary conditions at spatial infinity are found via the shooting method. They only exist for discrete values of the specific angular momentum a, each corresponding to a different node number n. In other words, bound states between Kerr–Newman black holes and synchronized

[d]Equations (13) and (18) can be written in terms of the black hole parameters $\{r_+, a, Q\}$ using $\Delta(r_+) = 0$.

states are thus restricted to closed surfaces in the 3-parameter space spanned by $\{M\mu, a\mu, Q\mu\}$. Fixing $Q\mu$, for instance, these surfaces reduce to line segments in the 2-parameter space spanned by $\{M\mu, a\mu\}$ or, alternatively, $\{M\mu, \Omega_{\rm H}/\mu\}$. These are commonly known as *existence lines*. This paper's main goal is to determine and compare the existence lines of synchronized scalar and vector states around Kerr and Kerr–Newman black holes. The defining features of these lines will be outlined, without loss of generality, for the Kerr spacetime ($Q\mu = 0$). This is also particularly convenient for the reader to compare the results presented herein with those already reported in the literature.[13,14,24,49] The subtleties introduced by a nonvanishing electric charge will then be briefly addressed.

4.1. *Kerr black holes*

When the black hole's gravitational radius, $R_{\rm G} = M$, is much smaller than the boson's reduced Compton wavelength, $\lambda_{\rm C} = \mu^{-1}$, the frequency spectra of scalar and vector quasi-bound states in Kerr spacetime can be written in the form[46,62,63]

$$\omega^{(\rm s)}_{|n,j,m_j\rangle} = \mu\left(1 - \frac{\alpha^2}{2\mathfrak{n}^2} - \frac{\alpha^4}{8\mathfrak{n}^4} + \frac{g(n,j,j)}{\mathfrak{n}^3}\alpha^4 + \frac{h(j,j)}{\mathfrak{n}^3}\frac{m_j a}{M}\alpha^5 + \cdots\right), \tag{27}$$

$$\omega^{(\rm v)}_{|n,\ell,j,m_j\rangle} = \mu\left(1 - \frac{\alpha^2}{2\mathfrak{n}^2} - \frac{\alpha^4}{8\mathfrak{n}^4} + \frac{g(n,\ell,j)}{\mathfrak{n}^3}\alpha^4 + \frac{h(\ell,j)}{\mathfrak{n}^3}\frac{m_j a}{M}\alpha^5 + \cdots\right), \tag{28}$$

where $\alpha = M\mu \ll 1$ is the so-called gravitational fine-structure constant, $\mathfrak{n} \equiv n + \ell + 1$ ($\mathfrak{n} \in \mathbb{N}$) may be referred to as principal quantum number and

$$g(n,\ell,j) = -\frac{4(6\ell j + 3\ell + 3j + 2)}{(\ell + j)(\ell + j + 1)(\ell + j + 2)} + \frac{2}{n + \ell + 1},$$
$$h(\ell, j) = \frac{16}{(\ell + j)(\ell + j + 1)(\ell + j + 2)}\,.$$

Note that $\omega^{(\rm v)}_{|n,j,j,m_j\rangle} = \omega^{(\rm s)}_{|n,j,m_j\rangle}$, which suggests that the magnetic-type vector states are somehow equivalent to the scalar states with the same total angular momentum. However, it is worth pointing out that, as opposed to the frequencies of the electric-type states, computed analytically via matched asymptotic expansions, Eq. (28) with $j = \ell$ is nothing but a conjecture. Nevertheless, all approximations are fairly accurate when $\alpha \lesssim 0.2$, even for near-extremal Kerr black holes.[63]

The instability rates of the quasi-bound states are proportional to the factor sign w, where $w \equiv (\omega - m_j\Omega_{\rm H})$, i.e. the states: grow exponentially with time when sign $w = -1$, thus being unstable; decay exponentially with time when sign $w = +1$, thus being stable; and are stationary (infinitely long-lived) when $w = 0$. The unstable states are superradiant, while the stable states are nonsuperradiant. The stationary states, which are synchronized with the black hole, exist precisely at the threshold of superradiance. Their existence lines will be presented for fixed values of $Q\mu$ in the $(M\mu, \Omega_{\rm H}/\mu)$-plane, in which the existence domain of Kerr(–Newman) black holes is shaded light gray. Note that the contour lines for which

$$\omega^{(\rm s)}_{|n,j,m_j\rangle} = m_j\Omega_{\rm H}, \tag{29}$$

$$\omega^{(\mathrm{v})}_{|n,\ell,j,m_j\rangle} = m_j \Omega_{\mathrm{H}} \tag{30}$$

constitute an analytical approximation to the existence lines of scalar and vector states, respectively. A comparison between *analytical* and *numerical* existence lines of some vector states can be found in Ref. 49. Overall, the agreement is excellent, except when $j = m_j$ and $\ell < j$.

When $Q\mu = 0$, the existence lines cover the entire range of the specific angular momentum a, with the endings matching the Schwarzschild ($a = 0$) and extremal ($a = M$) limits. The former (latter) coincides with the minimum (maximum) allowed value for the gravitational fine-structure constant $\alpha = M\mu$.

For a given m_j, the fundamental state does not possess any node in the radial direction and always has its total angular momentum completely aligned with the black hole's axis of symmetry ($j = m_j$). $|0, m_j, m_j\rangle$ thus represents fundamental scalar states. The fundamental vector states are those which cumulatively have the smallest possible orbital angular momentum, which corresponds to the electric-type states $|0, m_j - 1, m_j, m_j\rangle$. The existence lines for the fundamental scalar and vector states with $m_j = 1, 2, 3$ are shown in Fig. 1, where the markers pinpoint extreme ($a = M$) scalar states obtained by solving analytically Eq. (13) in terms of confluent hypergeometric functions.[21] These particular existence lines represent the threshold between Kerr black holes which are stable against all states with a given m_j and the ones which are unstable against at least one such state. Fundamental vector states

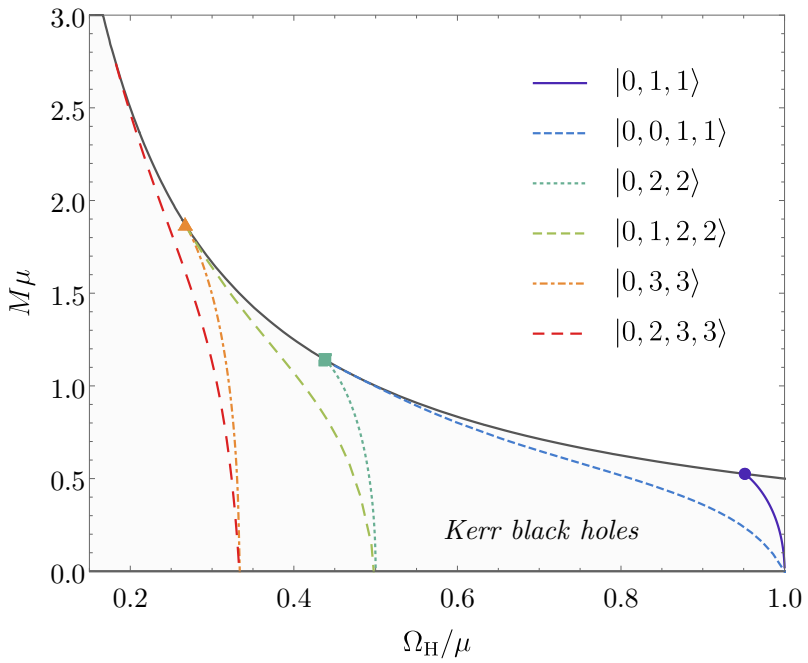

Fig. 1. Existence lines of the first fundamental scalar and vector states with $j = m_j$ in the $(M\mu, \Omega_{\mathrm{H}}/\mu)$-plane. The gray solid line refers to extremal ($a = M$) Kerr black holes. The markers pinpoint extreme ($a = M$) scalar states found analytically.[21] The vector states are less energetic than the corresponding scalar states, as they correspond to lower values of Ω_{H}.

always lie to the left with respect to the scalar state with the same m_j. The $\Omega_{\rm H}$-interval of the vector states are greater than that of the corresponding scalar cousins — e.g. it is approximately 10 times greater for $|0,0,1,1\rangle$ than for $|0,1,1\rangle$. Put it differently, for a given boson mass μ, Kerr black holes with sufficiently small horizon angular velocity may support vector, but not scalar states. These properties are a natural manifestation of the difference in strength of the superradiant instability, which is stronger for massive vector bosons.[8]

Excited states, on the other hand, must lie to the right with respect to the corresponding fundamental states in the $(M\mu, \Omega_{\rm H}/\mu)$-plane. For example, fixing $\{n, j, m_j\}$, existence lines migrate towards greater and greater horizon angular velocities as ℓ increases. This behavior is illustrated in Fig. 2. The impact of the orbital angular momentum on the existence lines is particularly relevant for near-extremal Kerr black holes. In the Schwarzschild limit, the lines converge to $(M, \Omega_{\rm H}) = (0, \mu)$, which amounts to saying that Schwarzschild black holes do not admit synchronized (scalar nor vector) bound states.[13] Figure 2 also shows the energy ordering of vector states with fixed j: the electric-type states $|n, j+1, j, m_j\rangle$ are more energetic than the magnetic-type states $|n, j, j, m_j\rangle$ and the latter more energetic than the electric-type states $|n, j-1, j, m_j\rangle$. This hierarchy matches the one found in the frequency spectrum of vector quasi-bound states.[46]

A similar rationale holds true when fixing $\{\ell, j, m_j\}$ and varying n, as shown in Fig. 3 for the states $|n, 1, 1\rangle$ and $|n, 0, 1, 1\rangle$, $n = 0, 1, 2$. The node number n plays a role somehow akin to that played by the orbital angular momentum ℓ. Large-n

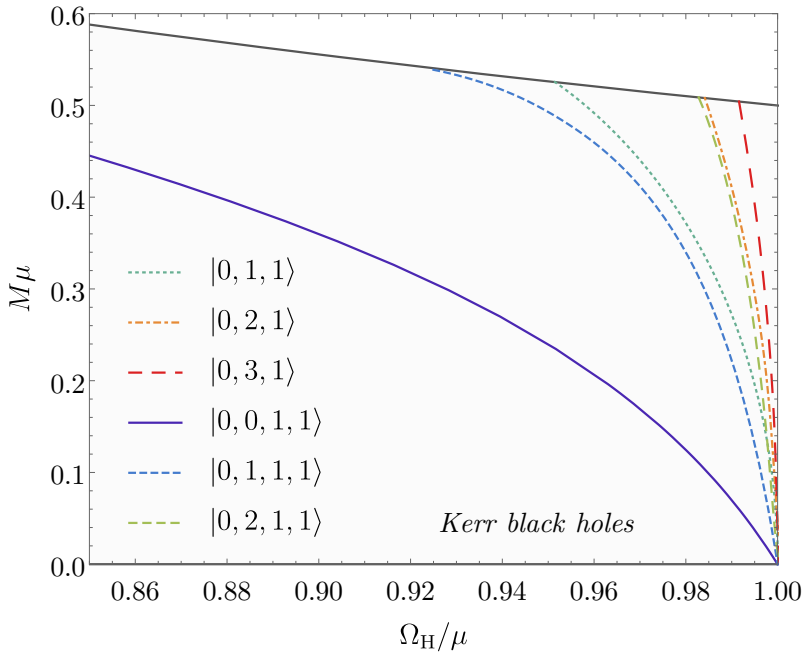

Fig. 2. Existence lines of the scalar states $|0,\ell,1\rangle$, $\ell = 1,2,3$ and vector states $|0,\ell,1,1\rangle$, $\ell = 0,1,2$ in the $(M\mu, \Omega_{\rm H}/\mu)$-plane. The gray solid line refers to extremal ($a = M$) Kerr black holes. The $\ell = 0$ vector states are the least energetic, as they correspond to lower values of $\Omega_{\rm H}$. The energy increases with ℓ.

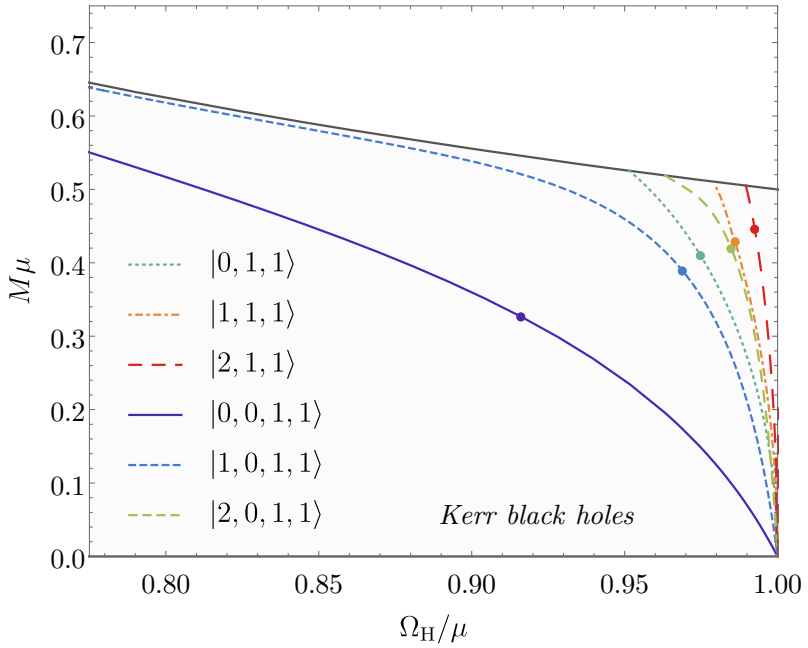

Fig. 3. Existence lines of the scalar states $|n,1,1\rangle$ and vector states $|n,0,1,1\rangle$, $n=0,1,2$ in the $(M\mu,\Omega_{\rm H}/\mu)$-plane. The gray solid line refers to extremal ($a=M$) Kerr black holes. The $n=0$ states are the least energetic, as they correspond to lower values of $\Omega_{\rm H}$. The energy increases with n. The plot markers are states with $r_+\mu=0.5$, whose radial profiles are shown in Fig. 4.

states require larger minimum horizon angular velocities for stationary equilibrium. Vector states are still less energetic than their scalar cousins. The radial profile of the states marked with bullets in Fig. 3 is depicted in Fig. 4. These states exist for Kerr black holes with $r_+\mu=0.5$ and have $n+1$ extrema. However, while the extrema of scalar states decrease towards spatial infinity, those of vector states increase. Vector states thus have wider spatial distributions.

The numerical solutions found using the direct-integration shooting method can be integrated from $r=r_+(1-\delta_+)$ to $r=r_-(1+\delta_-)$, with $\delta_-\ll 1$. Since the appropriate boundary conditions at both the outer horizon and spatial infinity are already imposed, there is no freedom left to set the desired behavior at the inner horizon. The latter rotates with an angular velocity different from $\Omega_{\rm H}$ and therefore synchronization is not possible there. The radial profiles of the states $|0,1,1\rangle$ and $|0,0,1,1\rangle$ marked in Fig. 3 is shown in Fig. 5 in the black hole's interior. They exhibit oscillatory character close to $r=r_-$. This suggests that Kerr black holes with synchronized hair do not possess a smooth Cauchy horizon, but rather a curvature singularity at $r=r_-$.[64]

4.2. *Kerr–Newman black holes*

The state of affairs does not change much when looking at synchronized states around Kerr–Newman black holes. The existence lines obtained when fixing the additional parameter $Q\mu$ coincide with those found for Kerr black holes ($Q\mu=0$) in the $(M\mu,\Omega_{\rm H}/\mu)$-plane. However, each point on the line now represents a black

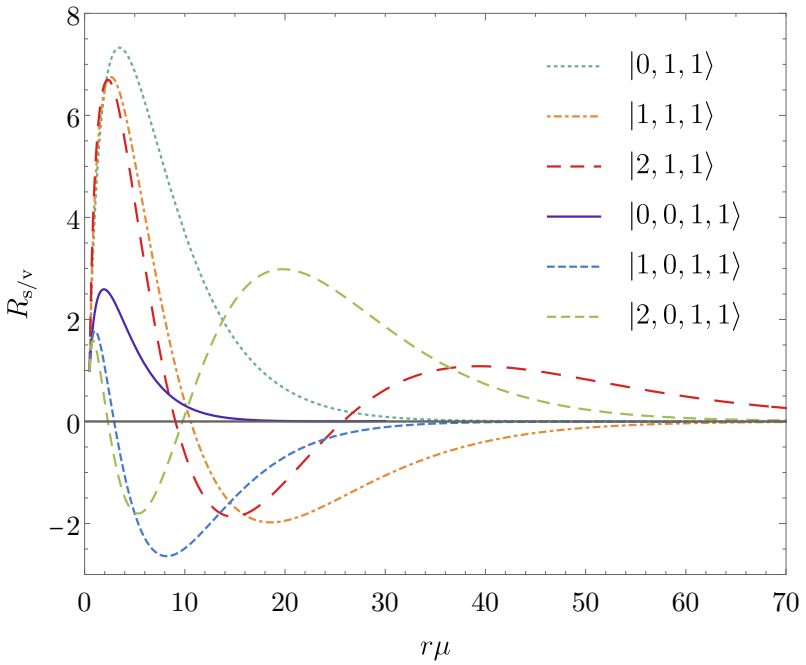

Fig. 4. Radial profiles of the states marked in Fig. 3 (bottom panel), characterized by $\mu r_+ = 0.5$. The radial functions are normalized so that $R(r_+) = 1$.

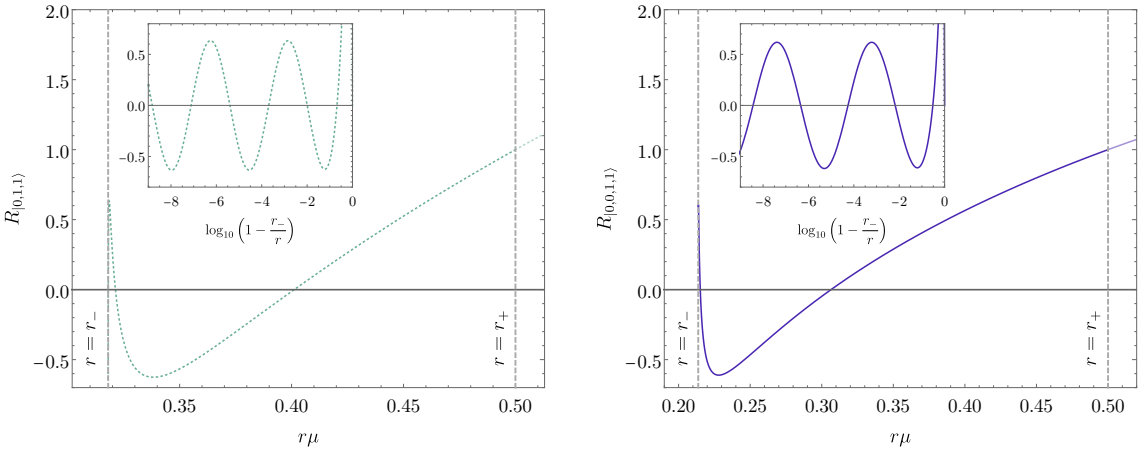

Fig. 5. Radial profiles of the states $|0,1,1\rangle$ (left panel) and $|0,0,1,1\rangle$ (right panel) marked in Fig. 3 inside the Kerr black hole, characterized by $r_+\mu = 0.5$. The radial functions are normalized so that $R(r_+) = 1$.

hole with nonvanishing specific electric charge Q/M. Moving towards greater horizon angular velocities, the specific angular momentum a/M decreases, whereas the specific electric charge Q/M increases. The black holes close to the line $M\mu = 0$ may be described as slowly-rotating extremal ($Q = M$) Reissner–Nordström black holes. Figure 6 shows where Kerr–Newman black holes with $a/M \in \{0.50, 0.80, 0.90, 0.95, 0.99\}$ lie on the existence line of the scalar state $|0,1,1\rangle$ for different values of $Q\mu$. Similar trends are found for vector states.

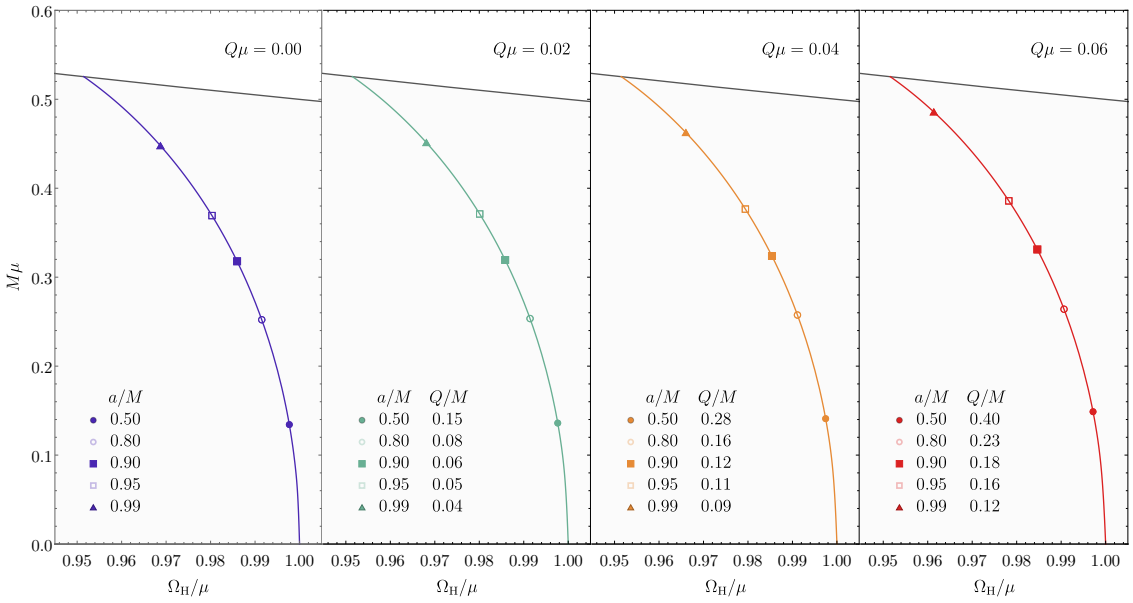

Fig. 6. Existence lines of the scalar states $|0, 1, 1\rangle$ in the $(M\mu, \Omega_H/\mu)$-plane for Kerr–Newman black holes with different normalized charges $Q\mu$. The gray solid line refers to extremal ($a = M$) Kerr black holes. The specific electric charge is presented for black holes with different specific angular momenta.

5. Conclusion

This paper aimed at providing a comparative analysis of stationary scalar and vector clouds around Kerr and Kerr–Newman black holes. The key physical property of these bound states is a solidary rotation of the cloud with the black hole. These configurations are akin to the atomic orbitals of an electron in a hydrogen atom and can similarly be described in terms of $\{n, \ell, j, m_j\}$. This set of *quantum numbers* label the existence lines of synchronized states in the parameter space of Kerr–Newman black holes and are continuously connected Kerr–Newman black holes with synchronized hair, solutions of Einstein–Maxwell theory minimally coupled to complex massive bosons.

In general, vector bound states have lower energies than their scalar cousins and also occur for Kerr–Newman black holes in a wider domain of the normalized horizon angular velocity. The fundamental states match in both cases the most unstable quasi-bound state and are characterized by $j = m_j$, $n = 0$ and the least possible value for the orbital angular momentum ℓ. The latter two have similar impact on the cloud's energy for fixed $\{j, m_j\}$. Additionally, states with vanishing orbital angular momentum ($\ell = 0$) are exclusive of vector bosons and are linked to a nonvanishing intrinsic angular momentum.

The motivation behind a new glance at stationary clouds around Kerr–Newman black holes follows from the recent separation of the Proca equation in the Kerr–NUT–(A)dS family of spacetimes. It would be of interest to apply the newfound ansatz to find synchronized states in other spacetimes and to construct stationary clouds in the time domain.

Acknowledgments

The authors are especially grateful for the hospitality during their visit to Pará University, where part of this project was developed. This work is supported by the Center for Astrophysics and Gravitation (CENTRA) and by the Center for Research and Development in Mathematics and Applications (CIDMA) through the Portuguese Foundation for Science and Technology (FCT — Fundação para a Ciência e a Tecnologia), references UIDB/04106/2020, UIDB/00099/2020 and UIDP/04106/2020. The authors acknowledge support from the projects PTDC/FIS-OUT/28407/2017 and CERN/FIS-PAR/0027/2019 and from national funds (OE), through FCT, I.P., in the scope of the framework contract foreseen in the numbers 4, 5 and 6 of the article 23, of the Decree-Law 57/2016, of August 29, changed by Law 57/2017, of July 19. This work has further been supported by the European Union's Horizon 2020 research and innovation (RISE) programme H2020-MSCA-RISE-2017 Grant No. FunFiCO-777740. The authors would like to acknowledge networking support by the COST Action CA16104.

References

1. R. Penrose, *Riv. Nuovo Cimento.* **1** (1969) 252.
2. R. M. Wald, *Astrophys. J.* **191** (1974) 231.
3. J. M. Bardeen, W. H. Press and S. A. Teukolsky, *Astrophys. J.* **178** (1972) 347.
4. Y. B. Zel'Dovich, *JETP Lett.* **14** (1971) 180.
5. Y. B. Zel'Dovich, *Sov. Phys. JETP* **35** (1972) 1085.
6. C. Misner, *Bull. Amer. Phys. Soc.* **17** (1972) 472.
7. R. Brito, V. Cardoso and P. Pani, *Superradiance: Energy Extraction, Black-Hole Bombs and Implications for Astrophysics and Particle Physics* (Springer, 2015).
8. W. H. Press and S. A. Teukolsky, *Nature* **238** (1972) 211.
9. W. E. East, F. M. Ramazanoğlu and F. Pretorius, *Phys. Rev. D* **89** (2014) 061503, `arXiv:1312.4529 [gr-qc]`.
10. N. Sanchis-Gual, J. C. Degollado, P. J. Montero, J. A. Font and C. Herdeiro, *Phys. Rev. Lett.* **116** (2016) 141101, `arXiv:1512.05358 [gr-qc]`.
11. W. E. East and F. Pretorius, *Phys. Rev. Lett.* **119** (2017) 041101, `arXiv:1704.04791 [gr-qc]`.
12. C. A. R. Herdeiro and E. Radu, *Phys. Rev. Lett.* **119** (2017) 261101, `arXiv:1706.06597 [gr-qc]`.
13. C. A. R. Herdeiro and E. Radu, *Phys. Rev. Lett.* **112** (2014) 221101, `arXiv:1403.2757 [gr-qc]`.
14. C. Herdeiro, E. Radu and H. Rńarsson, *Class. Quantum Grav.* **33** (2016) 154001, `arXiv:1603.02687 [gr-qc]`.
15. C. A. Herdeiro and E. Radu, *Int. J. Mod. Phys. D* **24** (2015) 1542014, `arXiv:1504.08209 [gr-qc]`.
16. J. D. Bekenstein, *Phys. Rev. D* **5** (1972) 1239.
17. J. Bekenstein, *Phys. Rev. D* **5** (1972) 2403.
18. J. Bekenstein, *Phys. Rev. Lett.* **28** (1972) 452.
19. R. Ruffini and J. A. Wheeler, *Phys. Today* **24** (1971) 30.
20. V. Cardoso and L. Gualtieri, *Class. Quantum Grav.* **33** (2016) 174001, `arXiv:1607.03133 [gr-qc]`.

21. S. Hod, *Phys. Rev. D* **86** (2012) 104026, arXiv:1211.3202 [gr-qc], Erratum **86** (2012) 129902.
22. S. Hod, *Eur. Phys. J. C* **73** (2013) 2378, arXiv:1311.5298 [gr-qc].
23. S. Hod, *Phys. Rev. D* **90** (2014) 024051, arXiv:1406.1179 [gr-qc].
24. C. L. Benone, L. C. Crispino, C. Herdeiro and E. Radu, *Phys. Rev. D* **90** (2014) 104024, arXiv:1409.1593 [gr-qc].
25. M. Wang and C. Herdeiro, *Phys. Rev. D* **93** (2016) 064066, arXiv:1512.02262 [gr-qc].
26. S. Hod, *Phys. Lett. B* **749** (2015) 167, arXiv:1510.05649 [gr-qc].
27. H. M. Siahaan, *Int. J. Mod. Phys. D* **24** (2015) 1550102, arXiv:1506.03957 [hep-th].
28. S. Hod, *J. High Energy Phys.* **01** (2017) 030, arXiv:1612.00014 [hep-th].
29. S. Hod, *Class. Quantum Grav.* **32** (2015) 134002, arXiv:1607.00003 [gr-qc].
30. Y. Huang and D.-J. Liu, *Phys. Rev. D* **94** (2016) 064030, arXiv:1606.08913 [gr-qc].
31. C. Bernard, *Phys. Rev. D* **94** (2016) 085007, arXiv:1608.05974 [gr-qc].
32. I. Sakalli and G. Tokgoz, *Class. Quantum Grav.* **34** (2017) 125007, arXiv:1610.09329 [gr-qc].
33. H. R. C. Ferreira and C. A. R. Herdeiro, *Phys. Lett. B* **773** (2017) 129, arXiv:1707.08133 [gr-qc].
34. M. Richartz, C. A. R. Herdeiro and E. Berti, *Phys. Rev. D* **96** (2017) 044034, arXiv:1706.01112 [gr-qc].
35. Y. Huang, D.-J. Liu, X.-H. Zhai and X.-Z. Li, *Class. Quantum Grav.* **34** (2017) 155002, arXiv:1706.04441 [gr-qc].
36. Y. Huang, D.-J. Liu, X.-h. Zhai and X.-Z. Li, *Phys. Rev. D* **98** (2018) 025021, arXiv:1807.06263 [gr-qc].
37. G. García and M. Salgado, *Phys. Rev. D* **99** (2019) 044036, arXiv:1812.05809 [gr-qc].
38. J. F. Delgado, C. A. Herdeiro and E. Radu, *Phys. Lett. B* **792** (2019) 436, arXiv:1903.01488 [gr-qc].
39. J. Kunz, I. Perapechka and Y. Shnir, *Phys. Rev. D* **100** (2019) 064032, arXiv:1904.07630 [gr-qc].
40. G. García and M. Salgado, *Phys. Rev. D* **101** (2020) 044040, arXiv:1909.12987 [gr-qc].
41. S. Teukolsky, *Phys. Rev. Lett.* **29** (1972) 1114.
42. S. A. Teukolsky, *Astrophys. J.* **185** (1973) 635.
43. V. P. Frolov, P. Krtouš, D. Kubizňák and J. E. Santos, *Phys. Rev. Lett.* **120** (2018) 231103, arXiv:1804.00030 [hep-th].
44. S. R. Dolan, *Phys. Rev. D* **98** (2018) 104006, arXiv:1806.01604 [gr-qc].
45. R. Cayuso, F. Gray, D. Kubizňák, A. Margalit, R. Gomes Souza and L. Thiele, *Phys. Lett. B* **795** (2019) 650, arXiv:1906.10072 [hep-th].
46. D. Baumann, H. S. Chia, J. Stout and L. ter Haar, *J. Cosmol. Astropart. Phys.* **12** (2019) 006, arXiv:1908.10370 [gr-qc].
47. N. Siemonsen and W. E. East, *Phys. Rev. D* **101** (2020) 024019, arXiv:1910.09476 [gr-qc].
48. R. Cayuso, O. J. Dias, F. Gray, D. Kubizňák, A. Margalit, J. E. Santos, R. Gomes Souza and L. Thiele, *J. High Energy Phys.* **04** (2020) 159, arXiv:1912.08224 [hep-th].
49. N. M. Santos, C. L. Benone, L. C. Crispino, C. A. Herdeiro and E. Radu arXiv:2004.09536 [gr-qc].
50. B. Carter, *Commun. Math. Phys.* **10** (1968) 280.

51. I. Semiz, *Phys. Rev. D* **45** (1992) 532, Erratum **47** (1993) 5615.
52. E. Berti, V. Cardoso and M. Casals, *Phys. Rev. D* **73** (2006) 024013, arXiv:gr-qc/0511111, Erratum **73** (2006) 109902.
53. J. B. Hartle, *Astrophys. J.* **150** (1967) 1005.
54. P. Pani, V. Cardoso, L. Gualtieri, E. Berti and A. Ishibashi, *Phys. Rev. Lett.* **109** (2012) 131102, arXiv:1209.0465 [gr-qc].
55. P. Pani, V. Cardoso, L. Gualtieri, E. Berti and A. Ishibashi, *Phys. Rev. D* **86** (2012) 104017, arXiv:1209.0773 [gr-qc].
56. O. Lunin, *J. High Enery Phys.* **12** (2017) 138, arXiv:1708.06766 [hep-th].
57. P. Krtouš, V. P. Frolov and D. Kubizňák, *Nucl. Phys. B* **934** (2018) 7, arXiv:1803.02485 [hep-th].
58. V. P. Frolov, P. Krtouš and D. Kubizňák, *Phys. Rev. D* **97** (2018) 101701, arXiv:1802.09491 [hep-th].
59. K. S. Thorne, *Rev. Mod. Phys.* **52** (1980) 299.
60. M. Maggiore, *Gravitational Waves. Volume 1: Theory and Experiments* (Oxford University Press, 2007).
61. P. Pani, *Int. J. Mod. Phys. A* **28** (2013) 1340018, arXiv:1305.6759 [gr-qc].
62. D. Baumann, H. S. Chia and R. A. Porto, *Phys. Rev. D* **99** (2019) 044001, arXiv:1804.03208 [gr-qc].
63. D. Baumann, H. S. Chia, R. A. Porto and J. Stout, *Phys. Rev. D* **101** (2020) 083019, arXiv:1912.04932 [gr-qc].
64. Y. Brihaye, C. Herdeiro and E. Radu, *Phys. Lett. B* **760** (2016) 279, arXiv:1605.08901 [gr-qc].

Chapter 3

Reprint of *Phys. Lett. B* 815 (2021) 13614

Physics Letters B 815 (2021) 136142

Contents lists available at ScienceDirect

Physics Letters B

www.elsevier.com/locate/physletb

Black holes, stationary clouds and magnetic fields

Nuno M. Santos [a,b,*], Carlos A.R. Herdeiro [b]

[a] Centro de Astrofísica e Gravitação — CENTRA, Departamento de Física, Instituto Superior Técnico — IST, Universidade de Lisboa — UL, Av. Rovisco Pais 1, 1049-001 Lisboa, Portugal
[b] Centre for Research and Development in Mathematics and Applications (CIDMA) and Departamento de Matemática da Universidade de Aveiro Campus de Santiago, 3810-183 Aveiro, Portugal

ARTICLE INFO

Article history:
Received 20 January 2021
Received in revised form 6 February 2021
Accepted 9 February 2021
Available online 12 February 2021
Editor: M. Trodden

Keywords:
Black holes
Magnetic fields
Scalar fields
Superradiance
Stationary clouds

ABSTRACT

As the electron in the hydrogen atom, a bosonic field can bind itself to a black hole occupying a discrete infinite set of states. When (i) the spacetime is prone to superradiance and (ii) a confinement mechanism is present, some of such states are infinitely long–lived. These equilibrium configurations, known as stationary clouds, are states "synchronized" with a rotating black hole's event horizon. For most, if not all, stationary clouds studied in the literature so far, the requirements (i)–(ii) are independent of each other. However, this is not always the case. This paper shows that massless neutral scalar fields can form stationary clouds around a Reissner–Nordström black hole when both are subject to a uniform magnetic field. The latter simultaneously enacts both requirements by creating an ergoregion (thereby opening up the possibility of superradiance) and trapping the scalar field in the black hole's vicinity. This leads to some novel features, in particular, that only black holes with a subset of the possible charge to mass ratios can support stationary clouds.

1. Introduction

Neutron stars and black holes in binary systems feed some of the most powerful astrophysical events in the Universe. Their gravitational–wave luminosity can reach a peak of approximately 10^{57} erg s^{-1} [1,2], only comparable to the electromagnetic luminosity of the most luminous gamma–ray bursts [3]. The Advanced LIGO/Virgo's first and second observation runs reported the detection of gravitational waves from ten different binary black hole mergers and a single binary neutron star merger. During the first half of the third observing run, a total of 39 gravitational–wave candidate events were observed, three of which may have originated from neutron star–black hole mergers [4]. Joint detections of gravitational and electromagnetic waves from neutron star–black hole coalescences are of particular interest for constraining the equation of state of dense nuclear matter [5] and measuring the Hubble constant [6]. Furthermore, some neutron stars, known as magnetars, are endowed with super–strong magnetic fields reaching 10^{12}–10^{15} G [7]. For instance, the magnetar SGR J1745–2900, which orbits the supermassive black hole Sagittarius A*, has a surface dipolar magnetic field of 10^{14} G. Neutron star–black hole binary systems are thus natural laboratories for probing the intricate interaction of black holes with magnetic fields.

A magnetic field B_0 permeating a black hole with mass M curves the spacetime in a non-negligible way beyond a threshold value set by $MB \sim 1$ [8], or reinstating familiar units

$$B \equiv \frac{c^4}{G^{3/2}M} \sim 10^{19}\left(\frac{M_\odot}{M}\right)\ \mathrm{G}\,, \tag{1}$$

where $M_\odot$ is the solar mass. A magnetic field of order B or larger warps significantly spacetime in the vicinity of the event horizon (without changing its topology). Since the field strength of a magnetic dipole falls off as the cube of the distance from it, it is unlikely that stellar–mass black holes or even supermassive black holes are subject to magnetic fields of order B.

Even if its strength is significantly smaller than B, the impact of a magnetic dipole on fields interacting with black holes may be non–negligible, as they can acquire an effective mass and be trapped in its vicinity. A massless field traversing the black hole's vicinity would then behave as if it had non–vanishing mass and its effective mass would depend on the magnetic field strength. In addition, if the field is bosonic, it can induce black–hole superradiance, i.e. the extraction of energy and angular momentum from rotating black holes (for a review, see [9]). Black–hole superradi-

* Corresponding author.
E-mail addresses: nunomoreirasantos@tecnico.ulisboa.pt (N.M. Santos), herdeiro@ua.pt (C.A.R. Herdeiro).

https://doi.org/10.1016/j.physletb.2021.136142

ance takes place when the phase angular velocity w of the bosonic field satisfies

$$w < m\Omega_{\mathcal{H}} \,, \tag{2}$$

where m is the azimuthal harmonic index and $\Omega_{\mathcal{H}}$ is the black hole's angular velocity. Together with a natural confinement mechanism, black–hole superradiance is responsible for bosonic fields to form quasi–bound states. These are continuously fed the extracted black hole's energy and angular momentum until Eq. (2) saturates, i.e. $w = m\Omega_{\mathcal{H}}$, and they become bound states. The new equilibrium state is expected to be a classical bosonic condensate in equilibrium with the slowed–down black hole, which for a complex bosonic field is a hairy black hole [10–14].

The bosonic field remains trapped in the vicinity of the black hole when it is massive. A non–vanishing intrinsic mass, however, is not always mandatory. Trapping can be attained even when the field is massless. For instance, a massless bosonic field interacting with a black hole immersed in a magnetic field is likely to form bound states. The magnetic field creates a potential barrier, confining the field into the neighborhood of the black hole.

An example that naturally embodies this idea is the interaction of a massless scalar field with a Reissner–Nordström black hole embedded in a uniform axial magnetic field.[1] The latter is described by the Reissner–Nordström–Melvin (RNM) solution [15,16], obtained via a solution–generating technique known as Harrison (or "magnetizing") transformation. Interestingly, the RNM solution is a stationary (rather than a static) solution of the Einstein–Maxwell theory. The rotation is sourced by the coupling between the black hole's electric charge and the external magnetic field. Besides, the spacetime features an ergoregion and, as a result, is prone to black–hole superradiance even for electrically neutral bosonic fields. This contrasts with the case of asymptotically–flat Reissner–Nordström black holes wherein (charged) superradiance is possible but only for *charged* bosonic fields [17] and a superradiant instability does not follow from a mass term; it requires, for instance, enclosing the black hole with a reflecting mirror – see, *e.g.*, [18–20].

The present paper focuses on bound states between a massless scalar field and a RNM black hole (cf. [21]). These real–frequency states are characterized by the threshold of superradiance $w = m\Omega_{\mathcal{H}}$, hereafter referred to as *synchronisation condition*, and were first reported in [22], in which the author named them *stationary clouds*. Much attention has been paid to such synchronized states since their discovery [14,23–42], yet most works rely on intrinsically massive fields. For the case under consideration here, the fields need not have a non-vanishing mass for stationary clouds to arise.[2] A peculiar feature of this model is that the scalar field's effective mass is proportional to the black hole's angular velocity, the proportionality constant being a function of the specific electric charge Q/M alone, where M and Q are, respectively, the black hole's mass and electric charge. Curiously enough, the condition for the existence of bound states is only met for values of Q/M in a subset of $[-1, 1]$.

The paper is organized as follows. First, the Einstein–Maxwell theory minimally coupled to a complex, ungauged scalar field is introduced in section 2. Together with a constant scalar field, the RNM solution is a particular case of the theory. Its main features are outlined in section 2.1, followed by a linear analysis of scalar field perturbations in section 2.2. The main results on stationary clouds are presented in section 3. A summary of the work can be found in section 4.

[1] Although this is not a realistic astrophysical scenario, it suffices to sketch the main argument of the paper.

[2] The same is true for AdS asymptotics – see, *e.g.*, [26].

Natural units ($G = c = 1$) are consistently used throughout the text. Additionally, the metric signature $(-,+,+,+)$ is adopted.

2. Framework

The action for the Einstein–Maxwell theory minimally coupled to a complex,[3] ungauged scalar field Ψ is

$$\mathcal{S} = \frac{1}{4\pi}\int \mathrm{d}^4x\sqrt{-g}\left[\frac{R}{4} - \frac{F^2}{4} - (\nabla^\mu\Psi^*)(\nabla_\mu\Psi)\right] , \tag{3}$$

where $\boldsymbol{F} = \mathrm{d}\boldsymbol{A}$ is the electromagnetic tensor and $\boldsymbol{A}$ is electromagnetic four–potential.

The corresponding equations of motion read

$$G_{\mu\nu} = 2\left[T^{(\boldsymbol{A})}_{\mu\nu} + T^{(\Psi)}_{\mu\nu}\right] \,,\ \Box\Psi = 0 \,,\ \nabla_\mu F^{\mu\nu} = 0 \,, \tag{4}$$

where $\Box \equiv \nabla_\mu\nabla^\mu$ is the d'Alembert operator and

$$T^{(\boldsymbol{A})}_{\mu\nu} \equiv F_\mu{}^\sigma F_{\nu\sigma} - \frac{1}{4}g_{\mu\nu}F_{\sigma\lambda}F^{\sigma\lambda}, \tag{5}$$

$$T^{(\Psi)}_{\mu\nu} \equiv 2\partial_{(\mu}\Psi^*\partial_{\nu)}\Psi - g_{\mu\nu}(\partial_\lambda\Psi^*)(\partial^\lambda\Psi) \tag{6}$$

are the stress–energy tensors of the electromagnetic and scalar fields, respectively. The action has a global $U(1)$ invariance with respect to the scalar field thanks to its complex character.

This field theory admits all of the stationary solutions of general relativity. These are characterized by $\Psi = \Psi_0$, for some constant Ψ_0. Linearizing the equations of motion around $\Psi = \Psi_0$, one obtains the ordinary Einstein–Maxwell equations together with the Klein–Gordon equation for the scalar field perturbation $\delta\Psi \equiv (\Psi - \Psi_0)$. This system describes the linear or zero–backreaction limit of the theory: the limit in which the backreaction of both the gravitational and electromagnetic fields to a non–constant scalar field is negligible. This first–order approximation suffices to capture potentially relevant astrophysical phenomena such as superradiant scattering. The framework allows one to solve the Klein–Gordon equation $\Box(\delta\Psi) = 0$ for a known solution $\{\boldsymbol{g}, \boldsymbol{A}\}$ of the Einstein–Maxwell equations.

2.1. Reissner–Nordström–Melvin black holes

This paper will focus on scalar field perturbations of RNM black holes. These solutions belong to a family of electrovacuum type D solutions of the Einstein–Maxwell equations which asymptotically resemble the magnetic Melvin universe. The latter describes a non–singular, static, cylindrically symmetric spacetime representing a bundle of magnetic flux lines in gravitational–magnetostatic equilibrium. It can be loosely interpreted as Minkowski spacetime immersed in a uniform magnetic field; but it should be kept in mind that such magnetic field, no matter how small, changes the global structure of the spacetime, in particular its asymptotics.

Given an asymptotically–flat, stationary, axi–symmetric solution of Einstein–Maxwell equations, it is possible to embed it in a uniform magnetic field via a solution–generating technique called Harrison transformation (also commonly known as "magnetizing" transformation). This possibility, first realized by Harrison [44], was explored for the Schwarzschild and Reissner-Nordström solutions [15] and for the Kerr and Kerr–Newman solutions [45].

The RNM solution, which describes a Reissner–Nordström black hole permeated by a uniform magnetic field, reads [16]

[3] Stationary clouds are not exclusive to complex scalar fields. A single real scalar field can equally form infinitely long–lived states at linear level – see [43].

$$\boldsymbol{g} = |\Lambda|^2\left(-\frac{\Delta}{r^2}\,\mathbf{d}t^2 + \frac{r^2}{\Delta}\mathbf{d}r^2 + r^2\mathbf{d}\theta^2\right) + \frac{r^2\sin^2\vartheta}{|\Lambda|^2}(\mathbf{d}\varphi - \Omega\mathbf{d}t)^2\,,$$

$$\boldsymbol{A} = \Phi_0\mathbf{d}t + \Phi_3(\mathbf{d}\varphi - \Omega\mathbf{d}t) \tag{7}$$

where $t\in(-\infty,+\infty)$, $r\in(0,+\infty)$, $\vartheta\in[0,\pi]$, $\varphi\in[0,2\pi)$ and

$$\Delta = r^2 - 2Mr + Q^2\,,$$

$$\Lambda = 1 + \frac{1}{4}B_0^2(r^2\sin^2\vartheta + Q_0^2\cos^2\vartheta) - iQB_0\cos\vartheta\,,$$

$$\Omega = -\frac{2QB_0}{r} + \frac{QB_0^3 r}{2}\left(1+\frac{\Delta}{r^2}\cos^2\vartheta\right)\,,$$

$$\Phi_0 = -\frac{Q}{r} + \frac{3}{4}QB_0^2 r\left(1+\frac{\Delta}{r^2}\cos^2\vartheta\right)\,,$$

$$\Phi_3 = \frac{2}{B_0} - \frac{1}{|\Lambda|^2}\left[\frac{2}{B_0} + \frac{B_0}{2}\left(r^2\sin^2\vartheta + 3Q^2\cos^2\vartheta\right)\right]\,.$$

B_0 is the strength of the magnetic field, which is assumed to be much weaker than the threshold value (1), i.e. $MB_0 \ll MB = 1$.

When applied to the Reissner–Nordström solution, the Harrison transformation produces a stationary (rather than a static) solution. The dragging potential Ω is directly proportional to the coupling QB_0, which suggests that the interaction between the charge Q and the magnetic field B_0 serves as a source for rotation.

The solution possesses two (commuting) Killing vectors, $\boldsymbol{\xi} = \partial_t$ and $\boldsymbol{\eta} = \partial_\varphi$, associated to stationarity and axi–symmetry, respectively. The line element has coordinate singularities at $\Delta = 0$ when $Q^2 \leq M^2$, which solves for $r_\pm = M \pm \sqrt{M^2 - Q^2}$. The hypersurface $r = r_+$ ($r = r_-$) is the outer (inner) horizon. Besides, there is an ergo–region that extends to infinity along the axial direction, but not in the radial direction. Here, ergo–region means the regions outside the outer horizon wherein $\boldsymbol{\xi}$ is spacelike.

The dragging potential Ω is constant (i.e. ϑ–independent) on $r = r_+$, where it has the value

$$\Omega_{\mathcal{H}} \equiv -\frac{2QB_0}{r_+}\left(1 - \frac{r_+^2 B_0^2}{4}\right)\,. \tag{8}$$

$\Omega_{\mathcal{H}}$ is the angular velocity of the outer horizon. The Killing vector $\boldsymbol{\chi} = \boldsymbol{\xi} + \Omega_{\mathcal{H}}\boldsymbol{\eta}$ becomes null on the hypersurface $r = r_+$ and it is timelike outside it.

2.2. Scalar field perturbations

In general, the Klein–Gordon equation $\Box(\delta\Psi) = 0$ does not admit a multiplicative separation of variables of the form

$$\delta\Psi(t,\mathbf{r}) = e^{-iwt}R(r)S(\vartheta)e^{+im\varphi}\,, \tag{9}$$

where w is the phase angular velocity, R and S are respectively the radial and angular functions and $m\in\mathbb{Z}$ is the azimuthal harmonic index. However, in the limit of sufficiently "weak" magnetic fields, i.e. neglecting terms of order[4] higher than $\mathcal{O}(B_0^2)$, the ansatz (9) actually reduces the problem to two differential equations in the coordinates r and ϑ. The radial and angular equations read [21]

$$\frac{\mathrm{d}}{\mathrm{d}r}\left(\Delta\frac{\mathrm{d}R}{\mathrm{d}r}\right) + \left[\frac{K^2}{\Delta} - (m^2B_0^2r^2 + \lambda)\right]R = 0\,, \tag{10}$$

$$\frac{1}{\sin\vartheta}\frac{\mathrm{d}}{\mathrm{d}\vartheta}\left(\sin\vartheta\frac{\mathrm{d}S}{\mathrm{d}\vartheta}\right) + \left(\lambda - \frac{m^2}{\sin^2\vartheta} - 3m^2Q^2B_0^2\cot^2\vartheta\right)S = 0\,, \tag{11}$$

respectively, where $K = r^2w + 2mQB_0r$ and λ is the separation constant. Equations (10)–(11) are both confluent Heun equations: the former (latter) has singular points at $r = r_\pm$ ($\vartheta = 0,\pi$). They are coupled via the Killing eigenvalues $\{w,m\}$, B_0, Q and the separation constant λ and remain invariant under the discrete transformation $\{w, mQB_0\}\to\{-w,-mQB_0\}$. This guarantees that, without loss of generality, one can take $\mathrm{sgn}(w) = \mathrm{sgn}(B_0) = +1$. When $mQB_0 = 0$, the angular equation reduces to the general Legendre equation, whose canonical solutions are the associated Legendre polynomials of degree ℓ and order m, $P_\ell^m(\vartheta)$, provided that $\lambda = \ell(\ell+1)$. Thus, if $|mQB_0| \ll 1$, the angular dependence of $\delta\Psi$ is approximately described by the scalar spherical harmonics of degree ℓ and order m, $Y_\ell^m(\vartheta,\varphi) = P_\ell^m(\vartheta)e^{+im\varphi}$.

Equation (10) can be cast in Schrödinger–like form, yielding

$$-\frac{\mathrm{d}^2\rho}{\mathrm{d}y^2} + V_{\mathrm{eff}}(y)\rho = w^2\rho\,, \tag{12}$$

where $\rho \equiv rR$ and y is the tortoise coordinate, defined by

$$y(r) = r + \frac{r_+^2}{r_+ - r_-}\log(r - r_+) - \frac{r_-^2}{r_+ - r_-}\log(r - r_-)\,,$$

which maps the interval $r\in[r_+,\infty)$ into $r_*\in(-\infty,+\infty)$. The effective potential V_{eff}, whose expression is omitted here, has the following limiting behavior:

$$\lim_{y\to-\infty} V_{\mathrm{eff}}(y) = w^2 - (w - m\Omega_{\mathcal{H}})^2\,, \tag{13}$$

$$\lim_{y\to+\infty} V_{\mathrm{eff}}(y) = m^2B^2\,. \tag{14}$$

The last limit suggests that a non–vanishing external magnetic field makes the scalar field acquire an effective mass $\mu_{\mathrm{eff}} = \sqrt{m^2B_0^2}$. It is important to remark, however, that the problem at hand is not equivalent to that of a massive scalar field perturbation on an asymptotically–flat stationary spacetime, wherein the mass dominates the asymptotic behavior of the field. Besides providing the field an effective mass, the magnetic field also changes the asymptotic behavior at infinity (to be that of the Melvin magnetic universe), which has similarities with AdS asymptotics in the sense that it is naturally confining.

Fig. 1 shows the effective potential as a function of the radial coordinate r for different (negative) specific electric charges. In an asymptotically–Melvin spacetime, the magnetic field acts like a potential barrier at $rB_0 \sim 1$, whose maximum, about ten times larger than $\mathcal{O}(B_0^2)$, approaches the outer horizon with decreasing Q/M (i.e. tending to extremality). Moreover, there is a potential well for all positive specific electric charges (not plotted in Fig. 1) as well as for negative ones above a certain threshold (away from extremality). The effective potential resembles a mirror placed at $rB_0 \sim 1$ and confines (low–frequency) scalar field perturbations in the black hole's vicinity [46,47]. It is then natural to impose a Robin (or mixed) boundary condition at $r = r_0$ as the outer boundary condition,

$$\tan(\zeta) = -\frac{R(r_0)}{R'(r_0)}\,, \tag{15}$$

[4] For a straightforward identification of the order of each term, it is convenient to introduce the dimensionless quantities $\{tB_0, rB_0, MB_0, QB_0, w/B_0\}$ so that all physical quantities are measured in units of the magnetic field strength. Note that the first four quantities are of order $\mathcal{O}(B_0)$, whereas the last is of order $\mathcal{O}(B_0^{-1})$.

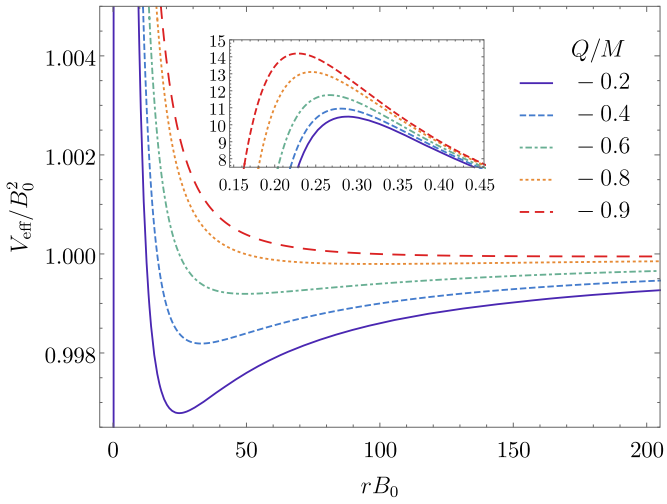

Fig. 1. Effective potential for scalar field perturbations with $\ell = m = 1$ and $w = 0.5B_0$ of RNM black holes with $MB_0 = 0.1$. (Inset) Zoom near $rB_0 \sim 1$ to display the maximum of the effective potential.

where r_0 is of order $\mathcal{O}(B_0^{-1})$, $\zeta \in [0, \pi)$, with $\zeta = 0$ ($\zeta = \pi/2$) corresponding to a Dirichlet (Neumann) boundary condition, and the prime denoting differentiation with respect to r.

In realistic astrophysical scenarios, magnetic fields occur in accretion disks around black holes. The "magnetic" potential barrier is then at a radial distance smaller than about the mean radius D of the disk, i.e. $r_0 \lesssim D$. Since the matter in the accretion disk is expected to be close to the innermost stable circular orbit, $D \sim 3M$ and it follows that $MB_0 \gtrsim 0.1$, which clashes with the assumption $MB_0 \ll 1$ (for a more complete discussion, see [47]). Despite this caveat, the main argument of the paper holds at least from a purely theoretical perspective.

Furthermore, physically meaningful solutions to the radial equation satisfy the inner boundary condition

$$R|_{y\to-\infty} \sim e^{-i(\omega - m\Omega_{\mathcal{H}})y} \,, \tag{16}$$

i.e. they behave as waves falling into (emanating from) the black hole when $w > m\Omega_{\mathcal{H}}$ ($0 < w < m\Omega_{\mathcal{H}}$).

3. Stationary scalar clouds

When the scalar field's phase angular velocity is a natural multiple of the black hole's angular velocity, i.e.

$$w = m\Omega_{\mathcal{H}} = -\frac{2mQB_0}{r_+} + \mathcal{O}(B_0^3) \,, \tag{17}$$

bound states, known as *stationary clouds*, are found. Equation (17) is called *synchronisation condition* and does depend on the scalar field's effective mass, $\mu_{\rm eff} = \sqrt{m^2 B_0^2}$. The ratio $|w/\mu_{\rm eff}| = 2|Q|/r_+$ is independent of B_0 and its absolute value is smaller than or equal to 2. Since it was assumed that $\mathrm{sgn}(w) = \mathrm{sgn}(B_0) = +1$, the synchronisation condition dictates that the bound states satisfy $\mathrm{sgn}(mQ) = -1$.

The synchronisation occurs in one–dimensional subsets of the two–dimensional parameter space of Reissner–Nordström–Melvin black holes, described by $\{M, Q\}$. These subsets – known as *existence lines* – are disjoint and can be labeled with a set of three "quantum" numbers: the number of nodes in the radial direction[5] n, the orbital/total angular momentum ℓ and the azimuthal harmonic index m. These states will be labeled with $|n, \ell, m\rangle$.

In the following, stationary scalar clouds around RNM black holes are obtained both (semi–)analytically and numerically. The existence lines will be plotted in the (M, Q)–plane normalized to the magnetic field strength B_0.

3.1. Analytical approach

The eigenvalue problem at hand can be solved using the matched asymptotic expansion method (see, *e.g.*, [48]), i.e. constructing approximations to the solutions of (10) that separately satisfy the inner and outer boundary conditions. The interval $r \in [r_+, r_0]$ is thus split into two: (i) the inner region, $r - r_+ \ll \lambda_c$, where $\lambda_c = \mu_{\rm eff}^{-1} \leq r_+/(m|Q|B_0)$ is the scalar field's Compton wavelength; inspection shows that $\lambda_c \gg M$; and (ii) the outer region, $r - r_+ \gg M$. The inner and outer expansions are then matched in the overlap region, where both conditions can hold simultaneously, defined by $M \ll r - r_+ \ll \lambda_c$.

3.1.1. Outer region

The outer region is well–defined only if the outer boundary is sufficiently far from the black hole, i.e. as long as $r_0 \gg M$. Given that $Q^2 \leq M^2$, one can take $\Delta \sim r^2$. Besides, if $r^2 \gg |2mQB_0/w|$, then $K \sim wr^2$. When the synchronization condition (17) holds, the latter approximation is equivalent to $r \gg r_+$, which is consistent with $r - r_+ \gg M$.

The radial equation (10) then reduces to that of a massless scalar field perturbation with phase angular velocity defined by $\varpi^2 \equiv w^2 - \mu_{\rm eff}^2 = m^2 B_0^2 (4Q^2/r_+^2 - 1)$ and angular momentum ℓ in Minkowski spacetime,[6]

$$\frac{\mathrm{d}^2}{\mathrm{d}r^2}(rR_+) + \left[\varpi^2 - \frac{\ell(\ell+1)}{r^2}\right](rR_+) = 0 \,, \tag{18}$$

where $R_+(r) \equiv \lim_{r\to r_0} R(r)$. The general solution is

$$R_+(r) = \alpha_+ j_\ell(\varpi r) + \beta_+ y_\ell(\varpi r) \,, \tag{19}$$

where j_ℓ and y_ℓ are the spherical Bessel functions of the first and second kinds, respectively, and $\alpha_+, \beta_+ \in \mathbb{C}$. For sufficiently large r, the spherical Bessel functions are a linear combination of ingoing and outgoing waves if ϖ is real, i.e. if $w^2 > \mu_{\rm eff}^2$. The Robin boundary condition (15) fixes the quotient

$$\gamma \equiv \frac{\beta_+}{\alpha_+} = \left[-\frac{j_\ell(\varpi r) + \tan(\zeta) j'_\ell(\varpi r)}{y_\ell(\varpi r) + \tan(\zeta) y'_\ell(\varpi r)}\right]\Bigg|_{r=r_0} \,. \tag{20}$$

The small–r behavior of the asymptotic solution (19) is

$$R_+(r) \sim \alpha_+ \frac{(\varpi r)^\ell}{(2\ell+1)!!} - \beta_+ \frac{(2\ell-1)!!}{(\varpi r)^{\ell+1}} \,. \tag{21}$$

3.1.2. Inner region

Near the outer horizon, the radial equation (10) reduces to

$$\frac{\mathrm{d}}{\mathrm{d}r}\left(\Delta \frac{\mathrm{d}R_-}{\mathrm{d}r}\right) - \ell(\ell+1)R_- = 0 \,, \tag{22}$$

where $R_-(r) \equiv \lim_{r\to r_+} R(r)$. Introducing the radial coordinate $z \equiv (r-r_+)/(r-r_-)$ and defining $R_-(z) = (1-z)^{\ell+1} F(z)$, one can bring the radial equation (22) into the form

$$z(1-z)\frac{\mathrm{d}^2 F}{\mathrm{d}z^2} + [c - (a+b+1)z]\frac{\mathrm{d}F}{\mathrm{d}z} - abF = 0 \,, \tag{23}$$

[5] The number of nodes in the radial direction does not include the node at $r = r_0$ when $\zeta = 0$ (Dirichlet boundary condition).

[6] Alternatively, one could say that Eq. (18) describes a scalar field with mass $\sqrt{m^2 B^2}$, phase angular velocity $m\Omega_{\mathcal{H}}$ and angular momentum ℓ.

with $a = b \equiv \ell + 1$ and $c \equiv 1$. Equation (23) is a Gaussian hypergeometric equation, which has three regular singular points: $z = 0, 1, \infty$. The most general solution is [11,49]

$$F(z) = \alpha_- F(a, a; 1; z) + \beta_- \left[F(a, a; 1; z) \log z + 2 \sum_{j=1}^{+\infty} f_{(j)} z^j \right] , \tag{24}$$

where

$$f_{(j)} = \left[\frac{(a)_j}{j!} \right]^2 [\psi(a + j) - \psi(a) - \psi(j + 1) + \psi(1)]$$

and $(a)_j = \Gamma(a + j)/\Gamma(a)$ and ψ is the digamma function. The second term in Eq. (24) diverges logarithmically as $z \to 0$ ($r \to r_+$). As the inner boundary condition must be regular, the constant β_- must vanish. In terms of the radial function R_-, the solution thus reads

$$R_-(z) = \alpha_- \frac{(2\ell + 1)!}{(\ell!)^2} \left[(-1)^{2\ell+1} R^{(\mathrm{D})}(z) + \frac{R^{(\mathrm{N})}(z)}{(\ell + 1)^2} \right] ,$$

where

$$R_-^{(\mathrm{D})}(z) = (1 - z)^{\ell+1} F(\ell + 1, \ell + 1; 2\ell + 2; 1 - z) ,$$
$$R_-^{(\mathrm{N})}(z) = (1 - z)^{-\ell} F(-\ell, -\ell; -2\ell; 1 - z) .$$

When $r \gg M$, $z \sim 1$ and $(1 - z) \sim (r_+ - r_-)/r$, meaning that

$$R_-^{(\mathrm{D})}(z) \sim (r_+ - r_-)^{\ell+1} r^{-\ell-1} ,$$
$$R_-^{(\mathrm{N})}(z) \sim (r_+ - r_-)^{-\ell} r^{\ell} .$$

3.1.3. Matching

It is clear that the larger–r behavior of the asymptotic solution R_- exhibits the same dependence on r as the small–r behavior of the asymptotic solution R_+. Matching the two solutions, one gets

$$\gamma = \frac{(\ell + 1)^2}{(2\ell + 1)!!(2\ell - 1)!!} [\varpi (r_+ - r_-)]^{2\ell+1} . \tag{25}$$

Using Eq. (20), one finally obtains

$$\tan(\zeta) = -\frac{j_\ell(\varpi r_0) + \gamma\, y_\ell(\varpi r_0)}{j'_\ell(\varpi r_0) + \gamma\, y'_\ell(\varpi r_0)} , \tag{26}$$

which establishes the existence condition for stationary scalar clouds around (non–extremal) RNM black holes. These exist as long as the field perturbation has a radial oscillatory character and therefore can satisfy a Robin boundary condition at $r_0 B_0 \sim 1$. This requirement is met provided that ϖ is real, i.e. if

$$w^2 > \mu_{\mathrm{eff}}^2 \Leftrightarrow \frac{4Q^2}{r_+^2} > 1 \implies \frac{Q^2}{M^2} > \frac{16}{25} , \tag{27}$$

or $|Q/M| \in (0.8, 1.0)$, where $\mathrm{sgn}(Q) = \pm 1$ for $\mathrm{sgn}(m) = \mp 1$ so that $\mathrm{sgn}(w) = +1$. Note that this restriction on the specific electric charge is a by–product of the proportionality between $w = m\Omega_{\mathcal{H}}$ and μ_{eff}.

3.2. Numerical approach

Stationary clouds can also be found by solving numerically the coupled equations (10)–(11). For that purpose, it is convenient to replace the mass M by the outer horizon radius r_+ and work with the dimensionless quantities $\{r_+ B_0, Q B_0, \Omega_{\mathcal{H}}/B_0\}$. To impose the correct inner boundary condition the radial function may be written as a series expansion around $r = r_+$ [50],

$$R|_{r \to r_+} \sim \sum_{j=0}^{+\infty} a_{(j)} (r - r_+)^j . \tag{28}$$

The coefficients $\{a_{(j)}\}_{j>0}$ are obtained by plugging (28) into (10), writing the resulting equation in powers of $(r - r_+)$ and setting the coefficient of each power separately equal to zero. The resulting system of equations must then be solved for $\{a_{(j)}\}_{j>0}$ in terms of $a_{(0)}$. The latter is set to 1 without loss of generality. The coefficients $\{a_{(j)}\}_{j>0}$ depend on the black hole's parameters $\{r_+, Q\}$, the Killing eigenvalue m and the separation constant λ. Instead of solving the angular equation (11), one approximates the latter by $\ell(\ell+1)$, which is accurate enough if $mQB_0 \ll 1$. Since $Q^2 \leq M^2$ and $MB_0 \ll MB = 1$, the approximation is valid for moderate values of m.

The parameters $\{r_+, \ell, m\}$ are assigned fixed values. By virtue of the regular singular point at $r = r_+$, Eq. (10) must be integrated from $r = r_+(1 + \delta)$, with $\delta \ll 1$, to $r = r_0$, where r_0 is the outer boundary radial coordinate. A simple shooting method finds the Q–values for which the numerical solutions satisfy a Robin boundary condition at $r = r_0$.

3.3. Existence lines

Fig. 2 displays the (numerical) existence lines for stationary clouds $|0, 1, 1\rangle$ with $r_0 B_0 \in \{4, 6, 8, 10\}$ and $\zeta \in \{0, \frac{\pi}{2}, \frac{\pi}{4}\}$. The shaded bands represent the allowed regions of the parameter space for the existence of bound states. The upper boundary, defined by $Q^2 = M^2$, corresponds to the *extremal line*. The RNM black holes in the lower boundary satisfy $Q^2 = 0.64M^2$, in accordance with the conclusion at the end of section 3.1.3.

The panels below the main plots show the absolute difference σ between each existence line and that corresponding to $r_0 B_0 = 4$ and the absolute difference ε between the *numerical* and *analytical* existence lines. As expected, given that the analytical condition (26) is valid when $MB_0 \ll 1$, $\varepsilon \to 0$ as $MB_0 \to 0$.

All existence lines lie within the shaded bands. Also, they converge to $(M, Q) = (0, 0)$, i.e. $\sigma \to 0$ as $MB_0 \to 0$, which is in agreement with the expectation that scalar field perturbations cannot attain stationary equilibrium with respect to asymptotically–Melvin black holes. Fixing MB_0, as the region of influence of the magnetic field decreases, i.e. as $r_0 B_0$ decreases, the Coulomb energy of the black hole supporting the stationary cloud increases. Vaster clouds thus require lower angular velocities so that they do not collapse into the black hole. Also, there is an overall decrease in the Coloumb energy as ζ varies continuously from 0 (Dirichlet boundary condition) to $\frac{\pi}{2}$ (Neumann boundary condition).

The existence lines for the states $|0, \ell, m\rangle$ with $\ell = m = 1, \ldots, 4$, $r_0 B_0 = 4$ and $\zeta = 0$ are plotted in Fig. 3. These approach the extremal line as $\ell = m$ decreases, a trend already noticed in previous works (see, *e.g.*, [25]).

The impact of the orbital angular momentum ℓ is enlightened in Fig. 4, in which the existence lines for the states $|0, \ell, 1\rangle$ with $\ell = 1, \ldots, 4$, $r_0 B_0 = 6$ and $\zeta = 0$ are shown. As ℓ increases, so does $|Q/M|$, which suggests that stationary clouds $|0, \ell, 1\rangle$ with $\ell > 1$ are more energetic than $|0, 1, 1\rangle$.

4. Conclusion

The RNM black hole stands out as a toy model for a rotating black hole immersed in an external axial magnetic field. In fact, it is the simplest stationary (but not static) solution of Einstein–Maxwell equations asymptotically resembling the magnetic Melvin

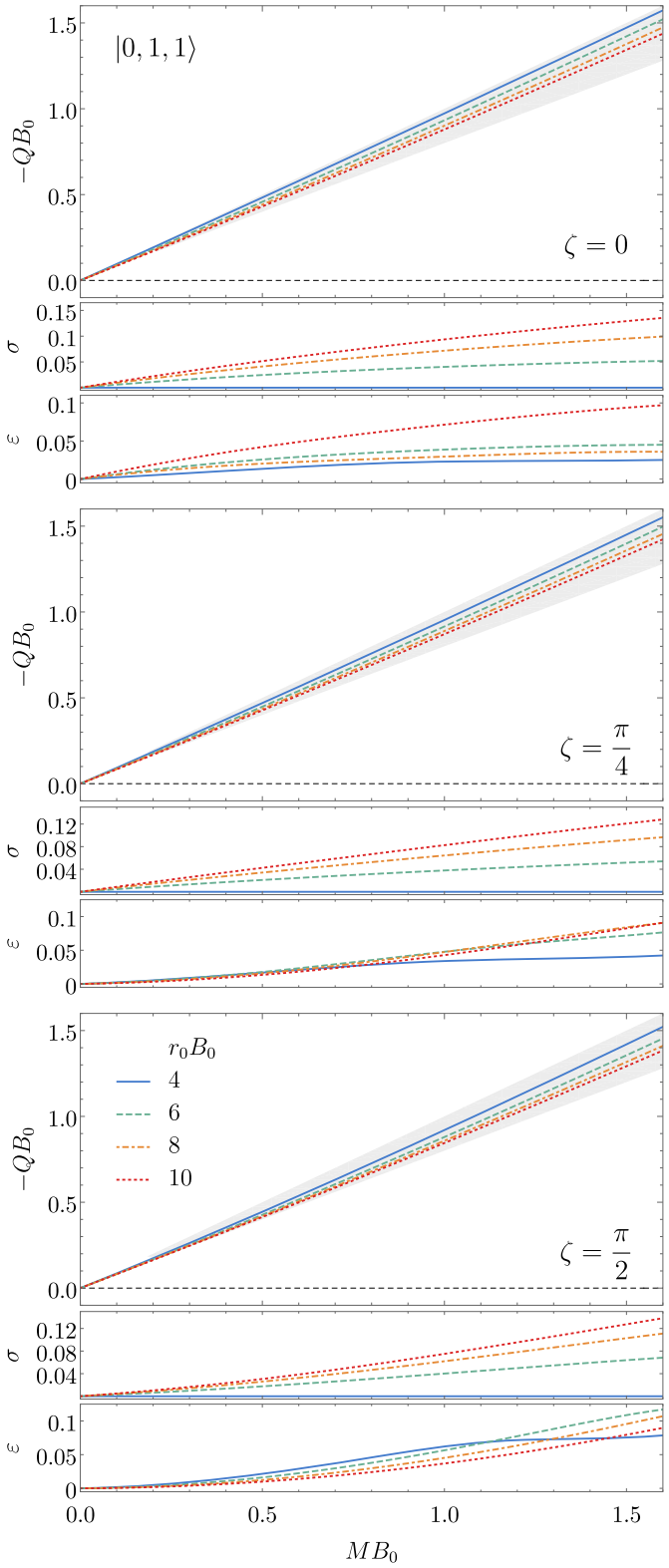

Fig. 2. Stationary scalar clouds $|n,\ell,m\rangle = |0,1,1\rangle$ around Reissner–Nordström black holes embedded in a uniform axial magnetic field of strength B_0, for different Robin boundary conditions, parametrized by ζ, at the outer boundary r_0.

universe. Frequently overlooked due to its astrophysical irrelevance, it is still worth studying as it may offer some insights into the interaction of black holes with magnetic fields.

The present paper aimed precisely to explore the interplay between bosonic fields and black holes when permeated by a uniform magnetic field. It was shown in particular that RNM black holes support synchronized scalar field configurations known as stationary clouds. They are somehow akin to atomic orbitals of the hydrogen atom in quantum mechanics in that they are both described by quantum number. In effect, stationary clouds are characterized by the number of nodes in the radial direction, n, the orbital angular momentum, ℓ, and the azimuthal harmonic index, m, which labels the projection of the orbital angular momentum along the direction of the magnetic field.

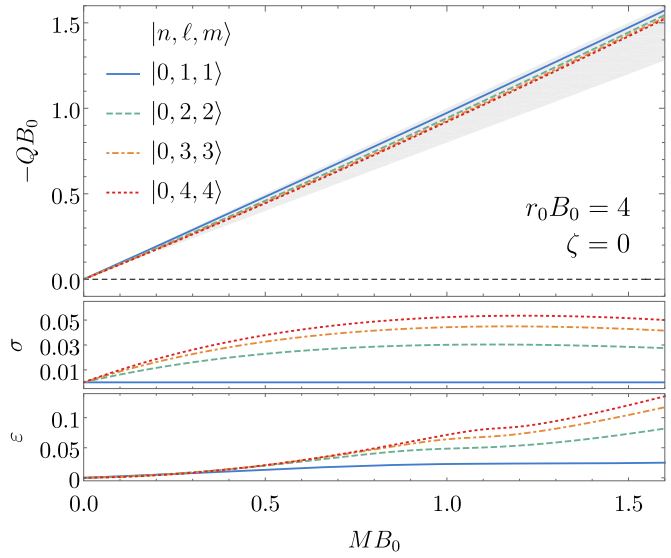

Fig. 3. Stationary scalar clouds $|n,\ell,m\rangle = |0,\ell,\ell\rangle$ around Reissner–Nordström black holes embedded in a uniform axial magnetic field of strength B_0 and satisfying a Dirichlet boundary condition ($\zeta = 0$) at $r_0 B_0 = 4$.

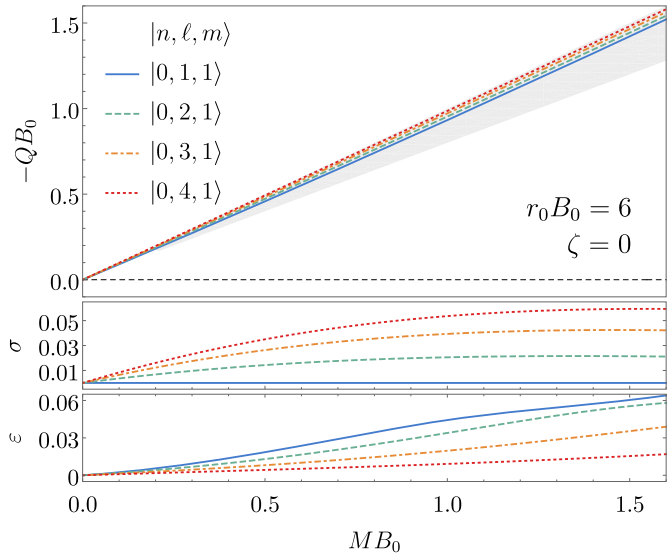

Fig. 4. Stationary scalar clouds $|n,\ell,m\rangle = |0,\ell,1\rangle$, with $\ell = 1,\ldots,4$, around Reissner–Nordström black holes embedded in a uniform axial magnetic field of strength B_0 and satisfying a Dirichlet boundary condition ($\zeta = 0$) at $r_0 B_0 = 6$.

It is now well known that stationary equilibrium is possible whenever a bosonic field at the threshold of superradiant instabilities (i.e. obeying the so–called syncrhonization condition) is confined in the black hole's vicinity. The confinement mechanism (either natural or artificial) creates a potential barrier which may prevent the field from escaping to infinity. As a result, infinitely long–lived configurations arise. For example, a massive bosonic field can form such stationary clouds around Kerr black holes – with the field's mass providing a natural confinement mechanism.

So does a massless charged scalar field in a cavity enclosing a Reissner–Nordström black hole – with the boundary of the cavity, a reflective mirror, sourcing an artificial confinement mechanism [18]. The properties of both equilibrium configurations are similar despite minor qualitative differences.

Additionally worth mentioning is the fact that, in two previous examples, the occurrence of superradiance does not rely on the existence of a confining environment; one could say that the two ingredients are added separately. However, in the setup under consideration, the magnetic field of the RNM black hole is responsible not only for developing an ergoregion and hence trigger superradiant phenomena but also for making low–frequency fields acquire an effective mass and thus be trapped, allowing the formation of stationary clouds. In view of this, it does not come as a surprise that both the black hole's angular velocity $\Omega_{\mathcal{H}}$ and the field's effective mass μ_{eff} – synonyms for superradiance and confinement, respectively – depend on B_0.

Lastly, a by–product of considering the RNM black hole was the realization that the quotient $m\Omega_{\mathcal{H}}/\mu_{\text{eff}}$ is a function of the black hole's specific electric charge Q/M only. Consequently, the condition for the existence of bound states constrains the values of Q/M for which stationary clouds can exist.

Declaration of competing interest

The authors declare that they have no known competing financial interests or personal relationships that could have appeared to influence the work reported in this paper.

Acknowledgements

This work has been supported by the Center for Astrophysics and Gravitation (CENTRA) and by the Center for Research and Development in Mathematics and Applications (CIDMA) through the Portuguese Foundation for Science and Technology (FCT – Fundação para a Ciência e a Tecnologia), references UIDB/00099/2020, UIDB/04106/2020 and UIDP/04106/2020. The authors acknowledge support from the projects PTDC/FIS-OUT/28407/2017, CERN/FIS-PAR/0027/2019 and PTDC/FIS-AST/3041/2020. N. M. Santos is supported by the FCT grant SFRH/BD/143407/2019. This work has further been supported by the European Union's Horizon 2020 research and innovation (RISE) program H2020-MSCA-RISE-2017 Grant No. FunFiCO-777740. The authors would like to acknowledge networking support by the COST Action CA16104.

References

[1] B. Abbott, et al., LIGO Scientific, Virgo, Phys. Rev. X 9 (2019) 031040, arXiv:1811.12907 [astro-ph.HE].
[2] V. Cardoso, T. Ikeda, C.J. Moore, C.-M. Yoo, Phys. Rev. D 97 (2018) 084013, arXiv:1803.03271 [gr-qc].
[3] D. Frederiks, et al., Astrophys. J. 779 (2013) 151, arXiv:1311.5734 [astro-ph.HE].
[4] R. Abbott, et al., LIGO Scientific, Virgo, arXiv:2010.14527 [gr-qc], 2020.
[5] G. Raaijmakers, et al., Astrophys. J. Lett. 893 (2020) L21, arXiv:1912.11031 [astro-ph.HE].
[6] S. Vitale, H.-Y. Chen, Phys. Rev. Lett. 121 (2018) 021303, arXiv:1804.07337 [astro-ph.CO].
[7] S. Olausen, V. Kaspi, Astrophys. J. Suppl. Ser. 212 (2014) 6, arXiv:1309.4167 [astro-ph.HE].
[8] V.P. Frolov, A.A. Shoom, Phys. Rev. D 82 (2010) 084034, arXiv:1008.2985 [gr-qc].
[9] R. Brito, V. Cardoso, P. Pani, Superradiance: Energy Extraction, Black-Hole Bombs and Implications for Astrophysics and Particle Physics, Vol. 906, Springer, 2015, arXiv:1501.06570 [gr-qc].
[10] C.A.R. Herdeiro, E. Radu, Phys. Rev. Lett. 112 (2014) 221101, arXiv:1403.2757 [gr-qc].
[11] C. Herdeiro, E. Radu, H. Ŕnarsson, Class. Quantum Gravity 33 (2016) 154001, arXiv:1603.02687 [gr-qc].
[12] W.E. East, F.M. Ramazanoğlu, F. Pretorius, Phys. Rev. D 89 (2014) 061503, arXiv:1312.4529 [gr-qc].
[13] C.A.R. Herdeiro, E. Radu, Phys. Rev. Lett. 119 (2017) 261101, arXiv:1706.06597 [gr-qc].
[14] N.M. Santos, C.L. Benone, L.C.B. Crispino, C.A.R. Herdeiro, E. Radu, J. High Energy Phys. 07 (2020) 010, arXiv:2004.09536 [gr-qc].
[15] F.J. Ernst, J. Math. Phys. 17 (1976) 54.
[16] G. Gibbons, A. Mujtaba, C. Pope, Class. Quantum Gravity 30 (2013) 125008, arXiv:1301.3927 [gr-qc].
[17] J. Bekenstein, Phys. Rev. D 7 (1973) 949.
[18] C.A.R. Herdeiro, J.C. Degollado, H.F. Rúnarsson, Phys. Rev. D 88 (2013) 063003, arXiv:1305.5513 [gr-qc].
[19] J.C. Degollado, C.A. Herdeiro, Phys. Rev. D 89 (2014) 063005, arXiv:1312.4579 [gr-qc].
[20] N. Sanchis-Gual, J.C. Degollado, P.J. Montero, J.A. Font, C. Herdeiro, Phys. Rev. Lett. 116 (2016) 141101, arXiv:1512.05358 [gr-qc].
[21] H. Vieira, V. Bezerra, Ann. Phys. 373 (2016) 28, arXiv:1603.02233 [gr-qc].
[22] S. Hod, Phys. Rev. D 86 (2012) 104026, arXiv:1211.3202 [gr-qc];
S. Hod, Phys. Rev. D 86 (2012) 129902, Erratum.
[23] S. Hod, Eur. Phys. J. C 73 (2013) 2378, arXiv:1311.5298 [gr-qc].
[24] S. Hod, Phys. Rev. D 90 (2014) 024051, arXiv:1406.1179 [gr-qc].
[25] C.L. Benone, L.C. Crispino, C. Herdeiro, E. Radu, Phys. Rev. D 90 (2014) 104024, arXiv:1409.1593 [gr-qc].
[26] M. Wang, C. Herdeiro, Phys. Rev. D 93 (2016) 064066, arXiv:1512.02262 [gr-qc].
[27] S. Hod, Phys. Lett. B 749 (2015) 167, arXiv:1510.05649 [gr-qc].
[28] H.M. Siahaan, Int. J. Mod. Phys. D 24 (2015) 1550102, arXiv:1506.03957 [hep-th].
[29] S. Hod, J. High Energy Phys. 01 (2017) 030, arXiv:1612.00014 [hep-th].
[30] S. Hod, Class. Quantum Gravity 32 (2015) 134002, arXiv:1607.00003 [gr-qc].
[31] Y. Huang, D.-J. Liu, Phys. Rev. D 94 (2016) 064030, arXiv:1606.08913 [gr-qc].
[32] C. Bernard, Phys. Rev. D 94 (2016) 085007, arXiv:1608.05974 [gr-qc].
[33] I. Sakalli, G. Tokgoz, Class. Quantum Gravity 34 (2017) 125007, arXiv:1610.09329 [gr-qc].
[34] H.R.C. Ferreira, C.A.R. Herdeiro, Phys. Lett. B 773 (2017) 129, arXiv:1707.08133 [gr-qc].
[35] M. Richartz, C.A.R. Herdeiro, E. Berti, Phys. Rev. D 96 (2017) 044034, arXiv:1706.01112 [gr-qc].
[36] Y. Huang, D.-J. Liu, X.-H. Zhai, X.-Z. Li, Class. Quantum Gravity 34 (2017) 155002, arXiv:1706.04441 [gr-qc].
[37] Y. Huang, D.-J. Liu, X.-h. Zhai, X.-z. Li, Phys. Rev. D 98 (2018) 025021, arXiv:1807.06263 [gr-qc].
[38] G. García, M. Salgado, Phys. Rev. D 99 (2019) 044036, arXiv:1812.05809 [gr-qc].
[39] J.F. Delgado, C.A. Herdeiro, E. Radu, Phys. Lett. B 792 (2019) 436, arXiv:1903.01488 [gr-qc].
[40] J. Kunz, I. Perapechka, Y. Shnir, Phys. Rev. D 100 (2019) 064032, arXiv:1904.07630 [gr-qc].
[41] G. García, M. Salgado, Phys. Rev. D 101 (2020) 044040, arXiv:1909.12987 [gr-qc].
[42] N.M. Santos, C.A.R. Herdeiro, Int. J. Mod. Phys. D 29 (2020) 2041013, arXiv:2005.07201 [gr-qc].
[43] C. Herdeiro, E. Radu, Class. Quantum Gravity 32 (2015) 144001, arXiv:1501.04319 [gr-qc].
[44] B.K. Harrison, J. Math. Phys. 9 (1968) 1744, https://doi.org/10.1063/1.1664508.
[45] F.J. Ernst, W.J. Wild, J. Math. Phys. 17 (1976) 182.
[46] R.A. Konoplya, Phys. Lett. B 666 (2008) 283, arXiv:0801.0846 [hep-th];
R.A. Konoplya, Phys. Lett. B 670 (2009) 459.
[47] R. Brito, V. Cardoso, P. Pani, Phys. Rev. D 89 (2014) 104045, arXiv:1405.2098 [gr-qc].
[48] V. Cardoso, P. Pani, M. Cadoni, M. Cavaglia, Class. Quantum Gravity 25 (2008) 195010, arXiv:0808.1615 [gr-qc].
[49] M. Abramowitz, I.A. Stegun, Handbook of Mathematical Functions with Formulas, Graphs and Mathematical Tables, Dover Publications, Inc., New York, 1965.
[50] P. Pani, Int. J. Mod. Phys. A 28 (2013) 1340018, arXiv:1305.6759 [gr-qc].

Chapter 4

Reprint of *Phys. Lett. B* 824 (2022) 136835

Physics Letters B 824 (2022) 136835

Contents lists available at ScienceDirect

Physics Letters B

www.elsevier.com/locate/physletb

A bound on energy extraction (and hairiness) from superradiance

Carlos A.R. Herdeiro [a], Eugen Radu [a], Nuno M. Santos [a,b,*]

[a] Departamento de Matemática da Universidade de Aveiro and Centre for Research and Development in Mathematics and Applications (CIDMA), Campus de Santiago, 3810-183 Aveiro, Portugal

[b] Centro de Astrofísica e Gravitação – CENTRA, Departamento de Física, Instituto Superior Técnico – IST, Universidade de Lisboa – UL, Avenida Rovisco Pais 1, 1049-001 Lisboa, Portugal

ARTICLE INFO

Article history:
Received 11 November 2021
Received in revised form 7 December 2021
Accepted 7 December 2021
Available online 13 December 2021
Editor: M. Trodden

ABSTRACT

The possibility of mining the rotational energy from black holes has far–reaching implications. Such energy extraction could occur even for isolated black holes, if hypothetical ultralight bosonic particles exist in Nature, leading to a new equilibrium state – a black hole with synchronised bosonic hair – whose lifetime could exceed the age of the Universe. A natural question is then: for an isolated black hole and at maximal efficiency, how large is the energy fraction ϵ that can be extracted from a Kerr black hole by the superradiant growth of the dominant mode? In other words, how hairy can the resulting black hole become? A thermodynamical bound for the total superradiance efficiency, $\epsilon \lesssim 0.29$ (as a fraction of the initial black hole mass), has long been known, from the area law. However, numerical simulations exhibiting the growth of the dominant mode only reached about one third of this value. We show that if the development of superradiant instabilities is approximately conservative (as suggest by the numerical evolutions), this efficiency is limited to $\epsilon \lesssim 0.10$, regardless of the spin of the bosonic field. This is in agreement with the maximum energy extraction obtained in numerical simulations for a vector field and predicts the result of similar simulations with a scalar field, yet to be performed.

1. Introduction

The recent successes of radio [1] and gravitational–wave astronomy [2–4] have put general relativity (GR) to the test as never before. A key issue is the observational confirmation of the *Kerr hypothesis*: that all astrophysical black holes (BHs), regardless of their scale, are well described by Kerr's solution to the vacuum Einstein's field equations [5]. From a theoretical standpoint, this paradigm relies on: (*i*) the *uniqueness theorems* of vacuum GR [6–8], which establish that its most general solution, regular on and outside the event horizon, is the Kerr metric, solely defined by its global charges, mass M and angular momentum J; (*ii*) a number of *no–hair theorems* (*e.g.* [9,10]) ruling out the existence of non–Kerr BHs in the presence of certain types of matter–energy, which otherwise could endow BHs with "hair". Consequently, these theorems support the *no–hair conjecture* [11], according to which the gravitational collapse of any type of matter–energy in GR always yields a Kerr BH.

At the time of writing there is no clear tension between the Kerr hypothesis and observations. Yet, fundamental open issues such as dark matter, dark energy and the inevitability of singularities in GR [12,13] strongly suggest going beyond GR and/or the standard model of particle physics. In this context, dynamically robust non–Kerr models are particularly welcome as exploratory scenarios of deviations from the Kerr hypothesis. Clearly, a formation scenario and sufficient stability are mandatory to make any alternative BH (or exotic compact object) model physically plausible and a potential actor on the astrophysical stage.

In this discussion, the phenomenon of superradiance [14] originates a novel possibility. Bosonic fields with a mass in an appropriate range can efficiently transfer the rotational energy of a Kerr BH into a cloud of bosonic particles, spinning down the BH – see *e.g.* [15]. When the BH spins down enough to meet the phase angular velocity of the dominant superradiant mode, the process stalls. The detailed phenomenology depends on the type of bosonic field. Real fields have a rich phenomenology related to the decay of the bosonic cloud via gravitational waves emission – see *e.g.* [15–17]. If the (scalar or vector) field is complex, on the other hand, the cloud is stationary after the synchronisation between the BH's and the field's angular velocities occurs, and a new stationary equilibrium state forms. This has been seen in the numerical evolutions of East and Pretorius, focusing on the case of vector bosonic fields [18]. The new equilibrium states were shown to match BHs

* Corresponding author.
E-mail address: nunomoreirasantos@tecnico.ulisboa.pt (N.M. Santos).

https://doi.org/10.1016/j.physletb.2021.136835

with synchronised Proca hair [19], first reported in [20] following the construction of BH solutions with synchronised scalar hair [21].

The BHs with synchronised hair (BHsSH) formed from the superradiant instability of Kerr are, themselves, prone to superradiant instabilities [22]. These, however, can be very long–lived; in particular, for supermassive BHs the lifetime of the superradiant instability of the newly formed hairy BH can take a timescale larger than a Hubble time to develop [23]. In other words, *superradiance can form a hairy BH on an astrophysical timescale, and the latter can be stable for a cosmological timescale*. This makes these hairy BHs resulting from the growth of the dominant superradiant mode of Kerr plausible players in astrophysical processes.

The superradiance scenario offers a formation mechanism for BHsSH with an interesting twist. Superradiance is quite sensitive to a matching of scales. The instability is strongest if the Compton wavelength of the bosonic particle, $1/\mu$, and the BH radius, $\sim M$, approximately match: $M\mu \sim 1$. Away from this sweet spot, the timescale of the instability grows with the exponential of $M\mu$ for $M\mu \gg 1$ [24] and as a large inverse power of $M\mu$ for $M\mu \ll 1$ [25]. Thus, BHs only become efficiently hairy (on an astrophysical timescale) in an island of the parameter space, determined by the mass of the bosonic particle μ. Sufficiently far from the resonance $M\mu \sim 1$, Kerr BHs are effectively stable against superradiance. Thus, in this scenario, Kerr and hairy BHs may co–exist in the Universe, with the latter belonging to an island in a narrow mass range around μ (and non–zero spin) and Kerr BHs composing the surrounding ocean of the BH mass spectrum.

For astrophysical BHs, known to exist within the mass range $M \in [1, 10^{10}]M_{\odot}$, the resonance $M\mu \sim 1$ means that the bosonic particle is ultralight, with the mass range $\mu \sim [10^{-10}, 10^{-20}]$ eV. This connects to the particular class of dark matter models known as fuzzy dark matter [26,27], which could have a stringy origin [28], or otherwise be embedded in simpler extensions of the standard model – see *e.g.* [29].

The foregoing discussion yields the exciting possibility that BHs (and in this case the hairiness of BHs) can become particle detectors of extremely light – and potentially inaccessible to colliders – dark matter particles, via astrophysical measurements. To assess this possibility, however, it is important to understand *how much energy* can be extracted from a Kerr BH from the growth of the dominant superradiant mode. Or, in the context of the complex bosons that endow BHs with hair, this translates into *how hairy* a BH can become, which naturally defines how non–Kerr its phenomenology may be. In his pioneering paper on the area law, Hawking noticed that no more than 29% of the initial BH mass could be extracted via superradiance [30]. Yet, the simulations by East and Pretorius, which followed the growth of the dominant superradiant mode, only reached about 9%. Was this because of the choice of parameters? Could the value be much closer to 29%? Is there a difference between scalar and vector superradiance concerning this maximal efficiency?

In this letter, we shall provide a simple argument that for both the scalar and vector case there is a roughly similar bound of around 10% for the maximal energy extraction due to the dominant superradiant mode from a Kerr BH; thus the efficiency is $\epsilon \lesssim 0.1$,[1] regardless the spin of the bosonic field. This bound is based on: (*i*) a scanning of the BHs solutions with synchronised scalar and Proca hair that can result from the growth of the dominant superradiant mode; (*ii*) the rationale that this superradiant evolution is approximately conservative, which is supported by the evolutions in [18]. Under this assumption, superradiance merely redistributes the mass and angular momentum of a Kerr BH, splitting it amongst the trapped region and the bosonic hair. Since Kerr BHs have a dimensionless spin j that obeys $j \leqslant 1$ (Kerr bound), the corresponding hairy BH that forms after the superradiant growth from Kerr must also obey this bound. We observe that generic hairy BHs *do not* obey $j \leqslant 1$ [21]. Scanning the parameter space, we can identify the hairiest solutions, under the constraint $0 \leqslant j \leqslant 1$. These occur precisely for hairy BHs with $j = 1$ and at a certain $M\mu$, which (slightly) depends on the spin of the field. Identifying the fraction of energy in the bosonic field in these solutions with the maximal efficiency, we obtain:

$$\begin{aligned} &\textbf{Scalar}: \ \epsilon_{\rm max} \sim 0.099 \ \ (\text{at } M\mu \approx 0.24)\ ; \\ &\textbf{Vector}: \ \epsilon_{\rm max} \sim 0.104 \ (\text{at } M\mu \approx 0.27)\ . \end{aligned} \tag{1}$$

In particular we observe that, for the vector case, the maximal energy extraction reported in [18], of $\sim 9\%$, occurred for $M\mu = 0.25$, which shows an interesting agreement with (1). Equation (1) is the main result in this letter. It *predicts* that numerical evolutions (yet to be performed) similar to those in [18] for the scalar case will lead to a similar result for the maximal efficiency, smaller than 10%. In the remaining of this paper we shall detail how the result (1) is obtained.

2. Black holes with synchronised hair

BHsSH are families of four–dimensional, asymptotically–flat, stationary solutions of Einstein's gravity minimally coupled to a complex bosonic field ψ with non–vanishing mass μ. The bosonic field can be a scalar (first discussed in [21]) or a vector (first discussed in [20]). Such spacetimes are regular on and outside an event horizon. The simplest solutions arise for free bosonic fields, but generalizations with interacting fields and/or non–minimal couplings are possible and have been studied, *e.g.* [31]. Besides the field's mass, which defines a scale and is set in the action, the space of solutions is conveniently characterised as a two–dimensional domain, spanned by two continuous dimensionless parameters: the ADM mass in units of the field's mass,[2] $M\mu$, and the oscillation frequency of the matter field in units of the field's mass, ω/μ. For each value of $(\omega/\mu, M\mu)$ there is a single BH solution in a certain two–dimensional domain – see Fig. 1. The range of *physical* masses M (say in solar masses) becomes defined after specifying the scale μ.

Actually, the continuous family of solutions just described is only one amongst an infinite discrete set of such continuous families of hairy BHs. This discrete set is labelled by two integers: the number of nodes of the appropriate radial functions, $n \in \mathbb{N}_0$, and the azimuthal harmonic index, $m \in \mathbb{Z}^+$, which, like ω, enters the bosonic field ansatz, $\psi \sim e^{-i\omega t + im\varphi}$. Both n and m can be seen as excitation numbers. Here we shall focus on the fundamental solutions with $(n, m) = (0, 1)$, which are the ones that naturally emerge as the equilibrium configurations from the growth of the dominant superradiant mode in Kerr [19], but some of the excited solutions have also been explicitly constructed – see *e.g.* [32,33].

BHsSH rely on a synchronisation between the event horizon's angular velocity Ω_H and the field's phase angular velocity ω/m, *i.e.* they satisfy the *synchronisation condition*

$$\Omega_H = \frac{\omega}{m}\ . \tag{2}$$

Thus, the $(\omega/\mu, M\mu)$ parameterization of the domain of existence can be equally seen as a $(m\Omega_H/\mu, M\mu)$ parameterization, which is a set of more physically intuitive quantities. Each solution in this

[1] ϵ is the fraction of the initial mass that is extracted in the process.

[2] For clarity we remark that, reinserting units, this dimensionless parameter is $M\mu/M_{\rm Pl}^2$, where $M_{\rm Pl}$ is the Planck mass.

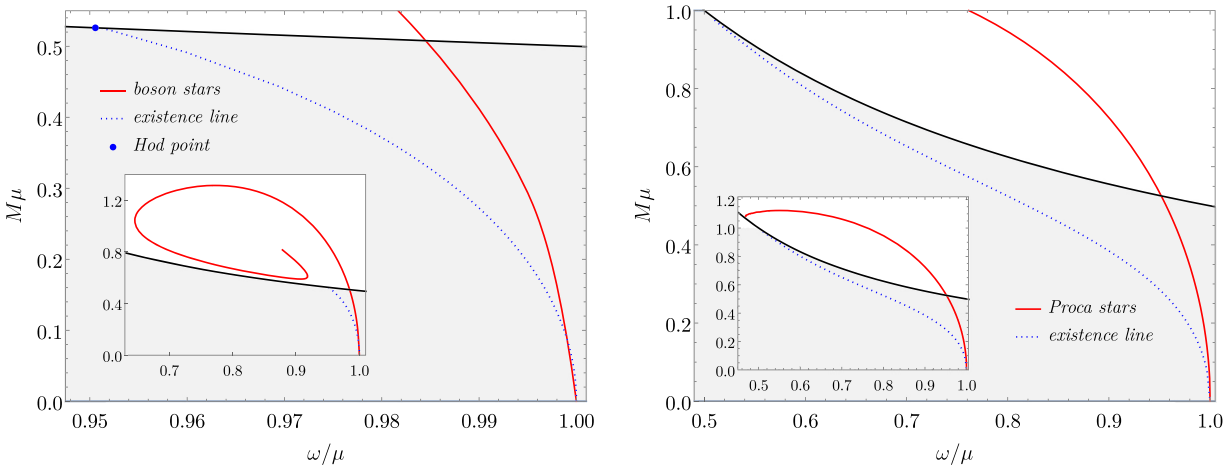

Fig. 1. Region of interest (cf. section 5) of the domain of existence of BHs with synchronised scalar (left panel) and vector (right panel) hair with $(n, m) = (0, 1)$ in the $M\mu$ *vs.* ω/μ plane. The insets in both panels show the full domain of existence.

domain has two extra global quantities, besides the ADM mass: the total angular momentum, $J\mu^2$, and the Noether charge associated with the global $U(1)$ symmetry provided by the complex nature of the bosonic field, $Q\mu^2$. Unlike the mass and angular momentum, the Noether charge is not associated with a Gauss law, meaning it cannot be measured by an observer at infinity. Since the domain of existence is two–dimensional, the three global quantities $(M\mu, J\mu^2, Q\mu^2)$ are not independent, but no simple relation between them is known.

The global charges M and J can be expressed as $M = M_H + M_\psi$ and $J = J_H + J_\psi$, where M_H and J_H (M_ψ and J_ψ) are the energy and angular momentum inside (outside) the event horizon, respectively. These are rigorously defined by Komar integrals – see *e.g.* [20,34]. It is convenient to define the dimensionless total and horizon angular momenta, $j \equiv J/M^2$ and $j_H \equiv J_H/M_H^2$, respectively. BHsSH can violate the Kerr bound, in terms of asymptotic and/or horizon quantities [35], and in fact do so in large extensions of their domain of existence, although their horizon *linear* velocity never exceeds the speed of light [36].

The proportion of energy and angular momentum in the bosonic field (*i.e.* outside the event horizon), for a given solution, is measured by the fractions

$$p \equiv \frac{M_\psi}{M} \,, \quad q \equiv \frac{J_\psi}{J} \,. \tag{3}$$

The quantities p and q measure the *hairiness* of the solutions. Note that $p, q \in [0, 1]$. They reduce to Kerr BHs in equilibrium with linearised bosonic fields when $p, q \to 0$ (*Kerr limit*) and to spinning bosonic stars when $p, q \to 1$ (*solitonic limit*). If a hairy BH is the equilibrium state obtained from the superradiance instability of Kerr, and under the aforementioned assumption of an approximately conservative process, then we identify the efficiency of the process as $\epsilon = p$.

3. Domain of existence

Fig. 1 shows the domain of existence of BHs with synchronised scalar (left panel) and vector (right panel) hair with $(n, m) = (0, 1)$. A detailed comparison between the two families can be found in [37]. The light grey shaded region represents the domain of existence of Kerr BHs in Einstein's gravity, which satisfy the Kerr bound, *i.e.* $j \leqslant 1$. Solutions saturating this bound fall into the black solid line. The domain of existence of BHsSH is bounded by: (i) the *existence line* (blue dotted line), a line segment comprised of solutions describing bound states between Kerr BHs and linearised bosonic fields ($p = q = 0$). This line segment joins the *Minkowski limit* ($M, J \to 0$) to the Kerr bound line. It is half–open, including the upper endpoint only. The latter is known as the *Hod point* [38] and can be found analytically for the scalar case (blue point in the left panel of Fig. 1). And (ii) the *bosonic star line* (red solid line), comprised of solutions describing spinning bosonic stars ($p = q = 1$).

As already discussed, the (dominant mode) superradiant instability of Kerr may form some of the hairy BHs in this domain of existence. This phenomenon occurs whenever the Kerr solution is exposed to a scalar field perturbation for which the field's phase angular velocity satisfies the *superradiant condition* $\omega/m < \Omega_H$. For a massless field, the rotational energy is radiated to infinity, leaving a Kerr BH with lower mass and angular momentum, in fact decreasing j. But for a bosonic field with non–vanishing mass and with a Compton wavelength comparable to, or larger than, the Kerr BH, a *superradiant instability* sets in, driving the configuration to a new equilibrium state (for complex fields).

Kerr BHs which lie to the right of the existence line are unstable when they are perturbed by linearized bosonic fields with the $m = 1$ azimuthal mode. The seed solutions of the evolutions described in [18] were Kerr BHs with initial mass M and dimensionless angular momentum $j = j_H = 0.99$ in the presence of a vector field with mass $M\mu \in \{0.25, 0.30, 0.40, 0.50\}$ and azimuthal number $m = 1$. These Kerr BHs gradually developed hair, attaining equilibrium when the horizon and the field synchronised. The corresponding migrations can be observed in Fig. 5 in [19].

4. Analytic bounds on "hairiness" for $j \leqslant 1$

Hawking's area theorem sets an upper limit of 29% for the efficiency of energy extraction from Kerr BHs by superradiance. This is simple to see. The horizon area of a Kerr BH with mass M_H and angular momentum J_H is $A = 8\pi M_H^2(1 + \sqrt{1 - j_H^2})$ (we recall that $M = M_H$, $J = J_H$ for a vacuum Kerr BH). The irreducible mass $M_{\rm irr}$ is defined as the mass of the Schwarzschild BH that results when all angular momentum has been extracted by reversible transformations, *i.e.* leaving the horizon area unchanged. The area theorem ($\delta A \geqslant 0$) then dictates that $\delta M_{\rm irr} \geqslant 0$. Like the area of the horizon, the irreducible mass remains unchanged (increases) in (ir)reversible transformations.

Starting from a Kerr BH, the maximum amount of energy that can be extracted from it is

$$M_H - M_{\rm irr} = M_H \left[1 - \frac{1}{\sqrt{2}} \left(1 + \sqrt{1 - j_H^2} \right)^{1/2} \right] , \tag{4}$$

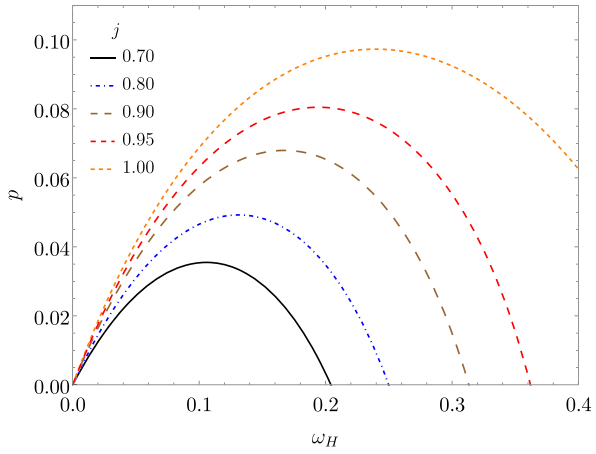

Fig. 2. Fraction of energy in the bosonic hair p according to relation (5).

resulting in a Schwarzschild BH with mass $M_{\rm irr}$. It is therefore possible to extract up to $1-1/\sqrt{2}\approx 29\%$ of the energy, with the upper limit corresponding to an initial extremal Kerr BH ($j_H=1$) and a final Schwarzschild BH. Of thermodynamic nature, this limit applies to any (reversible or irreversible) transformation whereby rotational energy is extracted from a Kerr BH, including superradiance.

In light of this maximal theoretical efficiency, $\epsilon \lesssim 0.29$, BHsSH grown from superradiance have $p\lesssim 0.29$. The simulations in [18] showed, however, only up to 9% of the initial energy is transferred into the (vector) field. Furthermore, they exhibit negligible dissipation. This suggests that the evolution of superradiant instabilities is nearly conservative, *i.e.* preserves the energy M and angular momentum J, thus leaving j almost unchanged. Accordingly, $j\leqslant 1$ should be satisfied throughout the evolution, since it is satisfied by the initial (Kerr BH) state.

It was already suggested in [19] that this upper limit on j places tighter constraints on the hairiness than the thermodynamic limit. This was done using an analytical model proposed therein to describe physical quantities of the hairy BHs which are Kerr–like. According to this model, BHsSH which are sufficiently Kerr–like have a fraction of energy in the bosonic field p obeying

$$p=1+\frac{1-\sqrt{1-16\omega_H^2(j\omega_H-1)^2}}{8\omega_H^2(j\omega_H-1)}\,,\quad \text{where}\ \ \omega_H=M\Omega_H\,. \tag{5}$$

In Fig. 2 we show how p derived from this relation varies with j and ω_H. The analysis shows that $j\leqslant 1$ implies $p\lesssim 0.10$, approximately one third of the thermodynamic bound.

5. A bound on "hairiness" from scanning BHsSH

Instead of using an approximate analytical model, we can in fact use the data on hairy BHs to see how large is p for $j\leqslant 1$. The region of interest, containing BHsSH that could emerge from the superradiant instability of Kerr BHs, is a subset of the domain of existence (shaded light orange in Fig. 3), bounded by two lines: the existence line and the $j=1$ line. These lines meet at the Hod point, which corresponds to an extremal Kerr BH ($j=j_H=1$). The "hairiness" trend is that, for fixed $M\mu$, p increases as ω/μ increases. Since the $p=0.29$ line always lies to the right of the $j=1$ line, the latter sets a tighter (frequency–dependent) upper limit on the hairiness than the former, as expected.

Table 1 lists the properties of BHsSH with $j=1$ and $M\mu\in\{0.25,0.30,0.40,0.50\}$ for both the scalar and vector cases. These illustrative values were chosen to match the ones taken in the simulations in [18], which were carried out for the vector case. According to our assumption that $\epsilon=p$, these are the hairiest solutions with such masses that can be formed from superradiance. For instance, a BH with synchronised scalar (vector) hair has at most about 9.7% (10.4%) of its energy in the field when $M\mu=0.25$. The results in Table 1 are compatible with the findings reported in [18], suggesting in particular that the superradiant amplification of the (vector) field in the maximal efficiency case reported therein, $M\mu=0.25$, is (approximately) as efficient as it can be.

Table 1
"Hairiness" of BHsSH with $(n,m)=(0,1)$ and $j=1$, for selected values of $M\mu$.

	$M\mu$	ω/μ	$M\omega$	p	q
Scalar	0.25	0.9921	0.2480	0.0971	0.3856
	0.30	0.9884	0.2965	0.0951	0.3132
	0.40	0.9774	0.3910	0.0686	0.1669
	0.50	0.9587	0.4794	0.0160	0.0303
Vector	0.25	0.9667	0.2417	0.1035	0.3984
	0.30	0.9496	0.2849	0.1038	0.3259
	0.40	0.9009	0.3604	0.0933	0.2057
	0.50	0.8356	0.4178	0.0738	0.1221

Table 2
Properties of the "hairiest" BHsSH with $(n,m)=(0,1)$ which are comparable to Kerr BHs (*i.e.* obey $j\leqslant 1$). These are characterised by $j=1$ and are pinpointed as black circles in Fig. 3.

Model	$M\mu$	ω/μ	$M\omega$	p	q	j_H
Scalar [21]	0.2445	0.9925	0.2426	0.0989	0.4010	0.7367
Vector [20]	0.2761	0.9584	0.2646	0.1042	0.3621	0.7981
Analytical [19]	–	–	0.2393	0.0973	0.4067	0.7282

A more comprehensive analysis is provided in Fig. 4. Starting from the Hod point, p increases as one moves downstream along the $j=1$ line, reaching a maximum and then decreasing towards the Minkowski limit. Solutions with fixed j values below unity show a similar behaviour. The maximum occurs at larger (lower) values of ω/μ (ω_H) as j decreases. The global maximum of p occurs at $M\mu\approx 0.24$ (0.27) and it is about 0.099 (0.104) in the scalar (vector) case, as shown in Table 2, corresponding to the values reported in Eq. (1). This suggests the maximal efficiency is not very sensitive to the spin of the bosonic field. The corresponding solutions satisfy the Kerr bound in terms of horizon quantities as well. Table 2 also shows they are well described by the analytical model introduced in [19], valid for any bosonic field.

6. Remarks

Some final remarks are in order. Firstly, this new (tighter) upper bound on the "hairiness" of BHsSH grown from superradiance (those represented by the region of interest) does not exclude the possibility that hairier BHs can appear from other dynamical formation channels, such as the merger of bosonic stars [39]. That is, the region of *dynamically viable solutions*, corresponding to those that can form by some mechanism and be sufficiently long–lived, can go beyond the region of interest discussed here.

Secondly, BHsSH in the region of interest can be arbitrarily close to Kerr BHs and therefore are quite Kerr–like: they are more accurately described as event horizons surrounded by a bosonic cloud rather than bosonic stars with an event horizon at its centre [37]. For instance, the areal radius of their shadow is at most 11% larger than that of comparable Kerr BHs [40].

Thirdly, like Kerr BHs, BHsSHs are prone to their own superradiant instability [22]. At fixed m, they are unstable against bosonic field modes with $\tilde{m}>m$. For constant $M\mu$, the strength of the instability decreases as the BHs become hairier (*i.e.* as one moves away from the existence line) [23]. In the region of interest, it is

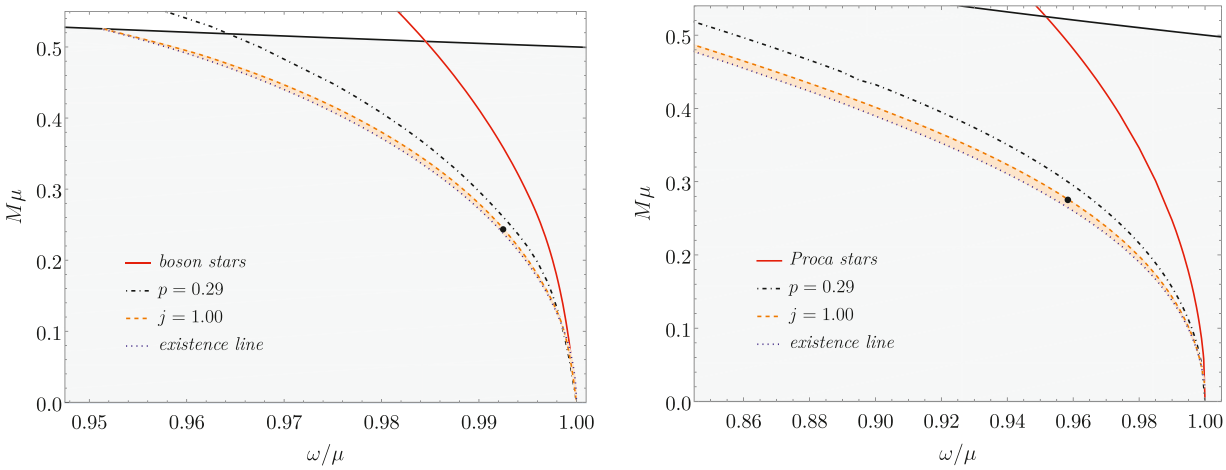

Fig. 3. Same as in Fig. 1, but with two additional lines: the dash–dotted black line separates BHsSH with less (to the left) and more (to the right) than 29% of the total energy in bosonic field, whereas the dashed orange line separates BHsSH satisfying (to the left) and violating (to the right) the Kerr bound. The light orange shaded region comprises BHsSH which satisfy this bound. The black circles represent the "hairiest" solutions in the region of interest (cf. Table 2).

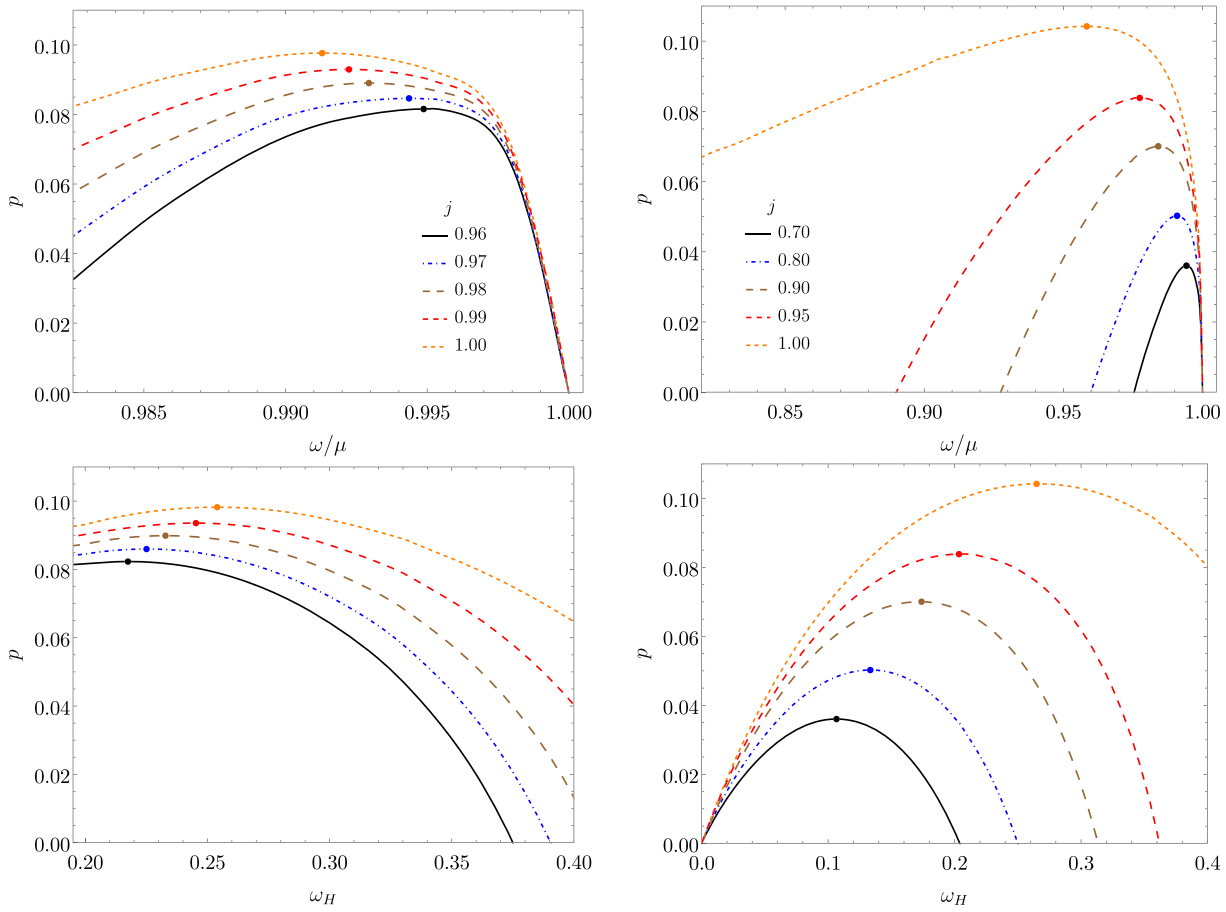

Fig. 4. Fraction p of the total energy contained in the bosonic field of BHs with synchronised scalar (left panels) and vector (right panels) hair for selected values of j. The top (bottom) panels show the dependence of p on ω/μ ($\omega_H = M\Omega_H$). The circles pinpoint the corresponding maximum.

minimum for BHs on the $j = 1$ line. If the timescale of the instability is larger than the age of the Universe, the hairy BH is effectively stable [23]. Effective stability is expected to occur for $M\mu \lesssim 0.25$. Interestingly, the "hairiest" BHs are characterised by $M\mu \approx 0.25$ (see Table 2) and thus might be stable on cosmological timescales, for the appropriate mass range.

Finally, let us comment on three potential limitations of our approach. The first one is that we have assumed that the evolution from Kerr into a hairy BH is conservative, unaltering j. If that would not be the case, and some of the system's energy is dissipated towards infinity by gravitational waves or gravitational cooling [41] (*i.e.* ejection of the bosonic field), would this challenge the bound? For the Kerr BH, superradiance with dissipation (*e.g.* via the scattering of a massless bosonic field), has a net effect of increasing the reduced area A/M^2. This implies a reduction of j. Thus, it seems likely that also for the hairy BHs any dissipation will reduce j further. Accordingly, the bound obtained under the assumption of a non–dissipative evolution is a robust, conservative

bound. The second potential limitation is that we have obtained the bound (1) from a specific set of solutions of BHsSH, namely those of the simplest bosonic model, without self–interactions. If we allow for self–interactions, is the bound significantly affected? Since the bosonic field is small in the region of interest, as it is very close to the existence line (cf. Fig. 3), any non–linearities will be negligible. Thus, we expect this bound to be universal, in the sense of also applying to models with generic self–interactions. Indeed, a preliminary investigation of the results reported in [31] confirms this expectation. That work studied BHsSH in a model with a massive complex scalar field with a *quartic* self–interaction, while the case of synchronised BH solutions with a self–interacting vector field has not yet been considered in the literature. As a final possible limitation, we have only considered isolated BHs, avoiding the issue of accretion. Accretion is known to spin up BHs and thus it may counter–act the effect of superradiance – see *e.g.* [39,42]. Our bound, however, is obtained for BHs with $j = 1$. For the Kerr case, this means no further accretion is possible. A similar sharp statement cannot be applied for the hairy BHs, since j can exceed unity. Yet, since these are Kerr–like BHs, it seems plausible that the impact of accretion may be small.

Declaration of competing interest

The authors declare that they have no known competing financial interests or personal relationships that could have appeared to influence the work reported in this paper.

Acknowledgements

This work is supported by the Center for Astrophysics and Gravitation (CENTRA) and by the Center for Research and Development in Mathematics and Applications (CIDMA) through the Portuguese Foundation for Science and Technology (FCT – Fundação para a Ciência e a Tecnologia), references UIDB/00099/2020, UIDB/04106/2020 and UIDP/04106/2020, and by national funds (OE), through FCT, I.P., in the scope of the framework contract foreseen in the numbers 4, 5 and 6 of the article 23, of the Decree-Law 57/2016, of August 29, changed by Law 57/2017, of July 19. The authors acknowledge support from the projects CERN/FIS-PAR/0027/2019 and PTDC/FIS-AST/3041/2020. N. M. Santos is supported by the FCT grant SFRH/BD/143407/2019. This work has further been supported by the European Union's Horizon 2020 research and innovation (RISE) programme H2020-MSCA-RISE-2017 Grant No. FunFiCO-777740.

References

[1] K. Akiyama, et al., First M87 Event Horizon Telescope results. I. The shadow of the supermassive black hole, Astrophys. J. 875 (1) (2019) L1.
[2] B.P. Abbott, et al., Observation of gravitational waves from a binary black hole merger, Phys. Rev. Lett. 116 (6) (2016) 061102.
[3] B.P. Abbott, et al., GWTC-1: a gravitational-wave transient catalog of compact binary mergers observed by LIGO and Virgo during the first and second observing runs, Phys. Rev. X 9 (3) (2019) 031040.
[4] R. Abbott, et al., GWTC-2: compact binary coalescences observed by LIGO and Virgo during the first half of the third observing run, Phys. Rev. X 11 (2021) 021053.
[5] R.P. Kerr, Gravitational field of a spinning mass as an example of algebraically special metrics, Phys. Rev. Lett. 11 (1963) 237–238.
[6] B. Carter, Axisymmetric black hole has only two degrees of freedom, Phys. Rev. Lett. 26 (1971) 331–333.
[7] D.C. Robinson, Uniqueness of the Kerr black hole, Phys. Rev. Lett. 34 (1975) 905–906.
[8] P.T. Chrusciel, J. Lopes Costa, M. Heusler, Stationary black holes: uniqueness and beyond, Living Rev. Relativ. 15 (2012) 7.
[9] J.D. Bekenstein, Transcendence of the law of baryon-number conservation in black hole physics, Phys. Rev. Lett. 28 (1972) 452–455.
[10] C.A.R. Herdeiro, E. Radu, Asymptotically flat black holes with scalar hair: a review, Int. J. Mod. Phys. D 24 (09) (2015) 1542014.
[11] R. Ruffini, J.A. Wheeler, Introducing the black hole, Phys. Today 24 (1) (1971) 30.
[12] R. Penrose, Gravitational collapse and space-time singularities, Phys. Rev. Lett. 14 (1965) 57–59.
[13] S.W. Hawking, R. Penrose, The singularities of gravitational collapse and cosmology, Proc. R. Soc. Lond. A 314 (1970) 529–548.
[14] R. Brito, V. Cardoso, P. Pani, Superradiance: New Frontiers in Black Hole Physics, Lect. Notes Phys., vol. 906, 2015, pp. 1–237.
[15] A. Arvanitaki, S. Dubovsky, Exploring the string axiverse with precision black hole physics, Phys. Rev. D 83 (2011) 044026.
[16] K.K.Y. Ng, S. Vitale, O.A. Hannuksela, T.G.F. Li, Constraints on ultralight scalar bosons within black hole spin measurements from the LIGO-Virgo GWTC-2, Phys. Rev. Lett. 126 (15) (2021) 151102.
[17] C. Yuan, R. Brito, V. Cardoso, Probing ultralight dark matter with future ground-based gravitational-wave detectors, Phys. Rev. D 104 (4) (2021) 044011.
[18] W.E. East, F. Pretorius, Superradiant instability and backreaction of massive vector fields around Kerr black holes, Phys. Rev. Lett. 119 (4) (2017) 041101.
[19] C.A.R. Herdeiro, E. Radu, Dynamical formation of Kerr black holes with synchronized hair: an analytic model, Phys. Rev. Lett. 119 (26) (2017) 261101.
[20] C. Herdeiro, E. Radu, H. Rúnarsson, Kerr black holes with Proca hair, Class. Quantum Gravity 33 (15) (2016) 154001.
[21] C.A.R. Herdeiro, E. Radu, Kerr black holes with scalar hair, Phys. Rev. Lett. 112 (2014) 221101.
[22] B. Ganchev, J.E. Santos, Scalar hairy black holes in four dimensions are unstable, Phys. Rev. Lett. 120 (17) (2018) 171101.
[23] J.C. Degollado, C.A.R. Herdeiro, E. Radu, Effective stability against superradiance of Kerr black holes with synchronised hair, Phys. Lett. B 781 (2018) 651–655.
[24] T.J.M. Zouros, D.M. Eardley, Instabilities of massive scalar perturbations of a rotating black hole, Ann. Phys. 118 (1979) 139–155.
[25] S.L. Detweiler, Klein-Gordon equation and rotating black holes, Phys. Rev. D 22 (1980) 2323–2326.
[26] A. Suárez, V.H. Robles, T. Matos, A review on the scalar field/Bose-Einstein condensate dark matter model, Astrophys. Space Sci. Proc. 38 (2014) 107–142.
[27] L. Hui, J.P. Ostriker, S. Tremaine, E. Witten, Ultralight scalars as cosmological dark matter, Phys. Rev. D 95 (4) (2017) 043541.
[28] A. Arvanitaki, S. Dimopoulos, S. Dubovsky, N. Kaloper, J. March-Russell, String axiverse, Phys. Rev. D 81 (2010) 123530.
[29] F.F. Freitas, C.A.R. Herdeiro, A.P. Morais, A. Onofre, R. Pasechnik, E. Radu, N. Sanchis-Gual, R. Santos, Ultralight bosons for strong gravity applications from simple Standard Model extensions, Jul. 2021.
[30] S.W. Hawking, Gravitational radiation from colliding black holes, Phys. Rev. Lett. 26 (1971) 1344–1346.
[31] C.A.R. Herdeiro, E. Radu, H. Rúnarsson, Kerr black holes with self-interacting scalar hair: hairier but not heavier, Phys. Rev. D 92 (8) (2015) 084059.
[32] Y.-Q. Wang, Y.-X. Liu, S.-W. Wei, Excited Kerr black holes with scalar hair, Phys. Rev. D 99 (6) (2019) 064036.
[33] J.F.M. Delgado, C.A.R. Herdeiro, E. Radu, Kerr black holes with synchronised scalar hair and higher azimuthal harmonic index, Phys. Lett. B 792 (2019) 436–444.
[34] C. Herdeiro, E. Radu, Construction and physical properties of Kerr black holes with scalar hair, Class. Quantum Gravity 32 (14) (2015) 144001.
[35] J.F.M. Delgado, C.A.R. Herdeiro, E. Radu, Violations of the Kerr and Reissner-Nordström bounds: horizon versus asymptotic quantities, Phys. Rev. D 94 (2) (2016) 024006.
[36] C.A.R. Herdeiro, E. Radu, How fast can a black hole rotate?, Int. J. Mod. Phys. D 24 (12) (2015) 1544022.
[37] N.M. Santos, C.L. Benone, L.C.B. Crispino, C.A.R. Herdeiro, E. Radu, Black holes with synchronised Proca hair: linear clouds and fundamental non-linear solutions, J. High Energy Phys. 07 (2020) 010.
[38] S. Hod, Stationary scalar clouds around rotating black holes, Phys. Rev. D 86 (2012) 104026, Erratum: Phys. Rev. D 86 (2012) 129902.
[39] N. Sanchis-Gual, M. Zilhão, C. Herdeiro, F. Di Giovanni, J.A. Font, E. Radu, Synchronized gravitational atoms from mergers of bosonic stars, Phys. Rev. D 102 (10) (2020) 101504.
[40] P.V.P. Cunha, C.A.R. Herdeiro, E. Radu, EHT constraint on the ultralight scalar hair of the M87 supermassive black hole, Universe 5 (12) (2019) 220.
[41] E. Seidel, W.-M. Suen, Formation of solitonic stars through gravitational cooling, Phys. Rev. Lett. 72 (1994) 2516–2519.
[42] R. Brito, V. Cardoso, P. Pani, Black holes as particle detectors: evolution of superradiant instabilities, Class. Quantum Gravity 32 (13) (2015) 134001.

Chapter 5

Reprint of *Phys. Rev. D* 106 (2022) 12

Thermodynamic stability of quasibald asymptotically flat black holes

Nuno M. Santos,[1,2,*] Carlos A. R. Herdeiro,[1,†] and Eugen Radu[1,‡]

[1]*Department of Mathematics, Centre for Research and Development in Mathematics and Applications (CIDMA), University of Aveiro, 3810–193 Aveiro, Portugal*

[2]*Departamento de Física, Instituto Superior Técnico—IST, Universidade de Lisboa—UL, Avenida Rovisco Pais 1, 1049–001 Lisboa, Portugal*

(Received 27 July 2022; accepted 7 November 2022; published 2 December 2022)

The local thermodynamic stability of a black hole (BH) in the canonical ensemble is defined by the positivity of the specific heat at constant global charges. Schwarzschild BHs in thermodynamic equilibrium with an energy reservoir are always unstable against small fluctuations of energy, whereas sufficiently near-extremal Reissner-Nordström/Kerr BHs are stable. One could expect that asymptotically flat hairy BHs branching off from such stable phases would also be, by continuity, locally thermodynamically stable for vanishingly little hair. We show this is not the case in some models, including scalarized BHs bifurcating from Reissner-Nordström and spinning BHs with synchronized hair bifurcating from Kerr. Specifically, it is found that quasibald BHs are locally thermodynamically unstable in the canonical ensemble for all global charges and regardless of being dynamically and entropically preferred over bald ones at fixed global charges.

DOI: 10.1103/PhysRevD.106.124005

I. INTRODUCTION

In 1973, Bardeen *et al.* formulated the four laws of black-hole mechanics [1] and noticed that the surface gravity κ and area A of the (spatial sections of the) event horizon of a stationary black hole (BH) bore a remarkable resemblance to temperature and entropy in classical thermodynamics, respectively. Soon after, Hawking made the remarkable discovery that BHs emit particles at a steady rate as if they were black bodies with temperature $T = \kappa/(2\pi)$ [2,3]. These four laws of black-hole mechanics are not mere analogies with the standard laws of thermodynamics; they actually describe BHs as thermodynamic systems. It is therefore natural to ask whether BHs are thermodynamically stable or not.

Thermodynamic stability can be local or global. Local stability refers to whether a certain equilibrium phase of a system corresponds to a *local* maximum of the entropy. It concerns the system's response to small fluctuations, determined by its thermodynamic variables under some fixed quantities, which amounts to a choice of ensemble. A system is said to be in a locally stable phase if any fluctuations produce a counteracting effect that ends up restoring the thermodynamic equilibrium. Global stability, on the other hand, refers to whether a certain equilibrium phase of a system corresponds to a *global* maximum of the entropy.

The local stability can be monitored by linear response functions such as the specific heat C. The specific heat dictates how much a system's temperature changes when it absorbs heat from the environment. Consider, for instance, a Schwarzschild BH with mass M at temperature $T = 1/(8\pi M)$ in contact with a heat reservoir R at fixed temperature T_R. Its specific heat is negative, $C = -1/(8\pi T)$. If $T < T_R$ (say), the BH will absorb energy from R. As a result, its temperature will decrease. Thus, the system runs away from thermal equilibrium and is (locally) unstable from a thermodynamic viewpoint. It is worth emphasizing that, in general, the thermodynamic stability of a family of BHs does not provide any information about its (linear) dynamical stability [4,5]. For instance, Schwarzschild BHs can be dynamically stable while being thermodynamically unstable.

In general, however, the BH may have nonvanishing electric charge Q and/or angular momentum J. Suppose now that a Kerr-Newman BH can exchange energy (at fixed temperature), but not electric charge nor angular momentum, with the reservoir (i.e., Q and J are kept fixed). This is the "canonical ensemble." The local thermodynamic stability is then characterized by the positivity of the specific heat at constant Q and J,

$$C_{Q,J} = \left(\frac{\partial M}{\partial T}\right)_{Q,J} = T\left(\frac{\partial S}{\partial T}\right)_{Q,J}, \tag{1.1}$$

where S is the BH entropy. As it turns out, there is a continuity with the Schwarzschild phase: the specific heat (at constant electric charge and angular momentum) is negative for sufficiently small Q *and* J. However, if [6]

*nunomoreirasantos@tecnico.ulisboa.pt
†herdeiro@ua.pt
‡eugen.radu@ua.pt

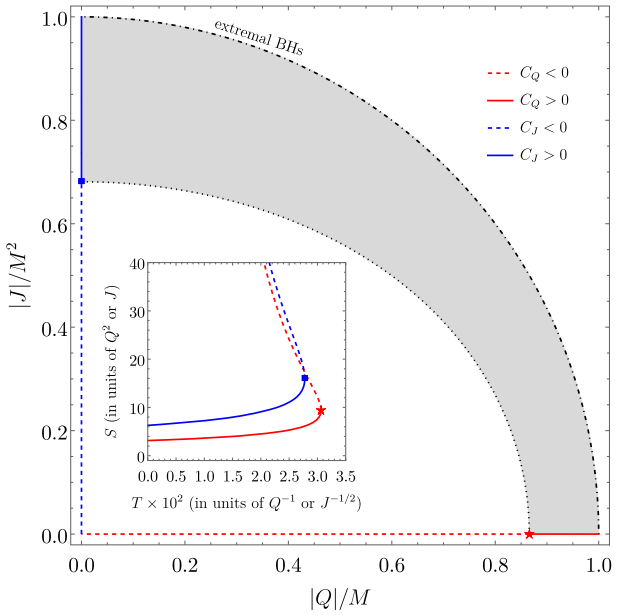

FIG. 1. Local thermodynamic stability of Kerr-Newman BHs in the canonical ensemble. Sign of the specific heat at constant electric charge Q and angular momentum J in the plane $(|Q|/M, |J|/M^2)$: $C_{Q,J} < 0$ in the (inner) white region, whereas $C_{Q,J} > 0$ in the gray region. Inset: entropy of Reissner-Nordström and Kerr BHs as a function of their temperature. The markers in both plots refer to Reissner-Nordström (red star) and Kerr (blue square) BHs with diverging specific heat.

$$J^4 + 6J^2M^4 + 4Q^2M^6 - 3M^8 > 0, \tag{1.2}$$

it becomes positive and the system becomes locally thermodynamically stable (in this ensemble). This corresponds to the gray region in Fig. 1. For Reissner-Nordström BHs ($J = 0$), this occurs when $\sqrt{3}M/2 < |Q| < M$ (horizontal red solid line). For Kerr BHs ($Q = 0$), on the other hand, it holds for $\sqrt{2\sqrt{3} - 3}M^2 < |J| < M^2$ (vertical blue solid line). For ease of notation, hereafter $C_Q \equiv C_{Q,J=0}$ and $C_J \equiv C_{Q=0,J}$. The sign of the specific heat can be inferred from the curve $S = S(T)$ for fixed Q and/or J. The inset of Fig. 1 shows the entropy of Reissner-Nordström and Kerr BHs as a function of their temperature. The black dotted line (in the main panel), together with the markers (in both panels), correspond to BHs with diverging specific heat, separating the stable and unstable phases. Such infinite discontinuity is commonly associated with second-order phase transitions.

The above description exhausts the discussion concerning electrovacuum BHs in the canonical ensemble. In the last few years, however, a number of non-Kerr-Newman (but still asymptotically flat) BHs became popular. They possess new macroscopic degrees of freedom not associated with gauge charges and collectively referred to as "hair"—see e.g., [7]. In particular, some of these models branch off from the Kerr-Newman family, thus being continuously connected to the electrovacuum BHs. In this context, one might wonder if a similar thermodynamic picture holds for asymptotically flat hairy BHs continuously connected to BHs in general relativity (GR)—i.e., are hairy BHs branching off from locally thermodynamically stable GR BHs also locally thermodynamically stable (in the same statistical ensemble)? By continuity, it seems intuitive that the answer should be positive for BHs with little hair. Indeed, this is what one observes in the Kerr-Newman family: adding Q (J) to Kerr (Reissner-Nordström) BHs, the Kerr-Newman solutions retain a positive specific heat in the neighborhood of Kerr (Reissner-Nordström) BHs with positive specific heat. However, the addition of hair (rather than global charges associated with gauge symmetries) can spoil the local thermodynamic stability of such electrovacuum BHs. In other words, locally thermodynamically stable GR BHs may become unstable when they grow (even very little) hair.

Asymptotically flat hairy BHs (in and beyond GR) may emerge from the reconsideration of the assumptions of no-hair theorems [7]. In the theories of relevance here, bald and hairy BHs coexist and, at some scales, the former become unstable to forming hair and evolve into the latter. In other words, such hairy BHs have a dynamical formation mechanism and are continuously connected to GR BHs in the linear limit of the theories (when the hair is vanishingly little) [8]. To address the question of local thermodynamic stability of such hairy BHs, two illustrative families will be considered here, both defined by the action

$$\mathcal{S} = \frac{1}{16\pi}\int \mathrm{d}^4x\sqrt{-g}R + \mathcal{S}_{\mathrm{M}}, \tag{1.3}$$

where R is the Ricci scalar of the metric g_{ab} with determinant g, $\mathcal{S}_{\mathrm{M}} = \int \mathrm{d}^4x\mathcal{L}_{\mathrm{M}}$ is the action for the matter field(s) and $\mathcal{L}_{\mathrm{M}} = \sqrt{-g}\hat{\mathcal{L}}_{\mathrm{M}}$ is the corresponding Lagrangian density ($\hat{\mathcal{L}}_{\mathrm{M}}$ is a scalar).

The first family comprises scalarized BHs in Einstein-Maxwell-scalar (EMS) theories [9–13]. These describe a massless real scalar field ϕ minimally coupled to Einstein's gravity and nonminimally coupled to Maxwell's electromagnetism, $\hat{\mathcal{L}}_{\mathrm{M}} = -2g^{ab}\phi_{;a}\phi_{;b} - f(\phi)\mathcal{I}$, where $\mathcal{I} = F_{ab}F^{ab}$, $F = \mathrm{d}A$ is the Maxwell tensor and $f(\phi)$ is a coupling function. For a judicious choice of $f(\phi)$, EMS theories admit both GR and scalarized BHs. In particular, the former can undergo spontaneous scalarization and become hairy (similar to neutron stars in scalar-tensor theories [14]).

The second family is composed of BHs with synchronized hair [15,16]. They are found in theories featuring a massive complex bosonic field minimally coupled to Einstein's gravity: $\hat{\mathcal{L}}_{\mathrm{M}} = -\Psi^*_{;a}\Psi^{;a} - \mu^2|\Psi|^2$ for a scalar field Ψ with mass μ, whereas $\hat{\mathcal{L}}_{\mathrm{M}} = -F^{ab}F^*_{ab}/4 - \mu^2A^aA^*_a/2$ for a vector field A with mass μ. Here, the asterisk denotes complex conjugation. In either case, BHs with synchronized hair coexist with Kerr BHs. At some scales, Kerr BHs

become unstable against superradiance, which results in the transfer of energy and angular momentum to a bosonic cloud orbiting the BH [8].

It is convenient to sketch the similarities and differences between the two families of hairy BHs. Scalarized BHs bear some resemblance with BHs with synchronized hair in the sense that they emerge from the growth and saturation of an instability. The instability (tachyonic for scalarized BHs and superradiant for BHs with synchronized hair) is present in the linear limit of the theory and is responsible for the development of hair when nonlinear effects are taken into account. Besides, both types of BHs are dynamically preferred over their bald counterparts. In fact, they are entropically favored, i.e., they maximize the entropy of the system in the microcanonical ensemble, i.e., for fixed global charges (M, Q, J).

There are, however, some differences one should note. While BHs with synchronized hair reduce to bosonic stars in the limit of vanishing horizon size, some EMS theories of scalarized BHs do not possess solitons, as established by some no-go theorems [17]. Even when they do, the solitons may not be continuously connected with the hairy BHs [18]. Another important distinction between the two families concerns the symmetries of the bosonic field. In the EMS theories, the scalar field shares the symmetries with the spacetime. As for BHs with synchronized hair, although the spacetime is stationary and axisymmetric, the bosonic field depends explicitly on time (but, since it is complex, the corresponding energy-momentum tensor is time independent). Finally, BHs with synchronized hair appear in models with a global $U(1)$ symmetry, which makes the hair *primary*, measured by a conserved (in the sense of a continuity equation) Noether charge. By contrast, the hair in scalarized BHs is *secondary* and the corresponding scalar "charge" is not conserved in any meaningful sense.

The thermodynamics of asymptotically flat hairy BHs is still poorly explored. Most studies focus on the thermodynamic stability in the microcanonical ensemble. The purpose of this paper is to provide an investigation of the local thermodynamic stability of the aforementioned families of hairy BHs in the canonical ensemble. Their specific heat (at constant global charges) is computed numerically and found to be negative for quasi-GR BHs, regardless of their specific electric charge or angular momentum.

II. SCALARIZED BLACK HOLES

In EMS theories, the equation of motion for the scalar field reads $\Box\phi = f_{,\phi}\mathcal{I}/4$. $\phi = 0$ solves the equation of motion if $f_{,\phi}(0) = 0$, in which case GR BHs remain solutions. However, they are not unique in general and coexist with BHs with a nontrivial scalar field (or "scalar hair"). These are usually dubbed "scalarized BHs."

One requires scalarized BHs to be continuously connected to GR BHs (i.e., the former reduce to the latter in the linear limit of the theory). These fall into subclass IIA in [10]. Such bifurcation may arise when GR BHs are afflicted by a linear tachyonic instability. The linearized Klein-Gordon equation reads $(\Box - \mu_{\rm eff}^2)\phi = 0$, with $\mu_{\rm eff}^2 = f_{,\phi\phi}(0)\mathcal{I}/4$. The coupling function together with the source term $\mathcal{I}$ act like a negative contribution to the field's mass provided that $f_{,\phi\phi}(0)\mathcal{I} < 0$. In that case, GR BHs become unstable to growing hair. For a purely electric field, $\mathcal{I} < 0$ and the previous inequality reduces to $f_{,\phi\phi}(0) > 0$. Some possible choices for the coupling function are then [10] exponential coupling, $f_E(\phi) = e^{-\alpha\phi^2}$ [9,11]; hyperbolic cosine coupling, $f_C(\phi) = \cosh(\sqrt{-2\alpha}\phi)$ [11]; and power coupling, $f_P(\phi) = 1 - \alpha\phi^2$ [11,19]. α will be referred to as the coupling constant and must be negative so that $f_{,\phi\phi}(0) > 0$. When $\alpha < 0$, f_E, f_C and f_P are monotonically increasing functions of ϕ.

Any static, spherically symmetric solution to the equations of motion can be cast in the form

$$ds^2 = -N(r)e^{-2\delta(r)}dt^2 + \frac{dr^2}{N(r)} + r^2(d\theta^2 + \sin^2\theta d\varphi^2), \tag{2.1}$$

in Schwarzschild coordinates (t, r, θ, φ), where $N(r) \equiv 1 - 2m(r)/r$ and $m(r)$ is the Misner-Sharp mass function, which can be regarded as the quasilocal mass contained within a sphere of radius r. Spherical symmetry imposes an electrostatic 4-vector potential (in the absence of a magnetic charge) as well as a radial-dependent scalar field, i.e., $A_a dx^a = V(r)dt$ and $\phi = \phi(r)$, where V is the electrostatic potential.

One assumes the existence of an event horizon at $r = r_H$, which is the largest root of N. The boundary conditions for m, δ, V and ϕ at the event horizon are found by requiring them to have a regular Taylor series at $r = r_H$, with $r_H = 2m(r_H)$, $\delta(r_H) = \delta_0$, $V(r_H) = 0$ and $\phi(r_H) = \phi_0$, where the gauge condition $V(r_H) = 0$ was imposed. In addition to $\{\alpha, \delta_0, \phi_0\}$, the solutions are characterized by the Arnowitt-Deser-Misner (ADM) mass M, the electric charge Q, the scalar charge Q_s and the (asymptotic) electrostatic potential Φ. When $\phi = 0$, all nonsingular (on and outside the event horizon) asymptotically flat, electrically charged BHs belong to the Reissner-Nordström family of BHs.

The BH entropy and temperature are

$$S = \pi r_H^2, \qquad T = \frac{e^{-\delta_0}}{4\pi r_H}\left[1 - \frac{Q^2}{r_H^2 f(\phi_0)}\right]. \tag{2.2}$$

Since the temperature cannot be negative, $r_H^2 f(\phi_0) \geq Q^2$. The mass M, the electric charge Q, the electrostatic potential Φ, the entropy S and the temperature T satisfy the Smarr relation $M = 2TS + \Phi Q$, the first law of BH mechanics being $dM = TdS + \Phi dQ$, and, what is more, the nonlinear relation $M^2 + Q_s^2 = 4T^2S^2 + Q^2$.

An important feature of these scalarized BHs is that the electric charge Q does not necessarily coincide with the

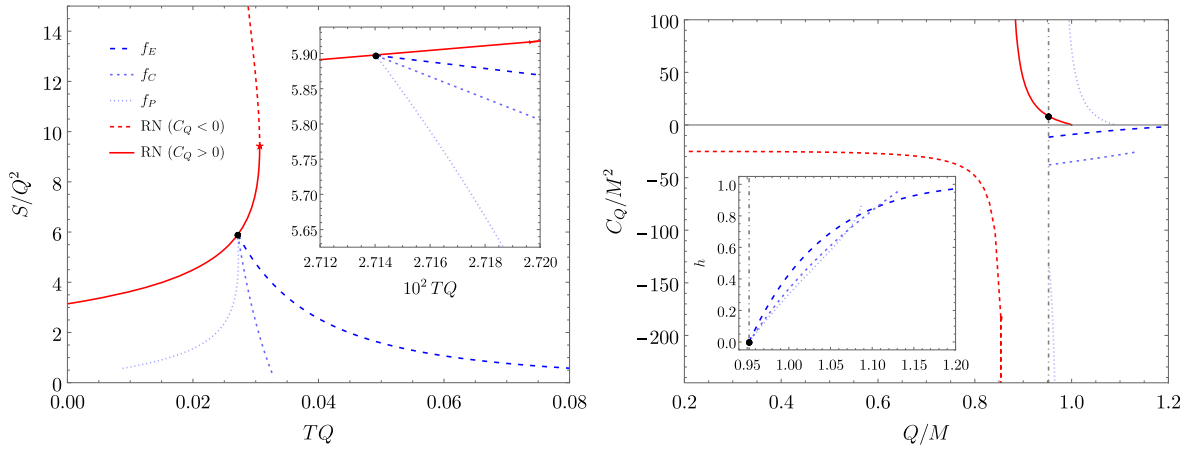

FIG. 2. Left: entropy of the scalarized BHs with $Q = 0.4$ as a function of their temperature, for different coupling functions. The inset shows the behavior of the curves close to the bifurcation point (black dot). Right: specific heat at constant electric charge of Reissner-Nordström (RN) BHs with $Q = 0.4$ as a function of their charge-to-mass ratio Q/M. The vertical dot-dashed line corresponds to the charge-to-mass ratio of the bifurcation point. The inset shows the hairiness h defined in Eq. (2.3).

electric charge *on* the event horizon Q_H. The latter is simply $Q_H = Q/f(\phi_0)$, which suggests that the nonminimal coupling between the scalar field and the 4-vector potential results in electric charge outside the event horizon. It is convenient to introduce the "hairiness" parameter

$$h \equiv 1 - \frac{Q_H}{Q} = 1 - \frac{1}{f(\phi_0)}, \tag{2.3}$$

which measures (through ϕ_0) the fraction of electric charge outside the event horizon (or, loosely speaking, how hairy a scalarized BH is). Note that $h \in [0, 1)$. In the linear limit of the theory ($\phi_0 = 0$), $f(\phi_0) = 1$, $Q = Q_H$ and $h = 0$.

A. Tachyonic instability and domain of existence

When $f_{,\phi\phi}(0) > 0$, the source term $\mathcal{I} = F_{ab}F^{ab}$ provides the scalar field with an imaginary (effective) mass, triggering a tachyonic instability. Such instability may arise even for a test field $\phi = \delta\phi$, with $|\delta\phi|M \ll 1$, turning Reissner-Nordström BHs unstable.

The scalar-free solutions at the onset of the tachyonic instability form an "existence line" on the plane defined by $(\alpha, |Q|/M)$. Since the second-order Taylor expansion of f_E and f_C around $\phi = 0$ coincides with f_P, the existence line is the same for the coupling functions considered herein. For each α, scalarized BHs branch off from the existence line and always have a charge-to-mass $|Q|/M$ ratio greater than that of the Reissner-Nordström BH at the bifurcation point. Moreover, they can exceed the usual extremal limit and have $Q^2 > M^2$. The solution space of scalarized BHs for the different couplings is qualitatively similar and can be found in [11]. Besides the existence line, it is bounded by a "critical line" composed of singular solutions, with vanishing entropy.

B. Local thermodynamic stability

As mentioned in Sec. I, Reissner-Nordström BHs with sufficiently small (large) electric charge-to-mass ratio Q/M are locally thermodynamically unstable (stable) in the canonical ensemble, i.e., their specific heat at constant electric charge C_Q is negative (positive). The state of affairs changes with the addition of a scalar field nonminimally coupled to electromagnetism to the theory. Scalarized BHs always have negative specific heat (at constant electric charge) in the linear limit, i.e., when $\phi_0 \to 0$, as we shall now discuss. This means scalarized BHs cannot be a local minimum of the action and therefore must have a negative mode [20], despite being dynamically preferred.

The blue lines in both panels of Fig. 2 correspond to scalarized BHs with $Q = 0.4$ for the different coupling functions. The value of the coupling constant ($\alpha = -2$) was chosen so that scalarized BHs bifurcate from locally thermodynamically stable Reissner-Nordström BHs. ϕ_0 (and thus h) increases monotonically as one moves down along the blue lines (see inset in the right panel of Fig. 2), signaling hairier and hairier BHs. The lines appear to terminate at singular solutions with vanishing entropy. The limiting behavior of the temperature differs: it appears to diverge for $f = f_E$, to tend to a nonvanishing finite value for $f = f_C$ and to vanish for $f = f_P$.[1] This distinction is

[1]In the latter case, because the temperature starts decreasing as the scalarized BHs become smaller and smaller, one could say that their behavior is akin to that of extremal Reissner-Nordström BHs. However, it should be kept in mind that extremal Reissner-Nordström BHs, having a finite entropy, are not singular. One can show in particular that these theories do not admit the near-horizon geometry of extremal Reissner-Nordström BHs as a solution.

connected to the higher-order terms in ϕ^2 of the Taylor expansion of f_E and f_C.

At first sight, the left panel of Fig. 2 may suggest that the specific heat is negative for scalarized BHs with exponential and hyperbolic cosine coupling to electromagnetism, but positive for those with a power coupling. On closer inspection (see inset in the left panel of Fig. 2), though, it becomes clear that the latter has negative specific heat in the linear limit. This indicates that the curve $S = S(T)$ goes through a point with infinite derivative (corresponding to a BH with diverging specific heat, and thus a second-order phase transition) and "turns around" at this point. $S(T)$ is then a multivalued function for $f = f_P$. Close to the critical temperature $T_c Q \approx 0.027$, the specific heat is characterized by the power-law $C_Q \propto (T - T_c)^k$, where the critical exponent k is $-1/2$, with a deviation below 1.5%. The specific heat at constant electric charge $Q = 0.4$ of Reissner-Nordström and scalarized BHs is shown in the right panel of Fig. 2. As the charge-to-mass ratio approaches its maximum value, it vanishes for $f = f_E, f_P$ and tends to a nonvanishing finite value for $f = f_C$.

Consider the case of the Reissner-Nordström BH at the point of intersection of the two sets of solutions (black dot in Fig. 2). This BH has $C_Q > 0$. Suppose that it absorbs a small amount of positive energy $\delta M > 0$ (without exchanging electric charge). The total mass M of the BH will increase by δM, thus reducing $|Q|/M$. The BH moves up along the red solid line, preserving its local thermodynamic stability. The event horizon absorbs all the energy so that the scalar field remains trivial. If, on the contrary, the Reissner-Nordström BH absorbs a small amount of negative energy $\delta M < 0$, M will decrease, yielding a BH with higher $|Q|/M$. This could either be a Reissner-Nordström BH or a scalarized BH. In general, in the region where the Reissner-Nordström and scalarized BHs coexist, the scalarized solutions maximize the entropy and thus are thermodynamically favored. The negative energy feeds the field, triggering the tachyonic instability, which results in a nontrivial field in equilibrium with the BH. Further absorption of negative energy enhances the tachyonic instability so that the BH migrates downward along the blue curves in Fig. 2 (left panel).

III. BLACK HOLES WITH SYNCHRONIZED HAIR

BHs with synchronized hair are four-dimensional, asymptotically flat, stationary solutions of Einstein's gravity minimally coupled to a complex bosonic field ψ with nonvanishing mass μ. As solutions describing BHs, they feature an event horizon at $r = r_H$, being regular on and outside it. The matter field is characterized by a harmonic time and azimuthal dependence, $\psi \sim e^{-i\omega t + im\varphi}$, where $\omega > 0$ and $m \in \mathbb{Z}^+$ are its frequency and azimuthal harmonic index, respectively. The ansatz and corresponding equations of motion as well as the boundary condition at the event horizon, spatial infinity and on the axis can be found in [21] for scalar hair ($\psi = \Phi$) and in [16] for vector hair ($\psi = A$).

A. Superradiant instability and domain of existence

This family of BHs is continuously connected to (a subset of) the family of Kerr BHs. This means BHs with synchronized hair can be realized in the linear limit of the theory, in which the backreaction of the spacetime to a nonconstant bosonic field is negligible. The corresponding limiting solutions are bound states between Kerr BHs and nontrivial bosonic fields, commonly known as "stationary clouds."

Stationary clouds are nothing but zero modes of the superradiant instability, i.e., equilibrium states defined by a bosonic field with vanishing momentum near the event horizon, which amounts to the synchronization condition

$$\Omega_H = \frac{\omega}{m}, \tag{3.1}$$

where Ω_H denotes the BH angular velocity. Equation (3.1) sets the onset of superradiance in Kerr BHs, which occurs whenever $\omega < m\Omega_H$. This condition follows directly from the first and second laws of BH mechanics. BH superradiance is rooted in the existence of an ergoregion, within which negative-energy physical states are possible. However, such possibility does not automatically translate into an instability, unless a confinement mechanism is present. This is here naturally provided by the bare mass of the bosonic field.

Linearizing the equations of motion around $\psi = \psi_0$, for some constant ψ_0, one can show that, when ω/Ω_H is not an integer, the field perturbation $\delta\psi \equiv (\psi - \psi_0)$ has a nonvanishing momentum and oscillates in space, namely in the radial direction, near the event horizon. On the contrary, when ω/Ω_H is an integer, the field becomes stationary and binds to the Kerr BH to form a stationary cloud, pretty much like an electron in a hydrogen atom.

When the backreaction of the spacetime is taken into account and Eq. (3.1) is satisfied, (some) Kerr BHs grow hair and turn dynamically into BHs with synchronized hair. These solutions were originally found for free scalar [15] and vector [16] fields and later generalized for self-interacting fields and/or nonminimal couplings [22].

The solution space of BHs with synchronized hair is fully described by (i) two continuous dimensionless parameters, namely the ADM mass $M\mu$ and the oscillation frequency ω/μ or, equivalently, the ADM angular momentum $J\mu^2$, in units of the field's mass; (ii) two discrete parameters, namely the number of nodes in the radial direction $n \in \mathbb{N}_0$ and the azimuthal harmonic index $m \in \mathbb{Z}^+$. The solutions live in a subset of the plane

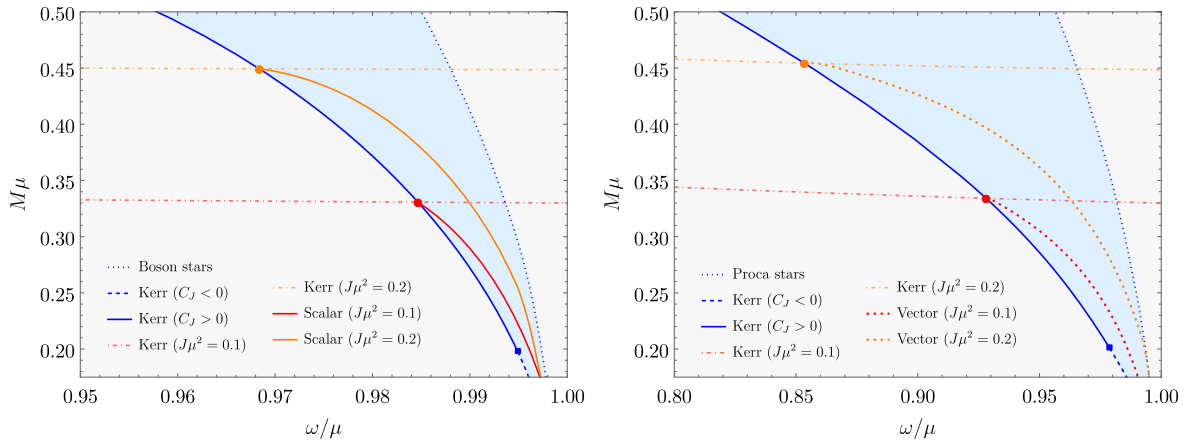

FIG. 3. Domain of existence of BHs with synchronized scalar (left) and vector (right) hair with $(n, m) = (0, 1)$ in the $(\omega/\mu, M\mu)$ plane (light blue region). Kerr BHs live in the light gray region. The blue square separates Kerr BHs with $|J| < \sqrt{2\sqrt{3} - 3}M^2$ ($C_J < 0$, dashed blue line) and $|J| > \sqrt{2\sqrt{3} - 3}M^2$ ($C_J > 0$, solid blue line). The red and orange solid lines define BHs with synchronized hair with $J\mu^2 = 0.1$ and $J\mu^2 = 0.2$, respectively. The circles represent the bifurcation points (cf. Table I).

defined by $(\omega/\mu, M\mu)$ (say). Fixing (n, m), they populate a spiral-shaped region, regardless of the spin of the bosonic field, a part of which is shown in Fig. 3 for BHs with synchronized scalar (left panel) and vector (right panel) hair with $(n, m) = (0, 1)$. They belong to the fundamental family of solutions, characterized by the lowest maximum ADM mass. The solution space is bounded by (i) the existence line, composed of stationary clouds around Kerr BHs (solutions with vanishing field) and (ii) the solitonic line, composed of spinning bosonic stars (solutions with vanishing horizon). BHs with synchronized hair interpolate between these two families of limiting solutions.

The global charges M and J, defined by Komar integrals, can be expressed as $M = M_H + M_\psi$ and $J = J_H + J_\psi$, where M_H and J_H (M_ψ and J_ψ) are the mass and angular momentum inside (outside) the event horizon, respectively. As before, it is convenient to have some measure of the hairiness of these solutions. These can be the proportion of energy and angular momentum in the bosonic field

$$p \equiv \frac{M_\psi}{M}, \qquad q \equiv \frac{J_\psi}{J}, \tag{3.2}$$

respectively, where $p, q \in [0, 1]$. Stationary clouds (bosonic stars) are characterized by $p = q = 0$ ($p = q = 1$).

B. Local thermodynamic stability

Just like Reissner-Nordström BHs, Kerr BHs with sufficiently large (small) specific angular momentum J/M^2 are locally thermodynamically stable (unstable) in the canonical ensemble. Given the similarities and differences between scalarized BHs and BHs with synchronized hair, *a priori*, it is not clear if the latter are also locally thermodynamically unstable in the canonical ensemble. Here, local thermodynamic stability is equivalent to the positivity of the specific heat at constant angular momentum C_J.

BHs with synchronized hair of constant angular momentum $J\mu^2$ define a line segment in the domain of existence joining the Minkowski limit $(M, J \to 0)$ to the existence line $(p, q \to 0)$. As $J\mu^2$ increases, the bifurcation point approaches the extremal line ($p = q = 0$, $J/M^2 = 1$). Figure 3 shows BHs with synchronized scalar (solid lines) and vector (dotted lines) hair with $J\mu^2 = 0.1$ (red lines) and $J\mu^2 = 0.2$ (orange lines). They bifurcate from locally thermodynamically stable Kerr BHs (blue solid line), since $|J| > \sqrt{2\sqrt{3} - 3}M^2 \approx 0.6813M^2$ (see Table I). However, as in Sec. II B, the hairy BHs turn out to be unstable. Indeed, the left panel of Fig. 4 shows their entropy decreases as the temperature increases, which means that $C_J < 0$. The hairiness p increases as the temperature increases (see right panel of Fig. 4). In the Minkowski limit, S vanishes and T diverges, with C_J approaching zero. This behavior bears close resemblance to that of scalarized BHs in EMS theories with an exponential coupling (see Fig. 2).

TABLE I. Bifurcation points of BHs with synchronized hair with $(n, m) = (0, 1)$ for the values of $J\mu^2$ presented in Fig. 3.

	$J\mu^2$	$M\mu$	ω/μ	$M\omega$	J/M^2
Scalar	0.10	0.3307	0.9847	0.3256	0.9146
	0.20	0.4494	0.9684	0.4352	0.9904
Vector	0.10	0.3341	0.9280	0.3101	0.8958
	0.20	0.4544	0.8534	0.3878	0.9686

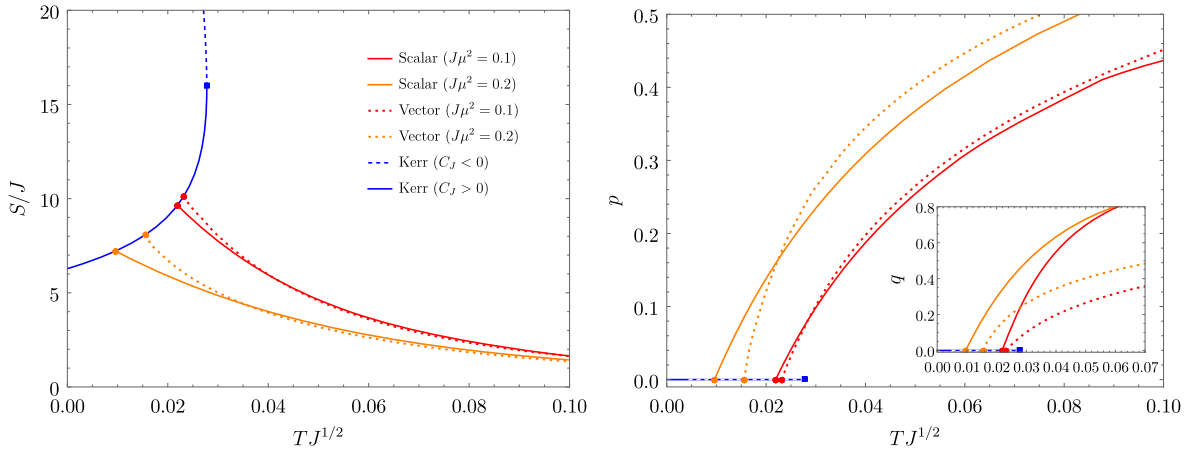

FIG. 4. Entropy (left) and hairiness p and q (right) of BHs with synchronized scalar and vector hair with $(n, m) = (0, 1)$ and $J\mu^2 = 0.1$ (red lines) and $J\mu^2 = 0.2$ (orange lines) as a function of their temperature.

IV. CONCLUSION

The issue of thermodynamical stability of BHs does not directly impact their astrophysical viability. For instance, Schwarzschild and slowly rotating Kerr BHs are thermodynamically unstable in the canonical ensemble. Yet, they may exist in the cosmos. This is because (i) the timescale of thermodynamic instabilities, dictated by the emission of Hawking radiation, is much larger than the age of the Universe for any astrophysical BH and (ii) Schwarzschild and Kerr BHs are dynamically stable in GR.

In fact, considering the grand-canonical ensemble, where BHs are also allowed to exchange electric charge (at fixed electrostatic potential) or angular momentum (at fixed angular velocity), all electrovacuum BHs are locally thermodynamically unstable. This is because another response function becomes negative precisely in the region where the specific heat becomes positive for both the Reissner-Nordström and Kerr cases [6].

Still, the issue of thermodynamic stability of BHs is relevant and quite fruitful, for instance, in the context of AdS/CFT [23]. Thus, it becomes an interesting question to understand how adding extra properties, such as hair, to a BH affects its thermodynamic stability.

This paper addressed the local thermodynamic stability in the canonical ensemble of two families of BHs with bosonic hair, namely scalarized BHs in a subclass of EMS theories and BHs with synchronized hair. Both these families are continuously connected to electrovacuum BHs and, therefore, provide examples where the BH hair can be arbitrarily small. Moreover, the former (latter) yields an example of secondary (primary) hair.

By studying their corresponding specific heat, it was found that the addition of a bosonic field minimally coupled to Einstein's gravity can change the thermodynamic behavior of BHs, even when the field strength is vanishingly small. Specifically, quasibald BHs are locally unstable in this statistical ensemble, regardless of their specific global charges (electric charge or angular momentum). This is particularly surprising for hairy BHs branching off from thermodynamically stable GR BHs.

This analysis provides a contrast between thermodynamical stability and dynamical stability. The Reissner-Nordström (Kerr) BHs with high specific electric charge (angular momentum) are the ones that are locally thermodynamically stable in the canonical ensemble. But when we enlarge the model to include the new fields and couplings of the models above, they are simultaneously the BHs more prone to the tachyonic (superradiant) instability that leads to the branching off toward the hairy solutions. The latter correspond to a new phase in which the BHs are thermodynamically locally unstable in the canonical ensemble, despite being entropically favored for fixed global charges and therefore the ones preferred in a conservative dynamical evolution.

Although the analysis herein was restricted to the aforesaid families, similar results were found for vectorized Reissner-Nordström BHs in Einstein-Maxwell-vector theories [24] in a preliminary investigation, suggesting a *universal* behavior. It would be interesting to perform a similar analysis on other families of hairy BHs continuously connected to the electrovacuum BHs of GR, e.g., scalarized Schwarzschild [25,26] or Kerr BHs [27] in the extended scalar-tensor Gauss-Bonnet theory. We emphasize that our two examples cover both primary and secondary hair, and that the observed behavior contrasts with the one observed when adding global charges, e.g., adding Q to Kerr or J to Reissner-Nordström, where a continuity in the thermodynamic stability properties is observed.

Besides considering the thermodynamic behavior in the canonical ensemble, one can also examine the stability of the hairy BHs in the grand-canonical ensemble. In this statistical ensemble, the electrostatic potential Φ and the angular velocity Ω_H of the event horizon are fixed and the

electric charge Q and the angular momentum J are free to vary. This is the most generic physical scenario. In this ensemble the whole Kerr-Newman family is unstable. The corresponding stability analysis of hairy BHs continuously connected to the Kerr-Newman family is left for future work.

ACKNOWLEDGMENTS

N. S. would like to thank Alexandre M. Pombo for sharing his knowledge on scalarized BHs and Jorge F. M. Delgado for fruitful discussion about BHs with synchronized hair. This work is supported by the Center for Research and Development in Mathematics and Applications (CIDMA) through the Portuguese Foundation for Science and Technology (FCT—Fundação para a Ciência e a Tecnologia), References No. UIDB/04106/2020 and No. UIDP/04106/2020 and by national funds (OE), through FCT, I. P., in the scope of the framework contract foreseen in the No. 4–6 of the article 23, of the Decree-Law 57/2016, of August 29, changed by Law 57/2017, of July 19. The authors acknowledge support from the Projects No. PTDC/FIS-OUT/28407/2017, No. CERN/FIS-PAR/0027/2019, No. PTDC/FIS-AST/3041/2020 and No. CERN/FIS-PAR/0024/2021. N. M. S. is supported by the FCT Grant No. SFRH/BD/143407/2019. This work has further been supported by the European Union's Horizon 2020 research and innovation (RISE) program H2020-MSCA-RISE-2017 Grant No. FunFiCO-777740.

[1] J. M. Bardeen, B. Carter, and S. W. Hawking, The four laws of black hole mechanics, Commun. Math. Phys. **31**, 161 (1973).
[2] S. W. Hawking, Particle creation by black holes, Commun. Math. Phys. **43**, 199 (1975).
[3] S. W. Hawking, Black hole explosions?, Nature (London) **248**, 30 (1974).
[4] S. Hollands and R. M. Wald, Stability of black holes and black branes, Commun. Math. Phys. **321**, 629 (2013).
[5] J. Keir, Stability, instability, canonical energy and charged black holes, Classical Quantum Gravity **31**, 035014 (2014).
[6] P. C. W. Davies, The thermodynamic theory of black holes, Proc. R. Soc. A **353**, 499 (1977).
[7] C. A. R. Herdeiro and E. Radu, Asymptotically flat black holes with scalar hair: A review, Int. J. Mod. Phys. D **24**, 1542014 (2015).
[8] C. A. R. Herdeiro, Black holes: On the universality of the Kerr hypothesis, arXiv:2204.05640.
[9] C. A. R. Herdeiro, E. Radu, N. Sanchis-Gual, and J. A. Font, Spontaneous Scalarization of Charged Black Holes, Phys. Rev. Lett. **121**, 101102 (2018).
[10] D. Astefanesei, C. Herdeiro, A. Pombo, and E. Radu, Einstein-Maxwell-scalar black holes: Classes of solutions, dyons and extremality, J. High Energy Phys. 10 (2019) 078.
[11] P. G. S. Fernandes, C. A. R. Herdeiro, A. M. Pombo, E. Radu, and N. Sanchis-Gual, Spontaneous scalarisation of charged black holes: Coupling dependence and dynamical features, Classical Quantum Gravity **36**, 134002 (2019).
[12] P. G. S. Fernandes, C. A. R. Herdeiro, A. M. Pombo, E. Radu, and N. Sanchis-Gual, Charged black holes with axionic-type couplings: Classes of solutions and dynamical scalarization, Phys. Rev. D **100**, 084045 (2019).
[13] J. L. Blázquez-Salcedo, C. A. R. Herdeiro, J. Kunz, A. M. Pombo, and E. Radu, Einstein-Maxwell-scalar black holes: The hot, the cold and the bald, Phys. Lett. B **806**, 135493 (2020).
[14] T. Damour and G. Esposito-Farèse, Nonperturbative Strong Field Effects in Tensor-Scalar Theories of Gravitation, Phys. Rev. Lett. **70**, 2220 (1993).
[15] C. A. R. Herdeiro and E. Radu, Kerr Black Holes with Scalar Hair, Phys. Rev. Lett. **112**, 221101 (2014).
[16] C. Herdeiro, E. Radu, and H. Rúnarsson, Kerr black holes with Proca hair, Classical Quantum Gravity **33**, 154001 (2016).
[17] C. A. R. Herdeiro and J. M. S. Oliveira, On the inexistence of solitons in Einstein–Maxwell-scalar models, Classical Quantum Gravity **36**, 105015 (2019).
[18] O. J. C. Dias, G. T. Horowitz, and J. E. Santos, Extremal black holes that are not extremal: Maximal warm holes, J. High Energy Phys. 01 (2022) 064.
[19] M. Boskovic, R. Brito, V. Cardoso, T. Ikeda, and H. Witek, Axionic instabilities and new black hole solutions, Phys. Rev. D **99**, 035006 (2019).
[20] H. S. Reall, Classical and thermodynamic stability of black branes, Phys. Rev. D **64**, 044005 (2001).
[21] C. Herdeiro and E. Radu, Construction and physical properties of Kerr black holes with scalar hair, Classical Quantum Gravity **32**, 144001 (2015).
[22] C. A. R. Herdeiro, E. Radu, and H. Rúnarsson, Kerr black holes with self-interacting scalar hair: Hairier but not heavier, Phys. Rev. D **92**, 084059 (2015).
[23] E. Witten, Anti-de Sitter space, thermal phase transition, and confinement in gauge theories, Adv. Theor. Math. Phys. **2**, 505 (1998).
[24] J. M. S. Oliveira and A. M. Pombo, Spontaneous vectorization of electrically charged black holes, Phys. Rev. D **103**, 044004 (2021).
[25] D. D. Doneva and S. S. Yazadjiev, New Gauss-Bonnet Black Holes with Curvature-Induced Scalarization in Extended Scalar-Tensor Theories, Phys. Rev. Lett. **120**, 131103 (2018).

[26] H. O. Silva, J. Sakstein, L. Gualtieri, T. P. Sotiriou, and E. Berti, Spontaneous Scalarization of Black Holes and Compact Stars from a Gauss-Bonnet Coupling, Phys. Rev. Lett. **120**, 131104 (2018).

[27] P. V. P. Cunha, C. A. R. Herdeiro, and E. Radu, Spontaneously Scalarized Kerr Black Holes in Extended Scalar-Tensor–Gauss-Bonnet Gravity, Phys. Rev. Lett. **123**, 011101 (2019).

Part II

Bosonic stars

Chapter 6

Reprint of *JCAP* 06 (2024) 068

Journal of Cosmology and Astroparticle Physics
An IOP and SISSA journal

Received: *April 18, 2024*
Accepted: *June 9, 2024*
Published: *June 26, 2024*

Radial stability of spherical bosonic stars and critical points

Nuno M. Santos,[a,b] **Carolina L. Benone**[c] **and Carlos A.R. Herdeiro**[a]

[a]*Departamento de Matemática da Universidade de Aveiro and, Centre for Research and Development in Mathematics and Applications (CIDMA), Campus de Santiago, 3810–193 Aveiro, Portugal*

[b]*Departamento de Física, Instituto Superior Técnico — IST, Universidade de Lisboa — UL, Avenida Rovisco Pais 1, 1049–001 Lisboa, Portugal*

[c]*Campus Universitário de Salinópolis, Universidade Federal do Pará, 68721–000, Salinópolis, Pará, Brazil*

E-mail: nunomoreirasantos@tecnico.ulisboa.pt, benone@ufpa.br, herdeiro@ua.pt

Abstract: We study radial perturbations of spherically symmetric spin-0 and spin-1 bosonic stars, computing numerically the squared frequency of the fundamental mode. We find that not all critical points — where the Arnowitt-Deser-Misner mass attains an extremum — correspond to zero modes. Thus, radial stability does not *always* change at such critical points. The results are in agreement with the so-called critical point method.

Keywords: gravity, stars

ArXiv ePrint: 2404.07257

https://doi.org/10.1088/1475-7516/2024/06/068

JCAP06(2024)068

Contents

1 Introduction

Self-gravity is key to the understanding of the physics of compact objects, such as white dwarfs, neutron stars, and black holes (BHs). Apart from the latter, which cannot support themselves at all against gravitational collapse, the equilibrium of compact objects relies on a balance between the attractive pull of gravity and a repulsive push of some sort. In the case of white dwarfs and neutron stars, the repulsion is nothing but degeneracy pressure of electrons and neutrons, respectively, caused by the Pauli exclusion principle and the Heisenberg uncertainty principle.

If compact objects are composed of something else rather than ordinary baryonic matter, they are said to be exotic. A number of exotic compact objects has been put forward over the past decades (see [1] for a review). Examples include boson stars (BSs) [2, 3], anisotropic stars [4], wormholes [5], gravastars [6], or fuzzballs [7]. BSs in particular have attracted much attention recently (see [8–10] for reviews). As first conceived by Kaup, they are solitonic solutions of Einstein's gravity minimally coupled to a massive, complex scalar field with harmonic time dependence. There is nothing special about scalar fields, though. Such compact objects may also consist of massive, complex vector (or Proca) fields, in which case they are known as Proca stars (PSs) [11]. Collectively, BSs and PSs are referred to as *bosonic stars*. Unlike white dwarfs and neutron stars, they are supported against gravitational

JCAP06(2024)068

collapse by the Heisenberg uncertainty principle only. From a theoretical standpoint, bosonic stars are particularly interesting because they appear in well-motivated and self-consistent physical theories and have a formation mechanism, known as gravitational cooling [12, 13]. From an observational standpoint, they stand out from the plethora of exotic compact objects as simple yet astrophysically viable compact objects, which can serve as a model (or a proxy) for lumps of ultralight dark matter [14–16].

Among the most pressing questions around the astrophysical viability of compact objects is that of stability. Bosonic stars are no exception: as hypothetical compact objects, they should be stable with respect to sufficiently small perturbations (or, in case they are unstable, be sufficiently long-lived). The linear stability of BSs was first addressed by Gleiser [17] and Jetzer [18] in the 80s, following Chandrasekhar's seminal work on perfect-fluid stars [19]. Both realized that, like normal stars, the fundamental set of BSs can be either radially stable or unstable, depending on the field value at the star's center ψ_0, and estimated upper bounds for the threshold of the instability. Gleiser and Watkins later solved numerically the linear perturbation equations (also referred to as "pulsation equations") and found that the instability trigger value matched the BS maximum Arnowitt-Deser-Misner (ADM) mass [20]. Soon afterward, Seidel and Suen studied the linear and nonlinear radial stability of mini-BSs using numerical relativity [21] and concluded that: stable mini-BSs oscillate (when perturbed), emitting bosonic radiation and losing mass as they relax to a configuration with lower mass and larger radius; unstable mini-BSs, on the other hand, either collapse to a black hole or migrate to a configuration in the stable branch. More recently, this picture was confirmed and extended, in both the time and frequency domains, to mini-BSs in the first excited mode [22] as well as massive-BSs in the fundamental and first excited modes [23, 24], and spherically symmetric PSs [25]. It has been reported in particular that some unstable solutions (also in the case of fundamental mini-BSs) disperse altogether due to having more energy than the corresponding collection of particles.

Radial perturbations correspond to physical, non-radiative degrees of freedom, describing changes in the mass of the system [26]. More precisely, they refer to polar (or even or electric) $\ell = 0$ perturbations of the equilibrium (spherically symmetric) background in the context of linear perturbation theory. Conclusions drawn from radial linear stability analysis must be taken with a pinch of salt: a compact object that is stable with respect to sufficiently small radial perturbations might be prone to instabilities grown out of an angular disturbance, for instance. Non-radial linear stability of mini-BSs as well as of massive and solitonic BSs has been studied in [27–29].

It is possible to analyze the radial linear stability of normal stars using the *critical point method* [30, Chap. 6]. On a plot of the equilibrium mass M vs. ψ_0, changes in stability, dictated by zero-frequency modes, are linked to critical points, i.e. solutions satisfying $\mathrm{d}M/\mathrm{d}\psi_0 = 0$. The linear perturbation equations pose a Sturm-Liouville boundary value problem on the finite interval $[0, R]$, where R is the star radius, for the perturbation frequency squared Ω^2. According to spectral theory, there are infinitely many real eigenvalues Ω_0^2, Ω_1^2, $\Omega_2^2, \ldots$, and the eigenfunction corresponding to the eigenvalue Ω_n^2, $n \in \mathbb{N}_0$, has exactly n zeros in the open interval $(0, R)$, i.e. n nodes. An eigenfunction with an odd (even) number of nodes is often referred to as an odd (even) mode. Additionally, the eigenvalues are ordered, i.e.

JCAP06(2024)068

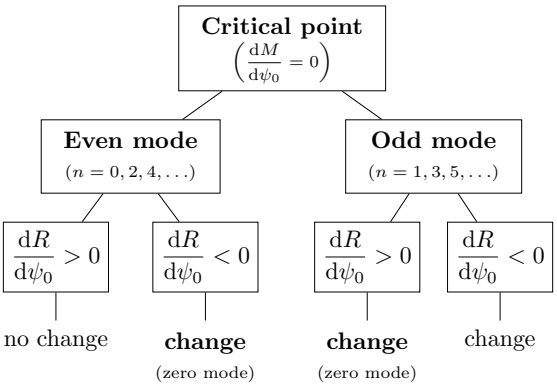

Figure 1. Assessment of stability-instability transitions with the critical point method.

$\Omega_0^2 < \Omega_1^2 < \Omega_2^2 < \ldots$. The stability can be analyzed by noting that $\mathrm{d}R/\mathrm{d}\psi_0 > 0$ ($\mathrm{d}R/\mathrm{d}\psi_0 < 0$) at a critical point corresponds to a change of sign of an odd (even) mode. The critical point method is summarized schematically in figure 1.

Unlike normal stars, BSs do not have a definite surface, i.e. a boundary outside which the energy density vanishes. In fact, the field extends to spacelike infinity and, for that reason, the corresponding linear perturbation equations form a *singular* Sturm-Liouville boundary value problem. Strictly speaking, the previous result on the eigenvalues cannot be applied to BSs. However, their energy density decay exponentially close to spacelike infinity, where its value is much smaller than the maximum. It is then reasonable to define the "surface" of a BS as a spherical surface enclosing most of its equilibrium mass. A popular choice is the circumferential radius containing 99% of M. Such a definition ensures the validity of the critical point method in this case.

While the critical point method suffices to identify zero-frequency modes and stability-instability transitions across the parameter space, it does not provide any estimates of the perturbation frequencies. These are important to understand the spectra of normal and quasinormal modes of stable BSs. To this end, the most straightforward approach is to (numerically) integrate the perturbation equations. One of the goals of this paper is to present the eigenvalues Ω_0^2 for mini-, solitonic [31] and axion [32] BSs as well as for PSs [11].

Another purpose of this paper is to clarify some ideas about BS stability present in the literature. An example is the statement [33] that the radial stability of a spherically symmetric BS changes whenever $\mathrm{d}M/\mathrm{d}\psi_0 = 0$. While it is true that transitions from stable to unstable configurations, and vice versa, only occur at critical points, defined by $\mathrm{d}M/\mathrm{d}\psi_0 = 0$, the examples herein make clear that not all critical points signal such transitions, as illustrated in figure 1.

The rest of the paper is organized as follows. In section 2, the action, equations of motion, and relevant physical quantities of different BS models are introduced. Section 3 is devoted to a brief review of the formulation describing spherically symmetric BSs, whereas section 4 formulates their first-order radial perturbations in the Zerilli gauge. In section 5, the space of solutions of both equilibrium and perturbed solutions is presented in a side-by-side comparison of the different models. An overview of the work is sketched in section 6, together with some final remarks.

JCAP06(2024)068

Notation. In the following, the speed of light c and the Planck constant $\hbar$ are set equal to one ($c = \hbar = 1$), unless stated otherwise. The mostly positive metric signature $(-+++)$ is adopted and Latin letters $(a, b, c, \ldots)$ are used for abstract index notation. Since the paper addresses first-order perturbations, every tensor field A can be expanded in powers of a bookkeeping parameter ϵ, $A(\epsilon) = A^{(0)} + \epsilon\, A^{(1)} + \ldots$, where $A^{(0)}$ is the unperturbed value and $A^{(1)}$ is the first-order perturbation of $A(\epsilon)$.

2 Framework

Consider the action describing a complex spin-s field, $s \in \{0, 1\}$, minimally coupled to Einstein's gravity:

$$\mathcal{S}_s = \int \mathrm{d}^4x\, \sqrt{-g} \left[\frac{R}{16\pi G} + \mathcal{L}_s \right] , \tag{2.1}$$

where G is the gravitational constant, g_{ab} is the metric, with determinant g and Ricci scalar R, and the matter Lagrangians read

$$\mathcal{L}_0 = -g^{ab} \nabla_a \Phi \nabla_b \bar{\Phi} - V_0(\Phi\bar{\Phi}) \,. \quad \mathcal{L}_1 = -\frac{1}{4} \mathcal{F}_{ab} \bar{\mathcal{F}}^{ab} - V_1(\mathcal{A}_a \bar{\mathcal{A}}^a) \,, \tag{2.2}$$

Φ is a complex scalar field, $\mathcal{A}_a \mathrm{d}x^a$ is a complex Proca field with strength $\mathcal{F} = \mathrm{d}\mathcal{A}$, and V_s is the corresponding spin-s field potential. Moreover, the overbar $\bar{\cdot}$ denotes complex conjugation.

This paper focuses on three particular forms of the scalar-field potential, namely

$$V_0(\Phi\bar{\Phi}) = \begin{cases} \mu^2 \Phi\bar{\Phi} & \text{(mini)} \,, \qquad (2.3a) \\ \mu^2 \Phi\bar{\Phi} \left(1 - \dfrac{2\Phi\bar{\Phi}}{v_0^2} \right)^2 & \text{(solitonic)} \,, \qquad (2.3b) \\ \dfrac{2\mu^2 f_a^2}{B} \left[1 - \sqrt{1 - 4B \sin^2 \left(\dfrac{\sqrt{\Phi\bar{\Phi}}}{2f_a} \right)} \right] & \text{(axionic)} \,, \qquad (2.3c) \end{cases}$$

and on the simplest form of the Proca-field potential,

$$V_1(\mathcal{A}_a \bar{\mathcal{A}}^a) = \frac{1}{2} \mu^2 \mathcal{A}_a \bar{\mathcal{A}}^a \,. \tag{2.4}$$

Bosonic stars in each model are known as mini-boson stars (MBSs), solitonic boson stars (SBSs), axionic boson stars (ABSs), and Proca stars (PSs), respectively. In the above potentials, $\{\mu, v_0, f_a\}$ are free parameters: $\mu = mc/\hbar$ is the inverse Compton wavelength of the corresponding spin-s field (and m is its bare mass), v_0 is the degenerate vacuum of the solitonic potential (2.3b) and f_a is the Peccei-Quinn symmetry breaking scale. Additionally, $B = z/(1+z)^2 \approx 0.22$, with $z \equiv m_u/m_d \approx 0.48$ being the up-quark-to-down-quark mass ratio. The second term in eq. (2.3c) is the standard QCD axion potential, which is non-zero when $\Phi = 0$. The first term is added so that $V_0(0) = 0$ and hence asymptotic flatness is ensured. Note that the potential in eq. (2.3a) is the linear approximation of both eqs. (2.3b)–(2.3c) around[1] $\Phi\bar{\Phi} = 0$.

[1]For the latter case, the linear approximation is valid when $\sqrt{\Phi\bar{\Phi}} \ll f_a$.

JCAP06(2024)068

Varying the action in eq. (2.1) with respect to the metric and to the matter field yields the equations of motion, namely Einstein equations,

$$E_{ab} \equiv G_{ab} - 8\pi G T^{[s]}_{ab} = 0\,, \tag{2.5}$$

where G_{ab} is the Einstein tensor, and $T^{[s]}_{ab}$ is the energy-momentum tensor of the spin-s field,

$$T^{[0]}_{ab} = \nabla_a\Phi\nabla_b\bar{\Phi} + \nabla_b\Phi\nabla_a\bar{\Phi} - g_{ab}\left[\frac{1}{2}g^{cd}\left(\nabla_c\Phi\nabla_d\bar{\Phi} + \nabla_d\Phi\nabla_c\bar{\Phi}\right) + V_0(\Phi\bar{\Phi})\right]\,, \tag{2.6a}$$

$$T^{[1]}_{ab} = \frac{1}{2}g^{cd}\left(\mathcal{F}_{ac}\bar{\mathcal{F}}_{bd} + \bar{\mathcal{F}}_{ac}\mathcal{F}_{bd}\right) - \frac{1}{4}g_{ab}F_{cd}\bar{F}^{cd} + \frac{1}{2}\mu^2\left(\mathcal{A}_a\bar{\mathcal{A}}_b + \bar{\mathcal{A}}_a\mathcal{A}_b - g_{ab}\mathcal{A}_c\bar{\mathcal{A}}^c\right)\,, \tag{2.6b}$$

and the matter equations

$$\nabla_a\nabla^a\Phi - \frac{\partial V_0}{\partial(\Phi\bar{\Phi})}\,\Phi = 0\,, \tag{2.7a}$$

$$\nabla_a\mathcal{F}^{ab} - \mu^2\mathcal{A}^b = 0\,. \tag{2.7b}$$

Equation (2.7a) is the Klein-Gordon equation, whereas eq. (2.7b) is the Proca equation. The latter implies the Lorenz condition $\nabla_a\mathcal{A}^a = 0$.

In either case, the action in eq. (2.1) possesses a global U(1) symmetry, i.e. it is invariant under the transformation $\{\Phi, \mathcal{A}_a\} \to e^{i\chi}\{\Phi, \mathcal{A}_a\}$, with χ constant. This implies the existence of the four-currents

$$j^a_0 = i(\Phi\nabla^a\bar{\Phi} - \bar{\Phi}\nabla^a\Phi)\,, \qquad j^a_1 = \frac{i}{2}\left(\bar{\mathcal{F}}^{ab}\mathcal{A}_b - \mathcal{F}^{ab}\bar{\mathcal{A}}_b\right)\,, \tag{2.8}$$

which are conserved, i.e. $\nabla_a j^a_s = 0$. There exists a Noether charge Q_s, obtained by integrating the timelike component of the four-currents on a spacelike surface Σ,

$$Q_s = \int_\Sigma \mathrm{d}^3x\ j^0_s\,. \tag{2.9}$$

Upon quantization, Q is nothing but the particle number.

The Komar mass reads

$$M_s = \frac{1}{4\pi G}\int_\Sigma \mathrm{d}V\, R_{ab}n^a\xi^b = 2\int_\Sigma \mathrm{d}V\left(T^{[s]}_{ab} - \frac{1}{2}g_{ab}T^{[s]}\right)n^a\xi^b\,, \tag{2.10}$$

where Σ is an asymptotically-flat spacelike hypersurface, n^α is a future-pointing unit vector normal to Σ, $\mathrm{d}V$ is the 3-volume form induced on Σ, and $T^{[s]} = g^{ab}T^{[s]}_{ab}$ is the trace of the energy-momentum tensor $T^{[s]}_{ab}$.

3 Equilibrium solutions

In this paper, only radial perturbations of spherically symmetric bosonic stars will be considered. For completeness, the construction and physical properties of the equilibrium solutions are reviewed in the following. The solutions are parametrized by the spin-s field value at the star's center ψ_0. This section follows closely the definitions and conventions in [34].

JCAP06(2024)068

3.1 Ansätze and equations of motion

A line element compatible with a static spherically-symmetric spacetime is

$$\mathrm{d}s^2 = g^{(0)}_{ab}\,\mathrm{d}x^a\mathrm{d}x^b = -\sigma(r)^2 N(r)\mathrm{d}t^2 + \frac{\mathrm{d}r^2}{N(r)} + r^2\left(\mathrm{d}\theta^2 + \sin^2\theta\,\mathrm{d}\varphi^2\right)\,, \quad N(r) = 1 - \frac{2G\mathcal{M}(r)}{r}\,, \tag{3.1}$$

where $\mathcal{M}$ is the Misner-Sharp mass function. Unlike the metric tensor, the matter fields are assumed to have a harmonic time-dependence:

$$\Phi^{(0)} = e^{-i\omega t}\,\phi(r)\,, \tag{3.2a}$$

$$\mathcal{A}^{(0)}_a\mathrm{d}x^a = e^{-i\omega t}\left[f(r)\,\mathrm{d}t + ig(r)\,\mathrm{d}r\right]\,, \tag{3.2b}$$

where $\{\phi, f, g\}$ are real functions. Without loss of generality, one assumes $\omega \in \mathbb{R}^+$.

Restricted to the above ansätze, the equations of motion in eqs. (2.5) and (2.7) yield a system of three (four) coupled ordinary differential equations for the scalar (Proca) field. The only non-zero components of E_{ab} are E_{tt}, E_{rr}, $E_{\theta\theta}$ and $E_{\varphi\varphi}$. The equations governing the metric functions N and σ read

$$\frac{1}{r^2\sigma}\partial_r(r\sigma N) - \frac{1}{r^2} + 8\pi G\mathcal{V}_s = 0\,, \tag{3.3a}$$

$$\frac{\partial_r\sigma}{\sigma} - 8\pi G\mathcal{W}_s = 0\,, \tag{3.3b}$$

where

$$\mathcal{V}_0 = V_0, \qquad \mathcal{V}_1 = \frac{1}{2}\left(\frac{\partial_r f - \omega g}{\sigma}\right)^2\,, \tag{3.4}$$

and

$$\mathcal{W}_0 = \left[(\partial_r\phi)^2 + \frac{\omega^2\phi^2}{\sigma^2 N^2}\right] r\,, \qquad \mathcal{W}_1 = \frac{\mu^2}{2}\left(\frac{f^2}{\sigma^2 N} + g^2\right) r\,. \tag{3.5}$$

On the other hand, the matter equations become

$$\frac{1}{r^2\sigma}\partial_r(r^2\sigma N\partial_r\phi) + \left(\frac{\omega^2}{\sigma^2 N} - V_0'\right)\phi = 0\,, \tag{3.6a}$$

$$\partial_r\left[\frac{r^2}{\sigma}(\partial_r f - \omega g)\right] - \mu^2\frac{r^2 f}{\sigma N} = 0\,, \quad \omega(\partial_r f - \omega g) + \mu^2\sigma^2 N g = 0\,, \tag{3.6b}$$

where $V_0^{(k)} \equiv \mathrm{d}^k V_0(\phi^2)/\mathrm{d}(\phi^2)^k$, $k \in \mathbb{N}$. The Lorenz condition reads

$$\frac{1}{r^2}\partial_r\left(r^2\sigma N g\right) + \frac{\omega f}{\sigma N} = 0\,. \tag{3.7}$$

3.2 Boundary conditions

Equations (3.3) together with eqs. (3.6) can be (numerically) integrated under the boundary conditions (BCs) summarized in table 1. The inner BCs result from the smoothness at $r = 0$,

JCAP06(2024)068

	Metric functions		Matter functions				
	$\mathcal{M}$	σ	ϕ	ϕ'	f	f'	g
Inner BCs ($r=0$)	0	σ_0	ϕ_0	0	f_0	0	0
Outer BCs ($r=\infty$)	M	1	0	0	0	0	0
	H_0	H_2	$\phi_\pm$	$\phi'_\pm$	$f_\pm$	$f'_\pm$	$g_\pm$
Inner BCs ($r=0$)	h_0	0	$\phi_\pm(0)$	0	$f_\pm(0)$	0	0
Outer BCs ($r=\infty$)	h_∞	0	0	0	0	0	0

Table 1. Boundary conditions (BCs) for both metric and matter functions of equilibrium and perturbed bosonic stars (see section 3.1 and section 4.2 for definitions).

required to avoid the poles there. In fact, it can be shown that

$$\mathcal{M}(r) = \frac{4\pi G}{3}\left[\omega^2\frac{\phi_0^2}{\sigma_0^2} + \tilde{V}_0\right] r^2 + \dots\,, \tag{3.8a}$$

$$\sigma(r) = \sigma_0 + \frac{4\pi G\phi_0^2}{\sigma_0}\omega^2 r^2 + \dots\,, \tag{3.8b}$$

$$\phi(r) = \phi_0 - \frac{1}{6}\left[\omega^2\frac{\phi_0}{\sigma_0^2} - \tilde{V}_0\right] r^2 + \dots\,, \tag{3.8c}$$

$$f(r) = f_0\left[1 + \frac{1}{6}\left(\mu^2 - \frac{\omega^2}{\sigma_0^2}\right)\right] r^2 + \dots\,, \tag{3.8d}$$

$$g(r) = -\frac{\omega}{3}\frac{f_0}{\sigma_0^2} r + \dots\,, \tag{3.8e}$$

where $\sigma_0 \equiv \sigma(0)$, $\phi_0 \equiv \phi(0)$ and $f_0 \equiv f(0)$ are as yet undetermined constants, and $\tilde{V}_0 \equiv V_0(\phi_0^2)$. Without loss of generality, one can assume that $\phi_0,\ f_0 \in \mathbb{R}^+$ thanks to the $\mathbb{Z}_2$-symmetry of the spin-s fields. Moreover, note that $m'(0) = \sigma'(0) = 0$.

On the other hand, the outer BCs ($r=\infty$) follow on from the requirement of asymptotic flatness. The leading-order asymptotic behavior of the functions is

$$N(r) = 1 - \frac{2GM}{r} + \dots\,, \tag{3.9a}$$

$$\log\sigma(r) = -\frac{c_0^2}{2}\frac{\mu^2\omega^2}{(\mu^2-\omega^2)^{3/2}}\frac{e^{-2r\sqrt{\mu^2-\omega^2}}}{r} + \dots\,, \tag{3.9b}$$

$$\phi(r) = \phi_\infty\frac{e^{-r\sqrt{\mu^2-\omega^2}}}{r} + \dots\,, \tag{3.9c}$$

$$f(r) = f_\infty\frac{e^{-r\sqrt{\mu^2-\omega^2}}}{r} + \dots\,, \tag{3.9d}$$

$$g(r) = f_\infty\frac{\omega}{\sqrt{\mu^2-\omega^2}}\frac{e^{-r\sqrt{\mu^2-\omega^2}}}{r} + \dots\,, \tag{3.9e}$$

where $\{c_0, \phi_\infty, f_\infty\}$ are constants.

JCAP06(2024)068

3.3 Physical quantities

The Noether charge (2.5) of the equilibrium solutions read

$$Q_0^{(0)} = 8\pi \int_0^\infty \mathrm{d}r\ r^2 \frac{\omega\phi^2}{\sigma N}\,, \tag{3.10a}$$

$$Q_1^{(0)} = 4\pi \int_0^\infty \mathrm{d}r\ r^2 \frac{g}{\sigma}(\partial_r f - \omega g)\,, \tag{3.10b}$$

whereas the Komar mass (2.7) yield

$$M_0^{(0)} = 4\pi \int_0^\infty \mathrm{d}r\ \frac{r^2}{\sigma N}\left[4\left(\omega^2 - \frac{\mu^2}{2}\sigma^2 N\right)\phi^2\right]\,, \tag{3.11a}$$

$$M_1^{(0)} = 4\pi \int_0^\infty \mathrm{d}r\ \frac{r^2}{\sigma N}\left[N(\partial_r f - \omega g)^2 + 2\mu^2 f^2\right]\,. \tag{3.11b}$$

Moreover, it is useful to introduce a definition for the radius. Unlike normal stars, such quantity is ill-defined due to the Yukawa-like asymptotic behavior of the matter fields. Here, the most common definition is adopted: the bosonic stars radius R is the circumferential radius containing 99% of the ADM mass.[2] The compactness of the equilibrium bosonic stars is then $\mathcal{C} \equiv GM/(c^2 R)$.

4 Perturbed solutions

In a spherically symmetric spacetime, metric perturbations can be written as a sum of 10 tensor spherical harmonics of degree $\ell \in \mathbb{N}_0$ and order $|\tilde{m}| \leq \ell$, which form an orthonormal basis. They can in particular be separated into polar (or even or electric) and axial (or odd or magnetic) perturbations according to their properties under parity transformations (see, e.g., [35, Chap. 12]). This section addresses radial perturbations of equilibrium bosonic stars. This amounts to considering polar $\ell = 0$ perturbations (also known as monopolar perturbations). Although in vacuum $\ell = 0$ perturbations can be removed by a gauge transformation (and do not contribute to radiative degrees of freedom of the gravitational field), they are not spurious in this case.

4.1 Ansätze and equations of motion

In the Zerilli gauge [26], the metric perturbation reads

$$g_{ab}^{(1)}\mathrm{d}x^a\mathrm{d}x^b = \sigma(r)^2 N(r)\tilde{H}_0(t,r)\,\mathrm{d}t^2 + \frac{\tilde{H}_2(t,r)}{N(r)}\,\mathrm{d}r^2\,, \tag{4.1}$$

while matter perturbations are assumed to have the form

$$\Phi^{(1)} = e^{-i\omega t}\,\phi_1(t,r)\,, \tag{4.2a}$$

$$\mathcal{A}_a^{(1)}\mathrm{d}x^a = e^{-i\omega t}\left[f_1(t,r)\,\mathrm{d}t + i g_1(t,r)\,\mathrm{d}r\right]\,, \tag{4.2b}$$

where $\{\tilde{H}_0, \tilde{H}_2\}$ are real functions, whereas $\{\phi_1, f_1, g_1\}$ are complex functions.

[2] Different definitions can be found in the literature [8, II.C].

JCAP06(2024)068

The first-order equations of motion include terms that prevent the existence of monochromatic (single-frequency) solutions. The simplest solutions are a superposition of two monochromatic waves with frequencies $\omega_\pm = \omega \pm \Omega$, where Ω is the perturbation frequency. The perturbation functions are of the form

$$\tilde{H}_0(t,r) = (e^{-i\Omega t} + e^{+i\Omega t})H_0(r)\,, \tag{4.3a}$$
$$\tilde{H}_2(t,r) = (e^{-i\Omega t} + e^{+i\Omega t})H_2(r)\,, \tag{4.3b}$$
$$\phi_1(t,r) = e^{-i\Omega t}\,\phi_+(r) + e^{+i\Omega t}\,\phi_-(r)\,, \tag{4.3c}$$
$$f_1(t,r) = e^{-i\Omega t}\,f_+(r) + e^{+i\Omega t}\,f_-(r)\,, \tag{4.3d}$$
$$g_1(t,r) = e^{-i\Omega t}\,g_+(r) + e^{+i\Omega t}\,g_-(r)\,. \tag{4.3e}$$

where $\{H_0,\, H_2,\, \phi_\pm,\, f_\pm,\, g_\pm\}$ are real functions. The resulting first-order equations of motion become an eigenvalue problem for Ω^2, which is real, i.e. Ω is either purely real or purely imaginary, the perturbed solution being either stable or unstable, respectively. Plugging eqs. (4.1) and (4.2) into ${E^t}_t$, ${E^t}_r$ and ${E^r}_r$, and keeping linear terms in the bookkeeping parameter ϵ, one gets, respectively,

$$\frac{1}{r}\partial_r(NH_2) + \frac{N}{r^2}H_2 - 8\pi G\mathcal{X}_s = 0\,, \tag{4.4a}$$
$$\Omega H_2 - 8\pi G r\mathcal{Y}_s = 0\,, \tag{4.4b}$$
$$\frac{N}{r}\partial_r H_0 + \frac{N}{r}\left(\frac{1}{r} + \frac{\partial_r N}{N} + \frac{2\partial_r\sigma}{\sigma}\right)H_2 + 8\pi G\mathcal{Z}_s = 0\,, \tag{4.4c}$$

where

$$\mathcal{X}_0 = \frac{\omega^2\phi^2}{\sigma^2 N}H_0 - N(\partial_r\phi)^2 H_2 + N(\partial_r\phi)\partial_r(\phi_+ + \phi_-) + \phi\left(\frac{\omega\omega_+}{\sigma^2 N} + V_0'\right)\phi_+ + \phi\left(\frac{\omega\omega_-}{\sigma^2 N} + V_0'\right)\phi_-\,, \tag{4.5a}$$
$$\mathcal{Y}_0 = (\partial_r\phi)(\omega_+\phi_+ - \omega_-\phi_-) - \omega\phi\,\partial_r(\phi_+ - \phi_-)\,, \tag{4.5b}$$
$$\mathcal{Z}_0 = \mathcal{X}_0 - 2\phi V_0'(\phi_+ + \phi_-)\,, \tag{4.5c}$$
$$\mathcal{X}_1 = \frac{\mu^2}{2}\frac{f}{\sigma^2 N}(fH_0 + f_+ + f_-) - \frac{\mu^2}{2}Ng^2H_2 - \frac{1}{2}\left[\frac{\omega_+(\partial_r f - \omega g)}{\sigma^2} - \mu^2 Ng\right]g_+ - \\ - \frac{1}{2}\left[\frac{\omega_-(\partial_r f - \omega g)}{\sigma^2} - \mu^2 Ng\right]g_- + \frac{\partial_r f - \omega g}{2\sigma^2}\left[(\partial_r f - \omega g)(H_0 - H_2) + \partial_r(f_+ + f_-)\right]\,, \tag{4.5d}$$
$$\mathcal{Y}_1 = \frac{\mu^2}{2}\left[g(f_+ - f_-) - f(g_+ - g_-)\right]\,, \tag{4.5e}$$
$$\mathcal{Z}_1 = \mu^2 Ng(g_+ + g_-) - \mathcal{X}_1 \tag{4.5f}$$

When $\mathcal{X}_s = \mathcal{Y}_s = \mathcal{Z}_s = 0$, eq. (4.4b) dictates that $\Omega = 0$, and one obtains from eq. (4.4a) that $H_2(r) \propto (rN)^{-1}$. On the other hand, close to the outer boundary, eq. (4.4c) retrieves $H_0(r) = a + H_2(r)$, where $a \in \mathbb{R}$ is a constant. The first-order Klein-Gordon equation reads

$$\begin{aligned}
&\frac{1}{r^2\sigma}\partial_r(r^2\sigma N\partial_r\phi_\pm) + \left(\frac{\omega_\pm^2}{\sigma^2 N} - V_0' - \phi^2 V_0''\right)\phi_\pm \\
&\quad = \phi^2 V_0''\phi_\mp + \frac{1}{2}N\partial_r\phi\,\partial_r(H_0 + H_2) - \frac{\omega\phi}{2\sigma^2 N}\left[(\omega + \omega_\pm)H_0 + (\omega - \omega_\mp)H_2\right] + \frac{H_2}{r^2\sigma}\partial_r(r^2\sigma N\partial_r\phi) \\
&\quad = \phi^2 V_0''\phi_\mp + \frac{1}{2}N\partial_r\phi\,\partial_r(H_0 + H_2) - \frac{\omega(\omega + \omega_\pm)\phi}{2\sigma^2 N}(H_0 + H_2) + \phi V_0' H_2\,,
\end{aligned} \tag{4.6}$$

JCAP06(2024)068

whereas the first-order Proca equation yields

$$\frac{1}{r^2\sigma}\partial_r\left[\frac{r^2}{\sigma}(\partial_r f_\pm-\omega_\pm g_\pm)\right]+\frac{H_0-H_2}{r^2\sigma}\partial_r\left[\frac{r^2}{\sigma}(\partial_r f-\omega g)\right]$$
$$+\frac{\partial_r f-\omega g}{2\sigma^2}\partial_r(H_0-H_2)-\frac{\mu^2}{\sigma^2 N}(fH_0+f_\pm)\,,$$
$$=\frac{1}{r^2\sigma}\partial_r\left[\frac{r^2}{\sigma}(\partial_r f_\pm-\omega_\pm g_\pm)\right]+\frac{\partial_r f-\omega g}{2\sigma^2}\partial_r(H_0-H_2)-\frac{\mu^2}{\sigma^2 N}(fH_2+f_\pm)=0\,, \quad (4.7a)$$

$$\omega_\pm(\partial_r f_\pm-\omega_\pm g_\pm)+\frac{\omega+\omega_\pm}{2}(\partial_r f-\omega g)(H_0-H_2)+\mu^2\sigma^2 N(g_\pm-gH_2)$$
$$=\omega_\pm(\partial_r f_\pm-\omega_\pm g_\pm)+\mu^2\sigma^2 N(g_\pm-gH_0)\mp\frac{1}{2}\frac{\omega_+-\omega_-}{\omega_++\omega_-}\mu^2\sigma^2 Ng(H_0-H_2)=0\,, \quad (4.7b)$$

Finally, the first-order Lorenz condition is

$$\frac{1}{r^2}\partial_r(r^2\sigma N g_\pm)-\frac{H_2}{r^2}\partial_r(r^2\sigma N g)+\frac{\omega_\pm f_\pm}{\sigma N}+\frac{(\omega+\omega_\pm)f}{2\sigma N}H_0-\frac{(\omega-\omega_\pm)f}{2\sigma N}H_2-\frac{1}{2}Ng\partial_r(H_0+H_2)$$
$$=\frac{1}{r^2}\partial_r(r^2\sigma N g_\pm)+\frac{\omega_\pm f_\pm}{\sigma N}+\frac{(\omega+\omega_\pm)f}{2\sigma N}(H_0+H_2)-\frac{1}{2}Ng\partial_r(H_0+H_2)=0\,. \quad (4.8a)$$

4.2 Boundary conditions

The perturbed functions $\{H_0,\, H_2,\, \phi_\pm,\, f_\pm,\, g_\pm\}$ must have regular Taylor series around $r=0$. Thus, the inner boundary conditions are

$$H_0(r)=\begin{cases}h_0-\dfrac{8\pi G}{3}\phi_0\left\{\dfrac{2\omega^2\phi_0}{\sigma_0^2}h_0+\left[\dfrac{2\omega\omega_+}{\sigma_0^2}-\tilde{V}_0'\right]\phi_+(0)+\left[\dfrac{2\omega\omega_-}{\sigma_0^2}-\tilde{V}_0'\right]\phi_-(0)\right\}r^2+\dots\,, & s=0\,,\\[2ex] h_0-\dfrac{8\pi G}{3}\dfrac{\mu^2 f_0}{\sigma_0^2}[f_0h_0+f_+(0)+f_-(0)]r^2+\dots\,, & s=1\,,\end{cases}$$

$$H_2(r)=\begin{cases}\dfrac{8\pi G}{3}\phi_0\left\{\dfrac{\omega^2\phi_0}{\sigma_0^2}h_0+\left[\dfrac{\omega\omega_+}{\sigma_0^2}+\tilde{V}_0'\right]\phi_+(0)+\left[\dfrac{\omega\omega_-}{\sigma_0^2}+\tilde{V}_0'\right]\phi_-(0)\right\}r^2+\dots\,, & s=0\,,\\[2ex] \dfrac{4\pi G}{3}\dfrac{\mu^2 f_0}{\sigma_0^2}\,[f_0h_0+f_+(0)+f_-(0)]\,r^2+\dots\,, & s=1\,,\end{cases}$$

$$\phi_\pm(r)=\phi_\pm(0)-\frac{1}{3}\left\{\frac{\omega(\omega+\omega_\pm)\phi_0}{4\sigma_0^2}h_0+\frac{1}{2}\left[\frac{\omega_\pm^2}{\sigma_0^2}-\tilde{V}_0'-\phi_0^2\tilde{V}_0''\right]\phi_\pm(0)-\frac{1}{2}\phi_0^2\tilde{V}_0''\phi_\mp(0)\right\}r^2+\dots\,,$$

$$f_\pm(r)=f_\pm(0)-\frac{1}{6}\left[\left(\frac{\omega_\pm^2}{\sigma_0^2}-\mu^2\right)f_\pm(0)+\frac{\omega_\pm(\omega+\omega_\pm)}{2}f_0h_0\right]r^2+\dots\,,$$

$$g_\pm(r)=-\frac{1}{3\sigma_0^2}\left[\omega_\pm f_\pm(0)+\frac{\omega+\omega_\pm}{2}f_0h_0\right]r+\dots\,,$$

where $\{h_0,\, \phi_\pm(0),\, f_\pm(0)\}$ are as yet undetermined constants, $\tilde{V}_0'\equiv V'(\phi_0^2)$ and $\tilde{V}_0''\equiv V''(\phi_0^2)$. The first-order matter equations are linear, which means that both $\phi_+(0)$ and $f_+(0)$ (say) can be set to unity without loss of generality. Since $\phi_+=\phi_-$ and $f_+=f_-$ when $\Omega=0$, one sets $\phi_+(0)=\phi_-(0)$ and $f_+(0)=f_-(0)$ and checks afterwards whether the outer boundary

JCAP06(2024)068

conditions hold,

$$H_0(r) \approx h_\infty + \frac{a_\infty}{r}\,, \tag{4.10a}$$

$$H_2(r) \approx \frac{a_\infty}{r}\,, \tag{4.10b}$$

$$\phi_\pm(r) \approx a_\pm \frac{e^{-r\sqrt{\mu^2-\omega_\pm^2}}}{r}\,, \tag{4.10c}$$

$$f_\pm(r) \approx b_\pm \frac{e^{-r\sqrt{\mu^2-\omega_\pm^2}}}{r}\,, \tag{4.10d}$$

$$g_\pm(r) \approx b_\pm \frac{\omega_\pm}{\sqrt{\mu^2-\omega_\pm^2}} \frac{e^{-r\sqrt{\mu^2-\omega_\pm^2}}}{r}\,. \tag{4.10e}$$

where $\{h_\infty, a_\infty, a_\pm, b_\pm\}$ are constants. The BCs are summarized in table 1.

4.3 Physical quantities

The Noether charge (2.5) and Komar mass (2.7) of the perturbed solutions are time-dependent, yielding, respectively, $Q_s = Q_s^{(0)} + \epsilon\, Q_s^{(1)} + \ldots$ and $M_s = M_s^{(0)} + \epsilon\, M_s^{(1)} + \ldots$, where

$$Q_s^{(1)} = 4\pi \int_0^\infty \mathrm{d}r\, r^2 \rho_{Q_s}^{(1)}\,, \tag{4.11a}$$

$$M_s^{(1)} = 4\pi \int_0^\infty \mathrm{d}r\, r^2 \rho_{M_s}^{(1)} = 8\pi \cos(\Omega t) \int_0^\infty \mathrm{d}r\, r^2 \mathcal{X}_s\,, \tag{4.11b}$$

and

$$\rho_{Q_0}^{(1)} = 2\cos(\Omega t)\frac{\phi}{\sigma^2 N}\left[2\omega\phi H_0 + (\omega+\omega_+)\phi_+ + (\omega+\omega_-)\phi_-\right]\,, \tag{4.12a}$$

$$\rho_{Q_1}^{(1)} = -\frac{\cos(\Omega t)}{\sigma^2}\left\{g\left[(\partial_r f_+ - \omega_+ g_+) + (\partial_r f_- - \omega_- g_-)\right] + (\partial_r f - \omega g)[g_+ + g_- + 2g(H_0 - H_2)]\right\}\,, \tag{4.12b}$$

The radial perturbations should leave the Noether charge unchanged, i.e. $Q_s = Q_s^{(0)}$, and thus $Q_s^{(1)} = 0$.

5 Results

The numerical results are obtained using MATHEMATICA [36], namely the built-in symbols NDSOLVE and FINDROOT. The results are presented in terms of dimensionless quantities, obtained from products or quotients of the mass m of the bosonic field. They are thus valid for any value of m. Assigning a specific value to m sets the characteristic scale of the system. To compare the physical properties of bosonic stars to those of other compact objects, one can express $\{M, Q, R, \omega, \Omega^2\}$ in convenient units (where $\hbar$ and c are reinstated for clarity):

$$M \approx 1.336 \left(\frac{10^{-10}\ \mathrm{eV}/c^2}{m}\right) \times \frac{M}{m_\mathrm{P}^2/m} \quad [M_\odot]\,, \tag{5.1a}$$

$$Q \approx 2.475 \left(\frac{10^{16}\ \mathrm{eV}/c^2}{m}\right)^2 \times \frac{Q}{m_\mathrm{P}^2/m^2} \quad [\mathrm{mol}]\,, \tag{5.1b}$$

JCAP06(2024)068

$$R \approx 1.973 \left(\frac{10^{-10}\ \mathrm{eV}/c^2}{m}\right) \times \frac{R}{\hbar/(mc)} \quad [\mathrm{km}]\,, \tag{5.1c}$$

$$\omega \approx 151.9 \left(\frac{m}{10^{-10}\ \mathrm{eV}/c^2}\right) \times \frac{\omega}{mc^2/\hbar} \quad [\mathrm{kHz}]\,, \tag{5.1d}$$

$$\Omega^2 \approx 23082 \left(\frac{m}{10^{-10}\ \mathrm{eV}/c^2}\right)^2 \times \left(\frac{\Omega}{mc^2/\hbar}\right)^2 \quad [\mathrm{kHz}^2]\,, \tag{5.1e}$$

where $m_\mathrm{P} = \sqrt{\hbar c/G}$ is the Planck mass. The values of the (dimensionless) quantities to the right of the multiplication signs can be readily read from the plots for a given solution. If $M/(m_\mathrm{P}^2/m) \sim \mathcal{O}(1)$ (say), bosonic fields with $m \lesssim 10^{-10}\,\mathrm{eV}/c^2$ are compatible with stellar-mass or even supermassive objects.

5.1 Equilibrium solutions

To find equilibrium bosonic stars, one fixes $\omega < \mu$, provides an initial guess for ψ_0 (either ϕ_0 or f_0), and solves the boundary value problem with the corresponding BCs. This amounts to numerically integrating eqs. (3.3) and (3.6) from $r\mu = \delta \ll 1$ (here, $\delta = 10^{-6}$) to $D\mu \sim \mathcal{O}(10)$, typically, where D is the (numerical) radial coordinate of the outer boundary.[3] Once a solution is found, the mass, Noether charge, radius, and compactness can be readily computed. The solutions presented herein are uniquely identified by the field's central value, thus being particularly convenient to display most physical quantities as functions of either ϕ_0 or f_0.

Figure 2 (left column) shows the parameter space of fundamental MBSs (see also figure 4). Their mass-radius relation is akin to that of neutron stars [30]. The minimum radius of MBSs is $4.12/\mu$. Like neutron stars, they also have a maximum mass, $M_\mathrm{MBSs}^{(\mathrm{max})} \approx 0.633\, m_\mathrm{P}^2/m$. The maximum-mass solution also maximizes the Noether charge, but its binding energy is negative. It is long known that this configuration marks a change in the stability of MBSs. This will be addressed in the following section.

The general features outlined above might change when adding self-interactions to the scalar-field potential. Recall, however, that both the solitonic and axionic potentials reduce to that of MBSs when $v_0 \gg |\Phi|$ and $f_a \gg \sqrt{\hbar}|\Phi|$, respectively. Of particular interest here are cases for which the mass has several critical points with respect to ϕ_0. This can occur in the complementary regimes $v_0 \lesssim |\Phi|$ and $f_a \lesssim \sqrt{\hbar}|\Phi|$, as it is clear from figure 2 (middle and right columns) for fundamental SBSs with $v_0 = 0.20$ and fundamental ABSs with $f_a = 0.08$, respectively. Their parameter space differs significantly from that of MBSs, displaying new branches, and hence new mass extrema. The inclusion of self-interactions can in particular make the first maximum a local (rather than a global) extremum. Although this is only shown for SBSs, the same is possible for ABSs with sufficiently small values of f_a [32]. In the neighborhood of the new maxima lie configurations with negative binding energy. Additionally, self-interacting BSs can be "smaller" and more compact than MBSs, as shown in figure 4.

The parameter space of fundamental MBSs and PSs, on the other hand, look very much alike, with f_0 playing the role of ϕ_0 in the latter — see figure 3 and figure 4 (bottom row). The maximum mass of PSs is significantly larger than that of MBSs, $M_\mathrm{PSs}^{(\mathrm{max})} \approx 1.058\, m_\mathrm{P}^2/m$.

[3] The numerical value of D should be such that the hypersurface $r = D$ encloses more than 99% of the mass, i.e. $D > R$. The stars become dilute when approaching the Newtonian limit ($\omega \to \mu$), in which one takes $D\mu \sim \mathcal{O}(100)$.

JCAP06(2024)068

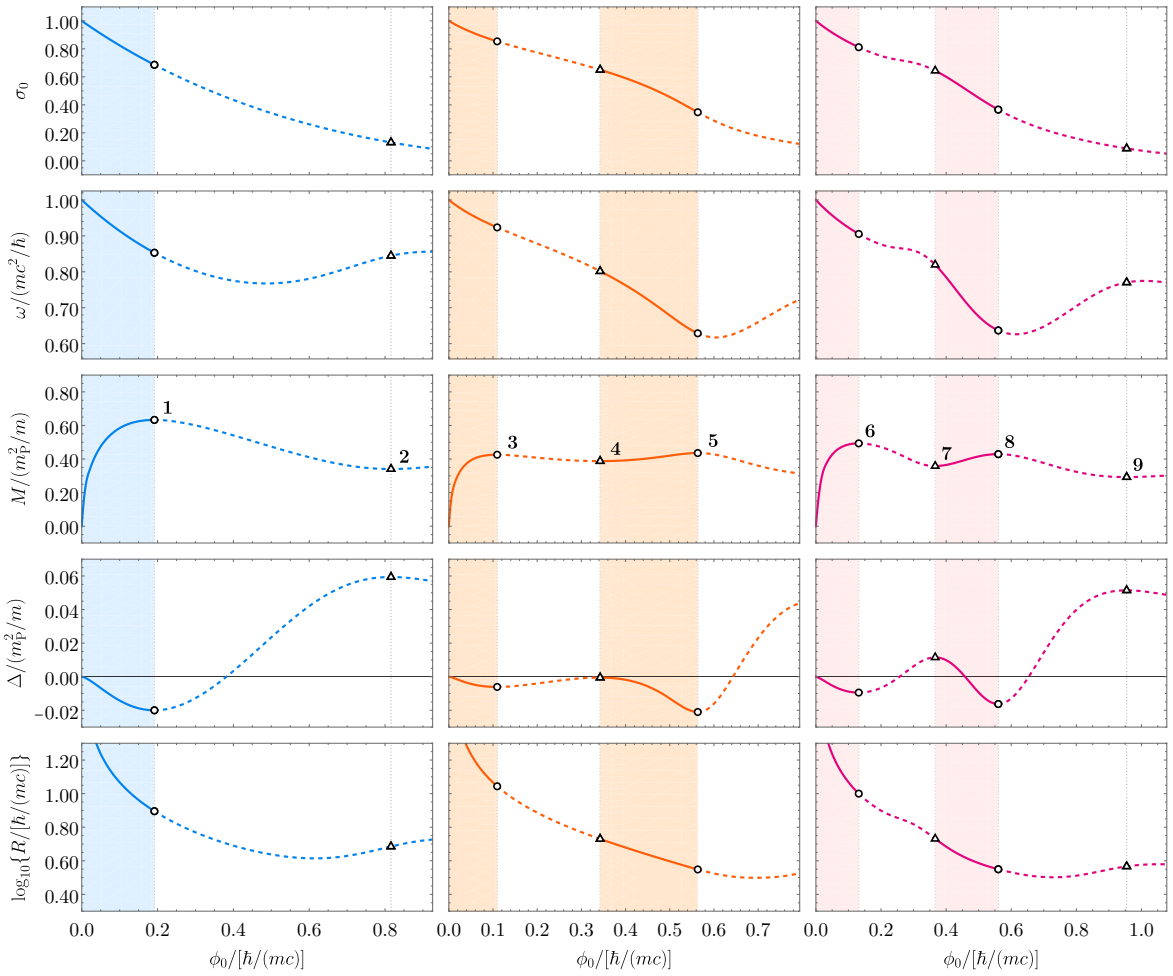

Figure 2. Spherically symmetric spin-0 boson stars in equilibrium. Central value of the metric function σ, σ_0 (first row), frequency (second row), mass (third row), binding energy, $\Delta \equiv M - mQ$ (fourth row), and radius (fifth row), all as functions of the shooting parameter ϕ_0, for mini-boson stars (left column), solitonic boson stars with $v_0 = 0.20$ (middle column), and axion boson stars with $f_a = 0.08$ (right column). The critical points, labeled numerically in the third row (cf. table 2), are represented by open circles (maxima) and open triangles (minima). Stars along solid (dashed) curves are stable (unstable), i.e. $\Omega^2 > 0$ ($\Omega^2 < 0$) (cf. figure 5).

As before, PSs can become heavier and more compact when (repulsive) self-interactions are taken into account [37], but this case is not considered here.

5.2 Perturbed solutions

Each equilibrium solution is expected to have an infinite countable number of squared perturbation frequencies $\{\Omega_n^2\}_{n=0}^{\infty}$, labeled by the node number n. The lowest-frequency mode is called the fundamental mode, whereas modes with $n > 0$ are excited modes. When, for a given solution, the fundamental mode is stable ($\Omega_0^2 > 0$), then all excited modes are stable, because $\Omega_0^2 < \Omega_1^2 < \Omega_2^2 < \ldots$. When it is unstable, the first excited mode can be either stable or unstable, because $\Omega_0^2 < \Omega_1^2$. If stable, all higher-n modes are also stable. If

JCAP06(2024)068

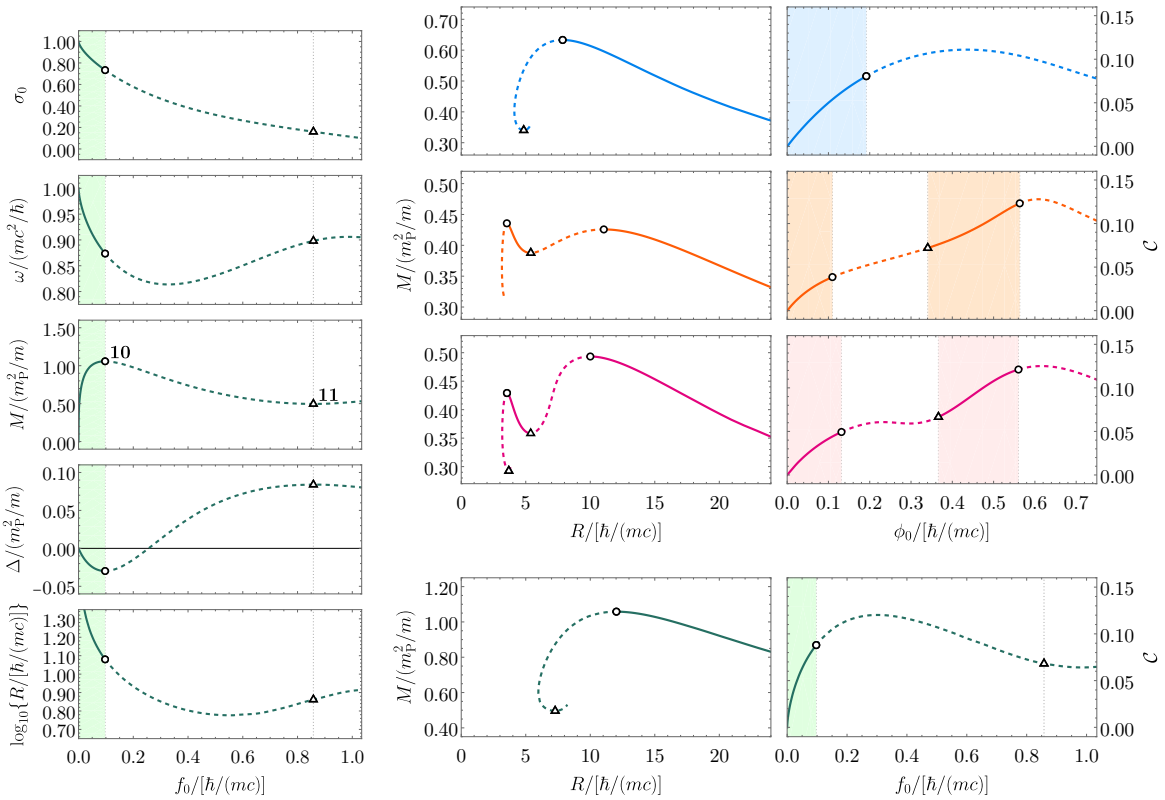

Figure 3. Same as in figure 2 but for spherically symmetric as a function of the shooting parameter ϕ_0 therein.

Figure 4. Mass-radius diagram (left column) and compactness as a function of the shooting parameter ψ_0 (right column) for the spin-1 boson stars in equilibrium spin-0 (top rows) and spin-1 (bottom row) boson stars in figure 2 (cf. figure 6). f_0 plays the role of and figure 3, respectively, where the colors match those therein.

JCAP06(2024)068

unstable, the second excited mode can be either stable or unstable, because $\Omega_1^2 < \Omega_2^2$. The very same reasoning can be generalized to the n-th mode. The fundamental mode is thus the most relevant to linear stability. Still, in the following, both fundamental ($n = 0$) and first ($n = 1$) excited modes are considered. The latter are only used to benchmark the results against those available in the literature (see appendix A).

To find perturbed BSs, one takes an equilibrium solution, provides an initial guess for $\{h_0, \Omega^2\}$, and solves the boundary value problem defined by eqs. (4.4) and eqs. (4.6) or (4.7). The squared fundamental frequencies Ω_0^2 of the equilibrium solutions presented in the previous section are shown in figure 5 and figure 6. As expected, they vanish in the Newtonian limit ($\omega \to \mu$). For MBSs and PSs, Ω_0^2 first increases with increasing ϕ_0 and f_0, respectively, reaches a maximum value and then drops to zero at the maximum-mass solution. The frequency Ω_0 ranges roughly between 0 and 10^{-2} (in units of $mc^2/\hbar$) in the first branch of both MBSs and PSs, but it is typically larger for the latter. The excited states are also stable. The zero mode ($\Omega_0^2 = 0$) marks the onset of the instability. Indeed, Ω_0^2 becomes negative as ϕ_0 and f_0 increase beyond their maximum-mass values, with shorter and shorter

instability timescales. In summary, both MBSs and PSs are linearly stable against radial perturbations in the first branch but succumb to instabilities otherwise. The dynamical evolution of perturbed MBSs [21, 22] corroborates this result: configurations in the first branch are set into oscillation, dominated by the fundamental frequency Ω_0, which results in a leak of scalar radiation and a decrease in the mass; configurations in the remaining branches either migrate towards the first branch, collapse into BHs or disperse altogether. It is worth noting that the aforementioned dynamical evolutions were performed by enforcing spherical symmetry, which prevents MBSs from decaying into non-spherical configurations in case such decay channels would be dynamically favored. The authors are not aware of any study of non-spherical perturbations of spherically symmetric bosonic stars. Lifting this restriction would make it possible to trigger non-monopolar modes that could change the dynamics. Given that spherical configurations are thought to be the ground state of MBSs, it is likely, though, that their stability properties remain unaltered. As for spherical PSs, recent dynamical evolutions have shown that, in the absence of spatial symmetries or even imposing a $\mathbb{Z}_2$-symmetry, configurations in the first branch, supposed to be stable according to linear perturbation theory, grow a dipolar mode and become prolate PSs [38]. This is because the former are not the true ground states of PSs, as first realized in the Newtonian limit [39].

The parameter space of both MBSs and PSs feature two critical points: a (global) maximum (**1** and **10**, respectively) and a (local) minimum (**2** and **11**, respectively). While the maxima do correspond to a change in the stability of the fundamental mode, it is clear from figure 5 and figure 6 that the minima do not signal any instability-stability transition, but rather represent unstable configurations. The very same conclusions can be drawn by applying the critical point method, i.e. computing the sign of $\mathrm{d}R/\mathrm{d}\psi_0$ at each critical point, as illustrated in table 2. These results show that critical points are *not always* zero modes, pinpointing stability reversals (either from stability to instability or vice versa).

Turning to self-interacting BSs, the spectrum of fundamental frequencies is richer, with (at least) two stable and two unstable branches. As before, the first branch, which contains the Newtonian limit, is stable, whereas the second branch is unstable. The instability timescale has a minimum value, though, which depends on the parameters σ_0 and f_a. The local minima **4** and **7** correspond to zero modes, meaning that the third branch is also stable. The frequency Ω_0 also attains a maximum value in this branch, about one order of magnitude larger than that of the first branch. The third and fourth branches are separated by the maxima **5** and **8**, for which $\Omega_0^2 = 0$. The parameter space of ABSs has another critical point, the local minimum **9**, which is not a zero mode: the fourth and the fifth branches are both unstable. Once again, the critical point method is in agreement with these conclusions, as shown in table 2.

6 Conclusion

Dynamical stability is a central notion in physics. A system in dynamic equilibrium is said to be dynamically stable if, when perturbed, all physical quantities associated with the perturbation remain bounded in time, and, ultimately, dynamic equilibrium is restored. Otherwise, the system is said to be dynamically unstable. This notion encompasses those of linear dynamical stability as well as mode stability. Although both refer to linear perturbations (i.e. sufficiently

JCAP06(2024)068

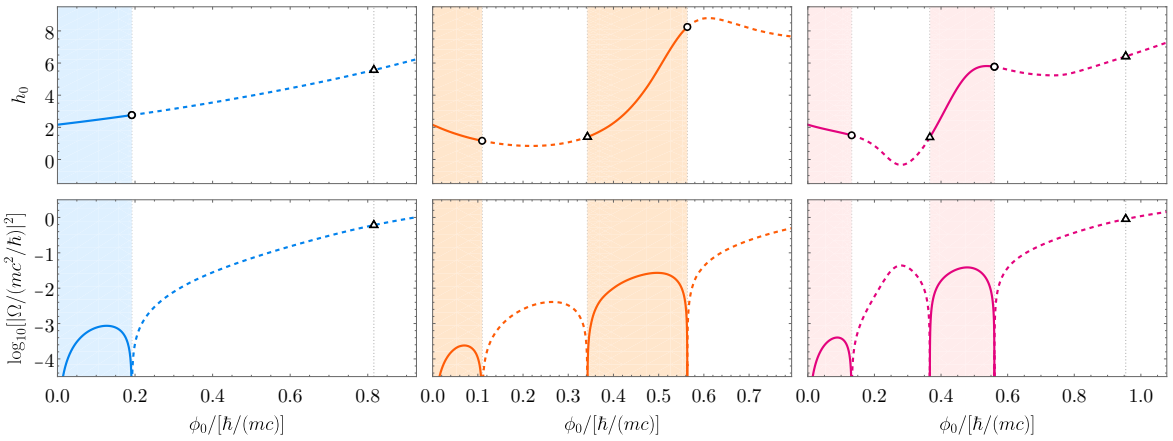

Figure 5. Perturbed spherically symmetric spin-0 boson stars. Central value of the metric function H_0, h_0 (first row), and squared fundamental frequency Ω_0^2, both as functions of the shooting parameter ϕ_0, for mini-boson stars (left column), solitonic boson stars with $v_0 = 0.20$ (middle column), and axion boson stars with $f_a = 0.08$ (right column), in a similar fashion to that in figure 2.

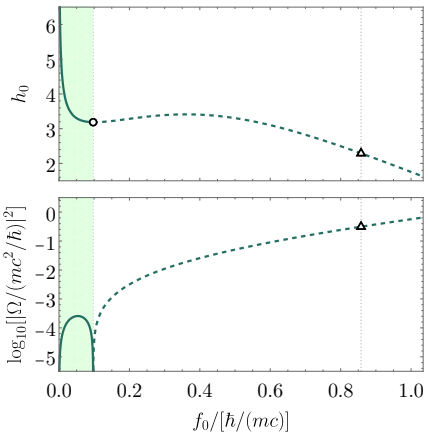

Figure 6. Same as in figure 5 but for spherically symmetric spin-1 boson stars. f_0 plays the role of ϕ_0 therein.

small disturbances), the latter concerns mode (i.e. fixed-frequency) perturbations. Mode stability guarantees that the system does not have exponentially growing mode solutions (with $\mathrm{Im}\,\Omega > 0$).

Dynamical stability implies linear dynamical stability, which in turn implies mode stability. It is then natural to assess the dynamical stability of a system by first studying its mode stability. This amounts to considering mode solutions to the equations governing linear perturbations. There has been a major effort to establish the mode stability of several compact objects, such as fluid stars, BSs, and BHs. This problem is generally intractable unless symmetries are imposed on the system. Spherical symmetry is frequently the starting point for such analysis, as it greatly simplifies the perturbation equations. A further simplification is to consider monopolar perturbations, i.e. study radial stability. Such oversimplification — narrowing dynamical stability down to radial stability — may seem pointless. However,

JCAP06(2024)068

Critical point	$\frac{\psi_0}{\hbar/(mc)}$	$\frac{\omega}{mc^2/\hbar}$	$\frac{M}{m_{\rm P}^2/m}$	$\frac{Q}{m_{\rm P}^2/m^2}$	$\frac{R}{\hbar/(mc)}$	$\frac{{\rm d}R}{{\rm d}\psi_0}$	$\left(\frac{\Omega_0}{mc^2/\hbar}\right)^2$
1	0.192	0.853	0.633	0.653	7.86	< 0	0
2	0.816	0.845	0.341	0.281	4.84	> 0	-0.606
3	0.109	0.924	0.426	0.432	11.1	< 0	0
4	0.342	0.802	0.388	0.388	5.37	< 0	0
5	0.563	0.629	0.436	0.457	3.54	< 0	0
6	0.132	0.905	0.493	0.503	10.0	< 0	0
7	0.366	0.820	0.358	0.347	5.39	< 0	0
8	0.560	0.637	0.429	0.445	3.55	< 0	0
9	0.955	0.770	0.294	0.241	3.69	> 0	-0.900
10	0.0971	0.874	1.06	1.09	12.0	< 0	0
11	0.858	0.898	0.496	0.412	7.28	> 0	-0.312

Table 2. Critical points identified in figure 2 and figure 3.

as far as spherically symmetric systems are concerned, radial stability analysis can provide a good proxy for linear dynamics, as reported in [22, 24] for BSs.

This paper addressed the radial stability of spherically symmetric mini-, solitonic, and axionic BSs as well as PSs. It focused on the numerical computation of their fundamental squared perturbation frequency. Previous works mostly looked into MBSs, and results for SBSs and ABSs were sparse or even lacking in the literature.[4] The addition of self-interactions to the scalar-field potential turns the parameter space more involved, with more branches and also zero-frequency modes. As for PSs, their radial stability was preliminarily studied in [11], wherein the fundamental mode frequency was presented for configurations in the neighborhood of the maximum-mass PS. These results were extended herein to the whole parameter space of PSs. Their spectrum turns out to bear a close resemblance to that of MBSs, featuring a stable branch and an unstable branch, divided by the maximum-mass solution. Nonetheless, spherically symmetric PSs along the stable branch (with respect to spherical perturbations) are not dynamically stable, as they decay into prolate configurations, the true ground states of static PSs [38]. This is a remarkable example of how (radial) mode stability may not translate into dynamical stability. In light of this result, it would be of particular interest to study dipolar perturbations of prolate PSs.

Another example of the aforementioned contrast is that of radially excited MBSs, i.e. configurations with at least one node in the radial direction. Figure 7 shows the parameter space of one-node MBSs is akin to that of the ground state, with a stable branch connecting the Newtonian limit to the maximum-mass solution. Such putatively stable configurations turn out to be *dynamically unstable*, either decaying to the ground state or collapsing into a BH [41]. In other words, mode stability may not persist when non-linear effects are taken into account.

[4] To the best of the author's knowledge, the radial stability of SBSs was only partially addressed in [40].

JCAP06(2024)068

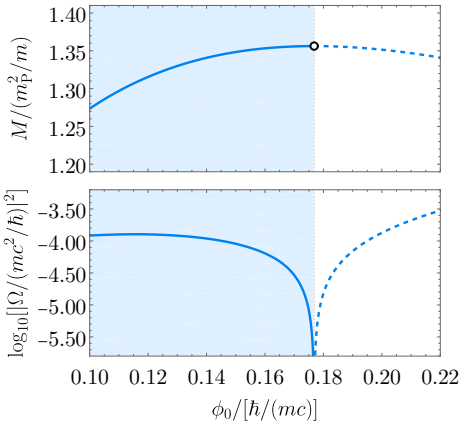

Figure 7. One-node spherically symmetric mini-boson stars. Mass (top row) and squared fundamental frequency Ω_0^2 (bottom row), both as functions of the shooting parameter ϕ_0.

The main take-home message from this study is that $\mathrm{d}M/\mathrm{d}\psi_0 = 0$ is not a sufficient condition for the existence of a zero-frequency mode and, therefore, for a stability-instability transition (as far as spherically symmetric bosonic stars are concerned[5]). This statement is not always made explicit in the literature — rather the opposite.[6] As a result, the condition $\mathrm{d}M/\mathrm{d}\psi_0 = 0$ can be easily misread as equivalent to $\Omega^2 = 0$. Table 2 makes the difference clear: all solutions listed therein satisfy $\mathrm{d}M/\mathrm{d}\psi_0 = 0$ but only those with $\Omega_0^2 = 0$ pinpoint changes in stability across the corresponding parameter space, as shown in figure 5 and figure 6. The authors hope the examples presented herein help clear up any misconceptions about the meaning of critical points on a plot of M vs. ψ_0, as they can lead to fallacious conclusions.

Acknowledgments

The authors would like to thank Richard Brito for discussions on the perturbation theory of PSs, and Eugen Radu for constructive comments and feedback on the manuscript. C.L.B. thanks the University of Aveiro for the kind hospitality during the development of part of this work.

This work is supported by the Center for Research and Development in Mathematics and Applications (CIDMA) through the Portuguese Foundation for Science and Technology (FCT — Fundação para a Ciência e a Tecnologia) through projects: UIDB/04106/2020 (DOI identifier https://doi.org/10.54499/UIDB/04106/2020); UIDP/04106/2020 (DOI identifier https://doi.org/10.54499/UIDP/04106/2020); PTDC/FIS-AST/3041/2020 (DOI identifier http://doi.org/10.54499/PTDC/FIS-AST/3041/2020); CERN/FIS-PAR/0024/2021 (DOI identifier http://doi.org/10.54499/CERN/FIS-PAR/0024/2021); and 2022.04560.PTDC (DOI identifier https://doi.org/10.54499/2022.04560.PTDC). This work has further been supported by the European Horizon Europe staff exchange (SE) programme HORIZON-MSCA-2021-SE-01 Grant No. NewFunFiCO-101086251. N.M.S. is supported by the FCT grant SFRH/BD/143407/2019 (DOI identifier https://doi.org/10.54499/SFRH/BD/143407/2019).

[5] See [42, 43] for a similar discussion on the critical point method applied to rotating relativistic stars.

[6] Exceptions exist, though. This subtlety has been properly addressed in the original work on ABSs [32].

JCAP06(2024)068

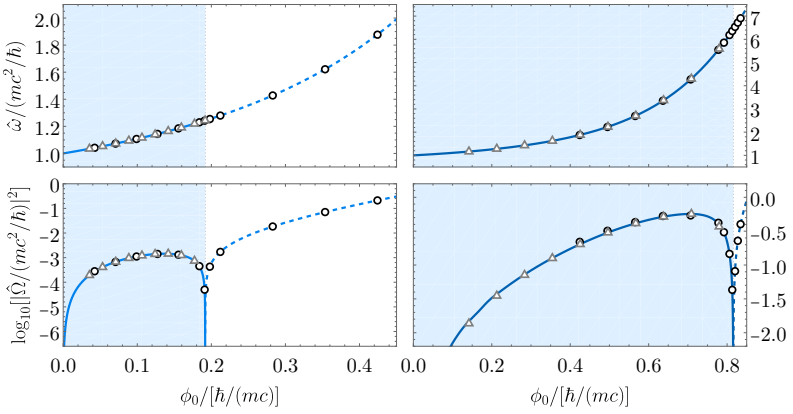

Figure 8. Spherically symmetric mini-boson stars. Rescaled frequencies $\{\hat{\omega}, \hat{\Omega}\}$ of the fundamental (left column) and first excited (right column) modes, both as a function of the shooting parameter ϕ_0. The black open circles and the gray open triangles are the data reported in [22] and [24], respectively.

C.L.B. acknowledges Conselho Nacional de Desenvolvimento Científico e Tecnológico (CNPq) and Fundação Amazônia Paraense de Amparo à Pesquisa (FAPESPA), from Brazil, for partial financial support.

A Comparison with the literature

For completeness, some of the results presented in section 5 are benchmarked against those available in the literature for the fundamental and first excited modes of MBSs [22, 24]. For that purpose, it is convenient to define the rescaled frequencies

$$\hat{\omega} \equiv \frac{\omega}{\sigma_0}\,, \qquad \hat{\Omega} \equiv \frac{\Omega}{\sigma_0}\,, \tag{A.1}$$

as they can be readily compared to those in [22]. Tables 3 and 4 (Tables 5 and 6) list relevant quantities of this work's solutions with values of ϕ_0 matching those selected in [22] ([24]) for the fundamental and first excited state, respectively. The last two columns of each table contains the values of $\hat{\omega}$ and $\hat{\Omega}_0^2$ (ω and Ω_0^2) reported therein. In general, the agreement is excellent, as clearly shown in figure 8, although there are some discrepancies in Ω_0^2 or $\hat{\Omega}_0^2$. This difference is likely to be linked to the cumulative errors when computing the perturbed solutions. This computation amounts to solving the "pulsation equations" using the equilibrium solutions, which, having been found numerically, already contain errors.

JCAP06(2024)068

$\frac{\phi_0}{\sqrt{2}\hbar/(mc)}$	σ_0	$\frac{\hat{\omega}}{mc^2/\hbar}$	$\frac{\omega}{mc^2/\hbar}$	$\frac{M}{m_{\rm P}^2/m}$	$\frac{Q}{m_{\rm P}^2/m^2}$	h_0	$\left(\frac{\Omega_0}{mc^2/\hbar}\right)^2$	$\left(\frac{\hat{\Omega}_0}{mc^2/\hbar}\right)^2$	$\left(\frac{\hat{\omega}}{mc^2/\hbar}\right)^2$ [22]	$\left(\frac{\hat{\Omega}_0}{mc^2/\hbar}\right)^2$ [22]
0.06	0.9222	1.0417	0.9606	0.4468	0.4523	0.1821	2.310×10^{-4}	2.716×10^{-4}	1.0417	2.8×10^{-4}
0.10	0.8732	1.0727	0.9367	0.5326	0.5427	0.1889	5.133×10^{-4}	6.732×10^{-4}	1.0727	6.7×10^{-4}
0.14	0.8263	1.1067	0.9144	0.5827	0.5968	0.1958	7.597×10^{-4}	1.113×10^{-3}	1.1067	1.11×10^{-3}
0.18	0.7814	1.1439	0.8939	0.6118	0.6289	0.2029	8.629×10^{-4}	1.413×10^{-3}	1.1440	1.41×10^{-3}
0.22	0.7384	1.1849	0.8749	0.6271	0.6462	0.2102	7.162×10^{-4}	1.314×10^{-3}	1.1849	1.31×10^{-3}
0.26	0.6973	1.2299	0.8576	0.6328	0.6527	0.2177	2.147×10^{-4}	4.415×10^{-4}	1.2299	4.5×10^{-4}
0.27	0.6872	1.2419	0.8535	0.6330	0.6530	0.2196	2.228×10^{-5}	4.717×10^{-5}	1.2419	0.5×10^{-4}
0.28	0.6773	1.2541	0.8495	0.6328	0.6528	0.2215	-2.010×10^{-4}	-4.380×10^{-4}	1.2542	-0.43×10^{-3}
0.30	0.6578	1.2796	0.8418	0.6315	0.6512	0.2254	-7.456×10^{-4}	-1.723×10^{-3}	1.2796	-1.71×10^{-3}
0.40	0.5664	1.4281	0.8088	0.6088	0.6236	0.2456	-5.896×10^{-3}	-1.838×10^{-2}	1.4281	-1.84×10^{-2}
0.50	0.4843	1.6215	0.7853	0.5703	0.5752	0.2672	-1.622×10^{-2}	-7.087×10^{-2}	1.6215	-7.09×10^{-2}
0.60	0.4109	1.8777	0.7715	0.5248	0.5167	0.2900	-3.568×10^{-2}	-2.114×10^{-1}	1.8777	-2.11×10^{-1}

Table 3. Comparison between this work's results and data reported in [22] for the fundamental mode (last two columns) of mini-boson stars.

$\frac{\phi_0}{\sqrt{2}\hbar/(mc)}$	σ_0	$\frac{\hat{\omega}}{mc^2/\hbar}$	$\frac{\omega}{mc^2/\hbar}$	$\frac{M}{m_{\rm P}^2/m}$	$\frac{Q}{m_{\rm P}^2/m^2}$	h_0	$\left(\frac{\Omega_0}{mc^2/\hbar}\right)^2$	$\left(\frac{\hat{\Omega}_0}{mc^2/\hbar}\right)^2$	$\left(\frac{\hat{\omega}}{mc^2/\hbar}\right)^2$ [22]	$\left(\frac{\hat{\Omega}_0}{mc^2/\hbar}\right)^2$ [22]
0.60	0.4108	1.8767	0.7715	0.5250	0.5169	0.3640	3.409×10^{-2}	2.019×10^{-1}	1.8777	0.22
0.70	0.3453	2.2240	0.7675	0.4773	0.4548	0.4011	3.581×10^{-2}	3.003×10^{-1}	2.2230	0.32
0.80	0.2871	2.6960	0.7741	0.4314	0.3953	0.4434	3.390×10^{-2}	4.113×10^{-1}	2.6963	0.43
0.90	0.2355	3.3536	0.7899	0.3908	0.3434	0.4915	2.860×10^{-2}	5.155×10^{-1}	3.3536	0.53
1.00	0.1902	4.2714	0.8123	0.3598	0.3046	0.5439	2.055×10^{-2}	5.682×10^{-1}	4.2714	0.54
1.10	0.1505	5.5470	0.8351	0.3428	0.2839	0.5956	9.284×10^{-3}	4.096×10^{-1}	5.5471	0.42
1.12	0.1433	5.8554	0.8390	0.3414	0.2822	0.6054	6.222×10^{-3}	3.031×10^{-1}	5.8555	3.05×10^{-1}
1.14	0.1362	6.1841	0.8425	0.3407	0.2813	0.6150	2.705×10^{-3}	1.457×10^{-1}	6.1842	1.46×10^{-1}
1.15	0.1328	6.3566	0.8442	0.3405	0.2812	0.6197	7.466×10^{-4}	4.233×10^{-2}	6.3566	4.30×10^{-2}
1.16	0.1294	6.5346	0.8457	0.3405	0.2812	0.6243	-1.360×10^{-3}	-8.123×10^{-2}	6.5346	-8.11×10^{-2}
1.17	0.1261	6.7184	0.8471	0.3407	0.2814	0.6289	-3.627×10^{-3}	-2.281×10^{-1}	6.7184	-2.28×10^{-1}
1.18	0.1228	6.9082	0.8485	0.3410	0.2818	0.6335	-6.064×10^{-3}	-4.020×10^{-1}	6.9083	-4.01×10^{-1}

Table 4. Comparison between this work's results and data reported in [22] for the first excited mode (last two columns) of mini-boson stars.

$\frac{\phi_0}{\sqrt{4\pi}\hbar/(mc)}$	σ_0	$\frac{\hat{\omega}}{mc^2/\hbar}$	$\frac{\omega}{mc^2/\hbar}$	$\frac{M}{m_{\rm P}^2/m}$	$\frac{Q}{m_{\rm P}^2/m^2}$	h_0	$\left(\frac{\Omega_0}{mc^2/\hbar}\right)^2$	$\frac{\omega}{mc^2/\hbar}$ [24]	$\left(\frac{\Omega_0}{mc^2/\hbar}\right)^2$ [24]
0.010	0.9346	1.0344	0.9668	0.4167	0.4211	0.1804	1.693×10^{-4}	0.9668	1.691×10^{-4}
0.015	0.9033	1.0531	0.9513	0.4853	0.4926	0.1846	3.345×10^{-4}	0.9513	3.344×10^{-4}
0.020	0.8729	1.0729	0.9365	0.5331	0.5432	0.1889	5.152×10^{-4}	0.9365	5.140×10^{-4}
0.025	0.8432	1.0939	0.9224	0.5673	0.5800	0.1932	6.806×10^{-4}	0.9224	6.798×10^{-4}
0.030	0.8144	1.1160	0.9089	0.5919	0.6069	0.1976	8.046×10^{-4}	0.9089	8.045×10^{-4}
0.035	0.7864	1.1395	0.8961	0.6093	0.6261	0.2021	8.617×10^{-4}	0.8961	8.617×10^{-4}
0.040	0.7591	1.1645	0.8840	0.6211	0.6394	0.2066	8.255×10^{-4}	0.8840	8.253×10^{-4}
0.045	0.7326	1.1909	0.8724	0.6284	0.6477	0.2112	6.698×10^{-4}	0.8724	6.697×10^{-4}
0.050	0.7067	1.2190	0.8615	0.6321	0.6520	0.2159	3.693×10^{-4}	0.8615	3.693×10^{-4}

Table 5. Comparison between this work's results and data reported in [24] for the fundamental mode (last two columns) of mini-boson stars.

$\frac{\phi_0}{\sqrt{4\pi}\hbar/(mc)}$	σ_0	$\frac{\hat{\omega}}{mc^2/\hbar}$	$\frac{\omega}{mc^2/\hbar}$	$\frac{M}{m_{\rm P}^2/m}$	$\frac{Q}{m_{\rm P}^2/m^2}$	h_0	$\left(\frac{\Omega_0}{mc^2/\hbar}\right)^2$	$\frac{\omega}{mc^2/\hbar}$ [24]	$\left(\frac{\Omega_0}{mc^2/\hbar}\right)^2$ [24]
0.04	0.7591	1.1645	0.8840	0.6212	0.6394	0.2521	8.530×10^{-3}	0.8840	7.892×10^{-3}
0.06	0.6571	1.2806	0.8415	0.6314	0.6511	0.2762	1.609×10^{-2}	0.8415	1.517×10^{-2}
0.08	0.5655	1.4299	0.8085	0.6084	0.6231	0.3020	2.319×10^{-2}	0.8085	2.277×10^{-2}
0.10	0.4833	1.6234	0.7851	0.5700	0.5748	0.3315	2.961×10^{-2}	0.7851	2.943×10^{-2}
0.12	0.4097	1.8814	0.7713	0.5242	0.5159	0.3646	3.414×10^{-2}	0.7713	3.406×10^{-2}
0.14	0.3442	2.2315	0.7676	0.4764	0.4537	0.4018	3.580×10^{-2}	0.7677	3.570×10^{-2}
0.16	0.2859	2.7078	0.7743	0.4305	0.3941	0.4444	3.382×10^{-2}	0.7743	3.379×10^{-2}
0.18	0.2344	3.3721	0.7904	0.3900	0.3423	0.4928	2.844×10^{-2}	0.7904	2.841×10^{-2}
0.20	0.1891	4.3001	0.8130	0.3592	0.3038	0.5453	2.030×10^{-2}	0.8130	2.028×10^{-2}
0.22	0.1495	5.5908	0.8357	0.3426	0.2836	0.5970	8.862×10^{-3}	0.8357	8.862×10^{-3}

Table 6. Comparison between this work's results and data reported in [24] for the first excited mode (last two columns) of mini-boson stars.

References

[1] V. Cardoso and P. Pani, *Testing the nature of dark compact objects: a status report*, *Living Rev. Rel.* **22** (2019) 4 [arXiv:1904.05363] [INSPIRE].

[2] D.J. Kaup, *Klein-Gordon Geon*, *Phys. Rev.* **172** (1968) 1331 [INSPIRE].

[3] R. Ruffini and S. Bonazzola, *Systems of selfgravitating particles in general relativity and the concept of an equation of state*, *Phys. Rev.* **187** (1969) 1767 [INSPIRE].

[4] R.L. Bowers and E.P.T. Liang, *Anisotropic Spheres in General Relativity*, *Astrophys. J.* **188** (1974) 657 [INSPIRE].

[5] M.S. Morris, K.S. Thorne and U. Yurtsever, *Wormholes, Time Machines, and the Weak Energy Condition*, *Phys. Rev. Lett.* **61** (1988) 1446 [INSPIRE].

[6] P.O. Mazur and E. Mottola, *Gravitational vacuum condensate stars*, *Proc. Nat. Acad. Sci.* **101** (2004) 9545 [gr-qc/0407075] [INSPIRE].

[7] S.D. Mathur, *The fuzzball proposal for black holes: An elementary review*, *Fortsch. Phys.* **53** (2005) 793 [hep-th/0502050] [INSPIRE].

[8] F.E. Schunck and E.W. Mielke, *General relativistic boson stars*, *Class. Quant. Grav.* **20** (2003) R301 [arXiv:0801.0307] [INSPIRE].

[9] S.L. Liebling and C. Palenzuela, *Dynamical boson stars*, *Living Rev. Rel.* **26** (2023) 1 [arXiv:1202.5809] [INSPIRE].

[10] L. Visinelli, *Boson stars and oscillatons: A review*, *Int. J. Mod. Phys. D* **30** (2021) 2130006 [arXiv:2109.05481] [INSPIRE].

[11] R. Brito, V. Cardoso, C.A.R. Herdeiro and E. Radu, *Proca stars: Gravitating Bose-Einstein condensates of massive spin 1 particles*, *Phys. Lett. B* **752** (2016) 291 [arXiv:1508.05395] [INSPIRE].

[12] E. Seidel and W.-M. Suen, *Formation of solitonic stars through gravitational cooling*, *Phys. Rev. Lett.* **72** (1994) 2516 [gr-qc/9309015] [INSPIRE].

[13] F.S. Guzman and L.A. Urena-Lopez, *Gravitational cooling of self-gravitating Bose-Condensates*, *Astrophys. J.* **645** (2006) 814 [astro-ph/0603613] [INSPIRE].

[14] A. Suárez, V.H. Robles and T. Matos, *A Review on the Scalar Field/Bose-Einstein Condensate Dark Matter Model*, *Astrophys. Space Sci. Proc.* **38** (2014) 107 [arXiv:1302.0903] [INSPIRE].

[15] L. Hui, J.P. Ostriker, S. Tremaine and E. Witten, *Ultralight scalars as cosmological dark matter*, *Phys. Rev. D* **95** (2017) 043541 [arXiv:1610.08297] [INSPIRE].

[16] F.F. Freitas et al., *Ultralight bosons for strong gravity applications from simple Standard Model extensions*, *JCAP* **12** (2021) 047 [arXiv:2107.09493] [INSPIRE].

[17] M. Gleiser, *Stability of Boson Stars*, *Phys. Rev. D* **38** (1988) 2376 [*Erratum ibid.* **39** (1989) 1257] [INSPIRE].

[18] P. Jetzer, *Dynamical Instability of Bosonic Stellar Configurations*, *Nucl. Phys. B* **316** (1989) 411 [INSPIRE].

[19] S. Chandrasekhar, *The Dynamical Instability of Gaseous Masses Approaching the Schwarzschild Limit in General Relativity*, *Astrophys. J.* **140** (1964) 417 [*Erratum ibid.* **140** (1964) 1342] [INSPIRE].

JCAP06(2024)068

[20] M. Gleiser and R. Watkins, *Gravitational Stability of Scalar Matter*, *Nucl. Phys. B* **319** (1989) 733 [INSPIRE].

[21] E. Seidel and W.-M. Suen, *Dynamical Evolution of Boson Stars. 1. Perturbing the Ground State*, *Phys. Rev. D* **42** (1990) 384 [INSPIRE].

[22] S.H. Hawley and M.W. Choptuik, *Boson stars driven to the brink of black hole formation*, *Phys. Rev. D* **62** (2000) 104024 [gr-qc/0007039] [INSPIRE].

[23] F.S. Guzman, *Evolving spherical boson stars on a 3-D Cartesian grid*, *Phys. Rev. D* **70** (2004) 044033 [gr-qc/0407054] [INSPIRE].

[24] B. Kain, *Boson stars and their radial oscillations*, *Phys. Rev. D* **103** (2021) 123003 [arXiv:2106.01740] [INSPIRE].

[25] N. Sanchis-Gual et al., *Numerical evolutions of spherical Proca stars*, *Phys. Rev. D* **95** (2017) 104028 [arXiv:1702.04532] [INSPIRE].

[26] F.J. Zerilli, *Gravitational field of a particle falling in a schwarzschild geometry analyzed in tensor harmonics*, *Phys. Rev. D* **2** (1970) 2141 [INSPIRE].

[27] Y. Kojima, S. Yoshida and T. Futamase, *Nonradial pulsation of a boson star. 1: Formulation*, *Prog. Theor. Phys.* **86** (1991) 401 [INSPIRE].

[28] S. Yoshida, Y. Eriguchi and T. Futamase, *Quasinormal modes of boson stars*, *Phys. Rev. D* **50** (1994) 6235 [INSPIRE].

[29] C.F.B. Macedo, P. Pani, V. Cardoso and L.C.B. Crispino, *Astrophysical signatures of boson stars: quasinormal modes and inspiral resonances*, *Phys. Rev. D* **88** (2013) 064046 [arXiv:1307.4812] [INSPIRE].

[30] S.L. Shapiro and S.A. Teukolsky, *Black holes, white dwarfs, and neutron stars: The physics of compact objects*, Wiley (1983) [DOI:10.1002/9783527617661] [INSPIRE].

[31] R. Friedberg, T.D. Lee and Y. Pang, *Scalar Soliton Stars and Black Holes*, *Phys. Rev. D* **35** (1987) 3658 [INSPIRE].

[32] D. Guerra, C.F.B. Macedo and P. Pani, *Axion boson stars*, *JCAP* **09** (2019) 061 [*Erratum ibid.* **06** (2020) E01] [arXiv:1909.05515] [INSPIRE].

[33] N. Siemonsen and W.E. East, *Stability of rotating scalar boson stars with nonlinear interactions*, *Phys. Rev. D* **103** (2021) 044022 [arXiv:2011.08247] [INSPIRE].

[34] C.A.R. Herdeiro, A.M. Pombo and E. Radu, *Asymptotically flat scalar, Dirac and Proca stars: discrete vs. continuous families of solutions*, *Phys. Lett. B* **773** (2017) 654 [arXiv:1708.05674] [INSPIRE].

[35] M. Maggiore, *Gravitational Waves. Vol. 2: Astrophysics and Cosmology*, Oxford University Press (2018).

[36] W.R. Inc., *Mathematica*, Version 13.3.

[37] K. Aoki and M. Minamitsuji, *Highly compact Proca stars with quartic self-interactions*, *Phys. Rev. D* **107** (2023) 044045 [arXiv:2212.07659] [INSPIRE].

[38] C.A.R. Herdeiro et al., *The non-spherical ground state of Proca stars*, *Phys. Lett. B* **852** (2024) 138595 [arXiv:2311.14800] [INSPIRE].

[39] Z. Wang, T. Helfer and M.A. Amin, *General relativistic polarized Proca stars*, *Phys. Rev. D* **109** (2024) 024019 [arXiv:2309.04345] [INSPIRE].

JCAP06(2024)068

[40] P. Ildefonso et al., *Self-interacting dipolar boson stars and their dynamics*, *Phys. Rev. D* **108** (2023) 064011 [arXiv:2307.00044] [INSPIRE].

[41] J. Balakrishna, E. Seidel and W.-M. Suen, *Dynamical evolution of boson stars. 2. Excited states and selfinteracting fields*, *Phys. Rev. D* **58** (1998) 104004 [gr-qc/9712064] [INSPIRE].

[42] K. Takami, L. Rezzolla and S. Yoshida, *A quasi-radial stability criterion for rotating relativistic stars*, *Mon. Not. Roy. Astron. Soc.* **416** (2011) L1 [arXiv:1105.3069] [INSPIRE].

[43] L.R. Weih, E.R. Most and L. Rezzolla, *On the stability and maximum mass of differentially rotating relativistic stars*, *Mon. Not. Roy. Astron. Soc.* **473** (2018) L126 [arXiv:1709.06058] [INSPIRE].

JCAP06(2024)068

Chapter 7

Outlook and perspectives

7.1 Outlook

Over the past decade, astronomers have made significant progress in testing the black hole paradigm and the Kerr hypothesis. Although state-of-the-art observations are consistent with the existence of Kerr black holes, the true nature of the most compact and extreme astrophysical objects in the Universe remains elusive. The evasiveness of black holes has its roots in the *teleological nature* of the event horizon [162], which refers to the fact that its location is determined by the whole future history of spacetime, i.e. by all the matter and energy that will ever fall into it. This results in its non-detectability: astronomers cannot detect the event horizon itself, but only test the consistency between observations and its existence. In addition to this property, the event horizon of canonical black holes harbours singularities—wherein general relativity breaks down—, and closed timelike curves—which violate causality. One can argue that these features do not raise concerns if the event horizon keeps them cloaked in secrecy, as suggested by the (weak) cosmic censorship conjecture. Even so, the event horizon itself is directly linked to the information loss paradox, arguably the most famous open problem in black hole physics.

The aforementioned theoretical challenges have prompted the search for alternatives, lumped together under the umbrella term "exotic compact objects", most of which (if not all) are inextricably tied to new physics. Given the congruence between observations and the current paradigm, one might ask oneself whether this is worth the effort. But the truth is that conjecturing and exploring exotic compact objects helps to deepen the understanding of the true nature of black holes, and gives a good head start on explaining hypothetical deviations from the paradigm. The failure of a given alternative

at describing the observable phenomenology of compact astrophysical objects reinforces the current paradigm. Its success, on the other hand, can challenge the prevailing framework in two ways: by either discarding the existence of astrophysical black holes or adding a new species to the zoo of compact objects. In other words, exotic compact objects can either take the place of black holes or coexist with them.

The design of astrophysically viable exotic compact objects is not an easy task: they should be described within well-motivated physical theories, have a dynamical formation mechanism, and be stable against sufficiently small perturbations [163]. Most of the proposals listed in Chapter 1 do not meet (at least one of) these requirements. Two families stand out from the rest in that regard: black holes with synchronized hair and bosonic stars. Both appear in Einstein's gravity minimally coupled to complex bosonic fields, one of the simplest yet rich classical field theories featuring exotic matter with potential astrophysical relevance—if ultralight, not only such putative bosonic fields can be part of the dark matter content of the Universe, but they can also form compact objects with astrophysical masses.

This doctoral thesis considered, for the most part, equilibrium properties of black holes with synchronized hair and bosonic stars, with a focus on their link to the formation and stability of these compact objects. Overall, the characteristics addressed herein are not very sensitive to the spin (either 0 or 1) of the bosonic field. In truth, minor differences apart, the parameter spaces of scalar and Proca field equilibrium solutions look very alike in shape, and possess similar trends and limits. As for black holes, the similitude extends to stationary clouds—e.g. their radial distribution is similar, both inside and outside the event horizon. Additionally, the variation of their "hairiness" in the neighborhood of the Kerr limit does not differ significantly, with superradiance-grown black holes storing at most 10% of their energy in the bosonic field. Finally, there is also no evidence that the spin has influence over the thermodynamic stability of black holes with synchronized hair (at least in the canonical ensemble)—they are unstable even if branched off from stable Kerr black holes.

Despite the close resemblance, there are, however, some relevant differences. Firstly, fixing the mass of the hypothetical bosonic field, the parameter space of comparable scalar and Proca field solutions spans over different ranges. The latter can be more massive and rotate slower than the former. Secondly, the elliptic solutions differ in the topology of the surfaces of constant energy density—they are spherical for a scalar field, but toroidal for a Proca field. This subtle dissimilarity turns out to be intimately connected with the dynamical stability of rotating bosonic stars [74]—boson stars are dynamically unstable, whereas Proca stars are dynamically stable. From an

astrophysical standpoint, Proca fields *might* be more viable than scalar fields. Whether this result holds in the presence of an event horizon or not, it remains unclear. Lastly, another difference, only briefly mentioned in Chapter 1 and Chapter 6, refers to the ground state of static bosonic stars, which do not share the same spatial symmetries—boson stars are spherical, and Proca stars are prolate.

The work presented herein fits into testing the theoretical and phenomenological viability of both black holes with synchornized hair and bosonic stars. This is a relevant and timely endeavour now that gravitational-wave astronomy is approaching its first precision era: the Laser Interferometer Space Antenna (LISA), a mission led by European Space Agency, is scheduled to launch in the mid-2030s, and is expected to deliver the ultimate test of the black hole paradigm and the Kerr hypothesis.

7.2 Perspectives

Extensions of the work presented herein are manifold. A natural avenue for future research is to obtain new equilibrium solutions of Einstein's equations (coupled or not to matter) describing compact objects. A fruitful approach to it has been looking for instabilities of known (exact or numerical) equilibrium solutions, as they are often associated with the existence of new ones.[1] A paradigmatic example of this connection is the Gregory-Laflamme instability of the black string [164, 165], whose zero mode generates a family of non-uniform black string solutions [166, 167]. Similarly, black holes with synchronized hair branch off from the zero mode of superradiant instabilities of Kerr black holes. The aforementioned instabilities are linear, i.e. they manifest themselves as exponentially-growing modes of the linearized equations of motion. Perturbation theory thus turns out to be particularly helpful to find such instabilities and provide approximations to new solutions (if any). This procedure has been used to obtain the original black holes with synchronized hair and their variants. Recently, a new variant has been suggested in the context of primordial magnetic monopoles [168]. If these are assumed to be magnetic black holes, massive charged bososnic fields can be superradiantly unstable in their vicinity, and, as expected, zero modes exist at the onset of the instability. Accordingly, new solutions branch out from them—they might be called magnetic black holes with synchronized hair. A distinctive feature of this family is that Dirac's quantization condition not only allows for the bosonic field's

[1] This is not necessarily the case. For instance, Myers-Perry black holes are prone to bar-mode (i.e. non-axisymmetric) instabilities but they do not branch off to new families of solutions.

winding number to be a rational number, but also can break its north-south symmetry. Their construction is underway, and the results shall be published soon.

A slightly different avenue is to search for quasi-equilibrium solutions of Einstein's equations, i.e. dynamical solutions that remain virtually unchanged for sufficiently long times (compared to either astrophysical or cosmological timescales). Dynamical resonances are a typical case of meta-equilibrium in black hole physics. These solutions describe slowly time-varying fields around black holes, and are closely related to quasi-bound states: the oscillation frequency (decay rate) of the former matches the real (imaginary) part of the frequency of the latter. However, while quasi-bound states are unphysical, as their energy density diverges at the event horizon, dynamical resonances are regular solutions with finite energy. They arise even when the metric is that of a Schwarzschild black hole [169, 170], evading no-hair theorems thanks to their dynamical nature. In the case of a massive scalar field, the half-life time of such solutions (also known in the literature as "wigs") can be larger than the Hubble time. The inclusion of (either attractive or repulsive) quartic self-interactions impacts the spatial distribution of the scalar field, but its effect upon the half-life time is subdominant [171]. An interesting variation on this setting is to replace the potential of the complex scalar field by a coupling to a real scalar field with a finite vacuum expectation value, that is, to consider the Friedberg-Lee-Sirlin field theory [172]. In this theory, which can be considered an ultraviolet completion of the aforementioned self-interacting scalar field theory, the real field generates mass for the complex field via a Higgs mechanism. A minimal coupling to Einstein's gravity allows for both equilibrium [173, 174] and quasi-equilibrium solutions. The computation and analysis of quasi-bound states and dynamical resonances of Schwarzschild black holes in this context is a work in progress.

Another avenue for future research is to study the stability of compact objects, a subject that is as crucial to their astrophysical viability as it is hard to tackle, namely away from spherical symmetry. There are two main approaches to address this issue: perturbation theory and numerical relativity. They typically offer different but complementary perspectives to the subject, and have been proven successful for different families of compact objects. Still, the stability of black holes with synchronized hair, albeit of great relevance, remains, for the most part, an open and challenging question. The only step in that direction concentrates on scalar hair and is based on linear perturbation theory [139]. The authors showed in particular that it is always possible to choose a gauge such that the linearized Klein-Gordon equation decouple from the metric perturbations. It would be interesting to exploit this simplification so as to extend the stability analysis therein, especially the computation of the quasinormal

mode spectrum, which is instrumental in the interpretation of the ringdown phase of compact binary mergers. Also of interest would be to consider Proca hair and check whether or not it is prone to stronger supperradiant instabilities, just as it happens in the absence of hair. Furthermore, a similar framework should likewise apply to bosonic stars, whose dynamical stability deserves further investigation, despite some enlightening recent developments [74, 9].

References

[1] N. M. Santos, C. L. Benone, L. C. B. Crispino, C. A. R. Herdeiro and E. Radu, *Black holes with synchronised Proca hair: linear clouds and fundamental non-linear solutions*, *JHEP* **07** (2020) 010 [2004.09536].

[2] N. M. Santos and C. A. R. Herdeiro, *Stationary scalar and vector clouds around Kerr–Newman black holes*, *Int. J. Mod. Phys. D* **29** (2020) 2041013 [2005.07201].

[3] N. M. Santos and C. A. R. Herdeiro, *Black holes, stationary clouds and magnetic fields*, *Phys. Lett. B* **815** (2021) 136142 [2102.04989].

[4] C. A. R. Herdeiro, E. Radu and N. M. Santos, *A bound on energy extraction (and hairiness) from superradiance*, *Phys. Lett. B* **824** (2022) 136835 [2111.03667].

[5] N. M. Santos, C. A. R. Herdeiro and E. Radu, *Thermodynamic stability of quasibald asymptotically flat black holes*, *Phys. Rev. D* **106** (2022) 124005 [2207.10089].

[6] N. M. Santos, C. L. Benone and C. A. R. Herdeiro, *Radial stability of spherical bosonic stars and critical points*, *JCAP* **06** (2024) 068 [2404.07257].

[7] A. M. Pombo, J. M. S. Oliveira and N. M. Santos, *Coupled scalar-Proca soliton stars*, *Phys. Rev. D* **108** (2023) 044044 [2304.13749].

[8] P. Ildefonso, M. Zilhão, C. Herdeiro, E. Radu and N. M. Santos, *Self-interacting dipolar boson stars and their dynamics*, *Phys. Rev. D* **108** (2023) 064011 [2307.00044].

[9] C. A. R. Herdeiro, E. Radu, N. Sanchis-Gual, N. M. Santos and E. dos Santos Costa Filho, *The non-spherical ground state of Proca stars*, *Phys. Lett. B* **852** (2024) 138595 [2311.14800].

[10] M. Carrasco-H., N. M. Santos and E. Contreras, *Spontaneous scalarization in Einstein-power-Maxwell-scalar models*, *Phys. Dark Univ.* **45** (2024) 101529 [2405.20442].

[11] J. A. Wheeler, *Our universe: the known and the unknown.*, *American Scientist* **56** (1968) 1.

[12] J. Michell, *On the Means of Discovering the Distance, Magnitude, &c. of the Fixed Stars, in Consequence of the Diminution of the Velocity of Their Light, in Case Such a Diminution Should be Found to Take Place in any of Them, and Such Other Data Should be Procured from Observations, as Would be Farther Necessary for That Purpose.*, *Phil. Trans. Roy. Soc. Lond.* **74** (1784) 35.

[13] P. de Laplace and I. du Cercle-Social, *Exposition du système du monde*, no. vol. 2 in Exposition du système du monde. De l'Imprimerie du Cercle-Social, rue du Théâtre Française, No. 4., 1796.

[14] A. Einstein, *Die Grundlage der allgemeinen Relativitätstheorie*, *Annalen der Physik* **354** (1916) 769.

[15] K. Schwarzschild, *On the gravitational field of a mass point according to Einstein's theory*, *Sitzungsber. Preuss. Akad. Wiss. Berlin (Math. Phys.)* **1916** (1916) 189 [physics/9905030].

[16] J. R. Oppenheimer and H. Snyder, *On Continued gravitational contraction*, *Phys. Rev.* **56** (1939) 455.

[17] R. P. Kerr, *Gravitational field of a spinning mass as an example of algebraically special metrics*, *Phys. Rev. Lett.* **11** (1963) 237.

[18] M. Schmidt, *3C 273 : A Star-Like Object with Large Red-Shift*, *Nature* **197** (1963) 1040.

[19] B. Carter, *Axisymmetric Black Hole Has Only Two Degrees of Freedom*, *Phys. Rev. Lett.* **26** (1971) 331.

[20] D. C. Robinson, *Uniqueness of the Kerr black hole*, *Phys. Rev. Lett.* **34** (1975) 905.

[21] P. T. Chrusciel, J. Lopes Costa and M. Heusler, *Stationary Black Holes: Uniqueness and Beyond*, *Living Rev. Rel.* **15** (2012) 7 [1205.6112].

[22] C. A. R. Herdeiro and E. Radu, *Asymptotically flat black holes with scalar hair: a review*, *Int. J. Mod. Phys. D* **24** (2015) 1542014 [1504.08209].

[23] M. S. Volkov, *Hairy black holes in the XX-th and XXI-st centuries*, in *14th Marcel Grossmann Meeting on Recent Developments in Theoretical and Experimental General Relativity, Astrophysics, and Relativistic Field Theories*, vol. 2, pp. 1779–1798, 2017, 1601.08230, DOI.

[24] S. Chandrasekhar, *Shakespeare, Newton and Beethoven or patterns of creativity*, *Current Science* **70** (1996) 810.

[25] R. Penrose, *Gravitational collapse and space-time singularities*, *Phys. Rev. Lett.* **14** (1965) 57.

[26] J. M. M. Senovilla, *Singularity Theorems and Their Consequences*, *Gen. Rel. Grav.* **30** (1998) 701 [1801.04912].

[27] NobelPrize.org, "All Nobel Prizes in Physics." https://www.nobelprize.org/prizes/lists/all-nobel-prizes-in-physics/, 2024.

[28] S. W. Hawking, *Black holes in general relativity*, *Commun. Math. Phys.* **25** (1972) 152.

[29] R. Penrose, *Gravitational collapse: The role of general relativity*, *Riv. Nuovo Cim.* **1** (1969) 252.

[30] J. D. Bekenstein, *Black holes and entropy*, *Phys. Rev. D* **7** (1973) 2333.

[31] J. M. Bardeen, B. Carter and S. W. Hawking, *The Four laws of black hole mechanics*, *Commun. Math. Phys.* **31** (1973) 161.

[32] S. W. Hawking, *Black hole explosions*, *Nature* **248** (1974) 30.

[33] S. W. Hawking, *Particle Creation by Black Holes*, *Commun. Math. Phys.* **43** (1975) 199.

[34] S. W. Hawking, *Breakdown of Predictability in Gravitational Collapse*, *Phys. Rev. D* **14** (1976) 2460.

[35] R. Genzel, F. Eisenhauer and S. Gillessen, *Experimental studies of black holes: status and future prospects*, 2404.03522.

[36] R. Giacconi, H. Gursky, F. R. Paolini and B. B. Rossi, *Evidence for x Rays From Sources Outside the Solar System*, *Phys. Rev. Lett.* **9** (1962) 439.

[37] R. Genzel, F. Eisenhauer and S. Gillessen, *The Galactic Center Massive Black Hole and Nuclear Star Cluster*, *Rev. Mod. Phys.* **82** (2010) 3121 [1006.0064].

[38] Event Horizon Telescope collaboration, *First Sagittarius A* Event Horizon Telescope Results. I. The Shadow of the Supermassive Black Hole in the Center of the Milky Way*, *Astrophys. J. Lett.* **930** (2022) L12 [2311.08680].

[39] Event Horizon Telescope collaboration, *First M87 Event Horizon Telescope Results. I. The Shadow of the Supermassive Black Hole*, *Astrophys. J. Lett.* **875** (2019) L1 [1906.11238].

[40] LIGO Scientific, Virgo collaboration, *Observation of Gravitational Waves from a Binary Black Hole Merger*, *Phys. Rev. Lett.* **116** (2016) 061102 [1602.03837].

[41] KAGRA, VIRGO, LIGO Scientific collaboration, *GWTC-3: Compact Binary Coalescences Observed by LIGO and Virgo during the Second Part of the Third Observing Run*, *Phys. Rev. X* **13** (2023) 041039 [2111.03606].

[42] V. Cardoso and P. Pani, *Testing the nature of dark compact objects: a status report*, *Living Rev. Rel.* **22** (2019) 4 [1904.05363].

[43] D. J. Kaup, *Klein-Gordon Geon*, *Phys. Rev.* **172** (1968) 1331.

[44] R. Ruffini and S. Bonazzola, *Systems of selfgravitating particles in general relativity and the concept of an equation of state*, *Phys. Rev.* **187** (1969) 1767.

[45] R. L. Bowers and E. P. T. Liang, *Anisotropic Spheres in General Relativity*, *Astrophys. J.* **188** (1974) 657.

[46] M. S. Morris, K. S. Thorne and U. Yurtsever, *Wormholes, Time Machines, and the Weak Energy Condition*, *Phys. Rev. Lett.* **61** (1988) 1446.

[47] P. O. Mazur and E. Mottola, *Gravitational vacuum condensate stars*, *Proc. Nat. Acad. Sci.* **101** (2004) 9545 [gr-qc/0407075].

[48] S. D. Mathur, *The Fuzzball proposal for black holes: An Elementary review*, *Fortsch. Phys.* **53** (2005) 793 [hep-th/0502050].

[49] M. S. Volkov and D. V. Galtsov, *NonAbelian Einstein Yang-Mills black holes*, *JETP Lett.* **50** (1989) 346.

[50] C. A. R. Herdeiro and E. Radu, *Kerr black holes with scalar hair*, *Phys. Rev. Lett.* **112** (2014) 221101 [1403.2757].

[51] D. D. Doneva and S. S. Yazadjiev, *New Gauss-Bonnet Black Holes with Curvature-Induced Scalarization in Extended Scalar-Tensor Theories*, *Phys. Rev. Lett.* **120** (2018) 131103 [1711.01187].

[52] H. O. Silva, J. Sakstein, L. Gualtieri, T. P. Sotiriou and E. Berti, *Spontaneous scalarization of black holes and compact stars from a Gauss-Bonnet coupling*, *Phys. Rev. Lett.* **120** (2018) 131104 [1711.02080].

[53] D. D. Doneva, F. M. Ramazanoğlu, H. O. Silva, T. P. Sotiriou and S. S. Yazadjiev, *Spontaneous scalarization*, *Rev. Mod. Phys.* **96** (2024) 015004 [2211.01766].

[54] J. Bovy and S. Tremaine, *On the local dark matter density*, *Astrophys. J.* **756** (2012) 89 [1205.4033].

[55] C. F. McKee, A. Parravano and D. J. Hollenbach, *Stars, Gas, and Dark Matter in the Solar Neighborhood*, *Astrophys. J.* **814** (2015) 13 [1509.05334].

[56] S. Sivertsson, H. Silverwood, J. I. Read, G. Bertone and P. Steger, *The localdark matter density from SDSS-SEGUE G-dwarfs*, *Mon. Not. Roy. Astron. Soc.* **478** (2018) 1677 [1708.07836].

[57] W. Hu, R. Barkana and A. Gruzinov, *Cold and fuzzy dark matter*, *Phys. Rev. Lett.* **85** (2000) 1158 [astro-ph/0003365].

[58] R. D. Peccei and H. R. Quinn, *CP Conservation in the Presence of Instantons*, *Phys. Rev. Lett.* **38** (1977) 1440.

[59] A. Arvanitaki, S. Dimopoulos, S. Dubovsky, N. Kaloper and J. March-Russell, *String Axiverse*, *Phys. Rev. D* **81** (2010) 123530 [0905.4720].

[60] F. F. Freitas, C. A. R. Herdeiro, A. P. Morais, A. Onofre, R. Pasechnik, E. Radu et al., *Ultralight bosons for strong gravity applications from simple Standard Model extensions*, *JCAP* **12** (2021) 047 [2107.09493].

[61] L. Hui, *Wave Dark Matter*, *Ann. Rev. Astron. Astrophys.* **59** (2021) 247 [2101.11735].

[62] J. A. Wheeler, *Geons*, *Phys. Rev.* **97** (1955) 511.

[63] F. E. Schunck and E. W. Mielke, *General relativistic boson stars*, *Class. Quant. Grav.* **20** (2003) R301 [0801.0307].

[64] S. L. Liebling and C. Palenzuela, *Dynamical boson stars*, *Living Rev. Rel.* **26** (2023) 1 [1202.5809].

[65] L. Visinelli, *Boson stars and oscillatons: A review*, *Int. J. Mod. Phys. D* **30** (2021) 2130006 [2109.05481].

[66] P. Jetzer and J. J. van der Bij, *CHARGED BOSON STARS*, *Phys. Lett. B* **227** (1989) 341.

[67] E. W. Mielke and F. E. Schunck, *Rotating boson stars*, .

[68] S. Yoshida and Y. Eriguchi, *Rotating boson stars in general relativity*, *Phys. Rev. D* **56** (1997) 762.

[69] T. D. Lee and Y. Pang, *Nontopological solitons*, *Phys. Rept.* **221** (1992) 251.

[70] S. Chandrasekhar, *The maximum mass of ideal white dwarfs*, *Astrophys. J.* **74** (1931) 81.

[71] M. Colpi, S. L. Shapiro and I. Wasserman, *Boson Stars: Gravitational Equilibria of Selfinteracting Scalar Fields*, *Phys. Rev. Lett.* **57** (1986) 2485.

[72] R. Brito, V. Cardoso, C. A. R. Herdeiro and E. Radu, *Proca stars: Gravitating Bose–Einstein condensates of massive spin 1 particles*, *Phys. Lett. B* **752** (2016) 291 [1508.05395].

[73] Z. Wang, T. Helfer and M. A. Amin, *General relativistic polarized Proca stars*, *Phys. Rev. D* **109** (2024) 024019 [2309.04345].

[74] N. Sanchis-Gual, F. Di Giovanni, M. Zilhão, C. Herdeiro, P. Cerdá-Durán, J. A. Font et al., *Nonlinear Dynamics of Spinning Bosonic Stars: Formation and Stability*, *Phys. Rev. Lett.* **123** (2019) 221101 [1907.12565].

[75] E. Seidel and W.-M. Suen, *Formation of solitonic stars through gravitational cooling*, *Phys. Rev. Lett.* **72** (1994) 2516 [gr-qc/9309015].

[76] F. S. Guzman and L. A. Urena-Lopez, *Gravitational cooling of self-gravitating Bose-Condensates*, *Astrophys. J.* **645** (2006) 814 [astro-ph/0603613].

[77] F. Di Giovanni, N. Sanchis-Gual, C. A. R. Herdeiro and J. A. Font, *Dynamical formation of Proca stars and quasistationary solitonic objects*, *Phys. Rev. D* **98** (2018) 064044 [1803.04802].

[78] F. Di Giovanni, S. Fakhry, N. Sanchis-Gual, J. C. Degollado and J. A. Font, *Dynamical formation and stability of fermion-boson stars*, *Phys. Rev. D* **102** (2020) 084063 [2006.08583].

[79] V. Cardoso, P. Pani, M. Cadoni and M. Cavaglia, *Ergoregion instability of ultracompact astrophysical objects*, *Phys. Rev. D* **77** (2008) 124044 [0709.0532].

[80] V. Cardoso, L. C. B. Crispino, C. F. B. Macedo, H. Okawa and P. Pani, *Light rings as observational evidence for event horizons: long-lived modes, ergoregions and nonlinear instabilities of ultracompact objects*, *Phys. Rev. D* **90** (2014) 044069 [1406.5510].

[81] P. V. P. Cunha, C. Herdeiro, E. Radu and N. Sanchis-Gual, *Exotic Compact Objects and the Fate of the Light-Ring Instability*, *Phys. Rev. Lett.* **130** (2023) 061401 [2207.13713].

[82] F. H. Vincent, Z. Meliani, P. Grandclement, E. Gourgoulhon and O. Straub, *Imaging a boson star at the Galactic center*, *Class. Quant. Grav.* **33** (2016) 105015 [1510.04170].

[83] H. Olivares, Z. Younsi, C. M. Fromm, M. De Laurentis, O. Porth, Y. Mizuno et al., *How to tell an accreting boson star from a black hole*, *Mon. Not. Roy. Astron. Soc.* **497** (2020) 521 [1809.08682].

[84] Event Horizon Telescope collaboration, *First Sagittarius A* Event Horizon Telescope Results. VI. Testing the Black Hole Metric*, *Astrophys. J. Lett.* **930** (2022) L17 [2311.09484].

[85] C. A. R. Herdeiro, A. M. Pombo, E. Radu, P. V. P. Cunha and N. Sanchis-Gual, *The imitation game: Proca stars that can mimic the Schwarzschild shadow*, *JCAP* **04** (2021) 051 [2102.01703].

[86] J. a. L. Rosa and D. Rubiera-Garcia, *Shadows of boson and Proca stars with thin accretion disks*, *Phys. Rev. D* **106** (2022) 084004 [2204.12949].

[87] I. Sengo, P. V. P. Cunha, C. A. R. Herdeiro and E. Radu, *The imitation game reloaded: effective shadows of dynamically robust spinning Proca stars*, 2402.14919.

[88] Z. Cao, A. Cardenas-Avendano, M. Zhou, C. Bambi, C. A. R. Herdeiro and E. Radu, *Iron Kα line of boson stars*, *JCAP* **10** (2016) 003 [1609.00901].

[89] T. Shen, M. Zhou, C. Bambi, C. A. R. Herdeiro and E. Radu, *Iron Kα line of Proca stars*, *JCAP* **08** (2017) 014 [1701.00192].

[90] eXTP collaboration, *The enhanced X-ray Timing and Polarimetry mission—eXTP*, *Sci. China Phys. Mech. Astron.* **62** (2019) 29502 [1812.04020].

[91] N. Franchini, P. Pani, A. Maselli, L. Gualtieri, C. A. R. Herdeiro, E. Radu et al., *Constraining black holes with light boson hair and boson stars using epicyclic frequencies and quasiperiodic oscillations*, *Phys. Rev. D* **95** (2017) 124025 [1612.00038].

[92] M. Bezares and C. Palenzuela, *Gravitational Waves from Dark Boson Star binary mergers*, *Class. Quant. Grav.* **35** (2018) 234002 [1808.10732].

[93] C. Palenzuela, I. Olabarrieta, L. Lehner and S. L. Liebling, *Head-on collisions of boson stars*, *Phys. Rev. D* **75** (2007) 064005 [gr-qc/0612067].

[94] V. Cardoso and P. Pani, *Tests for the existence of black holes through gravitational wave echoes*, *Nature Astron.* **1** (2017) 586 [1709.01525].

[95] V. Cardoso, S. Hopper, C. F. B. Macedo, C. Palenzuela and P. Pani, *Gravitational-wave signatures of exotic compact objects and of quantum corrections at the horizon scale*, *Phys. Rev. D* **94** (2016) 084031 [1608.08637].

[96] V. Cardoso, E. Franzin and P. Pani, *Is the gravitational-wave ringdown a probe of the event horizon?*, *Phys. Rev. Lett.* **116** (2016) 171101 [1602.07309].

[97] LIGO Scientific, Virgo collaboration, *GW190521: A Binary Black Hole Merger with a Total Mass of* $150M_\odot$, *Phys. Rev. Lett.* **125** (2020) 101102 [2009.01075].

[98] J. Calderón Bustillo, N. Sanchis-Gual, A. Torres-Forné, J. A. Font, A. Vajpeyi, R. Smith et al., *GW190521 as a Merger of Proca Stars: A Potential New Vector Boson of* 8.7×10^{-13} *eV*, *Phys. Rev. Lett.* **126** (2021) 081101 [2009.05376].

[99] J. Calderon Bustillo, N. Sanchis-Gual, S. H. W. Leong, K. Chandra, A. Torres-Forne, J. A. Font et al., *Searching for vector boson-star mergers within LIGO-Virgo intermediate-mass black-hole merger candidates*, *Phys. Rev. D* **108** (2023) 123020 [2206.02551].

[100] C. Herdeiro and E. Radu, *Ergosurfaces for Kerr black holes with scalar hair*, *Phys. Rev. D* **89** (2014) 124018 [1406.1225].

[101] J. F. M. Delgado, C. A. R. Herdeiro and E. Radu, *Violations of the Kerr and Reissner-Nordström bounds: Horizon versus asymptotic quantities*, *Phys. Rev. D* **94** (2016) 024006 [1606.07900].

[102] C. Herdeiro and E. Radu, *Construction and physical properties of Kerr black holes with scalar hair*, *Class. Quant. Grav.* **32** (2015) 144001 [1501.04319].

[103] B. Carter, *Hamilton-Jacobi and Schrodinger separable solutions of Einstein's equations*, *Commun. Math. Phys.* **10** (1968) 280.

[104] B. Carter, *Global structure of the Kerr family of gravitational fields*, *Phys. Rev.* **174** (1968) 1559.

[105] D. R. Brill, P. L. Chrzanowski, C. Martin Pereira, E. D. Fackerell and J. R. Ipser, *Solution of the scalar wave equation in a kerr background by separation of variables*, *Phys. Rev. D* **5** (1972) 1913.

[106] E. Berti, V. Cardoso and M. Casals, *Eigenvalues and eigenfunctions of spin-weighted spheroidal harmonics in four and higher dimensions*, *Phys. Rev. D* **73** (2006) 024013 [gr-qc/0511111].

[107] S. A. Teukolsky, *Rotating black holes - separable wave equations for gravitational and electromagnetic perturbations*, *Phys. Rev. Lett.* **29** (1972) 1114.

[108] S. Hod, *Stationary Scalar Clouds Around Rotating Black Holes*, *Phys. Rev. D* **86** (2012) 104026 [1211.3202].

[109] S. Hod, *Stationary resonances of rapidly-rotating Kerr black holes*, *Eur. Phys. J. C* **73** (2013) 2378 [1311.5298].

[110] S. Hod, *Quasi-Bound States of Massive Scalar Fields in the Kerr Black-Hole Spacetime: Beyond the Hydrogenic Approximation*, *Phys. Lett. B* **749** (2015) 167 [1510.05649].

[111] S. Hod, *The large-mass limit of cloudy black holes*, *Class. Quant. Grav.* **32** (2015) 134002 [1607.00003].

[112] S. Hod, *Spinning Kerr black holes with stationary massive scalar clouds: The large-coupling regime*, *JHEP* **01** (2017) 030 [1612.00014].

[113] M. Richartz, C. A. R. Herdeiro and E. Berti, *Synchronous frequencies of extremal Kerr black holes: resonances, scattering and stability*, *Phys. Rev. D* **96** (2017) 044034 [1706.01112].

[114] G. García and M. Salgado, *Regular scalar clouds around a Kerr-Newman black hole: Subextremal and extremal scenarios*, *Phys. Rev. D* **108** (2023) 104012 [2307.15888].

[115] S. Hod, *Kerr-Newman black holes with stationary charged scalar clouds*, *Phys. Rev. D* **90** (2014) 024051 [1406.1179].

[116] C. L. Benone, L. C. B. Crispino, C. Herdeiro and E. Radu, *Kerr-Newman scalar clouds*, *Phys. Rev. D* **90** (2014) 104024 [1409.1593].

[117] Y. Huang and D.-J. Liu, *Scalar clouds and the superradiant instability regime of Kerr-Newman black hole*, *Phys. Rev. D* **94** (2016) 064030 [1606.08913].

[118] C. Bernard, *Stationary charged scalar clouds around black holes in string theory*, *Phys. Rev. D* **94** (2016) 085007 [1608.05974].

[119] Y. Huang, D.-J. Liu, X.-H. Zhai and X.-Z. Li, *Scalar clouds around Kerr–Sen black holes*, *Class. Quant. Grav.* **34** (2017) 155002 [1706.04441].

[120] H. R. C. Ferreira and C. A. R. Herdeiro, *Stationary scalar clouds around a BTZ black hole*, *Phys. Lett. B* **773** (2017) 129 [1707.08133].

[121] M. A. A. de Paula, L. C. S. Leite, S. R. Dolan and L. C. B. Crispino, *Absorption and unbounded superradiance in a static regular black hole spacetime*, *Phys. Rev. D* **109** (2024) 064053 [2401.01767].

[122] O. J. C. Dias, J. E. Santos and B. Way, *Numerical Methods for Finding Stationary Gravitational Solutions*, *Class. Quant. Grav.* **33** (2016) 133001 [1510.02804].

[123] J. F. M. Delgado, C. A. R. Herdeiro, E. Radu and H. Runarsson, *Kerr–Newman black holes with scalar hair*, *Phys. Lett. B* **761** (2016) 234 [1608.00631].

[124] Y.-Q. Wang, Y.-X. Liu and S.-W. Wei, *Excited Kerr black holes with scalar hair*, *Phys. Rev. D* **99** (2019) 064036 [1811.08795].

[125] J. F. M. Delgado, C. A. R. Herdeiro and E. Radu, *Kerr black holes with synchronised scalar hair and higher azimuthal harmonic index*, *Phys. Lett. B* **792** (2019) 436 [1903.01488].

[126] C. A. R. Herdeiro, E. Radu and H. Rúnarsson, *Kerr black holes with self-interacting scalar hair: hairier but not heavier*, *Phys. Rev. D* **92** (2015) 084059 [1509.02923].

[127] J. F. M. Delgado, C. A. R. Herdeiro and E. Radu, *Kerr black holes with synchronized axionic hair*, *Phys. Rev. D* **103** (2021) 104029 [2012.03952].

[128] Y. Brihaye, C. Herdeiro and E. Radu, *Myers–Perry black holes with scalar hair and a mass gap*, *Phys. Lett. B* **739** (2014) 1 [1408.5581].

[129] C. Herdeiro, J. Kunz, E. Radu and B. Subagyo, *Myers–Perry black holes with scalar hair and a mass gap: Unequal spins*, *Phys. Lett. B* **748** (2015) 30 [1505.02407].

[130] O. J. C. Dias, G. T. Horowitz and J. E. Santos, *Black holes with only one Killing field*, *JHEP* **07** (2011) 115 [1105.4167].

[131] W. H. Press and S. A. Teukolsky, *Floating Orbits, Superradiant Scattering and the Black-hole Bomb*, *Nature* **238** (1972) 211.

[132] T. J. M. Zouros and D. M. Eardley, *INSTABILITIES OF MASSIVE SCALAR PERTURBATIONS OF A ROTATING BLACK HOLE*, *Annals Phys.* **118** (1979) 139.

[133] S. L. Detweiler, *KLEIN-GORDON EQUATION AND ROTATING BLACK HOLES*, *Phys. Rev. D* **22** (1980) 2323.

[134] S. R. Dolan, *Instability of the massive Klein-Gordon field on the Kerr spacetime*, *Phys. Rev. D* **76** (2007) 084001 [0705.2880].

[135] H. Yoshino and H. Kodama, *Bosenova collapse of axion cloud around a rotating black hole*, *Prog. Theor. Phys.* **128** (2012) 153 [1203.5070].

[136] A. Arvanitaki and S. Dubovsky, *Exploring the String Axiverse with Precision Black Hole Physics*, *Phys. Rev. D* **83** (2011) 044026 [1004.3558].

[137] W. E. East and F. Pretorius, *Superradiant Instability and Backreaction of Massive Vector Fields around Kerr Black Holes*, *Phys. Rev. Lett.* **119** (2017) 041101 [1704.04791].

[138] C. A. R. Herdeiro and E. Radu, *Dynamical Formation of Kerr Black Holes with Synchronized Hair: An Analytic Model*, *Phys. Rev. Lett.* **119** (2017) 261101 [1706.06597].

[139] B. Ganchev and J. E. Santos, *Scalar Hairy Black Holes in Four Dimensions are Unstable*, *Phys. Rev. Lett.* **120** (2018) 171101 [1711.08464].

[140] J. C. Degollado, C. A. R. Herdeiro and E. Radu, *Effective stability against superradiance of Kerr black holes with synchronised hair*, *Phys. Lett. B* **781** (2018) 651 [1802.07266].

[141] P. V. P. Cunha, C. A. R. Herdeiro, E. Radu and H. F. Runarsson, *Shadows of Kerr black holes with scalar hair*, *Phys. Rev. Lett.* **115** (2015) 211102 [1509.00021].

[142] P. V. P. Cunha, C. A. R. Herdeiro, E. Radu and H. F. Runarsson, *Shadows of Kerr black holes with and without scalar hair*, *Int. J. Mod. Phys. D* **25** (2016) 1641021 [1605.08293].

[143] P. V. P. Cunha, J. Grover, C. Herdeiro, E. Radu, H. Runarsson and A. Wittig, *Chaotic lensing around boson stars and Kerr black holes with scalar hair*, *Phys. Rev. D* **94** (2016) 104023 [1609.01340].

[144] P. V. P. Cunha, C. A. R. Herdeiro and E. Radu, *EHT constraint on the ultralight scalar hair of the M87 supermassive black hole*, *Universe* **5** (2019) 220 [1909.08039].

[145] P. V. P. Cunha and C. A. R. Herdeiro, *Shadows and strong gravitational lensing: a brief review*, *Gen. Rel. Grav.* **50** (2018) 42 [1801.00860].

[146] I. Sengo, P. V. P. Cunha, C. A. R. Herdeiro and E. Radu, *Kerr black holes with synchronised Proca hair: lensing, shadows and EHT constraints*, *JCAP* **01** (2023) 047 [2209.06237].

[147] F. H. Vincent, E. Gourgoulhon, C. Herdeiro and E. Radu, *Astrophysical imaging of Kerr black holes with scalar hair*, *Phys. Rev. D* **94** (2016) 084045 [1606.04246].

[148] S. Gimeno-Soler, J. A. Font, C. Herdeiro and E. Radu, *Magnetized accretion disks around Kerr black holes with scalar hair: Constant angular momentum disks*, *Phys. Rev. D* **99** (2019) 043002 [1811.11492].

[149] S. Gimeno-Soler, J. A. Font, C. Herdeiro and E. Radu, *Magnetized accretion disks around Kerr black holes with scalar hair: Nonconstant angular momentum disks*, *Phys. Rev. D* **104** (2021) 103008 [2106.15425].

[150] A. Cruz-Osorio, L. Rezzolla, F. D. Lora-Clavijo, J. A. Font, C. Herdeiro and E. Radu, *Bondi-Hoyle-Lyttleton accretion onto a rotating black hole with ultralight scalar hair*, *JCAP* **08** (2023) 057 [2301.06564].

[151] O. Donmez, O. Zanotti and L. Rezzolla, *On the development of QPOs in Bondi-Hoyle accretion flows*, *Mon. Not. Roy. Astron. Soc.* **412** (2011) 1659 [1010.1739].

[152] Y. Ni, M. Zhou, A. Cardenas-Avendano, C. Bambi, C. A. R. Herdeiro and E. Radu, *Iron Kα line of Kerr black holes with scalar hair*, *JCAP* **07** (2016) 049 [1606.04654].

[153] L. G. Collodel, D. D. Doneva and S. S. Yazadjiev, *Equatorial extreme-mass-ratio inspirals in Kerr black holes with scalar hair spacetimes*, *Phys. Rev. D* **105** (2022) 044036 [2108.11658].

[154] J. F. M. Delgado, C. A. R. Herdeiro and E. Radu, *EMRIs around $j = 1$ black holes with synchronised hair*, *JCAP* **10** (2023) 029 [2305.02333].

[155] LIGO Scientific, Virgo, KAGRA collaboration, *All-sky search for gravitational wave emission from scalar boson clouds around spinning black holes in LIGO O3 data*, *Phys. Rev. D* **105** (2022) 102001 [2111.15507].

[156] V. P. Frolov, P. Krtouš, D. Kubizňák and J. E. Santos, *Massive Vector Fields in Rotating Black-Hole Spacetimes: Separability and Quasinormal Modes*, *Phys. Rev. Lett.* **120** (2018) 231103 [1804.00030].

[157] V. P. Frolov, P. Krtous and D. Kubiznak, *Black holes, hidden symmetries, and complete integrability*, *Living Rev. Rel.* **20** (2017) 6 [1705.05482].

[158] M. A. Melvin, *Pure magnetic and electric geons*, *Phys. Lett.* **8** (1964) 65.

[159] S. W. Hawking, *Gravitational radiation from colliding black holes*, *Phys. Rev. Lett.* **26** (1971) 1344.

[160] P. C. W. Davies, *The Thermodynamic Theory of Black Holes*, *Proceedings of the Royal Society of London Series A* **353** (1977) 499.

[161] M. Gleiser and R. Watkins, *Gravitational Stability of Scalar Matter*, *Nucl. Phys. B* **319** (1989) 733.

[162] E. Poisson, *A Relativist's Toolkit: The Mathematics of Black-Hole Mechanics*. Cambridge University Press, 12, 2009, 10.1017/CBO9780511606601.

[163] C. A. R. Herdeiro, *Black Holes: On the Universality of the Kerr Hypothesis*, *Lect. Notes Phys.* **1017** (2023) 315 [2204.05640].

[164] R. Gregory and R. Laflamme, *Black strings and p-branes are unstable*, *Phys. Rev. Lett.* **70** (1993) 2837 [hep-th/9301052].

[165] R. Gregory and R. Laflamme, *The Instability of charged black strings and p-branes*, *Nucl. Phys. B* **428** (1994) 399 [hep-th/9404071].

[166] S. S. Gubser, *On nonuniform black branes*, *Class. Quant. Grav.* **19** (2002) 4825 [hep-th/0110193].

[167] T. Wiseman, *Static axisymmetric vacuum solutions and nonuniform black strings*, *Class. Quant. Grav.* **20** (2003) 1137 [hep-th/0209051].

[168] D. Pereñiguez, M. de Amicis, R. Brito and R. Panosso Macedo, *Superradiant Instability of Magnetic Black Holes*, 2402.05178.

[169] J. Barranco, A. Bernal, J. C. Degollado, A. Diez-Tejedor, M. Megevand, M. Alcubierre et al., *Are black holes a serious threat to scalar field dark matter models?*, *Phys. Rev. D* **84** (2011) 083008 [1108.0931].

[170] J. Barranco, A. Bernal, J. C. Degollado, A. Diez-Tejedor, M. Megevand, M. Alcubierre et al., *Schwarzschild black holes can wear scalar wigs*, *Phys. Rev. Lett.* **109** (2012) 081102 [1207.2153].

[171] A. Aguilar-Nieto, V. Jaramillo, J. Barranco, A. Bernal, J. C. Degollado and D. Núñez, *Self-interacting scalar field distributions around Schwarzschild black holes*, *Phys. Rev. D* **107** (2023) 044070 [2211.10456].

[172] R. Friedberg, T. D. Lee and A. Sirlin, *A Class of Scalar-Field Soliton Solutions in Three Space Dimensions*, *Phys. Rev. D* **13** (1976) 2739.

[173] J. Kunz, I. Perapechka and Y. Shnir, *Kerr black holes with synchronised scalar hair and boson stars in the Einstein-Friedberg-Lee-Sirlin model*, *JHEP* **07** (2019) 109 [1904.13379].

[174] J. Kunz and Y. Shnir, *Charged hairy black holes in the gauged Einstein-Friedberg-Lee-Sirlin model*, *Phys. Rev. D* **107** (2023) 104062 [2303.16562].